Quantifying Features of Arctic Odontocete Echolocation and Marine Habitat Variation in West Greenland

Marie Jo Zahn

A dissertation

submitted in partial fulfillment of the

requirements for the degree of

Doctor of Philosophy

University of Washington

2023

Reading Committee:

Kristin Laidre, Chair

Kathleen Stafford

Ian Fenty

Program Authorized to Offer Degree:

School of Aquatic and Fishery Sciences

© Copyright 2023
Marie J. Zahn

University of Washington

Abstract

Quantifying Features of Arctic Odontocete Echolocation and Marine Habitat Variation in West Greenland

Marie Jo Zahn

Chair of the Supervisory Committee:
Professor Kristin Laidre
School of Aquatic and Fishery Sciences

Monitoring Arctic cetacean habitat use enables identification of biologically important regions and predictions of climate change effects, both of which are critical to conservation efforts. The beluga (*Delphinapterus leucas*) and narwhal (*Monodon monoceros*) are the only toothed whale (odontocete) species that occupy Arctic waters year-round. As social animals, these species produce a variety of sounds to communicate with conspecifics and echolocate to forage and navigate. In recent decades, underwater recordings of their sounds have been collected to track seasonal movements and detect phenological shifts in response to sea ice declines. Yet, the vocal repertoires of belugas and narwhals are diverse, occur in similar frequency bands, and are only partially described, which can make it challenging to identify them in recordings. Furthermore, many questions remain surrounding what physical features of the marine environment explain

why belugas and narwhals occupy certain areas. This thesis takes a multidisciplinary approach to investigate Arctic odontocete echolocation and their marine habitat in West Greenland with goals to improve sustained observation methods. First, beluga echolocation click parameters were calculated using data from a 16-channel hydrophone array. Results revealed belugas had a narrow sonar beam emitted at high intensities, which was concordant with previous work showing the highly directional beam of narwhals. Second, beluga and narwhal click parameters were compared and found to be differentiable where beluga echolocation was distinguished by higher frequency content. Following this comparison, machine learning models were developed to classify the two species' clicks and the best model yielded highly accurate predictions (97.5% correct classification). Finally, this classifier was tested with a large acoustic dataset collected from seafloor-mounted moorings near glacier fronts in Melville Bay, Northwest Greenland. We present novel guidelines for visual identification of beluga and narwhal clicks using spectrograms from the moored recordings. Beluga clicks were characterized by frequencies >30 kHz whereas dominant narwhal click frequencies ranged from 20 to 30 kHz. Further, spectral energy in narwhal clicks quickly dropped below 20 kHz, providing a distinct lower frequency limit that was not visible in beluga clicks. These differences were reflected in one-third octave levels (TOL) calculated from click spectra. Narwhal clicks had a large increase between the 16 and 25 kHz TOL bands that was absent in beluga click spectra, and beluga clicks had a large increase between the 25 and 40 kHz TOL bands that was absent in narwhal click spectra. Compared to other variables, TOL ratios provided the strongest predictions to identify beluga and narwhal clicks. Our results provide compelling evidence to reliably identify beluga and narwhal clicks in long-term recordings and can be applied to future passive acoustic monitoring studies.

Often passive acoustic recording platforms also contain multiple oceanographic sensors to collect synchronous data on ocean conditions. In the final chapter of this thesis, synchronous year-round oceanographic observations were examined from the same moorings introduced in the preceding acoustic analyses. Results showed consistent seasonal hydrographic variability across sites. Differences in upwelling from subglacial plume mixing were found between sites where deep glaciers with higher freshwater runoff produced larger plumes. Maximum temperatures were observed in spring, priming deep glaciers for increased submarine melt during summer. Physical oceanographic variability has important implications for biological processes, including primary production, prey availability, and predator communities. Future work will continue to relate physical and biological processes at the glacier-ocean boundary and evaluate impacts from a warming ocean on ecosystem structure. Altogether, results from this thesis fill key knowledge gaps in Arctic odontocete click classification and ocean variability along Greenland's coast, enabling advancements in future passive acoustic and oceanographic observation procedures in the Arctic.

TABLE OF CONTENTS

LIST OF FIGURES

LIST OF TABLES

LIST OF SUPPLEMENTAL FIGURES

LIST OF SUPPLEMENTAL TABLES

ACKNOWLEDGEMENTS

I feel immense gratitude for the people who supported me throughout my graduate studies and influenced this work. My dissertation is the culmination of considerable effort by many individuals, most importantly my Ph.D. supervisory committee. I am indebted to my primary advisor, Kristin Laidre, for her constructive feedback and high standards, encouragement during uncertain times, and for modeling strength, kindness, and exceptional leadership in challenging circumstances. Kristin introduced me to Greenland where I had experiences that I will always cherish and that reaffirmed my dedication to polar ecology. It has been an incredible privilege to learn from Ian Fenty who has shown immense patience as I develop foundational knowledge in physical oceanography and taught me how to analyze hydrographic data with a critical and thoughtful eye. I am extremely thankful for Kristin and Ian's support to source funding for my Ph.D. research. I am deeply grateful to Kate Stafford for introducing me to the world of passive acoustics and being an invaluable resource on the topic. Kate has trusted my abilities and facilitated many important opportunities throughout my degree, including fieldwork and conferences, and I am truly thankful. I sincerely thank Mark Scheuerell for teaching me foundations in ecological modeling and paving the way for open and reproducible science within our SAFS community. I appreciate the positive presence and sincere interest from Randie Bundy as my GSR.

Data collection in the Arctic is a substantial feat, and my Ph.D. would not have been possible without the fieldwork completed by many individuals and institutions. I sincerely thank everyone who led and participated in the data acquisition for my thesis, in particular the 2013 Baffin Bay field team, the Oceans Melting Greenland (OMG) Narwhals project, and NASA OMG

program. I want to specifically thank collaborators and mentors who were instrumental in my progress: Jens Koblitz, Jennifer L. K. McCullough, Shannon Rankin, Malene Simon, and Michael Ladegaard. I am grateful to Mike Wood and Josh Willis for their help and willingness to share data and code to strengthen my research.

Outside of UW, my friends and family—near and far—kept me grounded and helped me maintain a healthy mindset during my degree. In particular, thank you Hannah Dawson, Kata Young, Alex Douglass, Courtney Hart, Nastia Rab, Leigh West, Duffy, Amy Van Cise, Jade Marcus, and Jimmy Paley for all the laughter and adventures. I thank the Laidre lab (past and present), the SAFS graduate student body, and my cohort for your friendship, community, and inspiration as we all endured the pandemic these last few years. Erica Escajeda, Ben Cohen, Jessie Lindsay, Helena McMonagle, Arial Brewer, Eileen Bates, Katie McElroy, Jenny Stern, Jessie Hale, Megan Feddern, and Liz Elmstrom always offered their generous support when I needed it. I owe a debt of gratitude to my partner, Sam, for his unwavering support, daily joy, and for always reminding me of my strengths when I had doubts. I am eternally grateful to my family, especially my mother and sister, for their endless encouragement, and finally, to grandma who would've been so proud to see me reach this milestone.

Lastly, I would like to thank the agencies who funded this work: the U.S. Office of Naval Research on K. L. Laidre's grant (award numbers: N00014-11-1-0201 and N00014-17-1-2774), the Vetlesen Foundation, NASA Oceans Melting Greenland EVS-2 mission, Cooperative Institute for Climate, Ocean, & Ecosystem Studies (CICOES) under NOAA Cooperative Agreement NA20OAR4320271, and the University of Washington's School of Aquatic and Fishery Sciences.

DEDICATION

To my father, David Zahn, who would've been proud to see this work completed, and to my mother, Kristie Zahn, who has always modeled strength and persistence.

Chapter 1. INTRODUCTION

1.1 GREENLAND IN A CHANGING ARCTIC

The Arctic is characterized by extremes, where dramatic seasonal cycles in temperature, light, and ice shape the physical, biological, and ecological landscapes. Arctic warming is occurring more than three-times as fast as the global mean and unequivocally altering marine and terrestrial ecosystems with global consequences (IPCC, 2021; 2022; Rantanen et al. 2022). Sea ice is one of the most important features of Arctic marine ecosystems because it drives biophysical processes and serves as critical habitat to resident species. Over the last four decades, the age, extent, and thickness of sea ice has declined at unprecedent rates and current models predict the Arctic will experience an ice-free summer by mid-century (Wang & Overland 2009; Overland & Wang 2013; Kwok 2018; Onarheim et al. 2018; Kacimi & Kwok 2022). Beyond environmental changes, longer open-water seasons due to sea ice declines are providing opportunities for human development in the Arctic (Comiso & Hall 2014; Kwok 2018; Overland et al. 2019). It is estimated that more than 80% of international trade in commodities by volume is transported by sea (UNCTAD, 2021). Accordingly, vessel traffic is expected to increase through previously inaccessible trans-Arctic shipping routes (i.e., the Northwest Passage and Northern Sea Route) and transform remote regions of the Arctic to commercial marine highways (Smith & Stephenson 2013; Reeves et al. 2014; Hauser et al. 2018; Mudryk et al. 2021). It is without question that major regime shifts in Arctic marine ecosystems are underway, and consequently, serious concern has grown surrounding negative impacts to native species and local human communities.

Greenland has experienced some of the most dramatic changes due to climate warming seen in the accelerated mass loss of its ice sheet (IMBIE Team 2020; Otosaka et al. 2023). In fact,

the loss of Greenland's ice sheet has caused global sea levels to rise by 13.7 mm since 1972, half of which occurred over the last eight years (Mouginot et al. 2019). As a result, Greenland has become a primary focus across many research disciplines as changes to its ice sheet, marine and land-terminating glaciers, and surrounding waters will have widespread physical and biological impacts at both local and global scales. Perhaps of most importance is Greenland's coast where large seasonal transformations occur and most ecological diversity is found. Human communities have settled in regions of high productivity, particularly on the west coast, to access the abundance of marine resources. Greenland's fjords, bays, and inlets host a variety of species during productive summer months including seabirds, fish, seals, whales, and polar bears (*Ursus maritimus*), all of which support local human subsistence and commerce. Interdisciplinary efforts have been made to couple ice, ocean, and atmospheric systems along Greenland's margins but resolving fine-scale physical and biological processes to predict ecosystem variability remains a considerable challenge (Straneo et al. 2022).

Within marine ecosystems, Arctic marine mammals are especially sensitive to sea ice declines, warming temperatures, and increased human activities in the Arctic (Laidre et al. 2008; Moore & Huntington 2008; Hauser et al. 2018; Halliday et al. 2020). Among Arctic marine mammals, cetaceans are especially at risk due to cumulative stressors from climate change (e.g., habitat loss) (Kovacs et al. 2011; Laidre et al. 2015), hydrocarbon development and commercial shipping (e.g., ship strikes, hearing damage, underwater noise disturbance) (Reeves et al. 2014; Hauser et al. 2018; Halliday et al. 2020), and insufficiently managed commercial or subsistence harvest, in particular for some Greenland subpopulations (Marcoux & Hammill 2016; Hobbs et al. 2019; Nammco 2022). The inaccessibility and hazardous conditions of the Arctic combined with

studying migrating animals that spend a fraction of their time at the ocean's surface makes studying Arctic cetaceans a difficult scientific endeavor.

This dissertation focuses on the acoustic ecology and marine habitat of two Arctic top predators in West Greenland: the beluga (*Delphinapterus leucas*) and narwhal (*Monodon monoceros*). Passive acoustic, oceanographic, and remote sensing technologies were used to describe foundational properties of the sounds produced by these species and their marine environment. Results help enable future long-term studies using passive acoustics and provide a firm understanding of seasonal ocean conditions in a previously understudied area in northwest Greenland. The following sections provide the biological and physical basis for this work.

1.2 Arctic Odontocetes

While numerous cetacean species migrate north into Arctic waters during summer, only belugas, narwhals, and bowhead whales (*Balaena mysticetus*) reside there year-round and are referred to as true Arctic cetaceans. The beluga and narwhal are closely related, mid-sized toothed whales (odontocetes) and sole members of the Monodontidae family. Known as Monodontids, they reach approximately 3–5 meters (~1,200–1,600 kg) as adults. Like bowhead whales, belugas and narwhals lack a dorsal fin, an evolutionary adaption to navigate ice-covered waters (Harington 2008). Juvenile belugas and narwhals are grayish in color, and upon maturity, develop their adult skin colors. Commonly known as the "white whale," adult belugas are white in color whereas adult narwhals have a mottled dark gray/blueish pattern on their dorsal side and are primarily white on their abdomen. Narwhals are known to be long-lived, some exceeding 100 years (Garde et al. 2007), and as individuals reach ages over ~15 years, their body color begins to fade to white. Current estimates of the beluga life span are ~80 years (Stewart et al. 2006).

Both species exhibit sexual dimorphism, where males tend to be larger than females (Garde et al. 2015; O'Corry-Crowe 2018). Specifically for the narwhal, males (very rarely females) develop an elongated, spiraled tooth out of the left side of their jaw, known as a tusk, that is understood to be a sexually selected trait used in male-to-male competition and to attract a mate (Graham et al. 2020). Male narwhals reach sexual maturity around 12–20 years and females between 8–9 years (Garde et al. 2015). Generally, narwhals have a calf every 3 years and mate in the spring (late May to early June), giving birth approximately 14 months later the following year during their annual northward migrations (Garde et al. 2007; Garde et al. 2022). Similarly, female belugas give birth approximately every 2–3 years once they reach sexual maturity between the ages of 9–12 years. Belugas mate in late winter to early spring and then give birth the following summer (July–August), although this can vary (O'Corry-Crowe 2018).

Belugas and narwhals are highly social species with complex community structures that are still not fully understood. It is estimated that there are 180,000 belugas and between 85,000–100,000 narwhals globally, though some subpopulations are poorly studied (NAMMCO 2017; Hobbs et al. 2019). As social animals, they travel in groups (pods) that range widely from a few individuals to tens or hundreds of individuals. Arctic odontocetes are composed of numerous subpopulations, or stocks, that are distinguished by their summering grounds. Belugas have an expansive range with 22 stocks (1 extirpated) that span Arctic and subarctic regions (Figure 1.1; Hobbs et al. 2019). While some beluga populations are resident, the majority are migratory and travel between coastal wintering grounds with minimal sea ice and northerly estuarine summering grounds to molt, feed, and give birth (Frost & Lowry 1990; Smith & Martin 1994; Innes et al. 2002; Lewis et al. 2009). Narwhals are only found in the Atlantic sector of the Arctic in 12 discrete stocks within the Canadian High Arctic, West and East Greenland, and western Russia (Richard

et al. 2010; Ahonen et al. 2019; Hobbs et al. 2019). It is well documented that narwhal populations in the Canadian Arctic and West Greenland undergo extensive annual migrations. They overwinter in the dense pack ice of Baffin Bay and Davis Strait and return to the same summering grounds in fjords and inlets with high site fidelity (Dietz et al. 2001; Heide-Jørgensen et al. 2003a). Migration pathways of narwhals in the eastern sector of the North Atlantic are not well known, but studies indicate that while some whales migrate between coastal and offshore environments similar to West Greenland stocks, others may remain offshore year-round (Heide-Jørgensen et al. 2015; Ahonen et al. 2019). In the recent global review of the status of Monodontids (Hobbs et al. 2019), greatest concern was identified for the Melville Bay and East Greenland narwhal stocks and several beluga stocks that are very small (Cook Inlet, St. Lawrence Estuary, Cumberland Sound, and Ungava Bay) and/or understudied (Eastern Hudson Bay and Barents-Kara-Laptev Seas).

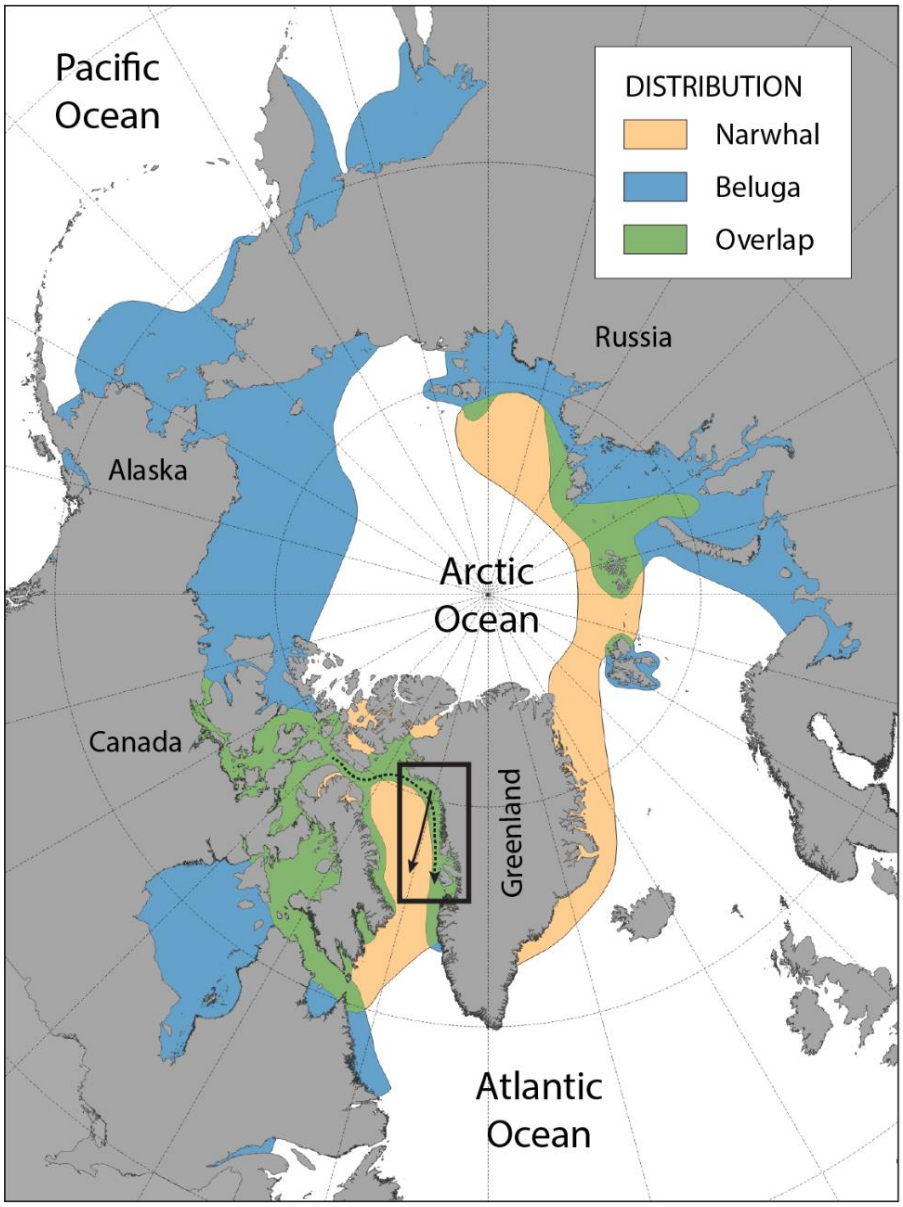

Figure 1.1. Beluga and narwhal distributions in the Arctic. Species ranges (beluga: blue; narwhal: amber/orange; overlap: green) are based on distributions outlined by Hobbs et al. (2019) and are inclusive of summering and wintering grounds as well as migratory areas. The black box outlines the study region for this thesis in West Greenland where both species occur. Lines with arrows show the general fall southward migration of the Eastern High Arctic-Baffin Bay beluga stock (dashed line) and Melville Bay narwhal stock (solid line). Note: some of this beluga subpopulation overwinters in the North Water polynya (Richard et al. 1998a; Richard et al. 1998b; Heide-Jørgensen et al. 2003b). Melville Bay stock movements are from narwhal telemetry studies (Dietz & Heide-Jørgensen 1995; M. P. Heide-Jørgensen et al. 2013).

As social species, Monodontids are vocal animals that use a wide variety of sounds to communicate and interact with one another, and as toothed whales, they have evolved the ability to echolocate for navigation and feeding (Au 1993; Madsen & Wahlberg 2007). Narwhals that overwinter in Baffin Bay are deep-divers, reaching depths greater than 1000 m deep (Laidre et al. 2002; Laidre et al. 2003). Diet studies examining stomach contents coupled with dive profiles found narwhals feed primarily in the winter on Arctic and polar cod (*Arctogadus glacialis* and *Boreogadus saida*), squid (*Gonatus* spp.), shrimp (*Pandalus* spp.), and Greenland halibut (*Reinhardtius hippoglossoides*) (Laidre et al. 2003; Laidre et al. 2004; Laidre & Heide-Jørgensen 2005; Garde et al. 2022). Diving behavior varies across sub-populations which is likely related to prey availability and foraging behavior. The beluga diet is much more variable than the narwhal diet given the beluga's wide distribution across the Arctic. As such, the beluga is more of a generalist predator across diverse habitats (Laidre et al. 2008). However, across the Arctic polar cod appears to be the most dominant prey species for many populations. Belugas can also dive to great depths but not as deep as those of narwhals. Recorded dives range from shallow depths to those >500 meters reaching the seafloor and are likely determined by regional prey abundance (Hauser et al. 2015; Lydersen & Kovacs 2021).

With ongoing climate warming, partial or complete beluga and narwhal habitat loss from warming ocean temperatures and sea ice declines is expected. The beluga and narwhal are ice-associated species and are found in coastal bays, fjords, leads, and pack ice (loose and dense) throughout the year. The life histories of migratory belugas and narwhals follow annual sea ice advance and retreat during their annual southward and northward movements. In a comprehensive study conducted by Laidre et al. (2008), the narwhal, along with the hooded seal (*Cystophora cristata*) and polar bear, was determined to be the most sensitive marine mammal species to

climate-induced habitat change. The beluga was classified as moderately sensitive. However, evaluating the relative sensitivity of Arctic marine mammals remains a considerable challenge given some subpopulations are still understudied and exposure to various threats is region specific. For example, in a more ice-free Arctic, cetaceans may benefit from increased prey as waters become more productive, but at the same time increased vessel traffic pose threats to some populations (Hauser et al. 2018; Moore & Reeves 2018). Narwhals are considered to be specialist predators and belugas generalist predators related to their dietary preferences summarized above. Narwhals are the most restricted in their distribution compared to bowhead and beluga whales and are adapted to winters in dense pack ice to feed (Laidre et al. 2004; Laidre & Heide-Jørgensen 2005). Further, narwhals occupy waters within narrow temperature ranges and prefer cold water below ~2°C (Chambault et al. 2020; Heide-Jørgensen et al. 2020). In addition to reduced suitable habitat, indirect and cumulative effects of climate change are more challenging to quantify. Climate-induced habitat change is likely to negatively impact both species, but the narwhal is at greater risk given its specialized diet, small population, thermal tolerance, and reduced distribution compared to the beluga (Laidre et al. 2008; Kovacs et al. 2011).

The largest spatiotemporal overlap between belugas and narwhals occurs in waters within the Canadian Arctic Archipelago and Baffin Bay, West Greenland (Figure 1.1). These regions also overlap with the Northwest Passage sea route and the vessel corridor for the Mary River Iron Ore Mine on Baffin Island where anthropogenic underwater noise is expected to increase (Stewart et al. 2011; Reeves et al. 2014; Halliday et al. 2021a; Kochanowicz et al. 2021). Underwater sounds from seismic surveys, drilling and oil production, military sonar, and motorized vessels can substantially disturb the acoustic environment that these whales depend on to communicate and forage (Erbe & Farmer 2000; Blackwell et al. 2004; Mads Peter Heide-Jørgensen et al. 2013;

Heide-Jørgensen et al. 2021; Kochanowicz et al. 2021). The Northwest Passage connects the Atlantic to the Pacific oceans via waterways along West Greenland, the Canadian High Arctic, and Alaska, and crosses key beluga and narwhal seasonal habitats. The peak commercial shipping season occurs in September which coincides with beluga and narwhal fall migrations into West Greenland waters. With increasing threats from vessel traffic in the region, there is a growing need to monitor beluga and narwhal movements and changes to their acoustic environment.

1.3 Greenland's Continental Shelf Waters

Passive acoustics can effectively address questions surrounding the distribution and behavior of belugas and narwhals, but studying changes to their marine environment requires oceanography. The large-scale circulation patterns along Greenland's continental shelf are generally agreed upon, but regional hydrography—in particular seasonal variability—is not well defined on a pan-Greenland scale. Greenland is bordered by Baffin Bay to the west, the Arctic Ocean to the north, the Nordic Seas (comprised of the Greenland, Icelandic, and Norwegian Seas) to the east, and the North Atlantic Ocean subpolar gyre to the south, including the Labrador and Irminger Seas (Figure 1.2). Northward transport of warm, saline subtropical Atlantic water (AW) originates from the Gulf Stream and North Atlantic Current (NAC) and meets cold Polar water (PW) as it circulates Greenland's coastline. The NAC branches and forms the Norwegian Atlantic Current to the east and the Irminger Current (IC) to the west following bathymetric contours that border the Irminger Sea. The Norwegian Atlantic Current runs along the coast of Ireland and through the Faroe-Shetland Ridge into the Nordic Seas where a branch joins the East Greenland Current (EGC) and moves south. The southward flow of the EGC follows the eastern boundary of Greenland and is formed from PW flowing through Fram Strait and AW from the Norwegian Atlantic Current. With a sill depth of ~2600 meters, Fram Strait acts as the main gateway for sea ice export and fresh

water from the Arctic. Fresh PW transported by the EGC occupies the shelf adjacent to the coastline and the upper layer in the water column. A warmer AW wedge of the EGC and IC flow farther offshore over the continental slope and below the PW layer. As the IC and EGC flow around Greenland's southern tip, the EGC becomes the West Greenland Current (WGC) that travels northward along the continent's western boundary. Bound by the bathymetric sill in Davis Strait (~640 m deep), a portion of the WGC recirculates south into the Labrador Sea and the western lobe of the North Atlantic subpolar gyre.

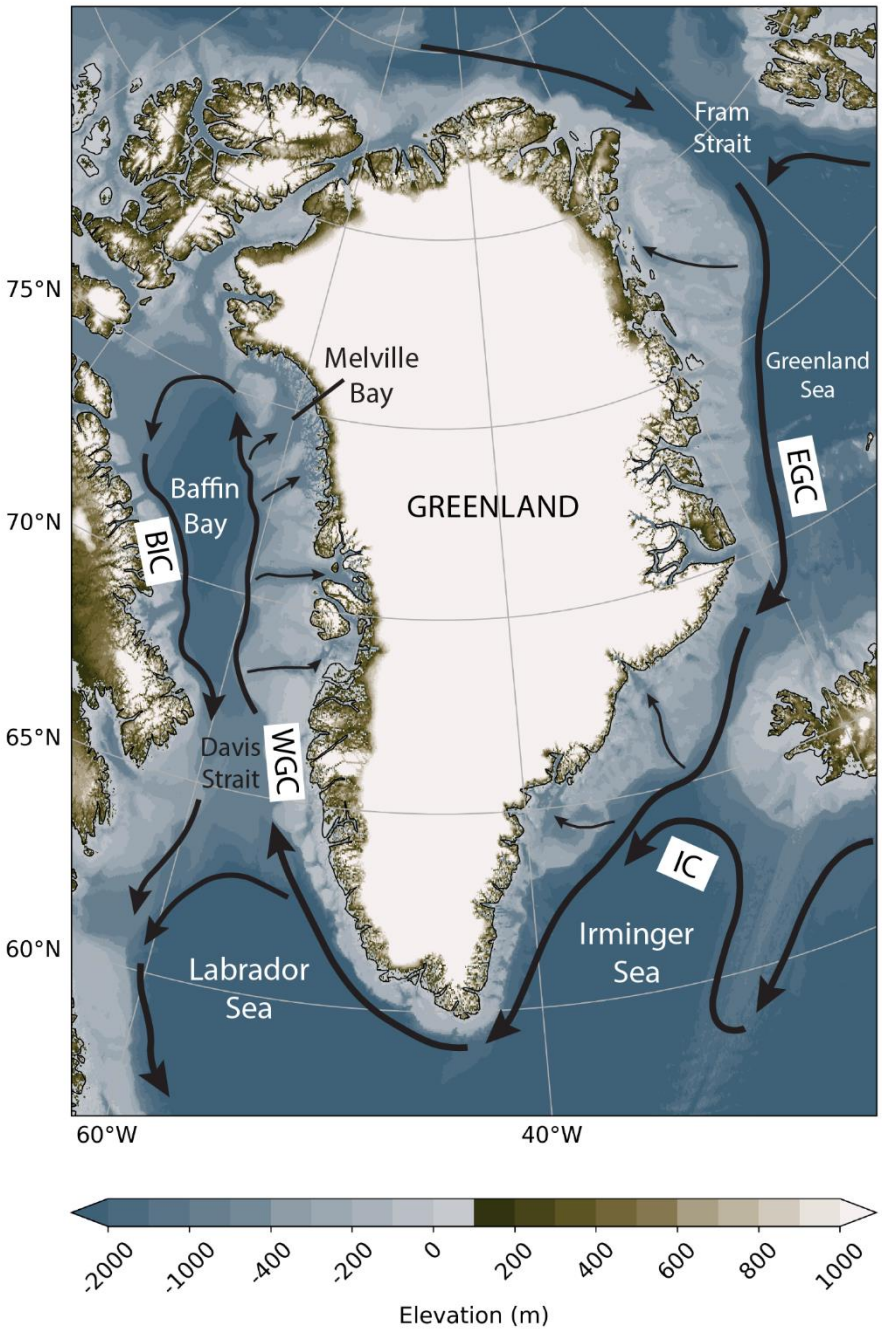

Figure 1.2. Dominant ocean currents surrounding Greenland. Black arrows indicate the major ocean currents: Irminger Current (IC), East Greenland Current (EGC), West Greenland Current (WGC), and Baffin Island Current (BIC). The dominant circulation patterns around Greenland are described by Talley et al. (2011) and summarized by many others (e.g., Cuny et al. 2002; Tang et al. 2004; Straneo et al. 2010; Straneo et al. 2012).

Ocean waters surrounding Greenland experience progressive heat loss as northbound warm, saline AW meet cold, fresh PW from outlets of tidewater glaciers and the Arctic Ocean. Waters along southeast Greenland and the Irminger Sea experience the warmest mean near-surface temperatures (~8 to 10°C), owing to their proximity to the NAC; the coldest mean near-surface temperatures are found in north and northwest Greenland (~ -1.5 to 2°C) where AW has mixed with PW and released heat during transit via air-sea temperature exchanges (Straneo et al. 2010; Rignot et al. 2012; Straneo et al. 2012; Rysgaard et al. 2020). Importantly, the Labrador Sea and Nordic Seas are where some of the greatest heat fluxes in the world take place, resulting in deep convection and the formation of North Atlantic Deep Water (NADW) and the upper limb of the Atlantic Meridional Overturning Circulation. Dramatic ocean heat/buoyancy loss in the winter is driven by cold air temperatures and surface winds, causing newly dense surface waters to sink to depths sometimes exceeding 2,000 meters (Marshall et al. 1998; Våge et al. 2009). The formation and flow of NADW is a primary means of freshwater transport equatorward and carbon sequestration to the deep ocean and has widespread effects as an important component of the global climate system.

Specifically in Baffin Bay, the dominant circulation is cyclonic (counterclockwise). The northbound WGC follows the coastline of Greenland's western boundary and is generally composed of a fresh PW coastal current on the shelf and AW on the slope. Terminology in the literature varies for the WGC where it may be referenced as a single water mass (Tang et al. 2004; Myers et al. 2007; Rykova et al. 2009) that carries warm water northward or as two partitioned components: an AW (offshore slope) and PW (onshore shelf) branch (Curry et al. 2011; Curry et al. 2014; Pacini et al. 2020). Warm, saline waters from the IC turn at Cape Farewell and a portion of it branches northward and crosses Davis Strait. Curry et al. (2011; 2014) refer to this water mass

as the West Greenland Slope Current (WGSC). The EGC has a fresh, PW inner continental shelf branch south of Denmark Strait called the East Greenland Coastal Current (EGCC; Sutherland & Pickart 2008; Harden et al. 2014). The EGCC and the low-salinity wedge of the EGC feed into the WGC's analogue named the West Greenland Coastal Current (WGCC) that also hugs the shoreline (Pacini et al. 2020). Inflowing waters on the eastern side of Davis Strait that comprise the WGC are modified during their cyclonic circulation in Baffin Bay where they meet the southward flowing Baffin Island Current (BIC) on the western boundary of Baffin Bay. The BIC transports cold, fresh water from the Canadian Arctic Archipelago southward (Cuny et al. 2002; Tang et al. 2004).

Generally, the water column surrounding Greenland and within its fjords is composed of a surface PW layer above an AW layer with a transition zone of intermediate water in between. The fresh, cold PW layer observed in the upper 100–200 m is more buoyant than the warm, saline dense AW typically found below 200 to 300 m (Straneo et al. 2010; Wood et al. 2021). However, the seasonal and interannual variability of Greenland's surrounding waters is not fully understood and is driven by thermohaline circulation, seafloor geometry, atmospheric forcing, and the annual sea ice cycle (Straneo et al. 2010; Harden et al. 2014; Carroll et al. 2018). On a large scale, throughout the year AW is circulating through the pathways described above, but summer melting of the ice sheet, glaciers, and seasonal sea ice delivers a seasonal freshwater pulse. The seasonal presence of fresh, PW originating from remote and local sources has been observed in fjords around Greenland, but the timing and magnitude varies.

The subpolar gyre has warmed since the 1990s (Bersch et al. 2007; Myers et al. 2007; Våge et al. 2011) with increased heat transport to high latitudes (Keil et al. 2020). Warming of AW has been hypothesized to be related to increased subsurface melt at the ice-ocean interface and

consequently glacier retreat (Holland et al. 2008; Straneo et al. 2010; Straneo & Heimbach 2013; Harden et al. 2014; Carroll et al. 2018; Rignot et al. 2021; Wood et al. 2021). Central to this hypothesis is the transport of heat from the subpolar North Atlantic Ocean to Greenland's marine-terminating glaciers via the network of coastal currents described above. Through these currents, AW is shunted across coastal shelves into drainage basins and fjords where it comes into direct contact with glacier fronts (Straneo et al. 2010; Straneo et al. 2016). However, the characteristics of tidewater glaciers and their drainage basins are highly diverse, and many factors contribute to the propensity of a given glacier to retreat in the presence of warming AW. Knowledge of ocean variability at the glacier-ocean interface is critical to accurately quantify the ocean's role in glacier retreat and infer how changes to physical processes along Greenland's coast due to warming temperatures will impact ecosystem structure. For top predators such as the beluga and narwhal, changes to their marine environment are expected to have cascading effects through the food web through trophic linkages as temperatures warm, sea ice declines, and nutrient fluxes and primary production shift.

1.4 Observation Methods

As the Arctic continues to experience unprecedented environmental changes, monitoring changes to the distribution, behavior, and marine habitat of belugas and narwhals is an increasing research priority. In particular, sustained observations (i.e., months and years) are needed to identify biologically important regions and quantify changes to marine ecosystems. Approaches widely used in marine mammal research include ship-based or aerial visual surveys, telemetry, experiments in captivity, and passive acoustics. For long-term studies to identify where and when animals are present in the Arctic, passive acoustics is likely the most effective tool. Passive acoustic instrumentation can be deployed for short (e.g., days using animal-borne tags) or long

(e.g., months using moorings) durations depending on the research objective (Mellinger et al. 2007). One of its greatest strengths is obtaining a continuous time series of animal occurrences spanning months to years that is coupled with a synchronous oceanographic dataset (e.g., temperature and salinity).

Passive acoustic monitoring relies on the ability to distinguish between species solely based on their characteristic sounds, which means specific sonic identifiers must be known for each species. Call types typically used in acoustic classification of odontocetes include echolocation clicks, burst pulses, whistles, and combined signals (Sjare & Smith 1986b; Chmelnitsky & Ferguson 2012; Marcoux et al. 2012; Garland et al. 2015; Rasmussen et al. 2015; Castellote et al. 2020; McCullough et al. 2021). Echolocation, also known as biosonar, is characterized by the emission of high frequency, relatively broadband clicks of high directionality and listening for returning echoes. It is a dominant sense for odontocetes, much like vision is for humans (Au 1993; Madsen & Wahlberg 2007). Burst pulses are a series of broadband pulses (clicks) with a high repetition rate (Ford & Fisher 1978; Sjare & Smith 1986b; Rasmussen et al. 2015). Whistles are narrow-band and frequency-modulated tonal vocalizations (Sjare & Smith 1986b; Rankin et al. 2017). Combined signals include overlaid or paired pulsed and tonal sounds (Shapiro 2006; Marcoux et al. 2012; Walmsley et al. 2020). Single or multiple call types may be used to differentiate species in acoustic classifiers. For the beluga and narwhal specifically, distinguishing between their sounds has proven challenging given the considerable overlap and variability in frequency ranges used by the two species (Ford & Fisher 1978; Marcoux et al. 2012; Stafford et al. 2012; Frouin-Mouy et al. 2017). Research objectives pursued in this dissertation specifically address improving methods for beluga and narwhal acoustic classification.

Coupled passive acoustic and oceanographic observations enable researchers to study marine mammal occurrence and ocean conditions separately, as well as investigate potential linkages between them. While large-scale circulation around Greenland has been described as summarized above, ocean observations at a sufficiently high resolution to characterize regional and seasonal hydrographic patterns along the continental shelf have been limited. In 2015, NASA launched the Earth Venture-Suborbital Oceans Melting Greenland (OMG) mission to improve ocean observations along Greenland's continental shelf to better understand the role of warm AW melting marine-terminating glaciers from below. Between 2015–2021, OMG launched several annual surveys: 1) ship-based and airborne expendable conductivity-temperature-depth (CTD and AXCTD) sensors to measure ocean properties (e.g., temperature, salinity, sound speed; Figure 1.2), 2) ship-based multibeam sonar and airborne gravimetry to map coastal bathymetry on the shelf and within fjords, and 3) airborne interferometric radar to measure surface topography including the extent and height of marine-terminating glaciers (Fenty et al. 2016). OMG's extensive sampling effort was performed principally to examine to what degree are Greenland's glaciers melting from submarine warm water. Results from OMG's effort show many of the >200 glaciers around Greenland terminate in deep fjords that consequently expose glacier ice to incoming warm Atlantic water (Fenty et al. 2016; Wood et al. 2021). While OMG's AXCTD mission has obtained oceanographic measurements around Greenland at an unprecedented spatial scale, it could not capture seasonal hydrographic variation given its yearly sampling regime. Identifying seasonal trends in temperature and salinity provides foundational knowledge about annual cycles in key ecosystem processes (e.g., subglacial plumes and spring blooms). Year-round observations also provide important baseline measurements to characterize the marine environment as ocean temperatures warm due to climate change.

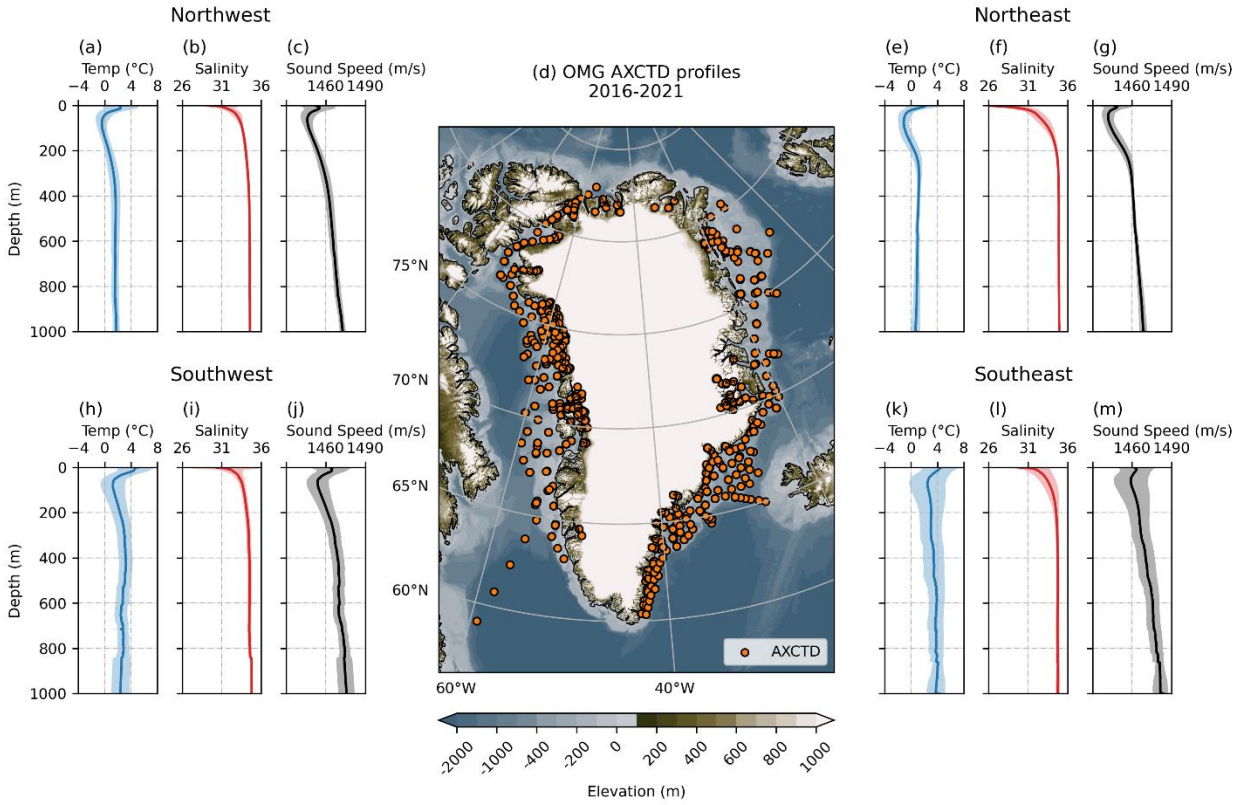

Figure 1.3. Oceans Melting Greenland (OMG) AXCTD locations and mean profiles. AXCTD profile sampling sites between 2016–2021 are shown in (d). Four regional sectors were defined to take average profiles: northwest (west of 45°W, north of 70°N), northeast (east of 45°W, north of 70°N), southwest (west of 45°W, south of 70°N), southeast (east of 45°W, south of 70°N). Mean temperature, salinity, and sound speed profiles for the northwest (a, b, c), northeast (e, f, g), southeast (h, i, j), and southwest sectors (k, l, m).

1.5 Thesis Overview

This dissertation seeks to address knowledge gaps in Greenland cetacean ecology and oceanography by quantifying features of beluga and narwhal echolocation and their marine environment. The work is motivated by an increasing need for sustained observations of Arctic odontocete behavior using passive acoustics and of ocean properties surrounding Greenland. At the outset of this research, advancements were needed to distinguish between beluga and narwhal

sounds to confidently identify them in mixed species recordings. Regions studied in this dissertation are within eastern Baffin Bay along the central and northwest Greenland continental shelf where the Eastern High Arctic-Baffin Bay beluga and Melville Bay narwhal stocks are found (Figure 1.1). Prior to this work, there had been no year-round ocean observations collected from northwest Greenland. Our findings provide an important hydrographic time series for Melville Bay, a region that supports narwhals during summer and belugas during their spring and fall migrations. In total, this thesis comprises four primary research studies (chapters 2–5) and a final section dedicated to concluding remarks (chapter 6).

Chapters 2 and 3 of this thesis quantify characteristics of beluga and narwhal echolocation in central Baffin Bay and develop methods to acoustically classify each species. Specifically, chapter 2 uses recordings from a 16-channel hydrophone array to describe properties of beluga echolocation (Zahn et al. 2021a). This work compliments the study by Koblitz et al. (2016) who reported narwhal echolocation parameters using a similar approach. In addition to providing baseline acoustic parameters, we report the first sonar beam width estimate of *in situ* recordings of wild belugas with an average -3 dB vertical beam width of 5.4° and source level of 212 dB pp re 1 µPa. Our findings reinforce the hypothesis that Arctic odontocetes have evolved a narrow echolocation beam with high source levels to reduce acoustic echoes from sea ice at the surface and to effectively identify open-water leads in pack ice (Koblitz et al. 2016; Jensen et al. 2018). Chapter 3 applies findings from Zahn et al. (2021a) and Koblitz et al. (2016) by examining whether beluga and narwhal clicks can be differentiated in acoustic recordings to support widespread use of passive acoustic monitoring of these species. We demonstrate belugas and narwhals can be classified acoustically using echolocation clicks with a high correct classification rate of 97.5% for the best model (Zahn et al. 2021b). Beluga echolocation was distinguished by more energy at

higher frequencies than narwhal clicks where spectral peaks, troughs, and center frequencies were generally >60 kHz and narwhal clicks <60 kHz. Results from chapter 3 provide strong support for using echolocation to distinguish between belugas and narwhals in passive acoustic studies.

The focus of chapters 4 and 5 shifts to northwest Greenland in the vicinity of narwhal summering areas and beluga migration pathways. Narwhals from the Melville Bay stock return to glacier fronts each summer with high site fidelity (Laidre et al. 2016). Seafloor-mounted ocean moorings outfitted with hydrophones and a suite of oceanographic sensors were strategically deployed near three glaciers with known narwhal presence. The aim of chapter 4 was to test and improve the acoustic classifier developed in chapter 3 using large acoustic datasets from these moorings. We compared changes in one-third octave levels (TOL) between two pairs of one-third octave bands and show narwhal clicks have a steep increase between the 16 and 25 kHz TOL bands whereas beluga clicks have a large increase between the 25 and 40 kHz TOL bands. Results from chapter 4 confirm our ability to accurately classify beluga and narwhal clicks using both manual and automated approaches and encourage the use of TOL metrics in future acoustic detection efforts.

Chapter 5 utilizes oceanographic measurements collected from the same moorings studied in chapter 4 to describe seasonal hydrographic variability and marine glacial habitats in Melville Bay. The high temporal resolution of the moored temperature and salinity observations (every 20–180 sec for two years) builds on the spatially robust dataset obtained by NASA's OMG program. Analysis of the moored hydrographic data revealed consistent seasonal hydrography across sites with differences in subglacial plume events where larger plumes were produced by deeper glaciers with large upstream ice basins. Glacier front ocean variability is greatest in the summer and fall, coincident with subglacial plumes and large wind events. Winter and spring are relatively stable

periods characterized by inshore advection from the WGC that feeds the renewal of warm, salty water. Coastal ecosystems near glacier fronts provide important habitat not only to narwhals during the summer but to a range of species. The variability described in chapter 5 can be linked to biological and ecological processes to better understand ecosystem-wide processes and seasonal trophic coupling. Results from chapter 5 will also help answer questions related to the sources and processes driving the retreat and acceleration of Greenland's glaciers more broadly.

The research presented in this thesis advances the current understanding of Arctic odontocete bioacoustics and Greenland seasonal hydrography and helps improve oceanographic and cetacean observation methods in the Arctic. The acoustic classifiers developed in chapters 3 and 4 provide evidence for reliable classification of beluga and narwhal clicks and a framework that can be applied to any odontocete species. Results from chapter 5 will help parameterize ice-ocean numerical models to make future projections about Greenland ice sheet dynamics and sea level rise under various climate warming scenarios. Altogether, this thesis highlights the strength of coordinating passive acoustic and oceanographic sampling for long-term observations in the Arctic and lays foundations for promising future research of belugas and narwhals.

Chapter 2. VERTICAL SONAR BEAM WIDTH AND SCANNING BEHAVIOR OF WILD BELUGAS (*DELPHINAPTERUS LEUCAS*) IN WEST GREENLAND

This chapter is published as:

Zahn, M. J., K. L. Laidre, P. Stilz, M. H. Rasmussen, J. C. Koblitz. (2021). Vertical sonar beam width and scanning behavior of wild belugas (*Delphinapterus leucas*) in West Greenland. *PLoS ONE* 16(9): e0257054. https://doi.org/10.1371/journal.pone.0257054

2.1 ABSTRACT

Echolocation signals of wild beluga whales (*Delphinapterus leucas*) were recorded in 2013 using a vertical, linear 16-hydrophone array at two locations in the pack ice of Baffin Bay, West Greenland. Individual whales were localized for 4:42 minutes of 1:04 hours of recordings. Clicks centered on the recording equipment (i.e., on-axis clicks) were isolated to calculate sonar parameters. We report the first sonar beam estimate of *in situ* recordings of wild belugas with an average -3 dB asymmetrical vertical beam width of 5.4°, showing a wider ventral beam. This narrow beam width is consistent with estimates from captive belugas; however, our results indicate that beluga sonar beams may not be symmetrical and may differ in wild and captive contexts. The mean apparent source level for on-axis clicks was 212 dB pp re 1 µPa and whales were shown to vertically scan the array from 120 meters distance. Our findings support the hypothesis that highly directional sonar beams and high source levels are an evolutionary adaptation for Arctic odontocetes to reduce unwanted surface echoes from sea ice (i.e., acoustic clutter) and effectively navigate through leads in the pack ice (e.g., find breathing holes). These results provide the first baseline beluga sonar metrics from free-ranging animals using a

hydrophone array and are important for acoustic programs throughout the Arctic, particularly for acoustic classification between belugas and narwhals (*Monodon monoceros*).

2.2 INTRODUCTION

Arctic cetacean species are faced with a growing threat of underwater noise pollution as vessel traffic is expected to increase with rising temperatures and ice-free conditions (Smith & Stephenson 2013; Reeves et al. 2014; Hauser et al. 2018). The Arctic is warming at a dramatic rate of two to three times the global mean with expected ice-free summers between 2030 to 2055 (Overland & Wang 2013; Runge et al. 2016; Overland et al. 2019). Endemic Arctic cetacean species have evolved to use sound to locate prey and communicate with each other in ice-dominant conditions. Man-made sounds such as engines, propellers, and air guns produce considerable noise underwater, interfering with the ability for cetaceans to sense their surroundings and find food (Mads Peter Heide-Jørgensen et al. 2013; Castellote et al. 2018; Hauser et al. 2018). The Northwest Passage and Northern Sea Route that are increasingly ice-free overlap spatially with key foraging areas and migration routes for these Arctic cetacean species (Reeves et al. 2014; Hauser et al. 2018). As the open-water season lengthens, human expansion in the Arctic through commercial shipping, fishing, and oil and gas exploration poses substantial risks to Arctic marine mammals in the form of vessel strikes, acoustic disturbance, and exposure to spilled or leaked oil and other harmful chemicals (Redfern et al. 2013; Reeves et al. 2014; Hauser et al. 2018). With these anticipated changes, scientists have an opportunity to inform management of human activities in the Arctic to minimize negative impacts on cetaceans through strategies such as restricting ship speed and rerouting vessels to avoid key habitat areas (Ragen et al. 2008; Silber et al. 2012; Redfern et al. 2013; Reeves et al. 2014).

Beluga whales (*Delphinapterus leucas*) are one of only two endemic Arctic odontocetes—along with the narwhal (*Monodon monoceros*)—that occupy the Arctic year-round. Unlike the narwhal, belugas have a circumpolar distribution. They are comprised of discrete subpopulations both in the Arctic and sub-Arctic (Innes et al. 2002; Reeves et al. 2014; Hauser et al. 2017b; Vacquié-Garcia et al. 2018). Given their large distribution and apex trophic position, belugas serve as an important ocean sentinel in a changing Arctic. While the eventual impacts of climate-induced habitat change on belugas remains unknown, monitoring their annual distribution and changes thereof are key to determine their responses and adaptations. Passive acoustic monitoring (PAM) is the most appropriate approach to study cetacean distributions, particularly for regions difficult to access such as the Arctic. It has been used to estimate range, seasonality, and population density of cetaceans (Mellinger et al. 2007; Marques et al. 2013), all of which are important considerations for managers to minimize spatial overlap and potentially harmful impacts of the developing shipping industry in the Arctic.

Affectionately named the "canaries of the sea," belugas are social and vociferous whales with highly variable acoustic profiles that use echolocation as a primary sense to target prey and spatially orient. They produce pulsed calls, combined calls, whistles, and echolocation clicks within broad frequency ranges from roughly 100 Hz to 20 kHz with some echolocation clicks reaching 120 kHz and higher (Au et al. 1985; Sjare & Smith 1986b; Garland et al. 2015). Despite the extensive work done on beluga acoustics, only three publications present information on echolocation of free-ranging animals (Schevill & Lawrence 1949; Sjare & Smith 1986b; Roy et al. 2010) with only one providing results on echolocation click parameters (Roy et al. 2010). Most studies focus on non-echolocation vocalizations (Sjare & Smith 1986b; Sjare & Smith 1986a; Chmelnitsky & Ferguson 2012; Garland et al. 2015), investigate the echolocation

capabilities of animals in captivity (Au et al. 1985; Penner et al. 1986; Au et al. 1987; Turl et al. 1987; Turl & Penner 1989; Turl et al. 1991; Lammers & Castellote 2009; Ames et al. 2020), or use recorded echolocation clicks as a proxy for animal presence during PAM (Castellote et al. 2013; Lammers et al. 2013; Castellote et al. 2015; Castellote et al. 2016; Castellote et al. 2020). Beluga echolocation occurs within a wide spectral range of 30 to 120 kHz where most of the click energy is concentrated within 30-50 kHz and can change depending on the ambient noise in their environment (Au et al. 1985; Sjare & Smith 1986b; Roy et al. 2010). Still, the spectral characteristics of free-ranging beluga echolocation have not been examined at a high resolution.

The acoustic field of view of an echolocating animal, referred to as its sonar beam, is controlled by the properties of functional range (intensity) and angular coverage (directionality) of the emitted clicks (Madsen et al. 2007; Madsen & Wahlberg 2007; Jensen et al. 2015). By producing short, high-frequency signals, the animal ensonifies a three-dimensional area and listens for echoes to interpret its surroundings and locate prey. The source level (SL) is known as the intensity of the signal recorded on the acoustic axis of the beam at a standardized 1 m distance from the source (Urick 1983; Møhl et al. 2000) and can conveniently be quantified as the peak-to-peak (pp) sound pressure level for stereotypical signals like toothed whale echolocation clicks. Echolocation clicks are highly directional such that the signal intensity rapidly decreases with increasing angle away from the acoustic axis (Au 1993; Madsen & Wahlberg 2007). Thus, directionality refers to the angular width in degrees (°) of the biosonar beam and is measured at the angle where the click intensity has decreased by half (-3 dB) relative to the on-axis click intensity.

There is evidence demonstrating toothed whales have active control over their sonar beam by adjusting output levels (Au et al. 1985; Au & Benoit-Bird 2003), beam width (Au et al.

1995; Wisniewska et al. 2012; Jensen et al. 2015), and the direction of the beam known as their acoustic gaze (Wisniewska et al. 2012; Koblitz et al. 2016; Ladegaard & Madsen 2019). Further, the biosonar beam is not only characterized by the signal itself, but the morphology of the sound generator and size of the animal (Jensen et al. 2018). However, reported beam width measurements from toothed whales converge around a narrow 5 – 14°, leading Jensen et al. (Jensen et al. 2018) to conclude that observed inverse frequency scaling where larger animals emit lower frequencies and smaller animals emit higher frequencies is driven by the evolutionary pressure to maintain a narrow acoustic field of view. A narrow beam facilitates precise sensory analysis of the animal's environment by reducing unwanted echoes and clutter (Koblitz et al. 2016; Jensen et al. 2018). Yet, the advantages of a narrow beam come with the cost of a small ensonified volume which can increase the risk of missed detections and reduce the animal's sensory awareness. Scanning behavior, where an animal surveys the surrounding area by actively moving its sonar beam at various angles, may mitigate the costs associated with a narrow beam by increasing search volume and aiding in the localization of live prey (Wisniewska et al. 2012; Beedholm et al. 2021). As the only Arctic odontocetes, the narwhal and beluga have evolved in a unique marine environment characterized by sea ice with similar evolutionary pressures shaping their acoustic profiles. Koblitz et al. (Koblitz et al. 2016) reported that the narwhal has the most directional sonar beam among all odontocetes with a 5° beam width. For the beluga, Au et al. (Au et al. 1987) conducted a captive experiment and determined the beluga beam width to be 6.5°. However, to date no estimate of beam width has been made for free-ranging belugas. Given the potential for variation in biosonar properties based on context, it is unknown whether belugas share an exceptionally narrow beam width like the narwhal in the wild.

Arguably the most important parameters that characterize whale biosonar systems are beam width, SL, and inter-click-interval as they provide information about how echolocation beams have evolved and how whales can be effectively monitored using passive acoustics (Urick 1983; Madsen & Wahlberg 2007). Yet, these metrics are especially difficult to measure in the wild because animal position estimates and methods to isolate on-axis clicks are required (Madsen & Wahlberg 2007). Here, we use data from a 16-channel vertical hydrophone array to determine baseline acoustic parameters including vertical beam width and SL of *in situ* beluga echolocation. Our results represent a unique dataset of beluga echolocation from a wild context, filling critical data gaps for the understudied population in Baffin Bay, West Greenland. We discuss how our findings provide foundational data useful for PAM programs and contribute to the broad understanding of beluga acoustic ecology, including how they have evolved to use sound to navigate, forage, and communicate with one another in an ice-dominant environment.

2.3 Materials and Methods

2.3.1 *Study Region and Acoustic Recordings*

During March 2013, helicopter-based surveys were conducted out of Niaqornat, West Greenland from an Air Greenland AS350. Suitable weather permitted seven flying days between 21 and 31 March and searches for whales occurred 100 to 150 km offshore in leads and cracks of pack ice >98% concentration (Figure 2.1). The primary objective of the study was to locate and record narwhals (Rasmussen et al. 2015; Koblitz et al. 2016), however, on two occasions pods of about 6 and 30 belugas were recorded opportunistically (Figure 2.1). Beluga whales were observed from the air and then sea ice conditions and weather were assessed for landing. As soon as possible after landing, a hydrophone array was deployed at the edge of a lead positioned in a

vertical, linear orientation. Belugas were visible the entire time during the recording period and no narwhals were in the vicinity.

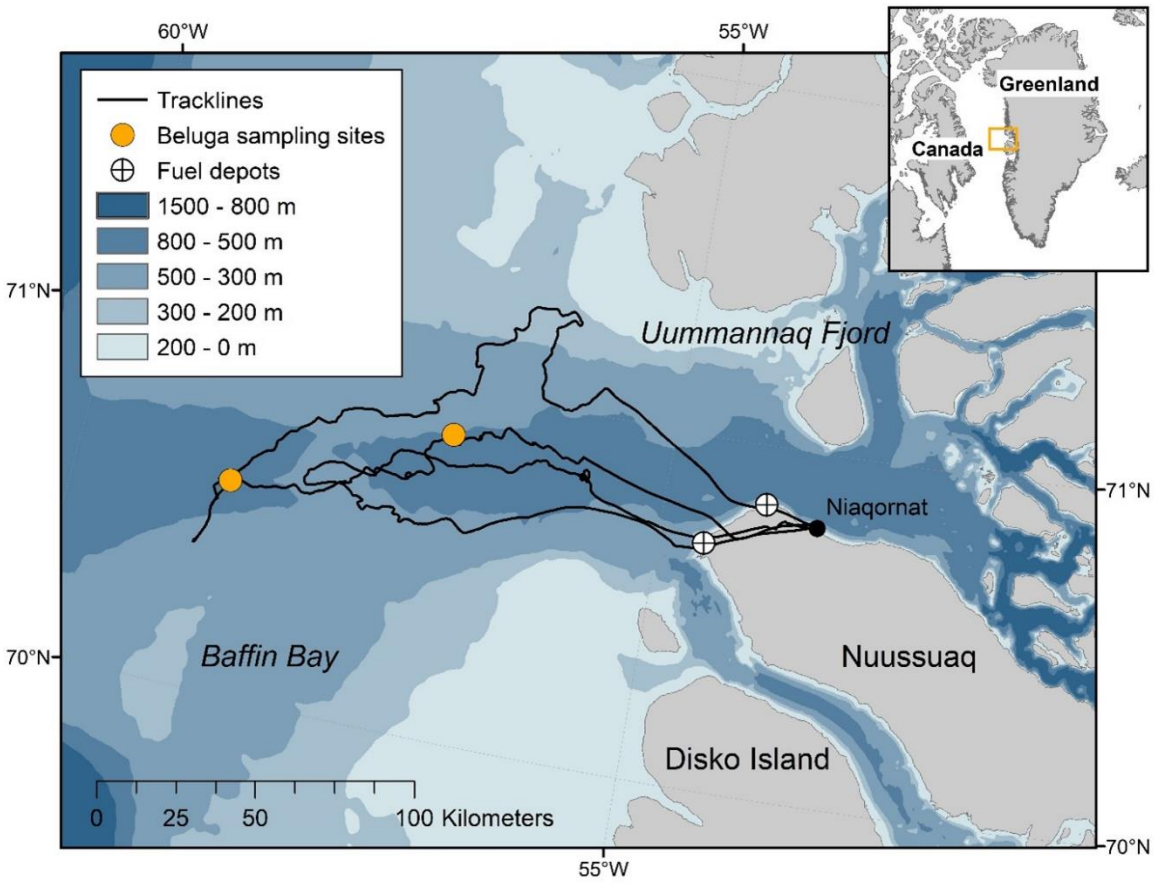

Figure 2.1. Map of study region in Baffin Bay, West Greenland. Includes track lines of search effort, fuel depots, and sampling locations on March 25 and 31st, 2013.

The array was composed of 16 individual Reson TC4013-5 hydrophones with a sensitivity of -215 dB +/- 2dB re 1V/µPa and flat (+/-2 dB) frequency response between 1–150 kHz. Each hydrophone was spaced 1 m apart on a 2 mm diameter line with the topmost hydrophone at 3 m below the surface, the lowest at 18 m, and a 4 kg weight was tied to the bottom to maintain verticality. A custom 16-channel amplifier was used to amplify hydrophone signals by 35 dB; the hydrophones functioned as a low pass filter (150 kHz, 1 pole) and no high

pass filter was applied. The recordings were converted from analog to digital with a sampling rate of 500 kHz and 16-bit resolution using two eight-channel National Instruments PXI-6123 A/D converters (voltage input range +/-10 V). A custom software MALTA (Microphone Array Localization Tool for Animals) by CAE Software & Systems was used to visualize recordings in real-time of multiple receivers. Recordings were partitioned, loss-less, in 5-second long WAV files as a safeguard against file corruption and for ease in data processing and analysis. Clipping level of the recording system was at 206 dB pp re 1 µPa at 100 kHz (Koblitz et al. 2016). All 16 hydrophones were calibrated prior to deployment, and the resulting frequency response of each receiver determined. Localization accuracy was determined in the field using playbacks of recorded clicks at known distances from the array (Koblitz et al. 2016).

2.3.2 *Localization and Assignment of Clicks to Individuals*

Recordings were visually inspected for the presence of beluga echolocation and then used for localization analysis. Clicks were detected using channel 10 just below the center of the array with a signal to noise ratio (SNR) greater than 12 dB. A time window of -5 and +6 ms (5500 samples) was extracted around each click detection for each channel and used for downstream analyses. The position of the individual at the time of click emission was calculated using the time of arrival difference (TOAD). Due to the vertical, linear organization of the hydrophones, the distance and depth of the whale were estimated but the direction in the horizontal plane could not be determined. Cross correlations of all 120 possible receiver pairs were calculated and the channel identified to have best match with other receivers was used as a reference. This reference channel was then used to compute TOADs between the 15 remaining channels and the beluga source position was determined based on a least square error optimization (Wahlberg et al. 2001). For best localization accuracy, up to eight channels were excluded from localization

calculations for instances where localizations based on this receiver substantially differed from the remaining channel combinations. In most cases, position estimates were based on all 16 channels but a minimum of eight channels were used. To confirm localization accuracy of the least square numerical solution for each click, the calculated source position was plotted over 28–120 hyperbolas from the receiver pair TOADs considered (Wahlberg et al. 2001; Madsen & Wahlberg 2007).

Manual assignment of clicks to echolocation sequences were based on the continuity between localized estimates of distance and depth, the sound pressure level recorded on each receiver—termed the received level (RL)—and inter-click interval (ICI). Clicks emitted beyond 150 m from the array were not considered due to high localization error at distances greater than ten times the array aperture (15 m). Inconsistent positions, ICI, and RL values indicated overlapping click trains from more than one individual. Using these patterns, clicks were assigned to individuals as separate tracks. Since multiple, successive echolocation sequences may be produced by the same whale, we used a conservative approach for identifying individuals using criteria of spatial and temporal proximity. Click sequences were assumed to originate from the same individual if 1) the whale's track line was consistently approaching the array, and 2) click sequences were not separated by more than 10 seconds or 10 meters in depth or distance. Localized clicks were isolated, bandpass filtered (1 kHz 4^{th} order high-pass and 240 kHz 4^{th} order low-pass), and sensitivity for each receiver incorporated to calculate source properties.

2.3.3 *Sonar Parameter Calculations and On-Axis Click Criteria*

Peak frequency (kHz), -3 dB and -10 dB bandwidth (kHz), -10 dB click duration (μs), apparent source level (ASL), ventral and dorsal -3 dB beam width (º), and the transmission beam

directivity index (DI; dB) were calculated for all localized clicks. Peak frequency was defined as the frequency of maximum amplitude in the spectrum (Madsen & Wahlberg 2007). The -3 dB and -10 dB bandwidth (kHz) were calculated as measures of the spectral variance around the centroid frequency of the spectrum, and the -10 dB click duration (μs) was determined using -10 dB spectral bounds relative to the peak of the waveform envelope (Madsen & Wahlberg 2007). The ASL was computed over the -10 dB click duration using the sonar equation and assumed geometric spreading and signal attenuation:

$$\mathrm{ASL} = \mathrm{RL} + \mathrm{TL} \tag{2.1}$$

$$\mathrm{TL} = 20\log(r) + \alpha r \tag{2.2}$$

where *RL* is received level, or sound pressure level recorded on each receiver, *TL* is transmission loss, α is the absorption (0.03 dB/m at 100 kHz) (Fisher & Simmons 1977), and *r* is the range, or derived distance of 1 m in front of the animal to the receiver. Following Møhl et al. (Møhl et al. 2000), the peak-peak apparent source level (ASL_{pp}) of each click was determined by the peak-peak measurement of its Hilbert transformation re 1 μPa and back-calculated to 1 m distance in front of the beluga. Given echolocation clicks are very short and broadband, it is possible that the actual peak amplitude of the signal is missed when sampling at 500 kHz. However, the amplitude of the Hilbert envelope effectively approximates the absolute analog amplitude despite sampling limitations. The root mean square apparent source level (ASL_{rms}) measured at 1 m was defined by the RL_{rms} pressure over the -10 dB click duration. The energy flux density source level at 1 m was the integrated energy of the signal over a -10 dB duration and was calculated by ASL_{rms}+10log(-10 dB click duration) (Madsen 2005).

Given the vertical orientation of the linear hydrophone array, only the vertical beam width was calculated. To calculate the vertical -3 dB beam width, vertical beam patterns based on measured RL at each receiver were merged and aligned at the receiver of maximal intensity,

identified as the center of the beam. Using the approximated -3 dB beam width, the sonar beam directivity index (DI) was then calculated following the approximation by Zimmer et al. (Zimmer et al. 2005): $\Theta = 185^{o} \times 10^{(-DI/20)}$, where Θ denotes -3dB beam width.

Echolocation clicks are highly directional where signals received oblique to the animal's acoustic axis are distorted (Au 1993; Madsen & Wahlberg 2007). Precise derivation of acoustic source properties thus depends on the isolation of clicks recorded as close to the whale's acoustic axis as possible, herein referred to as on-axis clicks (Madsen & Wahlberg 2007). On-axis clicks are characterized by the condition where the maximal intensity of the whale's beam is aimed directly towards the hydrophone array in both the vertical (up and down) and horizontal (left and right) dimensions (Figure 2.2). Following previous studies (Villadsgaard et al. 2007; Kyhn et al. 2009; Kyhn et al. 2010; Ladegaard et al. 2015; Koblitz et al. 2016), we selected on-axis clicks based on specific criteria. On-axis clicks in the vertical plane were recorded clicks where the whale's beam was centered between the top and bottom receivers (Figure 2.2A). If the whale's apparent beam maximum was detected at one of the outermost receivers, it was assumed that the beam axis was directed outside of the array, and at best, only part of the ventral or dorsal beam was captured. Therefore, clicks were identified as vertically on-axis when both the ventral and dorsal -3 dB beam width could be calculated within the array. Similarly, on-axis clicks in the horizontal plane were recorded clicks where the whale's beam is directed straight towards the receivers, not pointing to the left or right of the array (Figure 2.2B). Horizontal on-axis clicks were isolated by selecting the highest amplitude click that is part of a scan (i.e. click train where amplitude first increases then decreases) with the assumption that the animal maintains a constant source level and is scanning the array in both vertical and horizontal planes. All other

clicks were defined as being off-axis clicks. While up to eight channels were excluded for localization calculations, recordings from all 16 receivers were used for beam width estimates.

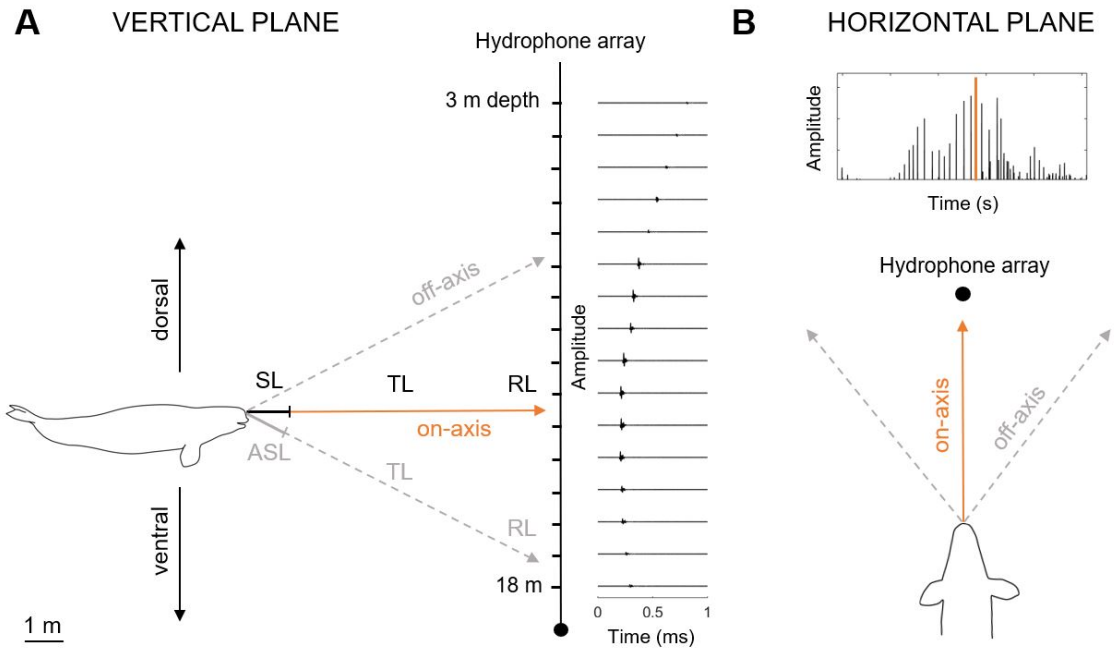

Figure 2.2. Schematic showing experimental setup and spatial criterion for on-axis click selection in the (A) vertical and (B) horizontal planes. The radiation pattern of an echolocation click is shown where the passive sonar equation was applied. The source level (SL) is the sound pressure level calculated from the received level (RL) and transmission loss (TL) on the acoustic axis; apparent source level (ASL) is the sound pressure level calculated for off-axis clicks/clicks of unknown recording aspect. Vertical on-axis clicks were isolated when the whale's acoustic axis (i.e. the maximal intensity of the whale's beam) was vertically centered on the array which was determined by -3dB beam width calculations. For each scanning sequence (i.e., click train with first ascending then descending amplitudes), the highest intensity click was isolated as a horizontal on-axis click where the whale was pointing its beam towards the array (not to the left or right), assuming constant SL.

Given the on-axis characteristics defined above, we selected clicks for final sonar parameter values when they fulfilled the following criteria: (1) localized within 120 m of the array; (2) part of a click train defined by a sequence of more than 10 clicks; (3) the maximal intensity was not recorded at one of the outermost receivers; (4) both the ventral and dorsal -3 dB beam width were calculated; (5) part of a scan; (6) highest amplitude click in the scan; (7) one click selected per track to avoid pseudo-replication of individuals. For comparison, sonar parameters were calculated for two subsets of data: (1) on-axis clicks in only the vertical plane (criteria 1 – 4), and (2) on-axis clicks in both the vertical and horizontal planes (criteria 1 – 7). Using these two datasets, the degree of click parameter distortion when introducing horizontal off-axis clicks was evaluated. Finally, clicks where the maximal intensity was recorded at the top- or bottom-most receiver were removed for a third subset of data that included only "non-edge clicks," where edge refers to the outermost receivers in the array (criteria 1 – 3). Non-edge clicks were used to examine angular variation in beluga spectra and waveforms to see how beluga signals change with increasing angle (2 – 20º) away from the whale's acoustic axis (0º).

Once clicks were isolated for on-axis clicks in the vertical plane and on-axis clicks in both the vertical and horizontal planes, final calculations of mean sonar parameter values were determined. To account for any minor hydrophone sensitivity fluctuations not explained in calibrations, all vertical beam width measurements were interpolated to a resolution of 0.5º by applying a flat smoothing function where 5 smoothing points were used for a moving average over 2º. The 2º width corresponded to the average localized source distances and sufficiently addressed any local peak artifacts from individual hydrophones. The final -3 dB beam width was determined by averaging individual -3 dB beam width values from on-axis clicks. The mean vertical beam pattern for all aligned on-axis clicks was smoothed (width of 2º) and normalized at

their center to zero. While the angle of the emitted click to the acoustic axis was unknown, we expected our ASL estimates to be close to the true source level by following the criteria outlined above for isolating on-axis clicks.

After on-axis clicks were selected, inter-click intervals (ICIs) were calculated for several conditions. ICIs are defined as the time interval in milliseconds between successive clicks. Median ICI values were calculated for: 1) the interval preceding each selected on-axis click (pre-click), 2) the interval proceeding each on-axis click (post-click), 3) a pooled sample of pre- and post-click intervals, and 4) intervals between all clicks from same localized click sequences, or tracks, that on-axis clicks were selected from.

2.4 RESULTS

Beluga recordings were made at two locations on March 25th and 31st 2013 for a total of 42:40 and 20:45 minutes, respectively. Beluga data reported in this study were from one site and individual whales were localized for 4:42 minutes. Each location was validated by comparing the least square localization estimate with hyperbolae for each hydrophone pairwise solution (see Figure 2.3). Out of 1,876 total clicks detected above a threshold of 146 dB pp re 1 µPa, 672 clicks were assigned to individuals in 17 separate tracks (see Figure 2.4). 133 clicks were isolated as on-axis in only the vertical plane and 12 clicks were selected as on-axis in both the vertical and horizontal planes. All on-axis clicks originated from 12 of the 17 total separate tracks and were used for sonar parameter calculations. For angular variation analysis, 351 clicks were isolated as being non-edge clicks where the maximal intensity of the click was not recorded at one of the outermost receivers. We estimate at minimum three to six individual belugas produced these tracks.

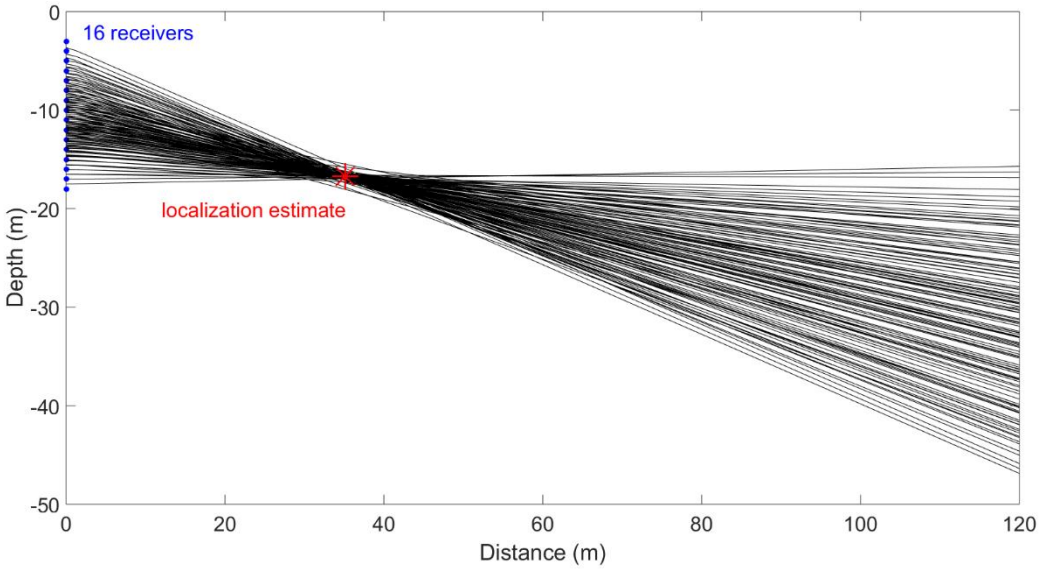

Figure 2.3. Hyperbolae for each of the 120 hydrophone pairs for a single click. Each blue dot on the y-axis indicates a hydrophone in the vertical array spaced 1 m apart. The red star demarcates the localization estimate in depth and distance from the array based on the least squares model. The hyperbolae intersect at the location of the analytical solution.

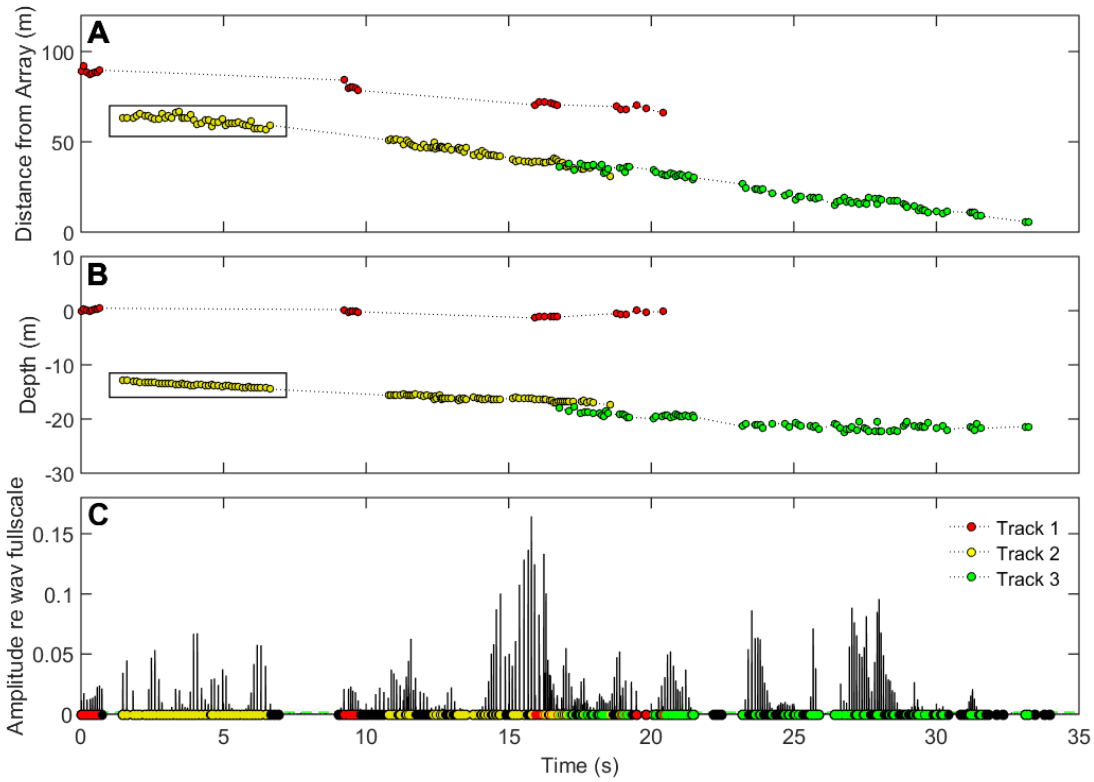

Figure 2.4. Echolocation localization tracklines assigned for at least three individual belugas. (A) localized distance from the array, (B) localized depth, and (C) Hilbert transform of the received amplitude for channel 10 recordings used for click detections. The black box indicates the click sequence used for Figure 2.7. Red circles are track 1, yellow circles track 2, and green circles track 3. Spatial information separates the individual shown in red from the individuals in yellow and green. Patterns in ICI, RL, and localized distance and depth allow for separation of the individuals assigned in yellow and green.

2.4.1 *Beluga Vertical Beam Width and Sonar Parameters*

Mean beluga sonar parameter values were similar between on-axis clicks in the vertical and horizontal planes and clicks on-axis only in the vertical plane (Table 2.1). A total of 133 clicks were on-axis in the vertical plane where both the ventral and dorsal -3 dB beam width could be determined, indicating that the echolocation beam was vertically centered on the array. Among

these, 12 clicks were determined to be on-axis in both the vertical and horizontal planes using the criteria outlined above. Mean beam width values for on-axis clicks in the vertical plane were larger (i.e., wider) and had larger ranges than clicks on-axis in both planes. Sonar parameter values for on-axis clicks in the vertical plane had greater variation than on-axis clicks in the vertical and horizontal planes (Table 2.1; Figure 2.5). All sonar parameter estimates are summarized in Tables 2.1 and 2.2.

Table 2.1. Mean (± s.d.) and range of wild beluga sonar parameters calculated for all on-axis clicks with values from previous work included for comparison. Subscript "pp" is peak-peak, "rms' is root-mean-square, and "EFD" is energy flux density. An asterisk (*) indicates significance ($p < 0.05$). References cited include Au et al. (Au et al. 1985; Au et al. 1987; Roy et al. 2010; Jensen et al. 2018) Roy et al. (Roy et al. 2010)[§], Castellote et al. (Castellote et al. 2013)[††]

	On-axis in horizontal and vertical planes (n = 12)		On-axis in vertical plane (n = 133)		Previous work	
Parameter	mean ± s.d.	range	mean ± s.d.	range	mean ± s.d.	range
-3 dB beam width (º)	5.4 ± 1.2	3.8 – 8.1	6.4 ± 2.4	2.4 – 18.3	6.5[‡]	
-3 dB dorsal beam width (º)	2.0 ± 1.0[*]	0.6 – 3.6	2.9 ± 2.0[*]	0.5 – 14.6		
-3 dB ventral beam width (º)	3.4 ± 1.0[*]	1.3 – 4.8	3.5 ± 1.5[*]	1.1 – 8.5		
DI (dB)	30.9 ± 1.8	27.2 – 33.7	29.8 ± 3.3	20.1 – 37.7	32.1[‡]	
ASL_{pp} (dB re 1 µPa)	212 ± 6	198 – 219	206 ± 8	184 – 219	198 ± 5 – 206 ± 6[†]; 218 ± 5[‡]; 164 ± 10[§]	NA – 222[†]; 206 – 218[‡]; 150 – 184[§]
ASL_{rms} (dB re 1 µPa)	206 ± 6	193 – 214	199 ± 9	175 – 214		
ASL_{EFD} (dB re 1 µPa^2s)	158 ± 6	144 – 164	152 ± 8	131 – 164	145 ± 5 – 149 ± 5[†]	NA – 165[†]
Peak frequency (kHz)	96.9 ± 7.4	88.0 – 110.0	90.1 ± 20.7	52.0 – 159.0	~55, ~105[†]; 107, 113[‡] 40 ± 6[§]; 73[††]	40 – 60, 100 – 120[†]; 10 – 54[§]; 32 – 90, 40 – 120[††]
-3 dB bandwidth (kHz)	39.8 ± 19.6	19.0 – 62.0	45.4 ± 18.1	15.0 – 115.0	~23, ~37[†]; 13 ± 4[§]	15 – 30, 30 – 65[†]; 6 – 38[§]
-10 dB bandwidth (kHz)	107.3 ± 21.1	68.0 – 137.0	97.2 ± 23.1	42.0 – 152.0	29 ± 10[§]	12 – 53[§]
$Duration_{-10\ dB}$ (µs)	14.5 ± 6.0	8.0 – 26.0	19.4 ± 8.6	8.0 – 60.0	163 ± 152[§]	35 – 1470[§]
Localized depth (m)	19.7 ± 16.0	0.2 – 44.0	18.2 ± 8.1	0.2 – 44.3		
Localized distance (m)	56.7 ± 32.3	13.4 – 99.9	37.9 ± 24.3	5.8 – 99.9		
Localized range (m)	61.1 ± 28.8	15.6 – 100.4	39.9 ± 23.3	7.3 – 100.4		

Table 2.2. Inter-click interval (ICI) values for on-axis clicks. Median ICI values were calculated for all clicks from same the click sequence, or track, as the selected on-axis clicks (all tracks), before the on-axis click (pre-click), after the on-axis click (post-click), and pooled pre- and post-intervals (pre + post). 25% and 75% quantiles (Q_1 and Q_3, respectively) and sample sizes of clicks considered (*n*) are included. All reported values are in milliseconds.

	On-axis in horizontal and vertical planes				On-axis in vertical plane			
Interval	median	Q_1	Q_3	*n*	median	Q_1	Q_3	*n*
All tracks	97.4	76.8	141.1	552	97.4	76.8	141.1	552
Pre-click	89.7	78.7	122.4	12	96.0	77.2	139.2	133
Post-click	108.7	84.2	147.0	12	99.0	77.5	154.6	133
Pre + post	95.0	78.7	133.4	24	105.4	78.2	154.2	166

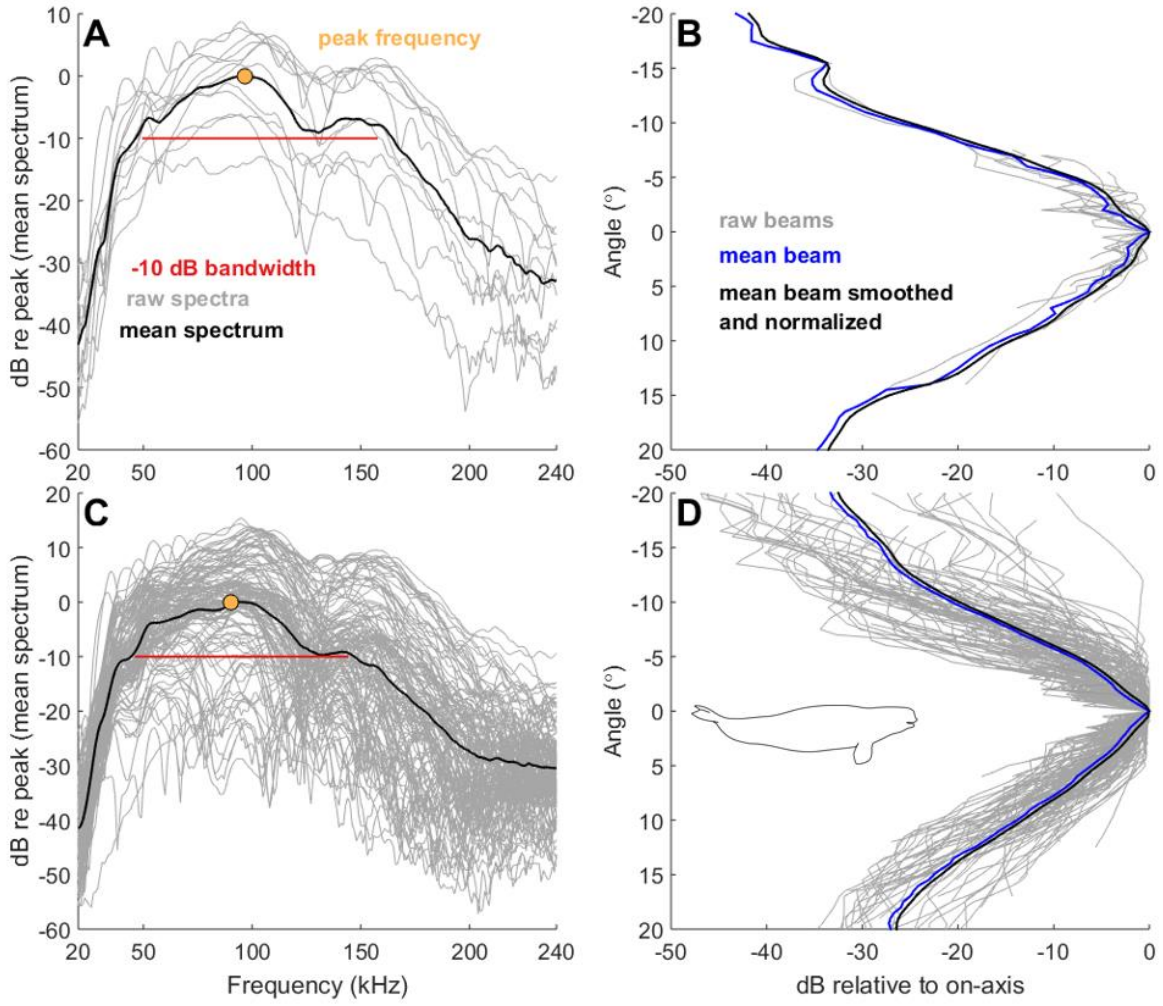

Figure 2.5. Beluga echolocation click spectra and beam pattern for on-axis clicks. (A) Beluga spectra and (B) vertical beam pattern for 12 on-axis clicks in both the vertical and horizontal planes. (C) Beluga spectra and (D) vertical beam pattern for 133 on-axis clicks in only the vertical plane. Spectra in (A) and (C) show raw spectra in gray, mean spectrum in black, peak frequency with a yellow point, and -10 dB bandwidth in red. Vertical beam patterns in (B) and (D) show raw beam patterns in gray, mean beam pattern in black, and the smoothed and normalized beam pattern in blue; negative angle values correspond to the dorsal vertical beam and positive values refer to the ventral beam.

A two-lobed spectral pattern was observed for mean beluga spectra (Figure 2.5A,C). The peak frequency for on-axis clicks in both spatial planes was 96.9 ± 7.4 (Table 2.1; Figure 2.5A,C). A spectral notch occurred at 130 kHz with a secondary peak at 150 kHz. This pattern was more pronounced in the 12 clicks that were on-axis in both planes (Figure 2.5A) but still evident for clicks that were on-axis in only the vertical plane (Figure 2.5C). The beluga echolocation mean waveform, consistent with all Delphinidae click shapes, showed an initial pressure increase followed by a strong pressure decrease and second pressure increase (Figure 2.6A). For all 351 non-edge clicks, signals measured by individual hydrophones away from the acoustic axis (i.e., maximal RL) were averaged in 2º wide angle bins relative to the central axis (0º) and plotted to show angular variation in beluga spectra and waveforms (Figure 2.6). The signal was increasingly distorted and diminished with increasing off-axis angle (Figure 2.6). The -3 dB beam width was 5.4 ± 1.2º, ranging between 3.8–8.1º and the ASL_{pp} was 212 ± 6 dB re 1 µPa, ranging between 198–219 dB (Table 2.1; Figure 2.5B,D). The ventral beam width was significantly wider than the dorsal beam width for on-axis clicks in the vertical plane (Paired *t*-test: $p = 0.015$) and on-axis clicks in both planes (Paired *t*-test: $p = 0.010$). ICIs were approximately 100 ms for selected on-axis clicks and associated click sequences (Table 2.2).

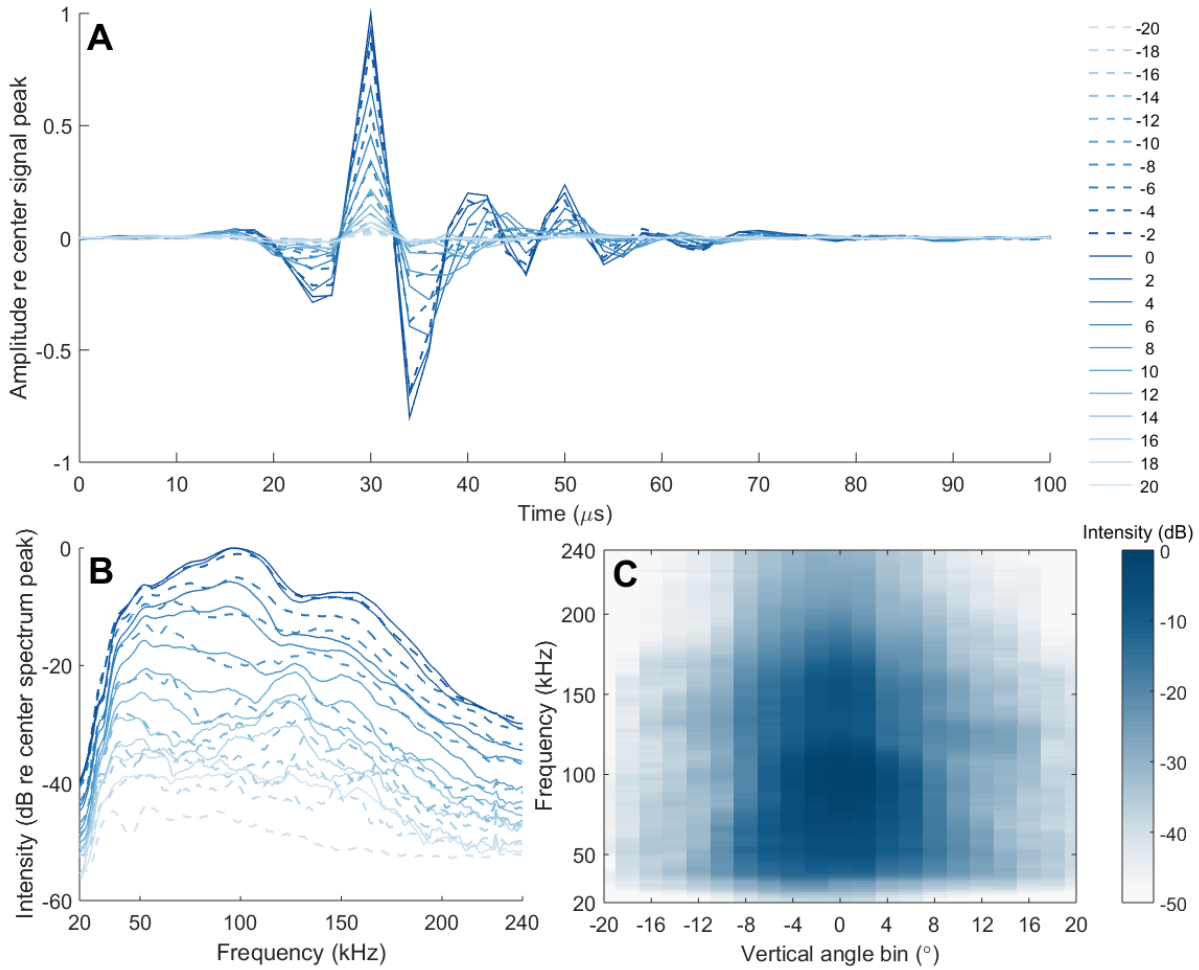

Figure 2.6. Mean angular variation for 351 non-edge clicks for beluga echolocation click (A) waveforms and (B, C) spectra. For all non-edge clicks selected where the RL of maximal intensity was not recorded at one of the outermost receivers, signals were received at various angles along the vertical hydrophone array where the center of the beam was at 0º. Angle bins between -20 to 20º (negative is dorsal; positive is ventral) show signal differences measured farther from the acoustic axis. The heatmap (C) in dB re center (0º) spectrum peak shows angle bin (º) and frequency ranges for the highest (dark blue) and lowest (white) spectral energy.

2.4.2 *Scanning Behavior*

Shifts in the acoustic gaze of belugas to probe their environment and increase their search volume—a behavior referred to as scanning—was observed in the vertical plane. Vertical

scanning was identified by sequential changes in the maximal RL on individual receivers throughout a click train revealing the upward and downward movement of their sonar beam over the array (Figure 2.7). All recordings used for analysis where individuals were localized between 10 and 120 meters distance from the array demonstrated this behavior. The maximum scanning angle for consecutive clicks for all analyzed click sequences containing on-axis clicks was 9º.

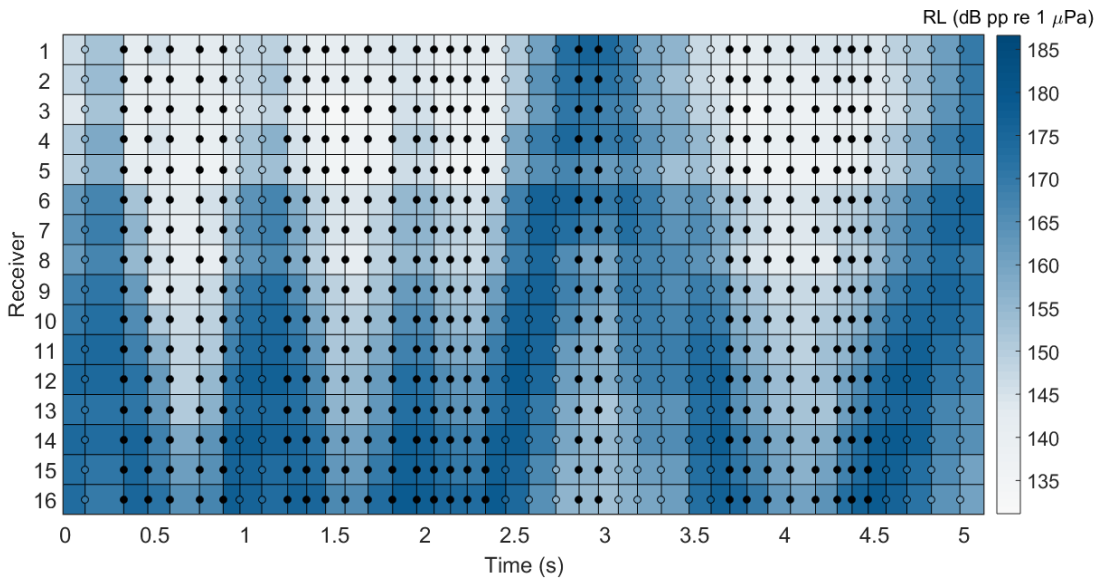

Figure 2.7. Vertical scanning of beluga sonar beam. Distribution of the received level (RL; represented via color spectrum) for each hydrophone for 41 clicks in 5 seconds, demonstrating vertical scanning of the array. Filled circles signify clicks where the hydrophone with the maximum RL was received by one of the outermost receivers and therefore was directed towards the edge of the array.

2.5 DISCUSSION

Despite significant ranges in body size, SL, and sonar frequency among odontocetes, toothed whale beam width remains strikingly consistent between 5–14º, suggesting there is selective pressure for long-range detection and spatial acoustic filtering to reduce unwanted echoes

(Jensen et al. 2018). Beam width and SL are defining characteristics of echolocation that provide insight into the evolution of biosonar systems and key information to biologists who employ passive acoustics for odontocete research and management (Madsen & Wahlberg 2007). Here, we present the first free-ranging beluga vertical beam width estimate of 5.4º and mean ASL of 212 dB pp re 1 µPa with concomitant vertical scanning behavior (i.e. adjustments in acoustic gaze) across all localized sequences. Beluga clicks with high directionality and intensity allow for spatial filtering and a longer detection range while scanning increases acoustic spatial coverage. In the acoustically complex environment of the Arctic, these properties are likely eco-evolutionary adaptations for belugas to reduce clutter and effectively navigate, particularly in the winter as they search for openings in the pack ice.

2.5.1 *Narrow Sonar Beam Width and High Source Level*

The majority of existing knowledge of beluga echolocation comes from experimental work where captive whales were held stationary with a hoop or bite plate to maintain a constant distance and angle to the hydrophone (Au et al. 1985; Penner et al. 1986; Au et al. 1987; Turl et al. 1987; Turl & Penner 1989; Turl et al. 1991; Lammers & Castellote 2009; Ames et al. 2020). No study has been conducted to measure beluga sonar beam width since the captive experiment completed by Au et al. (Au et al. 1987) where they determined the mean 3-dB vertical and horizontal sonar beam width to be a symmetrical 6.5º. Our results showing a vertical beam width of 5.4º (DI = 30.9 dB) confirm the narrow acoustic field of view of belugas, being 1.1º narrower than the estimate made by Au et al. (Au et al. 1987). Au et al. (Au et al. 1985) demonstrated how beluga biosonar changes in intensity and frequency for two environments with different ambient noise levels, an indication for the flexibility in echolocation behavior. The minor difference in vertical beam width determined in this study compared to Au et al. (Au et al. 1987) may indicate

individual or population-specific variation, environment-driven adaptation, or methodological differences.

Being that toothed whale biosonar beam width ranges between 5–14º, the beluga beam width is one of the most narrow among odontocetes, second only to the narwhal (Koblitz et al. 2016). The sperm whale (*Physeter macrocephalus*), Risso's dolphin (*Grampus griseus*), and bottlenose dolphin (*Tursiops spp.*) exhibit symmetrical half-power beam widths between 8 – 9º (Møhl et al. 2003; Wahlberg et al. 2011; Smith et al. 2016). Wider beam widths have been observed for the harbor porpoise (*Phocoena phocoena*) with a beam width of 11º and 13º in the horizontal and vertical planes, respectively (Koblitz et al. 2012) up to the Ganges river dolphins (*Platanista gangetica*) with a beam width of 14.5º (Jensen et al. 2013). Ganges river dolphins inhabit shallow, riverine waters that may explain their wider sonar beam when compared to pelagic species (Jensen et al. 2013). In contrast to species with restricted distributions like the narwhal (Heide-Jørgensen et al. 2003a), belugas occupy a diverse range of habitats given their circumpolar distribution in the Arctic and sub-Arctic (Innes et al. 2002; Reeves et al. 2014; Hauser et al. 2017b; Vacquié-Garcia et al. 2018) which may result in greater sonar variability across subpopulations. Here we show belugas occupying the deep, ice-covered waters in Baffin Bay present clicks with high directionality (DI > 30 dB), high SLs, and ICIs of ~100 ms which all facilitate long-range detection and spatial filtering. Environments like riverine or coastal systems with vegetation and shallow depths can create conditions with high acoustic clutter and reverberation levels when compared to open ocean conditions (Jensen et al. 2013; Ladegaard et al. 2015). Narrow, short-range biosonar systems adapt best to riverine environments to reduce reverberation and clutter. It may be that beluga subpopulations that predominantly inhabit rivers or coastal habitats present clicks with characteristics like the Ganges or Amazon river dolphins

with lower SLs (<200 dB re 1 μPa_{pp}), a slightly wider beam (>10º), and shorter ICIs (<50 ms) to adapt to their environment (Jensen et al. 2013). Future work to establish estimates of sonar parameters from several wild beluga stocks (e.g., Cook Inlet, Alaska (Lammers et al. 2013; Castellote et al. 2016; Blevins-Manhard et al. 2017) or the Canadian Arctic (Roy et al. 2010; Vergara & Mikus 2019)) will demonstrate whether characteristics of beluga biosonar including a narrow beam and high SLs remain consistent across diverging habitats.

As the only members of the Monodontid family, belugas and narwhals have broadband, high-frequency clicks and a narrow beam width, sonar properties that are broadly shared with other echolocating delphinids (McGowen et al. 2009; Jensen et al. 2018). Inverse frequency scaling where larger animals vocalize at higher source levels and lower sound frequencies compared to smaller animals has been an accepted hypothesis in acoustic communication for both terrestrial and marine environments (Fletcher 1992; Gillooly & Ophir 2010). Jensen et al. (Jensen et al. 2018) tested this hypothesis by claiming that this law operates differently for echolocating toothed whales. They examined how source level, directionality, and frequency vary with body size and reported that sonar output increased with body size at twice the rate than expected. As a result, having a narrow acoustic field of view, consistent for all toothed whales, is likely to be the primary evolutionary pressure for odontocete biosonar (Koblitz et al. 2012; Jensen et al. 2018). However, among toothed whales with average -3 dB beam widths between 5 to 14º, belugas and narwhals are outliers with both high source levels and narrow beam widths relative to their body size (Figures 2A and 3D in Jensen et al. (Jensen et al. 2018)). This suggests that although manydelphinids share common acoustic properties, Arctic odontocetes may have specific biosonar adaptations to increase their detection range, decrease surface reflections in their ice-dominated environment, and effectively navigate through leads in the pack ice. In dense

pack ice conditions, belugas and narwhals rely on openings in the ice to breathe at the surface, so there is a strong selective pressure to locate open water and ensure survival. Our results corroborate the notion that Arctic odontocetes are outliers among all toothed whales by having the narrowest acoustic field of view.

Echolocation is characterized by highly-directional acoustic emissions where signals become increasingly distorted off-axis to the center of the beam (Au 1993; Madsen & Wahlberg 2007; Au et al. 2012; Macaulay et al. 2020). As a result, accurate sonar parameter estimates are contingent on the ability to isolate on-axis clicks. While the criteria used in this study to isolate on-axis clicks (Figure 2.2) follows similar studies (Villadsgaard et al. 2007; Kyhn et al. 2009; Kyhn et al. 2010; Ladegaard et al. 2015; Koblitz et al. 2016), the true acoustic axis from which the echolocation signals originated remains unknown. However, the beam width measurement reported here closely compares to that of Au et al. (Au et al. 1987) where the acoustic axis was known. Furthermore, examination of signals recorded on receivers away from the maximal RL—assumed to be the center of the beam—show signal distortions (Figure 2.6). Finally, when comparing spectra between the 133 vertical on-axis clicks to the 12 horizontal and vertical on-axis clicks, it is apparent that high frequency content is lost as horizontal off-axis clicks are introduced in the sample (Figure 2.5 A,C). The 12 on-axis clicks isolated in this study retain high-frequency content and reveal a narrow beam width consistent with captive experiment estimates, indicating they are likely close to the whale's acoustic axis.

Au et al. (Au et al. 1987) reported highly variable and multilobed vertical beam patterns for low-amplitude clicks and for sequences where click intervals were less than 5 milliseconds. The authors further describe that the major axis of the composite vertical beam pattern was elevated 5º above the horizon, defined by the plane of the animal's teeth (Au et al. 1987). Due to

the *in situ* recording environment of the data analyzed here, the orientation of the animal's cranium and body was unknown. Moreover, identifying lobes in the acoustic beam pattern with any certainty was impossible due to the spatial arrangement of the receivers; the recording aperture was too wide to yield a sufficient resolution to capture lobes. Yet, our results show an asymmetrical vertical beam width with a wider ventral beam, providing further evidence for beluga biosonar adaptability and evolutionary adaptations in the Arctic environment. A sonar beam with a wider ventral beam more effectively filters surface clutter from the pack ice when compared to a symmetrical beam. It is possible that Au et al. (Au et al. 1987) observed a symmetrical sonar beam given the captive environment devoid of dense sea ice, whereas the free-ranging beluga beam width estimates reported here show context-specific biosonar adaptability in response to the ice-dominated setting.

Using the sonar equation and assuming a noise limited environment with spherical spreading, we computed a theoretical detection range for two scenarios: the maximum range for a beluga to ensonify a target prey and the maximum distance for a beluga click to reach an acoustic receiver. For both calculations, we used a SL of 212 dB re 1 µPa, which we computed from the 12 on-axis clicks used this study (Table 2.1). Transmission loss was calculated as $20\log(r) + \alpha r$ where r is the distance in meters from the source and α (absorption) is 0.03 dB/m (estimated at 100 kHz) (Fisher & Simmons 1977). The theoretical detection range for a beluga to ensonify a target prey, Arctic cod (*Boreogadus saida*), is approximately 300 meters using a prey target strength of -45 dB (Crawford & Jorgenson 1996) and beluga hearing threshold of 50 dB re 1 µPa (Castellote et al. 2014). However, beluga hearing thresholds have been shown to vary widely (>30 dB) (Castellote et al. 2014), and as a result, beluga prey detection ranges will also vary considerably. The estimated detection range for a beluga click reaching a hydrophone with

a broadband system noise level of 130 dB re 1 µPa, reflecting receivers used in this study, is approximately 800 meters. Indeed, there are many factors that drive the detection range of a beluga click, but these estimates along with the knowledge that belugas have a narrow beam provide important information when determining the density and spatial range to deploy future PAM receivers.

2.5.2 *Patterns in Frequency Spectra*

Beluga spectra from on-axis clicks showed a two-lobed pattern with characteristic peaks at 90 and 150 kHz and a slight notch at approximately 130 kHz that has not been previously reported in captive or wild beluga acoustic studies (Figures 2.5A,C and 2.6). However, the high peak frequencies for clicks on-axis in both the horizontal and vertical planes (97 kHz) and on-axis in only the vertical plane (90 kHz) are consistent with earlier work (Au et al. 1985; Castellote et al. 2013). It is possible that the animals used in experimental studies did not produce such high frequency, broadband clicks in the captive environment, or alternatively the sampling rate of the recording designs were too low to sufficiently capture the second peak. Nonetheless, we expect that the second peak at 150 kHz reported here was underestimated, and in reality, this peak is likely more pronounced given that higher frequencies attenuate faster than lower frequencies for broadband signals.

Apart from the bimodal frequency pattern, the broadband spectra reported here aligns with characteristic spectral patterns for *Delphinidae* species. Extant toothed whale echolocation has been classified into four main click types: 1) multi-pulsed sperm whale (*Physeteriidae*) clicks; 2) frequency modulated beaked whale (*Ziphiidae*) clicks; 3) broadband delphinid clicks; and 4) narrow-band, high frequency clicks (Jensen et al. 2018). As part of the delphinid click type, belugas produce broadband signals similar to those generated by riverine and marine

delphinids (e.g. *Tursiops* and *Orcaella* genera) (Au 1993; Jensen et al. 2013; Jensen et al. 2018). Beluga spectra reported here, however, demonstrate a broadband signal with the presence of a unique spectral lobe pattern that distinguishes it from other delphinids.

The broadband, lobed frequency pattern of beluga clicks shown in this study may provide necessary information to differentiate beluga echolocation from other species with similar acoustic profiles and spatial distributions, such as the killer whale (*Orcinus orca*) or narwhal. Increasing anecdotal and empirical evidence have showed range expansions of killer whales in the eastern Canadian Arctic and Baffin Bay, West Greenland, likely the result of declines in sea ice and increase in suitable habitat and foraging grounds (Lefort et al. 2020). Range shifts are likely as the Arctic changes, and knowledge of Arctic odontocete spectra are critical when choosing or designing recording equipment to measure echolocation parameters correctly and maximize characteristic echolocation features for species identification. When comparing killer whale and beluga spectra, broadband bimodal frequency spectra have been documented in killer whale clicks (Au et al. 2004; Simon et al. 2007) resembling the beluga lobed spectra we observed. Killer whale low and high frequency peaks occur at 24 and 108 kHz, respectively, (Simon et al. 2007) in contrast to the higher frequency peaks in beluga spectra reported here (97 and 147 kHz; Figure 2.5A). When comparing narwhal and beluga spectra, the narwhal presents a unimodal spectrum with no clear spectral notches (Koblitz et al. 2016). Additionally, beluga click peak frequency (97 kHz) is higher than that of the narwhal (~70 kHz) (Rasmussen et al. 2015; Koblitz et al. 2016) which may prove useful for species classification. Following work done by Soldevilla et al. (Soldevilla et al. 2008) where Risso's and Pacific white-sided dolphins (*Lagenorhynchus obliquidens*) were classified using spectral properties including unique peaks and notches, our results show promise for species identification using spectral information from

beluga echolocation and other odontocetes found in Arctic waters. However, particular attention to sampling rate and on-axis click criteria must be carefully considered, since the presence of defined spectral peaks diminishes with increasing off-axis angle (Figure 2.6) and recordings using low sampling rates may lack high frequency content.

2.5.3 *Scanning Behavior*

Biosonar scanning behavior, also referred to as shifts in acoustic gaze, has been well documented for bats in both field and laboratory settings (Ghose & Moss 2006; Surlykke et al. 2009; Seibert et al. 2013; Falk et al. 2014), but it is much less described for echolocating marine mammals. Scanning is typically identified using a hydrophone array where successive changes in the maximal RL on individual receivers throughout a click train are measured, revealing movement of the animal's sonar beam over time. Scanning of echolocating marine mammals was first reported by Schevill and Lawrence (Schevill & Lawrence 1956) and later by Kellogg (Kellogg 1959) and Norris et al. (Norris et al. 1961), though all accounts were largely qualitative descriptions for captive experiments with bottlenose dolphins (*Tursiops truncatus*). Recent studies with captive harbor porpoises (*Phocoena phocoena*) describe scanning behavior and speculate that it increases the animal's sensory volume, exploiting sonar beam directionality (Wisniewska et al. 2012; Ladegaard & Madsen 2019). Changes in an animal's acoustic gaze may also function to assist in moving target localization. Kloepper et al. (Kloepper et al. 2018) showed one captive bottlenose dolphin directed the center of its beam slightly off-axis to its target and concluded that the animal's off-axis emission strategy maximized angular position estimates of the target. In contrast, Beedholm et al. (Beedholm et al. 2021) gave two trained delphinids (*Tursiops truncatus* and *Pseudorca crassidens*) the same detection task and reported that while they rarely positioned their beam's axis directly on the target, in each trial the target

was ensonified within the animal's half-power beam width, likely to increase echo-to-noise ratios. A growing body of evidence has demonstrated the various ways animals adjust their acoustic gaze, including changes in beam width when approaching a target (Wisniewska et al. 2012; Jensen et al. 2015). Further research is needed to investigate potential differences in scanning behavior among delphinid species, examining whether directionality and scanning angle are inversely correlated or behavioral variations exist between coastal and marine environments. Nonetheless, vertical scanning was reported for narwhals by Koblitz et al. (Koblitz et al. 2016), and we similarly show this behavior for belugas (Figure 2.7). To our knowledge, our results mark the first account to quantify scanning behavior of belugas and support the assertion that scanning is a compensatory trait that widens the whale's acoustic gaze in response to a highly directional sonar beam. The degree to which wild beluga beam width changes during target selection remains to be studied.

2.5.4 *Error Estimation and Limitations*

Localization error was determined using methods and results outlined in Koblitz et al. (Koblitz et al. 2016) and is consistent with other studies using linear arrays for localization (Kyhn et al. 2009; Kyhn et al. 2010; Jensen et al. 2013; de Freitas et al. 2015). Beluga recordings analyzed here were from the same field season and used the same instruments as Koblitz et al. (Koblitz et al. 2016) so error estimation equally applies. Accordingly, the source distance is expected to be underestimated by approximately 20%, resulting in an underestimation of the ASL by 1 to 4 dB. The beam width is likely overestimated as it is inversely proportional to the localized distance; further, our methods to account for any fluctuations in individual hydrophone sensitivities by interpolating and smoothing beam patterns resulted in a conservative vertical beam width estimate. When considering the distances that whales were recorded (up to 100 meters) for this

study, our vertical beam width measurement is estimated to be 1 to 2° wider than the true beluga vertical beam width. Thus, the true beluga vertical beam width is likely narrower and bears a higher directivity than what is reported here (5.4°).

Although the sample sizes used here for on-axis clicks are comparable to other biosonar studies (Villadsgaard et al. 2007; Kyhn et al. 2009; Kyhn et al. 2010; Koblitz et al. 2016), there are limitations to the conclusions presented in this study to parameterize wild beluga echolocation given the small samples and number of individuals considered. Based on the localization analyses and individual tracks (i.e., click sequences) produced, we estimated 3 to 12 individuals produced the on-axis clicks that were used for sonar parameter calculations (12 on-axis clicks in both the horizontal and vertical planes; 133 clicks on-axis in the vertical plane). These data likely originated from the same group of individuals, which indicates that any potential variation in echolocation characteristics across different groups or stocks would not be represented in the parameter estimates presented here. Yet, the parameters reported here provide a strong foundation on which future work will continue to refine. In particular, continued research is needed to quantify how beluga echolocation varies across subpopulations that inhabit a variety of environments and how it broadly compares to odontocete echolocation in and outside of the Arctic.

2.5.5 *Implications for PAM in a Changing Arctic*

An increase in human activities and ambient underwater sound levels pose significant risks to Arctic cetaceans as warming temperatures lead to sea ice loss and a longer open-water season (Reeves et al. 2014; Hauser et al. 2018). Anthropogenic noise (e.g. commercial ships, pile drivers, helicopters, outboard motors) has been shown to mask beluga communication and hearing for the Cook Inlet population (Castellote et al. 2018) and could similarly threaten

populations in West Greenland. Human expansion northward into the Arctic is expected for oil and gas exploration, fishing, and recreation as regions like the Northwest Passage become ice-free and navigable. In order to develop management plans and regulations that proactively minimize threats to Arctic cetaceans, monitoring programs that provide baseline data for cetacean ecology and their habitats are needed.

PAM that uses multiple hydrophones over large spatiotemporal scales is the most viable tool to study Arctic cetacean populations in remote regions and identify ecologically important areas for management, including migration routes and mating grounds (Castellote et al. 2013; Sousa-Lima et al. 2013; Frouin-Mouy et al. 2017; Ahonen et al. 2019; Castellote et al. 2020; Zhong et al. 2020). Our results provide fundamental sonar parameters for belugas that can be implemented in Arctic and sub-Arctic PAM programs, particularly for the comparison and differentiation between belugas and narwhals. We also provide an approximation of 800 m as the range at which a beluga click can be detected using a PAM receiver similar to the instruments used in this study. Understanding the spatial resolution at which whales can be detected is important when designing the extent and frequency of PAM receivers to be deployed. Classification using echolocation is a promising tool, given its primary role in beluga and narwhal foraging ecology, and is increasingly being incorporated into classification regimes (Soldevilla et al. 2008; Baumann-Pickering et al. 2015; Rankin et al. 2017). To fully implement PAM using echolocation identifiers, appropriate acoustic receivers with a high sampling rate must be used. Arctic odontocetes use echolocation frequently as it is the primary way they sense their environment and locate prey, and as a result, echolocation data are especially useful for classification during times where vocalizations (e.g., whistles) are absent. This *in situ* study of

beluga biosonar provides foundational information for PAM programs and a baseline for future comparative studies with species that have overlapping ranges and similar acoustic profiles.

2.6 ACKNOWLEDGEMENTS

We thank Niaqornat's community members for their support, Greenland Institute of Natural Resources for local housing, Mikkel Villum Jensen for his assistance in the field, Air Greenland pilot Geir Akse for ensuring safe travel to and from field locations, Ben Cohen for graphics support, and the University of Tübingen, the German Oceanographic Museum Stralsund, and the Greenland Institute of Natural Resources for providing equipment. This work was funded by the US Office of Naval Research (https://www.onr.navy.mil/) on a grant to K.L.L. (N00014-11-1-0201) and research permits were provided by the Government of Greenland. M.J.Z. was supported by the School of Aquatic and Fishery Sciences, University of Washington (https://fish.uw.edu/) and the Vetlesen Foundation (https://www.vetlesenfoundation.org/). The funders had no role in study design, data collection and analysis, decision to publish, or preparation of the manuscript.

Chapter 3. ACOUSTIC DIFFERENTIATION AND CLASSIFICATION OF WILD BELUGAS AND NARWHALS USING ECHOLOCATION CLICKS

This chapter is published as:

Zahn, M. J., S. Rankin, J. L. K. McCullough, J. C. Koblitz, F. Archer, M. H. Rasmussen, K. L. Laidre. (2021). Acoustic differentiation and classification of wild belugas and narwhals using echolocation clicks. *Scientific Reports* 11:22141. https://doi.org/10.1038/s41598-021-01441-w

3.1 ABSTRACT

Belugas (*Delphinapterus leucas*) and narwhals (*Monodon monoceros*) are highly social Arctic toothed whales with large vocal repertoires and similar acoustic profiles. Passive Acoustic Monitoring (PAM) that uses multiple hydrophones over large spatiotemporal scales has been a primary method to study their populations, particularly in response to rapid climate change and increasing underwater noise. This study marks the first acoustic comparison between wild belugas and narwhals from the same location and reveals that they can be acoustically differentiated and classified solely by echolocation clicks. Acoustic recordings were made in the pack ice of Baffin Bay, West Greenland, during 2013. Multivariate analyses and Random Forests classification models were applied to eighty-one single-species acoustic events comprised of numerous echolocation clicks. Results demonstrate a significant difference between species' acoustic parameters where beluga echolocation was distinguished by higher frequency content, evidenced by higher peak frequencies, center frequencies, and frequency minimums and maximums. Spectral peaks, troughs, and center frequencies for beluga clicks were generally > 60 kHz and narwhal clicks < 60 kHz with overlap between 40–60 kHz. Classification model

predictive performance was strong with an overall correct classification rate of 97.5% for the best model. The most important predictors for species assignment were defined by peaks and notches in frequency spectra. Our results provide strong support for the use of echolocation in PAM efforts to differentiate belugas and narwhals acoustically.

3.2 INTRODUCTION

Only three species of cetaceans occupy the Arctic year-round: the beluga (*Delphinapterus leucas*), narwhal (*Monodon monoceros*), and bowhead whale (*Balaena mysticetus*). As toothed whales (odontocetes), the beluga and narwhal are closely related and are the only two members of the Monodontidae family. They use echolocation to identify objects and locate prey, unlike the bowhead whale, a baleen whale, that has not evolved this sense (Au 1993; Madsen & Wahlberg 2007). Belugas are circumpolar in their distribution with approximately 22 subpopulations, or stocks, some of which are highly migratory and others resident in both Arctic and sub-Arctic waters (Smith & Martin 1994; Lydersen et al. 2001; Innes et al. 2002; Reeves et al. 2014; Hauser et al. 2017b; Vacquié-Garcia et al. 2018; Hobbs et al. 2019). Most populations migrate from wintering regions among the pack ice and return to the same estuarine summering areas to feed, molt, and give birth (Frost & Lowry 1990; Smith & Martin 1994; Lewis et al. 2009). In contrast, narwhals occur in approximately 12 stocks and have a more restricted distribution occupying waters of the Canadian Arctic, West and East Greenland, and western Russia within the Atlantic Arctic (Heide-Jørgensen et al. 2003a; Richard et al. 2010; Ahonen et al. 2019). Narwhals in the Canadian Arctic and West Greenland undergo extensive annual migrations with high site fidelity from their summer ranges in fjords of Greenland and Baffin Island to their wintering grounds in Baffin Bay and northern Davis Strait (Dietz et al. 2001; Heide-Jørgensen et al. 2003a; Reeves et al. 2014). Across their respective distributions, belugas

and most of the world's narwhals overlap for much of the year in the waters of the Canadian Arctic and Baffin Bay, West Greenland, during their annual migrations (Figure 3.1a).

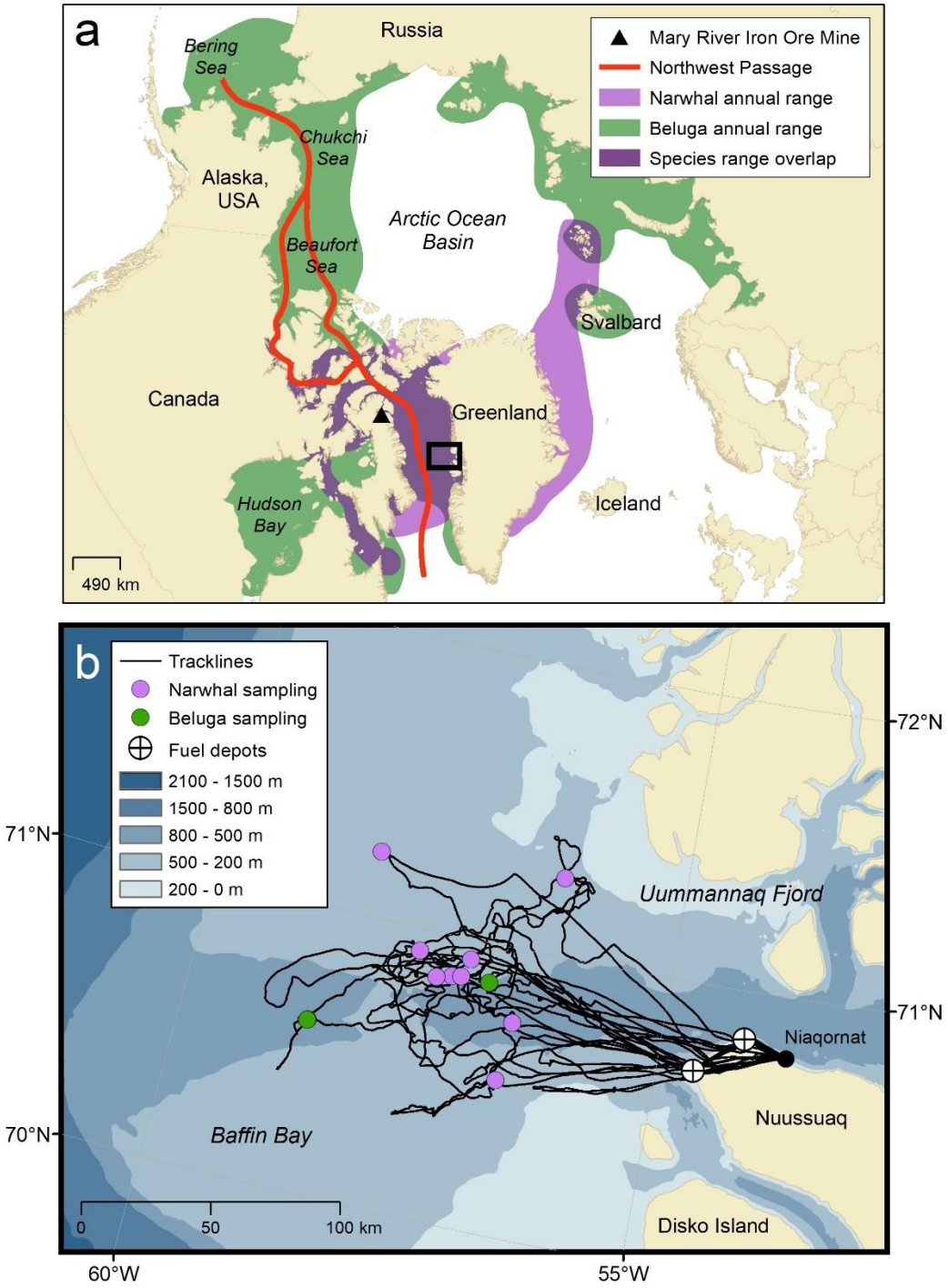

Figure 3.1. Top panel: map of narwhal (purple) and beluga (green) annual ranges (a). Overlapping beluga and narwhal annual ranges is visible in dark purple. The Northwest Passage sea route between the Atlantic and Pacific oceans is shown in red. Bottom panel: map showing

track lines of search effort, fuel depots, and recording sites for narwhals and belugas in Baffin Bay, West Greenland, between March 21st and 31st, 2013 (b). The black inset box in (a) demarcates the area shown in (b).

In addition to the use of visual surveys and telemetry to study wild beluga and narwhal populations, Passive Acoustic Monitoring (PAM) uses hydrophones over large spatiotemporal scales to localize regions of ecological importance (Castellote et al. 2013; Sousa-Lima et al. 2013; Frouin-Mouy et al. 2017; Ahonen et al. 2019; Castellote et al. 2020; Zhong et al. 2020). Despite this, the acoustic profiles of Arctic odontocetes remain largely understudied, particularly during non-summer months, because they reside under sea ice much of the year and the deployment and recovery of acoustic equipment in the Arctic is challenging and costly (Ahonen et al. 2019). Further, PAM relies on the ability to distinguish between species solely based on their characteristic sounds (i.e., calls or echolocation clicks), which means individual or a combination of specific sonic identifiers must be known for each species. Call types typically used in acoustic classification of odontocetes include echolocation clicks, burst pulses, whistles, and combined signals (Sjare & Smith 1986b; Chmelnitsky & Ferguson 2012; Marcoux et al. 2012; Garland et al. 2015; Rasmussen et al. 2015; Castellote et al. 2020; McCullough et al. 2021). Echolocation, sometimes referred to as biosonar, is characterized by the emission of high frequency, relatively broadband clicks of high directionality and listening for returning echoes; it is a dominant sense for odontocetes, much like vision is for humans (Au 1993; Madsen & Wahlberg 2007). Burst pulses, or “buzzes,” are short bursts or a series of broadband pulses (clicks) with a high repetition rate (Ford & Fisher 1978; Sjare & Smith 1986b; Rasmussen et al. 2015). Whistles are narrow-band and frequency-modulated tonal vocalizations (Sjare & Smith 1986b; Rankin et al. 2017). Finally, combined signals, or “mixed calls,” include overlaid or

paired pulsed and tonal sounds (Shapiro 2006; Marcoux et al. 2012; Walmsley et al. 2020). Acoustic classifiers may use a single call type or multiple call types to differentiate species (Simões Amorim et al. 2019).

Belugas and narwhals have large vocal repertoires that feature similar acoustic profiles (Ford & Fisher 1978; Marcoux et al. 2012; Stafford et al. 2012; Frouin-Mouy et al. 2017), which can make it difficult to distinguish between them acoustically without visual confirmation of species identity. To date, only one study has differentiated between belugas and narwhals acoustically (Frouin-Mouy et al. 2017) since other PAM studies have focused on regions where they do not co-occur (Lammers et al. 2013; Castellote et al. 2016; Ahonen et al. 2019). Frouin-Mouy *et al.* (2017) identified narwhals when they observed whistles or buzzes combined with low-frequency echolocation clicks, and belugas were detected when bird-like whistles were combined with high-frequency clicks. When whistles and buzzes were absent, they used an increase in spectral power around the 20 kHz frequency band to identify narwhal mid-frequency clicks (Frouin-Mouy et al. 2017). However, their comparison was narrow in scope as it was not their primary research objective. Thorough analyses of echolocation clicks have been conducted separately on belugas (Au et al. 1985; Sjare & Smith 1986b; Au et al. 1987; Rutenko & Vishnyakov 2006; Roy et al. 2010; Zahn et al. 2021a) and narwhals (Ford & Fisher 1978; Rasmussen et al. 2015; Koblitz et al. 2016; Podolskiy & Sugiyama 2020), but no comparative study with data from the same region exists. The broadband signals of beluga and narwhal echolocation extend frequencies between 2–150 kHz, but high-frequency clicks have been reported for both species with energies up to 200 kHz (Rasmussen et al. 2015; Zahn et al. 2021a). Measurements of beluga click peak frequencies in captive and wild environments vary widely between 40–120 kHz (Au et al. 1985; Au et al. 1987; Roy et al. 2010; Castellote et al.

2013; Zahn et al. 2021a). Unlike belugas, narwhals have not been held in captivity where controlled experiments can occur, and as a result, narwhal phonation is poorly described compared to belugas and other delphinids. Narwhal echolocation has been characterized by clicks with frequency maxima between 30–70 kHz (Miller et al. 1995; Shapiro 2006; Marcoux et al. 2011; Rasmussen et al. 2015), with some as low as 2–10 kHz and 7–14 kHz (Stafford et al. 2012). Still, among these studies, differences in study design, sampling equipment, and location make direct comparisons between beluga and narwhal click characteristics challenging.

As the Arctic continues to experience profound environmental changes due to climate warming (Comiso & Hall 2014; Kwok 2018; Overland et al. 2019), monitoring changes to the seasonal presence of belugas and narwhals is a growing research priority. Projections suggest that trans-Arctic shipping routes like the Northwest Passage and Northern Sea Route will be ice-free by midcentury (Overland & Wang 2013; Smith & Stephenson 2013), leading to concerns surrounding the effects of increased human activities on Arctic cetaceans (Hauser et al. 2018; Halliday et al. 2020). Importantly, the spatiotemporal overlap of belugas and narwhals also overlaps with the vessel corridor for the Mary River Iron Ore Mine on Baffin Island and the Northwest Passage (Figure 3.1a) where potentially large increases in underwater noise are expected in the coming decades (Stewart et al. 2011; Reeves et al. 2014; Halliday et al. 2021a; Kochanowicz et al. 2021). Arctic odontocetes are especially at risk to northward human expansion as hydrocarbon development and commercial shipping pose substantial threats via ship strikes, hearing damage, vessel disturbance, and increased underwater noise (Reeves et al. 2014; Hauser et al. 2018; Halliday et al. 2020). Underwater anthropogenic sounds from seismic surveys, drilling and oil production, military sonar, and motorized vessels can substantially disturb the acoustic environment which they depend on (Erbe & Farmer 2000; Blackwell et al.

2004; Mads Peter Heide-Jørgensen et al. 2013; Heide-Jørgensen et al. 2021; Kochanowicz et al. 2021; Yang et al. 2021).

Here, we use data collected from an offshore region in Baffin Bay, West Greenland to compare beluga and narwhal echolocation clicks. Our research objectives were twofold: (1) determine whether spectral properties between beluga and narwhal echolocation are significantly different, and (2) build an acoustic classifier to determine whether belugas and narwhals can be classified using only echolocation parameters. Employing methods to differentiate belugas and narwhals acoustically will equip scientists with the necessary tools to monitor their distribution and habitat-use changes. Further, using PAM to study Arctic odontocetes year-round will help managers mitigate any negative consequences of climate change and vessel traffic on these sentinel species.

3.3 METHODS

3.3.1 *Data Collection*

Aerial searches for narwhals and belugas were conducted out of Niaqornat, West Greenland, from an Air Greenland AS350 helicopter in spring 2013 (Figure 3.1b). All field operations were in accordance with IACUC procedures as approved by the University of Washington (#4155–01, PI Laidre) and the US Office of Naval Research. The Government of Greenland and Greenland Institute of Natural Resources, Nuuk provided K. L. Laidre permission to conduct research in Greenland waters. All methods were carried out in accordance with relevant guidelines and regulations. Weather conditions allowed seven days between 21 and 31 March to search for whales 100–150 km offshore in leads and cracks in the pack ice > 98% concentration. When narwhals or belugas were observed, an aerial search radius of at least 5 km was required to ensure that the ice conditions were safe for landing, during which sightings for other whales and

species in the vicinity were made. On the ice, a hydrophone array was deployed at the edge of a lead and all recordings were paired with visual identification of each species. Only one species was observed and recorded at each sampling location, so there were no occurrences in which both narwhals and belugas were present. Since the detection range for echolocation is < 1 km (Zahn et al. 2021a) and our search radius was > 5 km, we assume our data are single-species recordings.

The hydrophone array was composed of 16 individual Reson TC4013-5 receivers (sensitivity -215 dB +/- 2dB re 1V/µPa; flat +/- 2dB frequency response 1–150 kHz) positioned in a vertical, linear orientation. Prior to deployment, each hydrophone was calibrated and its frequency response determined. Each receiver was located 1 m apart along a 2 mm diameter line with the topmost hydrophone at 3 m below the surface and the bottom hydrophone at 18 m. A 4-kg weight attached to the bottom maintained a vertical orientation of the array. While recording, a custom software, MALTA (Microphone Array Localization Tool for Animals by CAE Software & Systems), was used to visually examine recordings of all 16 receivers in real-time. Hydrophone signals were amplified by 35 dB using a custom amplifier, and recordings were converted from analog to digital (500 kHz sampling rate; 16-bit resolution) using two eight-channel National Instruments PXI-6123 A/D converters. No high pass filter was applied, and the hydrophones served as a low pass filter (150 kHz, 1 pole). The clipping level was at 206 dB pp re 1 µPa at 100 kHz (Koblitz et al. 2016; Zahn et al. 2021a). To safeguard against potential file corruption and facilitate data post-processing, whale recordings were partitioned, loss-less, in 5-second-long sound files.

3.3.2 *Event Selection and Acoustic Parameter Estimation*

Individual echolocation clicks were detected using the open source passive acoustic analysis software PAMGuard (v. 2.01.03f) (Gillespie et al. 2008). Based on localization analyses using the same data (Koblitz et al. 2016; Zahn et al. 2021a), the highest amplitude signals were recorded on hydrophones 10 and 11 (positioned at 12 and 13 m deep, respectively) and thus provided the highest quality recordings. For species differentiation analyses and classification models, only data from clicks recorded on hydrophone 10 (12 m depth) were used to avoid pseudo-replication. Using the Click Detector module in PAMGuard, clicks were detected from hydrophone 10 recordings with a 14 dB signal-to-noise minimum threshold. To minimize false detections on low-frequency sounds, the detector included a 4^{th} order IIR Butterworth high-pass filter with a 4 kHz corner frequency. No additional frequency filters were used. Click detections were labeled using PAMGuard click classifiers that were defined by specified frequency bins according to the peak frequency within each click. Each classifier was given a unique numeric code that corresponded to the target detection frequency range: 1 (4–20 kHz), 2 (20–50 kHz), 3 (50–70 kHz), 4 (70–100 kHz), 5 (100–150 kHz), 6 (150–250 kHz), and 0 (unclassified).

Groups of clicks (i.e., click trains) were then manually assigned to individual detection "events" using the bearing/time display in PAMGuard's Viewer Mode (v. 2.01.03f). Although data from only one hydrophone were necessary for our analyses, bearing angles produced from two channels (hydrophones 10 and 11) were needed to effectively visualize and isolate click trains. Since the classification models employed in downstream analyses utilized subsamples of the entire dataset to evaluate model performance—much like a testing and training dataset—we assigned clicks to acoustic events using predetermined time windows to facilitate random partitioning of the data across all recordings. Two-minute intervals were used for narwhal

recordings and one-minute intervals were used for beluga recordings in an effort to obtain a similar number of clicks per acoustic event between species, because the beluga recordings had more overlapping click trains. For all events, we included clicks where the maximal intensity of the beam was both centered (i.e., on-axis) and not centered (i.e., off-axis) on the recording system to reflect the nature of most PAM data. Once all clicks were assigned to events, a suite of acoustic parameters was calculated (Table 3.1). Using the *PAMpal* package (v. 0.12.6) (Sakai 2021) in R (v. 4.1.0) (R Core Team 2021), echolocation parameter values were calculated for the click sequences selected in PAMGuard using standard measurement criteria (Baumann-Pickering et al. 2010; Griffiths et al. 2020; Sakai 2023). Default *PAMpal* settings were used that included a 10 kHz Butterworth high-pass filter and a FFT window length of 2.5 ms to use in calculations. Parameter values were calculated for individual clicks and then the mean parameter values determined for a given event, except for inter-click-interval (ICI) where the mode value was approximated for each acoustic event.

Table 3.1. Descriptions of echolocation acoustic parameters used as variables in species differentiation analyses and classification models. All parameters outlined here were used for the standard Random Forests classification model and BANTER's first stage call classifier. Variable codes marked with an asterisk (*) indicate which acoustic parameters were used for multivariate differentiation analyses. A full list and the process used by the *PAMpal* package (Sakai 2021) for calculating click parameters can be found in the R package documentation (Sakai 2023).

Variable Code	Variable Name	Unit	Description
peak*	Peak frequency	kHz	Frequency value with the highest dB level
peak2*	Second peak frequency	kHz	Frequency value with the second highest dB level
peak3*	Third peak frequency	kHz	Frequency value with the third highest dB level
trough*	Frequency trough	kHz	Frequency value between peak and peak2 with the lowest dB value; also called spectral notch
trough2*	Second frequency trough	kHz	Frequency value between peak2 and peak3 with the lowest dB value
peakToPeak2*	First peak to second peak	kHz	Difference between the frequency values of peak and peak2
peakToPeak3*	First peak to third peak	kHz	Difference between the frequency values of peak and peak3
peak2ToPeak3*	Second peak to third peak	kHz	Difference between the frequency values of peak2 and peak3
Q_10dB	-10 dB resonant quality factor	kHz	Metric of frequency pureness at -10 dB calculated by dividing the center frequency by the bandwidth
Q_3dB*	-3 dB resonant quality factor	kHz	Metric of frequency pureness at -3 dB calculated by dividing the center frequency by the bandwidth
fmin_10dB	-10 dB frequency minimum	kHz	-10 dB frequency minimum
fmin_3dB*	-3 dB frequency minimum	kHz	-3 dB frequency minimum
fmax_10dB	-10 dB frequency maximum	kHz	-10 dB frequency maximum
fmax_3dB*	-3 dB frequency maximum	kHz	-3 dB frequency maximum
BW_10dB	-10 dB bandwidth	kHz	-10 dB bandwidth
BW_3dB*	-3 dB bandwidth	kHz	-3 dB bandwidth
centerHz_10dB	-10 dB center frequency	kHz	[min frequency + (max frequency - min frequency)]/2 at -10 dB
centerHz_3dB*	-3 dB center frequency	kHz	[min frequency + (max frequency - min frequency)]/2 at -3 dB
duration*	Click duration	µs	Time defined by the number of samples above 100 times the 40th percentile of the Teager Kaiser energy level
ici*	Inter-click interval	sec	Time interval between consecutive clicks; mode approximated for each event

3.3.3 *Species Differentiation*

Multivariate analyses were used to assess potential differences in beluga and narwhal echolocation. When both the -3 dB and -10 dB measurement was calculated for acoustic parameters, only -3 dB parameters were considered for differentiation analyses to remove redundant variables (see Table 3.1). To ensure -10 dB measurements did not have a substantial contribution, we ran our analyses with both -3 dB and -10 dB measurements and our results were unaffected. Each acoustic parameter across all acoustic events was z-score transformed and a Euclidean distance dissimilarity matrix generated. A permutational multivariate analysis of variance (PerMANOVA; 999 permutations) was performed to test for differences between species among mean acoustic parameter values (Anderson 2001). However, a significant result from a perMANOVA can result from differences in the mean positions of each group in multivariate space, differences in within-group variance in multivariate space, or a combination of the two. Therefore, a permutation test of multivariate homogeneity of dispersions (PERMDISP; 999 permutations) was used to analyze whether within-group variance in multivariate space between beluga and narwhal acoustic parameter values was different (Anderson 2006; Anderson 2017). Differences between beluga and narwhal acoustic parameter values were visualized using principal component analysis (PCA) performed on a correlation matrix (Pearson 1901). As an ordination technique, PCA reduces a high-dimensional dataset with correlated variables into fewer, uncorrelated dimensions called principal components (PCs) (Lever et al. 2017). PCA variable loadings, or eigenvectors, on each PC were used to explore differences among groups. PCA eigenvalues provide the amount of variance explained by each PC and are used to determine which PCs are statistically significant. By applying the broken-stick rule and examining a scree plot, eigenvalues that are higher than what is expected by

chance are considered to explain a significant amount of the variance in the original data (Jackson 1993). All statistical analyses were conducted in R using the *vegan* package (v. 2.5-7) (Oksanen et al. 2020).

3.3.4 *Species Classification Using Random Forests*

We used a Random Forests (RF) classification model (Breiman 2001) to classify beluga and narwhals using echolocation click parameters. RF has demonstrated to be an effective approach for bioacoustic studies (Ross & Allen 2014; Archer et al. 2020; Yang et al. 2020) as it is unaffected by nonparametric data and can accommodate many correlated variables. An RF model consists of many individual decision trees; each of these trees uses a random subset of samples and predictors. By combining thousands of trees, the final aggregated ensemble tree explores differences among species across the entire space of predictors in the original data and maximizes predictive power. RF models do not use a separate testing dataset to assess model accuracy. The random subsample drawn for each individual tree is termed the "in-bag" sample, while the remainder of the data not included are referred to as "out-of-bag" (OOB). OOB samples are used to test model performance by calculating an OOB classification error rate.

The two primary parameters for RF classification are the number of randomly selected predictors to choose from at each node, *mtry*, and the number of randomly selected samples to classify in each tree, *sampsize*. We conducted a sensitivity analysis for *mtry* and *sampsize* to ensure we used parameter values that prevented overfitting and maximized classification accuracy. The model was fit over all possible combinations of both parameters within possible ranges (*mtry*: 2–19; *sampsize*: 2–18) and the model accuracy determined. For all combinations, the correct classification rate did not vary by more than 0.05%, and therefore the model result was not sensitive to *mtry* and *sampsize*. Thus, we used the default value for *mtry* (square root of

the number of predictors) and used half of the total sample size for the smallest species class for *sampsize*.

For our final model, species were assigned *a priori* to acoustic events in PAMGuard and 20 acoustic parameters were used as predictors to classify belugas and narwhals (Table 3.1). Each predictor (i.e., acoustic parameter) was the calculated mean across all individual clicks for each acoustic event. A randomized subset of four acoustic parameters (*mtry*) was used to split observations at each node. Each tree was grown using a randomized subset of nine acoustic events (*sampsize*) from each species group. The model was structured such that equal subsamples were drawn from each species class without replacement to account for our unbalanced dataset and to capture as much variation in the acoustic data as possible. For passive acoustics, there are occasions when individual whales may dominate the recordings with stereotyped calls; therefore, if we sampled with replacement, our model may underestimate the variation in the data. Model stability was visualized by plotting the trace of cumulative OOB error rate by number of trees and plotting the distribution of the fraction of trees that objects were in-bag. Ten thousand trees were constructed in the forest (*ntree*) to achieve model stability. To determine whether our model correct classifications rates were significantly greater than what was expected by chance alone (50%), a binomial test for statistical significance of model performance was conducted. Our classification model was built using the *randomForest* (v. 4.6-14) (Liaw & Wiener 2002) and *rfPermute* (v. 2.5) (Archer 2021) packages in R.

3.3.5 *Species Classification Using BANTER*

For comparison with the singular RF model above, we also employed BANTER (Bio-Acoustic eveNT classifiER), a supervised acoustic classification method that can utilize multiple call types (Rankin et al. 2017) to classify belugas and narwhals. BANTER consists of two stages of RF

models (Rankin et al. 2017). The first stage is referred to as the "call classifier" in which individual classification models are built for each call type or detector. From the call classifier, BANTER produces a distribution of classification probabilities for each call type or detector. The second stage is the "event classifier" and uses the results from the first stage to classify acoustic events (collections of calls) to each species.

Although BANTER has the potential to use information from multiple call types (e.g., whistles or burst pulses), our objective was to determine whether belugas and narwhals can be classified using echolocation signals alone. Therefore, our call classifier consisted of separate RF models for each of the echolocation click detectors used in PAMGuard. Two click detectors (1 and 6) from the PAMGuard classification were removed due to insufficient data. For each detector, an RF model was built using 20 acoustic parameters (Table 3.1) to classify all individual echolocation clicks from that detector. RF models using default settings draw bootstrap samples from one pool containing the entire training dataset from all classes. Therefore, when an RF model is applied to an unbalanced dataset, the classifier will tend to correctly classify the dominant class. To offset this effect, BANTER draws equal random subsamples without replacement from each species group. Each model randomly selected 50 clicks from each species (*sampsize*) without replacement and each forest contained 20,000 trees. The number of parameters randomly selected to choose from at each node was set to the default (square root of the total number of parameters). Results from the call classifier provide mean assignment probabilities for each click detector. For example, the click detector 2 model produces the mean probability that clicks from detector 2 will be assigned to a beluga or narwhal. The call classifier also determines the proportion of each detector present for a given event. For example, all events that do not have clicks detected by click detector 2 will have a

proportion of zero, and for events that do have clicks from detector 2 will have a proportion value between 0 and 1.

Results from the call classifier (i.e., mean assignment probabilities for each click detector and proportions of each detector per event) were then applied to the second stage event classifier as variables. The mode inter-click interval for each event was added as an additional event-level variable. The event classifier assigned all acoustic events to either a beluga or narwhal using a single RF model. Parameterization of this model was the same as the call classifier (*mtry* = default; *ntree* = 20,000), except the number of events randomly selected (*sampsize*) was set to nine. Relative variable importance was examined for both the call and event classifiers. To determine whether the correct classification rates of our BANTER call and event classifiers were significantly greater than what was expected by chance alone (50%), binomial tests for statistical significance were conducted for each model. Our BANTER classification model was built using the *banter* (v. 0.9.4) (Rankin et al. 2017) and *rfPermute* (Archer 2021) packages in R.

For the previous analyses, recordings were subdivided into one- and two-minute acoustic events for belugas and narwhals, respectively. As an alternate approach to using standardized temporal intervals, we examined BANTER performance using events assigned to independent acoustic encounters. Acoustic encounters are defined by separate sightings of groups of whales and can vary in recording duration, ambient noise, and environmental and recording conditions (e.g., greater distance or different orientation between whales and receivers). Here, individual encounters were comprised of several acoustic events. If sounds from independent sightings were substantially different, encounters that have a larger number of events will have a greater representation in the species classification model used above. Using the same BANTER framework, we tested whether unique encounters for each species were similar. To accomplish

this, a series of BANTER classification training models were created using all events from one encounter for each species (*mtry* = default; *ntree* = 10,000; *sampsize* = half the smallest class sample size) and then used to predict events from encounters that were not included. All unique pairwise combinations of acoustic encounters between species were used to build separate BANTER models. The correlation between the training confusion matrices and the prediction (validation) confusion matrices were then calculated. The presence of correlation (> 0.5) indicates that events from separate encounters are similar because the prediction classification scores are similar to the training scores.

3.4 RESULTS

A total of 1:03 hours of beluga recordings and 7:38 hours of narwhal recordings were made 100 km or more offshore in the pack ice of Baffin Bay (Figure 3.1b). Belugas were observed and recorded at two unique locations and narwhals at nine unique locations, in pods of approximately six to thirty individuals. Narwhal recordings used for analyses originated from five independent sightings (i.e., encounters) and beluga recordings from two. We estimate there were approximately 22–36 individual belugas and 63–120 narwhals sampled across all seven encounters. Recordings were paired with visual confirmation of species, so all echolocation clicks were labeled as originating from belugas or narwhals. Species groups were assigned to events created in PAMGuard. A total of 11,319 clicks were assigned to 81 separate events with a median of 71 clicks per event (Supplementary Table S3.1). Out of the 81 events, 19 were belugas (2,537 clicks) and 62 were narwhals (8,782 clicks). Twenty acoustic parameters were used to compare beluga and narwhal echolocation (Table 3.1). Signal parameter measurements for each species across all acoustic events are summarized in Table 3.2. Beluga acoustic events had a higher mean peak frequency (68.7 ± 10.1 kHz), -3 dB center frequency (69.6 ± 10.6 kHz), and -

10 dB center frequency (70.2 ± 9.2 kHz) than narwhal events (43.7 ± 7.8 kHz, 43.8 ± 7.8 kHz, and 46.2 ± 8.5 kHz, respectively). Spectral peaks, troughs, and center frequencies (variables: peak, peak2, peak3, trough, trough2, centerHz_10dB, and centerHz_3dB) for beluga clicks were generally > 60 kHz and narwhal clicks < 60 kHz with overlap between 40–60 kHz (Table 3.2).

Table 3.2. Summary of signal parameter measurements for beluga and narwhal echolocation for all 81 acoustic events (beluga: *n* = 19; narwhal: *n* = 62). Mean ± standard deviation (s.d.) and range (min – max) are provided.

		Beluga		Narwhal	
Variable	Unit	Mean ± s.d.	Range	Mean ± s.d.	Range
peak	kHz	68.7 ± 10.1	54.4 – 96.7	43.7 ± 7.8	28.0 – 58.8
peak2	kHz	67.6 ± 7.9	50.9 – 89.5	49.3 ± 6.8	34.9 – 63.3
peak3	kHz	65.5 ± 10.7	43.0 – 86.4	46.1 ± 8.1	17.3 – 65.2
trough	kHz	68.7 ± 8.9	51.3 – 90.4	48.2 ± 6.5	32.1 – 64.3
trough2	kHz	63.8 ± 9.4	42.4 – 77.4	44.2 ± 9.5	16.8 – 65.1
peakToPeak2	kHz	16.6 ± 2.4	13.3 – 24.0	19.4 ± 2.8	11.0 – 25.1
peakToPeak3	kHz	16.4 ± 2.4	11.6 – 22.2	15.3 ± 2.6	5.8 – 21.2
peak2ToPeak3	kHz	23.5 ± 3.1	17.2 – 31.4	19.4 ± 4.8	6.2 – 31.8
Q_10dB	kHz	6.1 ± 4.7	1.7 – 16.0	3.3 ± 1.4	1.3 – 10.6
Q_3dB	kHz	33.3 ± 24.7	8.8 – 93.6	15.0 ± 5.6	6.0 – 34.8
fmin_10dB	kHz	53.1 ± 8.1	42.4 – 71.7	33.1 ± 5.5	22.2 – 51.3
fmin_3dB	kHz	65.0 ± 9.7	50.1 – 88.1	40.5 ± 6.6	26.3 – 57.0
fmax_10dB	kHz	87.4 ± 15.2	61.7 – 119.0	59.3 ± 13.8	33.9 – 90.0
fmax_3dB	kHz	74.2 ± 12.4	54.3 – 103.3	47.1 ± 9.3	29.6 – 66.6
BW_10dB	kHz	34.3 ± 15.9	9.3 – 65.5	26.2 ± 12.1	10.4 – 58.8
BW_3dB	kHz	9.2 ± 6.9	0.9 – 25.3	6.5 ± 3.9	1.9 – 17.8
centerHz_10dB	kHz	70.2 ± 9.2	53.1 – 93.6	46.2 ± 8.5	28.1 – 65.5
centerHz_3dB	kHz	69.6 ± 10.6	52.2 – 95.7	43.8 ± 7.8	28.1 – 58.9
duration	µs	659.7 ± 479.9	53.4 – 1487.0	592.9 ± 488.0	15.0 – 1667.1
ici	ms	177.9 ± 174.6	2.9 – 696.5	143.5 ± 70.1	20.3 – 334.2

3.4.1 *Species Acoustic Differentiation*

Results from the perMANOVA reveal significant differences between beluga and narwhal echolocation characteristics ($F_{1,79}$ = 42.35, p = 0.001; Supplementary Table S3.2). Beluga acoustic events also demonstrated a higher dispersion in multivariate space than narwhal acoustic events (PERMDISP, $F_{1,79}$ = 8.37, p = 0.004; Supplementary Table S3.2). The PCA further displayed strong evidence for beluga and narwhal acoustic differentiation; beluga events were more dispersed than narwhal events (Figure 3.2a). Within the two-dimensional space of PC1 and PC2, 72.9% of the original trait variation was explained where most was captured by the first dimension (58.4%; Figure 3.2a). According to the broken-stick model, PC1 was the only dimension found to explain a significant amount of the variation in the original data. Beluga acoustic events are largely located on the right side of the PCA ordination space, representing higher echolocation click parameter values as compared to narwhal acoustic events that are on the left side (Figure 3.2b; Supplementary Figure S3.1). These findings are consistent with average spectra, acoustic event spectrograms, and mean parameter values for each species where beluga spectra present more energy at higher frequencies than narwhal spectra (Figure 3.3; Table 3.2).

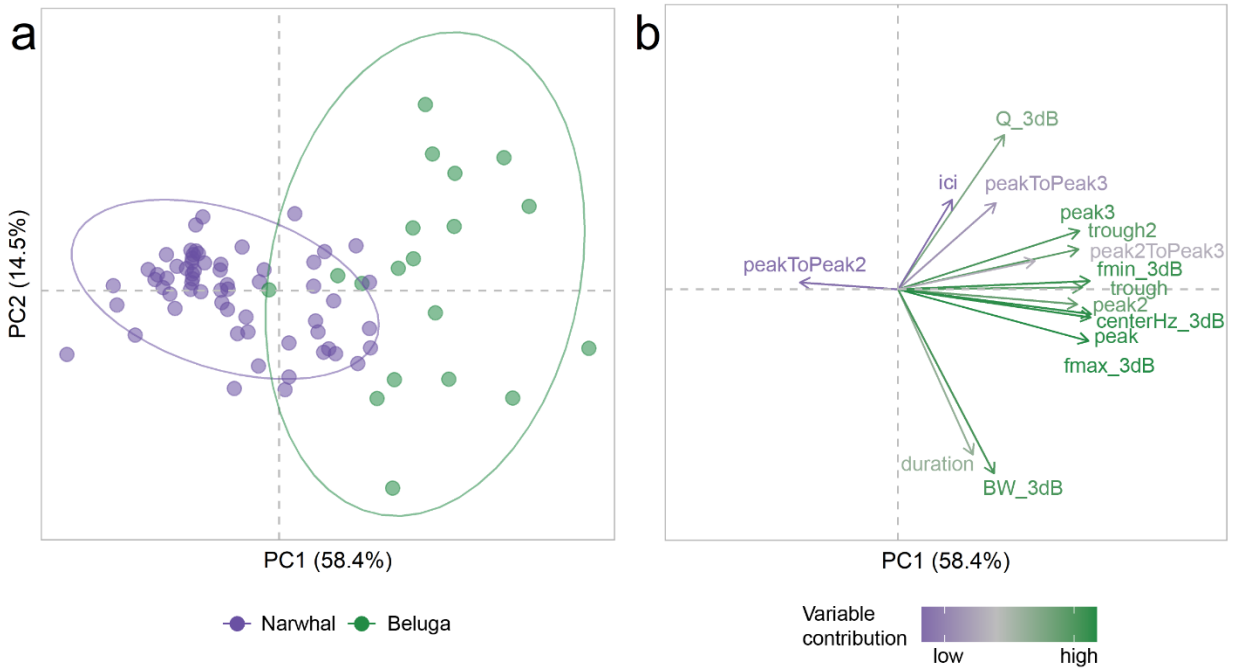

Figure 3.2. Multivariate PCA ordination plot for beluga or narwhal acoustic events (a) and acoustic parameter eigenvectors (b). Principle component (PC) 1 explains 58.4% of the variation and PC2 explains 14.5%. The total variable contribution is shown in vector length and color, where purple is a low contribution and green is high. Ellipses in (a) show 95% confidence intervals. (a) and (b) represent the same multidimensional space.

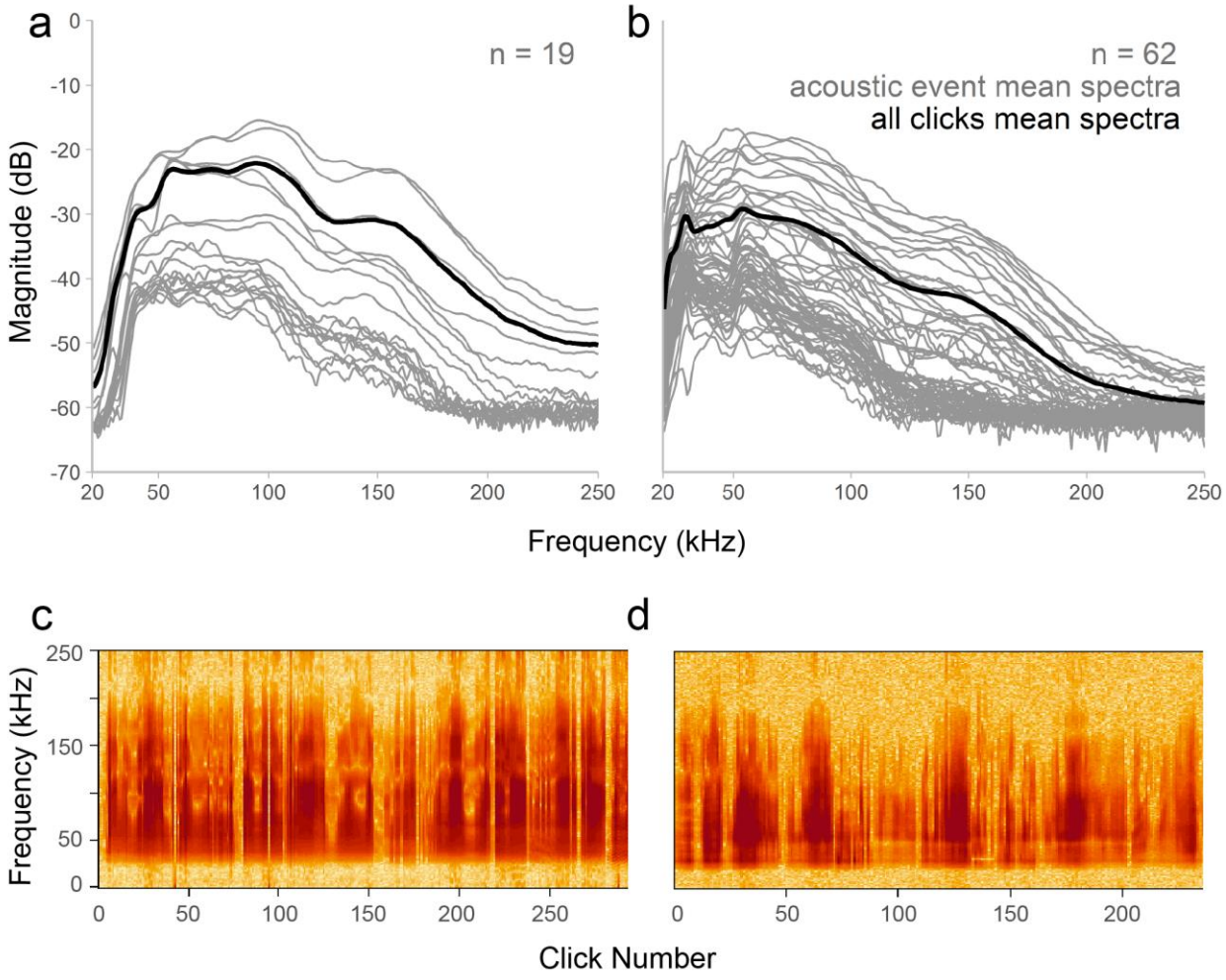

Figure 3.3. Average spectra and example concatenated spectrograms for beluga (a,c) and narwhal (b,d) acoustic events. Gray lines in (a) and (b) show average spectra for individual acoustic events: 19 beluga events and 62 narwhal events. Black lines in (a) and (b) represent the mean spectra for all echolocation clicks assigned to events for each species: 2,537 beluga clicks and 8,782 narwhal clicks. Example concatenated spectrograms in (c) and (d) show one acoustic event for each species (1024 point FFT; Hanning window).

3.4.2 *Species Acoustic Classification*

Both the RF and BANTER species classification models performed well with high OOB correct classification rates ($P < 0.001$ for all models; Table 3.3). The overall correct classification rate

for the RF model was 92.6% (95% CI: 84.6–97.2%); 94.7% correct classification for beluga acoustic events and 91.9% for narwhal events. One beluga and five narwhal acoustic events were misclassified (Figure 3.4a) and the most important predictors for species classification were -3 dB and -10 dB frequency minimums and peak frequency (Figure 3.4b). Average spectra and waveforms for misclassified events presented signal patterns characteristic of off-axis clicks (i.e., clicks recorded away from the whale's longitudinal acoustic axis) when compared to those that were correctly classified (Figure 3.5).

Table 3.3. Confusion matrices for the (a) standard Random Forest model, (b) BANTER call classifiers (Detectors 2, 3, 4, and 5), and (c) BANTER event classifier. The total number of correct and incorrect classifications of echolocation clicks are shown between the groups identified *a-priori* (rows) and predictions by the classifier (columns). Out-of-bag (OOB) percent correct (95% confidence interval) classification rates demonstrate model performance. Binomial test *P*-values using a prior probability of 0.5 are provided where an asterisk (*) represents statistical significance ($P < 0.05$).

	Beluga	Narwhal	Correct classification (95% CI)	*P*-value
(a) Standard Random Forest model				
Beluga	18	1	94.7% (74.0 – 99.9%)	<0.001*
Narwhal	5	57	91.9% (82.2 – 97.3%)	<0.001*
Overall			92.6% (84.6 – 97.2%)	<0.001*
(b) BANTER call classifier				
Detector 2				
Beluga	351	31	91.9% (88.7 – 94.4%)	<0.001*
Narwhal	886	5022	85.0% (84.1 – 85.9%)	<0.001*
Overall			85.4% (84.5 – 86.3%)	<0.001*
Detector 3				
Beluga	1007	122	89.2% (87.2 – 90.9%)	<0.001*
Narwhal	540	1632	75.1% (73.3 – 76.9%)	<0.001*
Overall			80.0% (78.5 – 81.3%)	<0.001*
Detector 4				
Beluga	710	136	83.9% (81.3 – 86.3%)	<0.001*
Narwhal	121	449	78.8% (75.2 – 82.1%)	<0.001*
Overall			81.9% (79.7 – 83.8%)	<0.001*
Detector 5				
Beluga	131	39	77.1% (70.0 – 83.1%)	<0.001*
Narwhal	22	72	76.6% (66.7 – 84.7%)	<0.001*
Overall			76.9% (71.3 – 81.8%)	<0.001*
(c) BANTER event classifier				
Beluga	19	0	100% (82.4 – 100%)	<0.001*
Narwhal	2	60	96.8% (88.8 – 99.6%)	<0.001*
Overall			97.5% (91.4 – 99.7%)	<0.001*

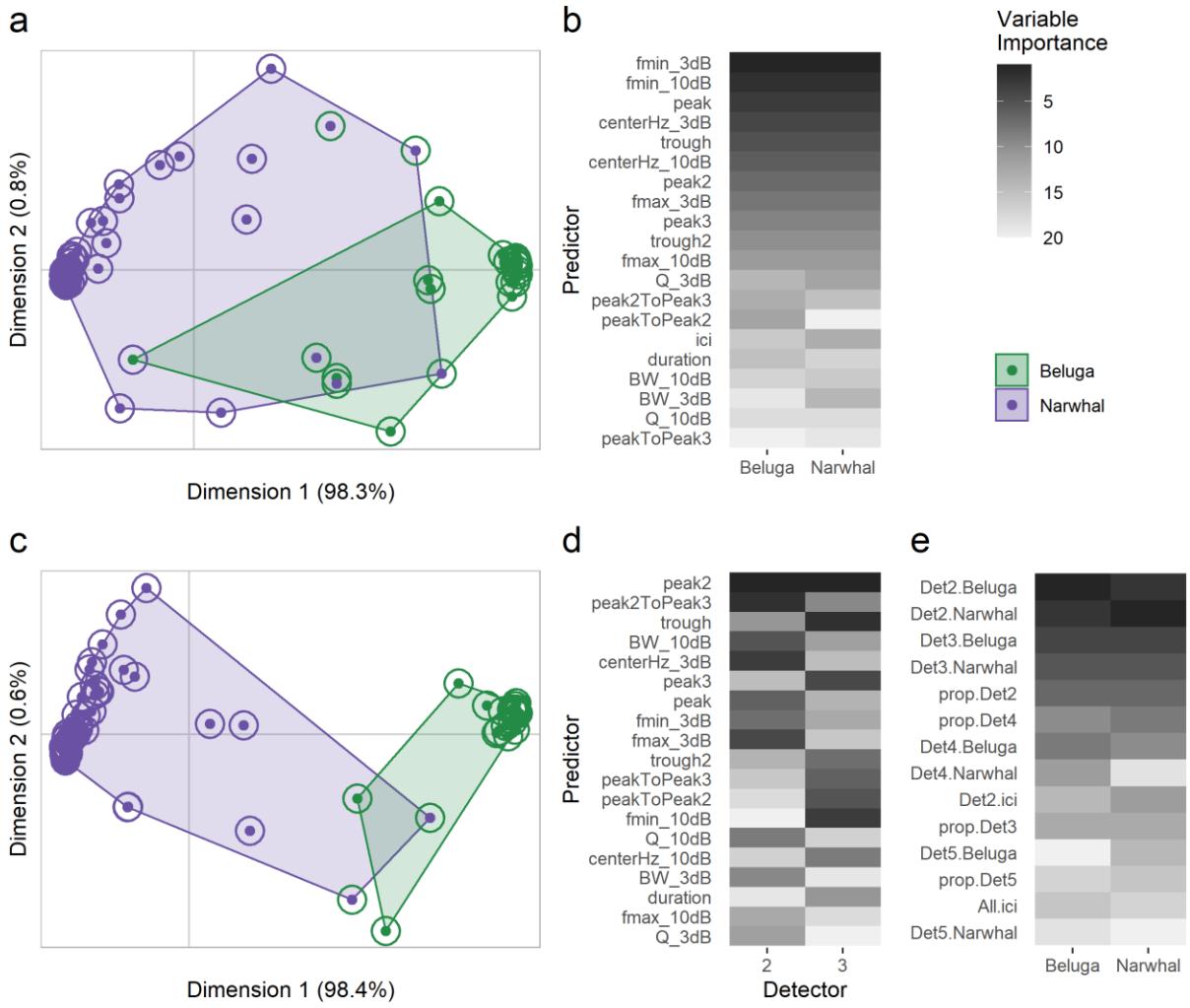

Figure 3.4. Ordination plots (a, c) from a multidimensional scale (MDS) conversion of Random Forest (RF) proximity scores to visualize species classification predictions. The top panel (a, b) corresponds to the single RF classification model and the bottom panel (c, d, e) are the results from the BANTER classification model. RF proximity scores are calculated for each pair of objects (i.e., acoustic events) to produce a NxN matrix, where N is the total number of objects. If objects occupy the same terminal node for one tree, their proximity score increases by one. All proximities are normalized by dividing by the total number of trees in the forest. Shaded regions show *a-priori* species groups with points colored according to their original (inner) and predicted (outer) species. Dimension 1 in (a) and (c) explains 98.3% and 98.4% of the total variation for the RF and BANTER models, respectively, and dimension 2 explains 0.8% and 0.6% of the variation, respectively. Relative variable importance is shown for both models (b, d, e). The

heatmaps show ranked variable importance from the least important (light gray) to most important (dark gray). Descriptions of predictors are provided in Table 3.1 and Supplementary Table S3.2.

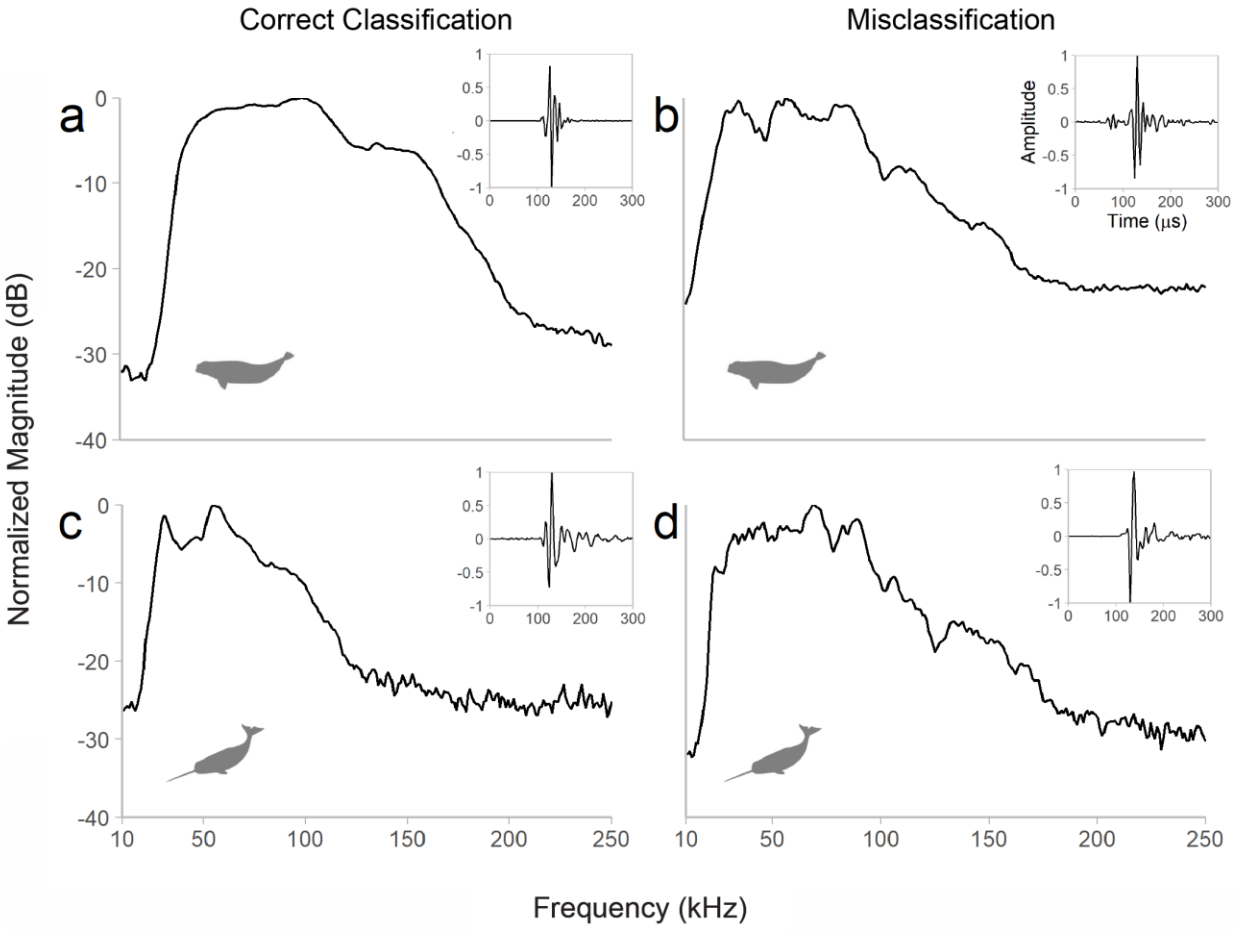

Figure 3.5. Example average spectra for beluga (a, b) and narwhal (c, d) acoustic events that were correctly classified (a, c) and misclassified (b, d). The waveforms of the highest amplitude click for each event are provided. The beluga acoustic event in (b) was misclassified by only the Random Forest model ansd the narwhal acoustic event in (d) was misclassified by both the Random Forest and BANTER classification models.

BANTER's two-stage approach achieved a higher accuracy than the standard RF model. The BANTER first stage call classifier used here consisted of four separate models for click

detectors 2, 3, 4, and 5 (Table 3.3), each producing mean species assignment probabilities and click detector proportions that were subsequently used as variables for the second stage event classifier (Supplementary Table S3.3). BANTER's event classifier achieved a correct classification score of 97.5% (95% CI: 91.4–99.7%); 100% correct classification for beluga acoustic events and 96.8% for narwhal events (Table 3.3). Among the event-level variables, detectors 2 (20–50 kHz) and 3 (50–70 kHz) were the most important classifiers (Figure 3.4e). By examining the relative importance of the predictors (i.e., acoustic parameters; Table 3.1) for detector 2 and 3 call classifiers, the second peak frequency, the frequency difference between the second and third peaks, and the frequency trough were the most important for classification of individual clicks (Figure 3.4d). However, since the event classifier uses mean assignment probabilities from each detector classifier as predictors, the most important variables for the detector 2 and 3 classifiers are not necessarily important variables for the event classifier. Examination of the vote distributions for the detector 2 and 3 call classifiers revealed that the detector 2 call classifier produced confident species classifications (i.e., the majority of samples were classified at high probability) compared to the detector 3 classifier (Supplementary Figure S3.2). Overall, the BANTER model demonstrated strong predictive power with only two narwhal event misclassifications (Table 3.3; Figure 3.4c). For correctly classified events, the model had high confidence for its species assignment evidenced by its vote distribution (Supplementary Figure S3.3).

The correlation test to examine similarity between acoustic encounters revealed that events among different encounters were similar. A positive correlation between training confusion matrices (from models built using one encounter per species) and validation confusion matrices (from training models that predicted events from encounters not used in training model)

indicated similarity between encounters. With the exception of one pair, all encounter pairs had a positive correlation and 6 of the 10 pairs had a correlation greater than 0.5 (Supplementary Table S3.4).

For both the single RF and BANTER models, the majority of the predictions for beluga and narwhal acoustic events were tightly clustered (Figure 3.4a,c). These tightly clustered, correctly classified events were marked by clear differences between beluga and narwhal spectral characteristics. Beluga average spectra tended to be smoother, have a larger bandwidth, and higher -3 and -10 dB frequency minimums and maximums (Figures 3.3a & 3.5a). Conversely, narwhal average spectra presented peaks and notches, a lower bandwidth, and lower frequency minimums and maximums (Figures 3.3b & 3.5c). Average spectra from events that were misclassified and showed properties of both beluga and narwhal spectral characteristics generally had lower signal magnitudes (dB), smaller click sample sizes, and spectral variations that suggest a higher proportion of off-axis clicks (i.e., clicks not centered on the recording equipment; Figures 3.3 & 3.5).

3.5 DISCUSSION

Passive acoustics has been a primary method to monitor beluga and narwhal populations year-round in remote regions of the Arctic, providing insight into their seasonal distribution and migratory routes (Roy et al. 2010; Marcoux et al. 2011; Castellote et al. 2013; Castellote et al. 2016; Frouin-Mouy et al. 2017). Yet, prior to this study, the acoustic profiles of these two species were examined separately, despite their shared habitat ranges and acoustic features. Our results provide the first acoustic comparison between belugas and narwhals from the same region and reveal that they can be acoustically differentiated and classified using echolocation clicks alone. Belugas and narwhals have considerable acoustic overlap and variability in their social

calls which makes species classification using acoustic parameters challenging (Ford & Fisher 1978; Marcoux et al. 2012; Stafford et al. 2012; Frouin-Mouy et al. 2017). Our analysis of beluga and narwhal recordings from the same region, during the same season, and acquired using the same equipment delivers a rare *in situ* comparison that fills a critical knowledge gap in the acoustic ecology for each species. We also provide a robust BANTER classification model that sets a precedent and foundation for echolocation parameters to be used in future PAM classification efforts, whether for belugas and narwhals or other odontocete species.

Our multivariate analyses showed significant differences between beluga and narwhal echolocation characteristics (perMANOVA: $p = 0.001$) where beluga acoustic parameters were more dispersed and distinguished by higher frequency content (Figures 3.2 & 3.3). Spectral peaks, troughs, and center frequencies for beluga clicks tended to be > 60 kHz and narwhal clicks < 60 kHz with overlap between 40–60 kHz (Table 3.2). The greater variation observed among beluga acoustic events may be due to the sample size being smaller ($n = 19$) than the narwhal dataset ($n = 62$) or may reflect the true variation in beluga echolocation. Additionally, the lower frequency content observed in narwhal echolocation may indicate that narwhals have a longer echolocation detection range for prey and PAM receivers than belugas. Previous work to quantify beluga echolocation parameters reveals high variability and evidence of biosonar adaptability (Gurevich & Evans 1976; Au et al. 1985; Au et al. 1987; Rutenko & Vishnyakov 2006; Castellote et al. 2013). For example, estimates of beluga echolocation peak frequencies range widely between 40–120 kHz across captive and wild environments (Gurevich & Evans 1976; Au et al. 1985; Au et al. 1987; Rutenko & Vishnyakov 2006; Roy et al. 2010; Lammers et al. 2013) and have been shown to change depending on the ambient sound levels of the environment (Au et al. 1985). Narwhal echolocation has been largely characterized by lower

frequency clicks with maxima between 30–70 kHz (Miller et al. 1995; Shapiro 2006; Marcoux et al. 2011; Stafford et al. 2012), but high-frequency clicks have been reported where the entire bandwidth can extend up to 200 kHz (Rasmussen et al. 2015). Frouin-Mouy *et al.* (2017) used a difference in spectral power around the 20 kHz frequency band to distinguish between species for mid-frequency clicks with peaks within 30–60 kHz (Frouin-Mouy et al. 2017). However, their sample sizes were small with 20 beluga and 17 narwhal click trains (162 and 186 individual clicks, respectively), and their recordings came from five different locations and three different receivers which can introduce classification errors (Roch et al. 2015). Our findings are consistent with their preliminary comparison in which narwhal spectra contain more energy between 20–50 kHz than beluga spectra (Figure 3.3). Yet, it remains unknown to what degree the variation observed in beluga and narwhal echolocation is due to context-specific active biosonar adjustments made by the whales, the orientation of whales relative to the receiver, differences in sound propagation in the water, population- or individual-specific characteristics, and/or differences in sampling design, recording equipment, or data processing.

Between the two classification models presented in this study, the BANTER model proved to be the strongest classifier with a correct classification rate of 97.5%. The BANTER event classifier accurately predicted all beluga events (100%) and misclassified only two narwhal events (3.2%; Table 3.3). As a balanced design, the BANTER classifier does not bias towards either species, but it reveals that beluga events are more diagnosable evidenced by the correct prediction of all beluga events by the event classifier. This may occur because a higher proportion of the beluga events—the smaller sample size group—was randomly selected for the training dataset compared to the narwhal group across all *n* trees. Results from BANTER's two-stage approach identifies which frequency ranges contain the most useful information for species

classification. The call classifiers for detectors 2 (20–50 kHz) and 3 (50–70 kHz) were found to be the most important for BANTER's event classifier, suggesting clicks with peak frequencies between 20–70 kHz largely contained the information necessary for correct species assignment to acoustic events (Figure 3.5a,c). Higher frequencies attenuate faster than lower frequencies (Madsen & Wahlberg 2007); therefore, it is possible that the lower frequency classifiers (detectors 2 and 3) were the most important because lower frequency signals were detected more than higher frequency signals. These results also indicate that the BANTER model will be less affected by variations in detection distances between species that would more largely influence the higher frequency detector 4 and 5 classifiers.

While BANTER's call classifiers used acoustic parameters for predictors, the event classifier used mean assignment probabilities and detector proportions for predictors. The most important predictors for the event classifier were the mean assignment probabilities for detector 2 (Figure 3.4e). Given the reasonably high overall classification rate (85.4%) and vote distribution for the detector 2 call classifier, it is likely that the most important variables for this classifier were also important for the event classifier. For the detector 2 call classifier, the second peak frequency, frequency difference between the second and third peaks, and -3 dB center frequency were the most important variables for the classification of clicks (Figure 3.4d). Soldevilla *et al.* (2008) demonstrated that Risso's (*Grampus griseus*) and Pacific white-sided dolphins (*Lagenorhynchus obliquidens*) could be classified using spectral peak and notch patterns from echolocation clicks. Here, we similarly demonstrate the efficacy of using unique spectral properties to classify belugas and narwhals.

Our results from the single RF model demonstrate how a simple RF classifier using only echolocation parameters can still achieve a high correct species classification rate (92.6%). The

RF model accurately predicted beluga events more than narwhal events, with one beluga misclassification (5.3%) and five narwhal misclassifications (8.1%; Table 3.3). Much like the BANTER model, the lower misclassification rate of beluga events may be in part due to the unbalanced dataset; a higher proportion of the beluga events were randomly selected in the RF model because it was the smaller sample size group. However, it is also possible that beluga events contain more diagnosable features and thus yield higher classification scores. The most important acoustic parameters for species classification in the standard RF model differed from those in BANTER's detectors 2 and 3 call classifiers. Among all 20 acoustic parameters used in the RF model, frequency minimum (-3 dB and -10 dB) and peak frequency were the most important variables for species assignment (Figure 3.4b).

Using echolocation predictors for species classification is an effective approach, particularly given its primary sensory role for odontocetes. There is evidence for individual and group-specific call types among belugas (Vergara et al. 2010; Morisaka et al. 2013; Panova et al. 2016; Vergara & Mikus 2019) and narwhals (Ames et al. 2021), which contributes to the variation in their vocal repertoire but also makes acoustic classification challenging. However, it is likely that echolocation clicks are characterized by more stable features due to their sensory function. There are occasions where whales are only echolocating and not producing other call types (e.g., whistles, burst pulses) (Frouin-Mouy et al. 2017), and as such, a classifier that uses echolocation may offer more reliable year-round detections. While it is likely that the addition of other call types (e.g., burst pulses or whistles) would improve classification (Roch et al. 2015; Rankin et al. 2017), the BANTER classifier presented here demonstrates belugas and narwhals can be classified by clicks alone. Echolocation is increasingly being incorporated into PAM classification programs (Soldevilla et al. 2008; Baumann-Pickering et al. 2015; Rankin et al.

2017; Yang et al. 2020) and is specifically gaining traction for monitoring belugas(Castellote et al. 2013; Castellote et al. 2016; Zhong et al. 2020). Noise from ice floes, vessels, or industrial activities below 40 kHz can mask lower frequency social calls (e.g., Lammers et al. 2013; Halliday et al. 2021b). The broadband, high frequency nature of echolocation clicks is largely protected from masking by lower frequency anthropogenic sounds. As vessel traffic is expected to increase in the Arctic, echolocation may be a stronger metric for PAM classification.

Yet, the directionality and high-frequency nature of echolocation clicks pose their own limitations to species detectability and classification. Acoustic receivers will record echolocation sounds when the whale is facing the receiver but are unlikely to detect whales that are pointing their sonar beam away from the recorder. Narwhals are known to forage for Greenland halibut (*Reinhardtius hippoglossoides*) and *Gonatus* squid species at depths often > 1,000 meters in the winter (Laidre et al. 2003; Laidre et al. 2004), so they may be detected by seafloor recorders during these months. While belugas can dive to depths > 500 meters and reach the seafloor, they do not prey upon benthic species like narwhals; instead, they target fish species like the Arctic cod (*Arctogadus glacialis*) and polar cod (*Boreogadus saida*) that occupy shallower depths (Hauser et al. 2015; Lydersen & Kovacs 2021). Therefore, due to the differences in prey selection by belugas and narwhals, they may not be detected by seafloor recorders with the same confidence depending on the recording depth of the instrument. Additionally, the rapid attenuation of ultrasonic echolocation signals (Madsen & Wahlberg 2007) results in a smaller detection range for echolocation clicks (<1 km; Zahn et al. 2021a) compared to lower-frequency social calls. Multiple receivers and the inclusion of other call types (e.g., whistles) in the classifier may be required to detect whales at a sufficiently large spatial resolution. In addition to deploying more receivers, the instruments required to record echolocation clicks must record

higher frequencies with higher sampling rates, which typically depend on more battery power and memory storage. Ongoing development of acoustic receivers to be both economical and reliable will support monitoring populations using echolocation clicks at large scales.

This study provides a unique case in which the methods employed were identical for each species studied, so confounding variables that can substantially affect parameterization, like differences in the frequency responses of recording systems used (Roch et al. 2015), are absent. However, the data used to build the classifiers originated from a limited number of independent acoustic encounters: two beluga and five narwhal. When testing for the similarity between independent acoustic encounters using a BANTER framework, our results indicate that there is likely not a strong effect of encounter on species classification. Additional data from multiple, independent groups of whales are needed to more accurately reflect the true variation in beluga and narwhal echolocation. While we show it is possible to differentiate and classify belugas and narwhals using echolocation clicks, incorporating data from additional independent encounters and other call types will strengthen the classifier against any individual- or pod-specific acoustic characteristics that may be present.

Future work to test the BANTER classification model presented here will elucidate its efficacy for PAM applications. Acoustic recordings used in this study were collected with a hydrophone deployed off the ice-edge positioned at a depth of 12 meters. Assuming the new data follow the methodology employed here—including the recording equipment and sampling rate (500 kHz sampling rate; 16-bit resolution)—our model has the potential to be used on novel data. However, it remains unclear how effective the model presented here will be when data collected at depth, such as seafloor recorders where detectability of echolocation may decrease and recordings are expected to have a higher proportion of off-axis clicks, are applied. Additional

examination is needed to assess the degree to which differences in recording equipment (e.g., Scripps Institution of Oceanography High-frequency Acoustic Recording Package [HARPs] or Ocean Instruments' SoundTrap recorders) or receiver depth would affect the outcome of the presented classifier. Likewise, further consideration of which acoustic parameters are more stable across various equipment may mitigate effects of differing platforms (Roch et al. 2015; Rankin et al. 2017).

Insufficient data on beluga and narwhal populations has made it difficult to determine major threats to populations and thus hindered specific conservation efforts (Ragen et al. 2008). Narwhals have been identified as one of the most sensitive Arctic marine mammals to climate change due to their specialized habitat niche and restricted distribution range (Laidre et al. 2008). Both belugas and narwhals have been shown to have high site fidelity to their summering and wintering grounds, but little is known about what factors (e.g., prey availability or ice conditions) cause these behavior (Heide-Jørgensen et al. 2002; Laidre et al. 2004; Hauser et al. 2014). Furthermore, global climate warming is causing a lengthened open-water season in the Arctic that has galvanized opportunities for increased hydrocarbon exploration and commercial and recreational shipping development (Ragen et al. 2008; Huntington 2009; Overland & Wang 2013; Reeves et al. 2014). Some of the largest unexploited hydrocarbon reserves are found in the Arctic, particularly Baffin Bay (Gregersen et al. 2013; McCauley et al. 2017), and most global trade depends on maritime transport. Over half of the distribution ranges of the three endemic Arctic whale species overlaps with known or anticipated offshore hydrocarbon deposits (Reeves et al. 2014). Stakeholders of international trade and hydrocarbon exploration need to be informed of what regions are critical to belugas and narwhals for vital processes (e.g., calving, feeding, migrating) in order to mitigate industrial activities (Frouin-Mouy et al. 2017). Strict regulations

on vessel speed, appropriate shipping lanes, and types of permissible activities will be needed to avoid harmful consequences (Ragen et al. 2008).

As advances in PAM increase efficiency and robustness of data collection and analyses in the Arctic, present and future distributions of belugas and narwhals can be recorded with greater confidence and resolution, thereby improving efforts to monitor their changes in response to climate change and increased underwater noise. The multivariate nature of acoustic parameters lends itself to the interactive effects between variables, making methods like RF classifiers that can handle correlated variables robust for PAM species detection. BANTER increases classification accuracy beyond a standard RF model by using information from misclassifications at the call classification stage to inform the overall event classifier. Results from this study fill a critical data gap in the acoustic ecology of belugas and narwhals and provide a promising approach for future PAM programs. As recording systems advance and training datasets expand, classification programs such as the one presented here will develop greater predictive power and allow acousticians to reliably monitor Arctic odontocete populations long-term. Despite the variation in beluga and narwhal acoustic repertoires, our study suggests that the use of echolocation parameters for species classification may provide the most reliable method to differentiate these iconic species.

3.6 Acknowledgements

We are grateful to Niaqornat's community members and Greenland Institute of Natural Resources for their local support, Mikkel Villum Jensen for his help in the field, Air Greenland pilot Geir Akse for safe field operations, and the University of Tübingen and the German Oceanographic Museum Stralsund for providing recording equipment. We thank Jessica Crance, Taiki Sakai, and Dan Ovando for their support in implementing our analyses. We also thank Jay

Barlow and Angela Szesciorka for providing R script and Pina Gruden for providing Matlab code. Funding was provided by the U.S. Office of Naval Research on K. L. Laidre's grant (N00014-11-1-0201). The School of Aquatic and Fishery Sciences, University of Washington, and the Vetlesen Foundation supported M. J. Zahn.

3.7 Data Availability

All code used for model design and implementation are freely available via Github: https://github.com/mjzahn/beluga_narwhal_classifier.

3.8 SUPPLEMENTAL MATERIALS

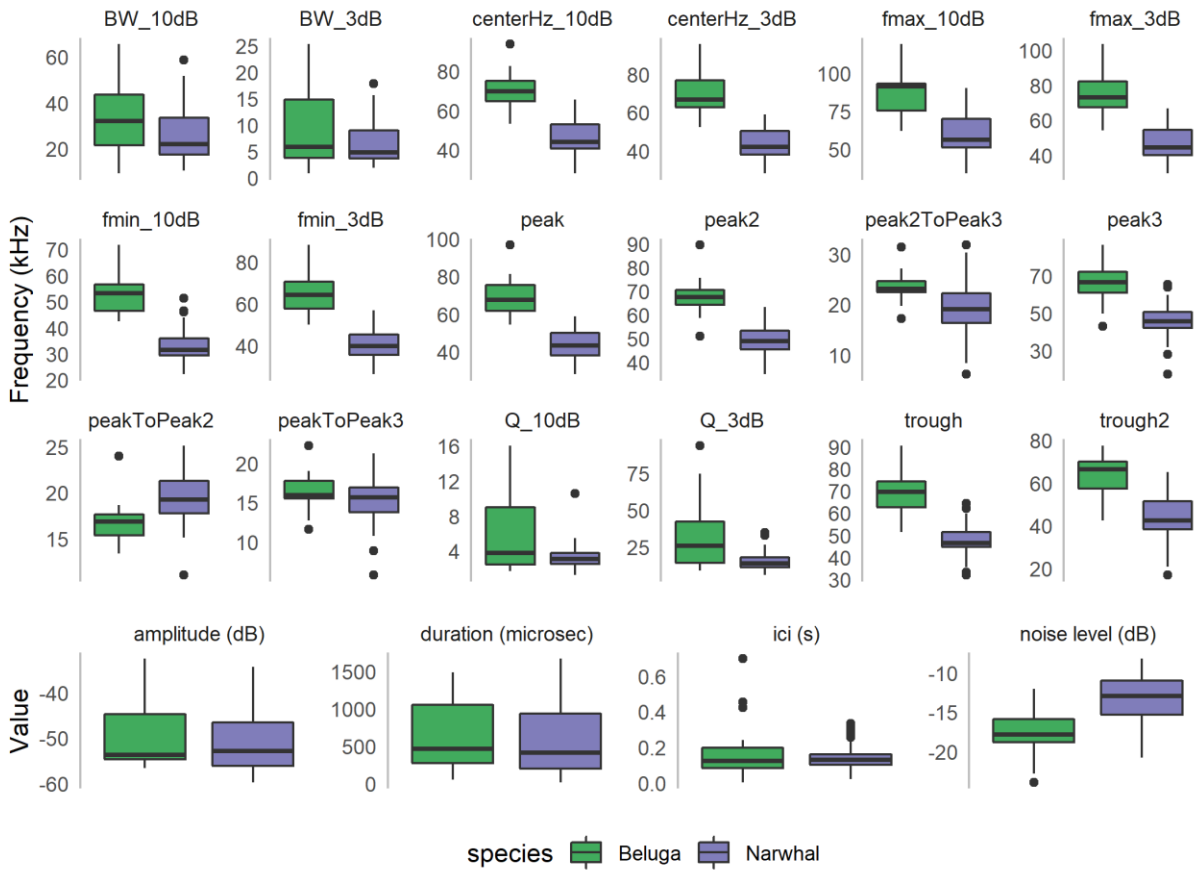

Figure S3.1. Beluga (green) and narwhal (purple) echolocation parameter variation for each of the variables calculated in the *PAMpal* R package. Click amplitude and noise level were not used in analyses.

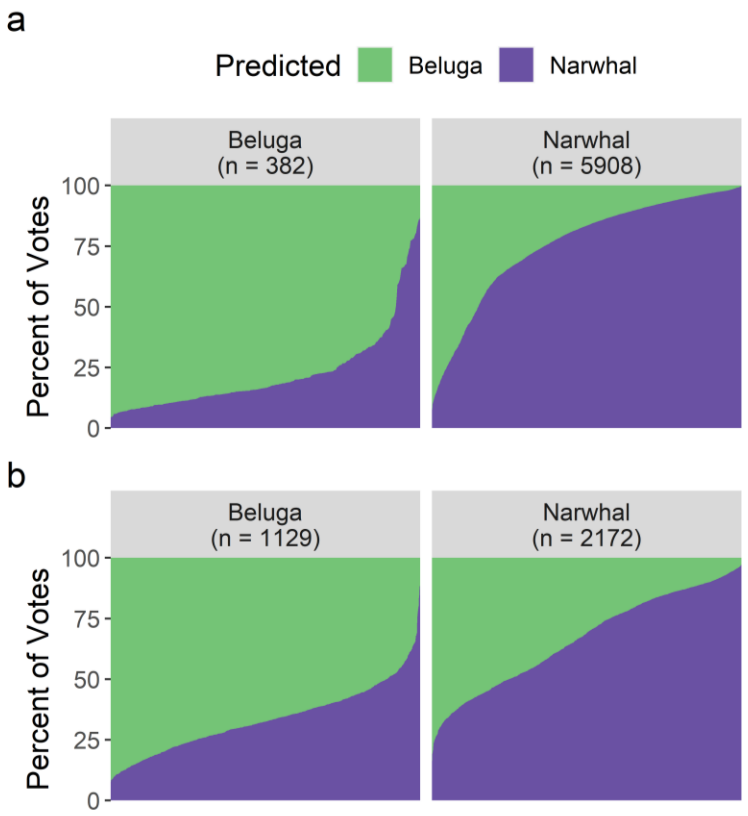

Figure S3.2. Distribution of model votes (beluga or narwhal classification) for each click that was assigned *a priori* to a species class for the detector 2 (a) and detector 3 (b) BANTER call classifiers. The distribution demonstrates the overall confidence of the call classifier results.

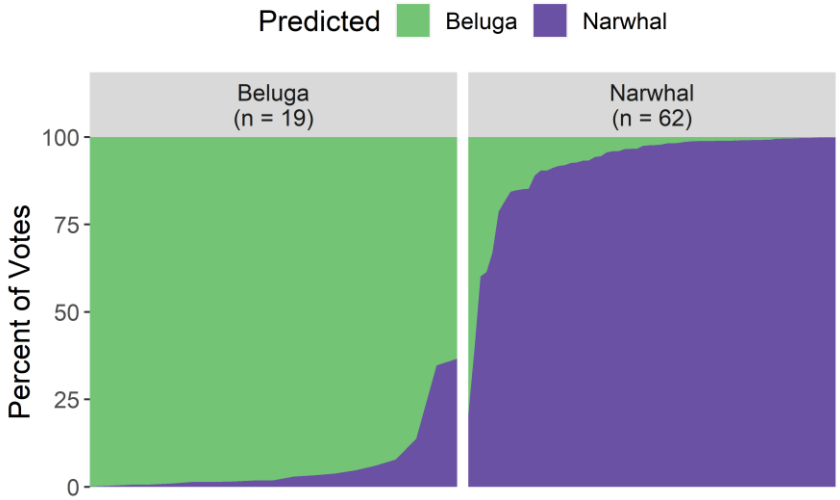

Figure S3.3. Distribution of model votes (beluga or narwhal classification) for each event that was assigned *a priori* to a species class. The distribution demonstrates the overall confidence of the BANTER event classifier results.

Table S3.1. Summary of the number of echolocation clicks assigned to each acoustic event in PAMGuard for each species (N = narwhal; B = beluga).

Event	Species	# Clicks	Event	Species	# Clicks
1	N	17	42	N	462
2	N	65	43	N	49
3	N	280	44	N	252
4	N	27	45	N	279
5	N	20	46	N	26
6	N	17	47	N	64
7	N	39	48	N	204
8	N	444	49	N	364
9	N	131	50	N	208
10	N	6	51	N	472
11	N	203	52	N	41
12	N	111	53	N	126
13	N	158	54	N	52
14	N	284	55	N	274
15	N	401	56	N	235
16	N	119	57	N	239
17	N	48	58	N	11
18	N	93	59	N	24
19	N	130	60	N	17
20	N	238	61	N	18
21	N	71	62	N	13
22	N	155	63	B	120
23	N	52	64	B	57
24	N	31	65	B	10
25	N	117	66	B	20
26	N	14	67	B	292
27	N	337	68	B	928
28	N	608	69	B	37
29	N	6	70	B	20
30	N	14	71	B	183
31	N	305	72	B	498
32	N	137	73	B	89
33	N	102	74	B	19
34	N	266	75	B	16
35	N	28	76	B	24
36	N	150	77	B	18
37	N	8	78	B	12
38	N	55	79	B	171
39	N	22	80	B	13
40	N	57	81	B	11
41	N	134			

Table S3.2. PerMANOVA and PERMDISP test results on z-score transformed data to assess the differences between beluga and narwhal echolocation. The asterisk (*) indicates a statistically significant result ($P < 0.05$).

	df	SSE	MSE	*F*	R^2	*P*-value
PerMANOVA						
Species	1	418.78	418.78	42.35	0.35	0.001*
Residuals	79	781.22	9.89		0.65	
Total	80	1200.00			1.00	
PERMDISP						
Groups	1	12.95	12.95	8.37		0.004*
Residuals	79	122.17	1.55			
Total	80	135.12				

Table S3.3. Descriptions of predictors used for BANTER's event classifier. Values for these predictors are determined from BANTER's call classifier. The 'X' in variable codes is a placeholder for either 'beluga' or 'narwhal.'

Variable Code	Description
Det2.X	Mean probability that Detector 2 clicks (20–50 kHz) for a given event will be assigned to species X
Det3.X	Mean probability that Detector 3 clicks (50–70 kHz) for a given event will be assigned to species X
Det4.X	Mean probability that Detector 4 clicks (70–100 kHz) for a given event will be assigned to species X
Det5.X	Mean probability that Detector 5 clicks (100–150 kHz) for a given event will be assigned to species X
prop.Det2	Proportion of Detector 2 clicks (20–50 kHz) for a given event
prop.Det3	Proportion of Detector 3 clicks (50–70 kHz) for a given event
prop.Det4	Proportion of Detector 4 clicks (70–100 kHz) for a given event
prop.Det5	Proportion of Detector 5 clicks (100–150 kHz) for a given event
Det2.ici	Time interval (in sec) between consecutive clicks for only Detector 2 clicks; mode approximated for each event
All.ici	Time interval (in sec) between consecutive clicks across all detectors; mode approximated for each event

Table S3.4. Results for the correlation test to examine the similarity between independent acoustic encounters. Each row corresponds to a separate BANTER classification model that used one encounter for each species as training data (10 unique combinations). The number of events comprising each encounter and out-of-bag (OOB) percent correct classification rsates (95% confidence interval) for model performance are reported. The correlation between the validation confusion matrices (made predictions on encounters that were not used in the training model) and the training model confusion matrices indicates degree of similarity between encounters.

Encounter ID		# Events		Training model correct classification (95% CI)	Confusion matrix correlation
Beluga	Narwhal	Beluga	Narwhal		
2	4	16	2	94.4% (72.7 – 99.9%)	-0.54
2	3	16	8	95.8% (78.9 – 99.9%)	0.08
2	6	16	8	91.7% (73.0 – 99.0%)	0.12
7	4	3	2	100% (47.8 – 100%)	0.37
2	5	16	14	100% (88.4 – 100%)	0.53
7	5	3	14	100% (80.5 – 100%)	0.63
2	1	16	30	97.8% (88.5 – 99.9%)	0.82
7	6	3	8	90.9% (58.7 – 99.8%)	0.83
7	1	3	30	100% (89.4 – 100%)	0.96
7	3	3	8	100% (71.5 – 100%)	0.98

Chapter 4. ACCURATE SPECIES CLASSIFICATION OF ARCTIC TOOTHED WHALE ECHOLOCATION CLICKS USING ONE-THIRD OCTAVE RATIOS

4.1 ABSTRACT

Passive acoustic monitoring has been an effective tool to study cetaceans in remote regions of the Arctic. Here, we improve and validate methods to acoustically identify the only two Arctic toothed whales, the beluga (*Delphinapterus leucas*) and narwhal (*Monodon monoceros*), using echolocation clicks. Performance of an acoustic classifier was tested with long-term datasets from moorings in Northwest Greenland, and it correctly predicted >94% of acoustic events. Visual species identification was possible using spectrograms where beluga clicks had most energy >30 kHz and narwhal clicks had a sharp lower frequency limit near 20 kHz. We then compared changes in one-third octave levels (TOL) between two pairs of one-third octave bands from over one million click spectra. Narwhal clicks had a steep increase between the 16 and 25 kHz TOL bands that was absent in beluga click spectra. Conversely, beluga clicks had a steep increase between the 25 and 40 kHz TOL bands that was absent in narwhal click spectra. Random Forest classification models built using TOL statistics accurately predicted the species identity of acoustic events (100%). Our findings support the use of echolocation TOL profiles in future automated click detectors and classifiers for acoustic monitoring of Arctic toothed whales.

4.2 INTRODUCTION

In the Arctic, passive acoustic monitoring enables observations of biotic and abiotic processes over spatiotemporal scales that would otherwise be unfeasible (e.g., Halliday et al. 2021a; Mattmüller et al. 2022; Stafford et al. 2022). Notably, observations of cetacean occurrence acquired from passive acoustic data provide key information about changes in habitat-use and timing of life history events, or phenology, of Arctic species due to climate change (Ahonen et al. 2021; Stafford et al. 2021; Moore et al. 2022). The Arctic has warmed at rates more than three times the global mean, and sea ice extent at its September minimum has declined by more than 12% per decade (Onarheim et al. 2018; relative to 1981–2010 mean; IPCC, 2022; Rantanen et al. 2022). Greater accessibility in Arctic waters has spurred increased human activities, such as commercial shipping and oil and gas exploration, that have heightened underwater noise levels and the risk of acoustic disturbance (e.g., behavioral changes, masking, or hearing damage) to marine mammals (Finneran et al. 2002; Erbe et al. 2016; Halliday et al. 2020; Southall et al. 2021). Studies using passive acoustics effectively track changes to natural and anthropogenic sounds, but they require knowledge of unique properties of specific sounds to accurately identify them in recordings. Given the efficacy and need for long-term passive acoustic monitoring in the Arctic, a firm understanding of acoustic parameters must be established for key species to ensure reliable acoustic classification.

Narwhals (*Monodon monoceros*) and belugas (*Delphinapterus leucas*) are ice-associated Arctic toothed whales (Monodontidae family). Narwhals inhabit waters in the Atlantic sector of the Arctic around Greenland, Canada, Svalbard, and Russia, while the beluga range is circumpolar and extends into subarctic territories (Innes et al. 2002; Reeves et al. 2014; Hobbs et al. 2019). Migratory belugas and narwhals follow the annual sea ice cycle where their autumn

southward and spring northward movements are linked to sea ice advance and retreat, respectively. They return to the same summer and winter locations with high site fidelity, particularly the narwhal (Dietz et al. 2001; Innes et al. 2002; Heide-Jørgensen et al. 2003a). Phenological and distribution shifts have been documented for both species where animals are departing later during years with delayed sea ice freeze-up and expanding their range (Nielsen 2009; Heide-Jørgensen et al. 2010; Hauser et al. 2017a; Louis et al. 2020; Shuert et al. 2022). Further, narwhals have been shown to be extremely sensitive to ship noise and seismic airgun pulses (Heide-Jørgensen et al. 2021; Williams et al. 2022; Radtke et al. 2023; Tervo et al. 2023) and are considered one of the most sensitive Arctic marine mammals to climate change due to their preference for cold waters and specialization in habitat and prey (Laidre et al. 2008; Heide-Jørgensen et al. 2020). Belugas are also strongly affected by anthropogenic noise disturbance (Lesage et al. 1999; Erbe & Farmer 2000; Halliday et al. 2021b) and some stocks have had significant declines from cumulative climate and anthropogenic stressors (Hobbs et al. 2019; Lesage 2021).

Narwhals and belugas have been studied using short- and long-term passive acoustic methods (Schevill & Lawrence 1949; Au et al. 1985; Møhl et al. 1990; Marcoux et al. 2011; Lammers et al. 2013; e.g., Ahonen et al. 2019). Both species are highly social with complex community structures, and accordingly, individuals produce a variety of vocalizations to interact with conspecifics and sense their environment. Call types produced by these whales are broadly categorized into whistles, pulsed calls (or “burst pulses”), and combined calls that contain both pulsed and tonal sounds (Blackwell et al. 2018). Vocalizations produced for sensory tasks (e.g., navigation and prey localization) include echolocation clicks and terminal buzzes that are found at the end of click sequences (Roy et al. 2010; Blackwell et al. 2018; Castellote et al. 2021;

Chambault et al. 2023). Pulsed calls and buzzes are defined by their short duration and high-repetition rate signals. Although there is a considerable body of literature studying their sounds, beluga and narwhal vocalizations remain partially described due to recording limitations and the diversity in their social calls within and between subpopulations (Sjare & Smith 1986b; Marcoux et al. 2012; Garland et al. 2015). For regions where belugas and narwhals overlap in West Greenland and the Canadian High Arctic, distinguishing between their vocalizations is essential for passive acoustic monitoring of these two species.

Scientific studies have historically estimated key acoustic parameters for each species individually (Au et al. 1985; Au et al. 1987; Møhl et al. 1990; Miller et al. 1995; Roy et al. 2010; Stafford et al. 2012; Rasmussen et al. 2015; Koblitz et al. 2016; Zahn et al. 2021a). The first direct species comparison was done by Frouin-Mouy et al. (2017) where they examined beluga and narwhal recordings and found narwhal clicks had a substantial increase in energy between the 16 and 20 kHz one-third octave bands which was lacking in beluga clicks. Jones et al. (2022) presented differences in two key parameters (peak frequency and inter-click interval). It is now well established that beluga and narwhals produce high-frequency, broadband clicks from ~20 kHz to well over 100 kHz (Rasmussen et al. 2015; Koblitz et al. 2016; Zahn et al. 2021a), and beluga clicks contain more energy at higher frequencies (>40 kHz) than narwhal clicks (Frouin-Mouy et al. 2017; Zahn et al. 2021b; Jones et al. 2022). Outside of descriptive statistics, Zahn et al. (2021b) reported the first attempt to automatically classify beluga and narwhal clicks from parameter estimates using machine learning Random Forest (RF) models.

Here, we build on previous work and verify methods to classify beluga and narwhal clicks using manual and automated approaches on recordings from passive acoustic instruments mounted near glacier fronts in Northwest Greenland. Our primary objectives were twofold: 1)

test the narwhal and beluga acoustic classifier developed by Zahn et al. (2021b) with new acoustic data recorded with receivers and sampling rates that differed from the model's training data, and 2) investigate the predictive capacity of two additional model parameters derived from one-third octave levels (TOL). The first objective investigated whether a classifier trained with data from high sampling rate recordings could predict observations from lower sampling rate recordings. Our findings provide an important step in automating beluga and narwhal detection in long-term acoustic recordings using echolocation signals, and thus improve methods to monitor these species.

4.3 METHODS

4.3.1 *Study Area*

This study was conducted in Northwest Greenland and was part of a larger project to study the ecological importance of narwhal summering grounds in Melville Bay (Figure 4.1). Melville Bay (Greenlandic: *Qimusseriarsuaq*) is found on the northwest Greenland continental shelf (74°N – 76.5°N) with a large trough that opens southwest into Baffin Bay. Both belugas and narwhals utilize regions along the eastern portion of Baffin Bay throughout the year. The Eastern High Arctic-Baffin Bay beluga stock occupies estuaries, bays, and inlets in the Canadian Arctic Archipelago during summer months (Hobbs et al. 2019). Over winter, a portion of the stock resides in the North Water polynya while the majority travel south during fall along the West Greenland coast remaining in mostly ice-free waters (Doidge & Finley 1993; Richard et al. 1998b; Richard et al. 1998a; Heide-Jørgensen et al. 2003b). The Melville Bay narwhal stock spends summer months near glacier fronts in Melville Bay and migrates south to overwinter in the dense pack-ice of Baffin Bay and Davis Strait (Dietz & Heide-Jørgensen 1995; Dietz et al. 2008; Laidre & Heide-Jørgensen 2011; Laidre et al. 2016). Narwhals are temporary summer

residents of Melville Bay. Belugas transit through the area during their fall and spring migrations.

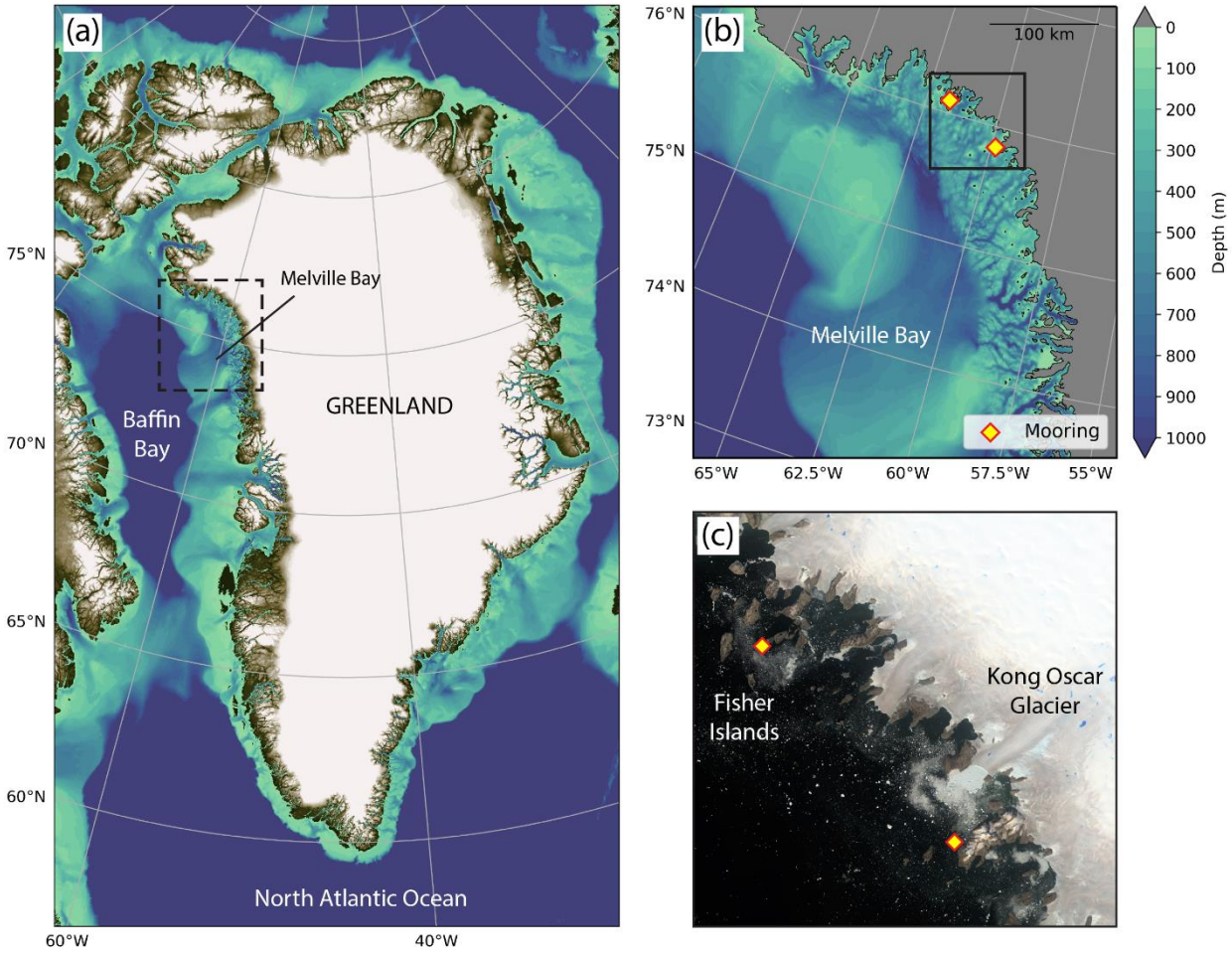

Figure 4.1. Map of the study region in Melville Bay, Northwest Greenland (a). The dashed outline in (a) demarcates the region (b), and the black box in (b) shows the region displayed in (c). Ocean mooring locations are marked with yellow diamonds (b, c). Mooring positions near Kong Oscar glacier and in the Fisher Islands are shown on a Landsat 8 image converted to natural color from 18 August 2019 (c) courtesy of the U.S. Geological Survey. Ocean bathymetry (a, b) is from the International Bathymetric Chart of the Arctic Ocean (Jakobsson et al. 2012).

4.3.2 *Acoustic Data Collection*

Between 2019 and 2020, three seafloor-mounted ocean moorings were deployed from the R/V *Sanna* (Greenland Institute of Natural Resources) near glacier fronts in Melville Bay. Each mooring was equipped with a sound recorder and an array of oceanographic sensors to study the habitat of narwhals during summer. Instruments and floats were attached to 6 mm Dyneema line, and an 800 kg anchor connected to an acoustic release (PORT LF, Edgetech Instruments) mounted the mooring to the seafloor. After deployment in August 2019, one mooring was destroyed by icebergs and two were successfully retrieved in August 2020. These two moorings were positioned in the Fisher Islands and in front of Kong Oscar glacier, also known as Nuussuup Sermia (Figure 4.1). We refer to these mooring locations as the Fisher Islands and Kong Oscar sites.

Moorings included SoundTrap ST500 STD (Ocean Instruments, New Zealand) acoustic recorders (Table 4.1). The SoundTrap instruments sampled at 144 kHz (16-bit) with a Nyquist frequency of 72 kHz to record beluga and narwhal echolocation clicks that contain most of their energy above 20 kHz (Koblitz et al. 2016; Frouin-Mouy et al. 2017; Zahn et al. 2021a; Jones et al. 2022). Specifications of the SoundTrap ST500 STD recorders included a system peak clipping level of 173 dB re µPa, bandwidth of 20 Hz to 60 kHz (±3 dB), and self-noise <36 dB re 1 µPa above 2 kHz and better than sea-state zero at 100 Hz to 2 kHz. Acoustic data were logged 40 minutes per hour. This duty cycle was selected to ensure the recorders maximized recording coverage each hour while retaining sufficient battery to last into winter, well after the area was covered in fast ice and whales had departed.

Table 4.1. Summary of acoustic data collected from the moored SoundTrap ST500 STD recorders in Melville Bay.

Site	Recording period	Latitude (°N)	Longitude (°W)	Seafloor depth (m)	Sampling rate (kHz)	Duty cycle	Instrument depth (m)
Fisher Islands	5 Aug 2019 – 20 Dec 2019	76.1038	61.7270	370	144	40 min/hr	194
Kong Oscar	5 Aug 2019 – 16 Jan 2020	75.8418	59.8431	250	144	40 min/hr	158

4.3.3 *Acoustic Data Processing and Species Assignment*

Raw acoustic data were processed using the open-source passive acoustic monitoring software PAMGuard (version 2.02.09; Gillespie et al. 2008). Echolocation clicks were detected using PAMGuard's Click Detector when the amplitude of a transient signal exceeded 14 dB above the measured background noise. Subsets of the SoundTrap data were processed to adjust filter settings and determine an effective approach to reduce false detections (i.e., noise) while maximizing the detection of echolocation clicks. A 4-pole Butterworth 1 kHz high pass filter ("digital pre filter" in PAMGuard) was applied to remove a low frequency noise peak. Then, a 4-pole Butterworth 20 kHz high pass filter ("digital trigger filter") was applied for click detection. Signal waveforms from click detections were labeled and extracted from the 1 kHz high pass filtered data for subsequent analysis.

Following the click detection stage, sound clips were labeled according to their peak frequency from power spectra within PAMGuard. Each classifier, or detector, in PAMGuard categorized clicks with a unique numeric code (i.e., detector number) when their peak frequencies fell within a specified frequency range. For consistency, we used the same classifier set as in Zahn et al. (2021b) but removed detectors 4 (70–100 kHz), 5 (100–150 kHz), and 6

(150–250 kHz) since the upper limit of the SoundTrap recording bandwidth was 72 kHz. Accordingly, detectors 1 (4–20 kHz), 2 (20–50 kHz), and 3 (50–70 kHz) labeled detections when clicks had peak frequencies within the respective target frequency range. Initial processing of the data revealed that detector 1 included only false detections (i.e., non-echolocation sounds), so only detectors 2 and 3 were enabled for downstream analyses. Further inspection of false detections showed that power spectra from transient noise signals decreased in energy with increasing frequency. Therefore, to further reduce abiotic transient sounds (e.g., ice or glacier calving), an additional constraint was added to detector 2 whereby clicks were only labeled as echolocation clicks when there was a >5 dB difference in energy between 10–20 kHz and 30–40 kHz. Unclassified detections (detector 0) were discarded.

Detections identified and labeled as clicks within PAMGuard were then processed into hourly acoustic events using the *PAMpal* package (version 1.0.4; Sakai 2021) in R (version 4.3.1; R Core Team 2023). Upon ingestion of the PAMGuard detector output into R, twenty acoustic parameters were calculated for each detection using a fast Fourier transform (FFT) window length of 2.5 ms (360 samples). Due to the close proximity of the moorings to glacier termini, ambient noise levels were high for frequencies extending up to 20 kHz. A 4-pole 20 kHz Butterworth high pass filter was applied to remove the prevailing noise signal before calculating echolocation parameters. Any corner frequency below this drastically increased the risk of noise peaks rising above echolocation signal peaks and yielding erroneous variable estimates. Narwhal clicks can contain energy between 3.5–5 and 7–14 kHz (Stafford et al. 2012), but these components are relatively low in energy and thus echolocation peak frequencies are expected to be above 20 kHz. A full parameter list with descriptions is provided in Supplementary Material Table S4.1. Click parameter estimation by *PAMpal* follows methods outlined by Griffiths et al.

(2020) and Soldevilla et al. (2008) and further information about the process used can be found in the R package documentation (Sakai 2023). Detections were binned into 1-hour long acoustic events with unique identification numbers. Each event contained all the detections that occurred within a given hour from the start to end date of the recording period for each site (Table 4.1). Events that had fewer than 30 detections were found to generally contain only false detections and were removed.

Concatenated click spectrograms and mean power spectra for all acoustic events were manually examined to identify each event's source and classify them as beluga or narwhal. Events that contained only noise from crackling sea ice, glacier ice, and calving were removed from subsequent classification analyses. Beluga and narwhal events were identified based on differences in the energy distribution of each species' clicks in the frequency domain. Belugas produce higher frequency clicks compared to those generated by narwhals as demonstrated by estimated peak frequencies being consistently >20 kHz higher in beluga clicks than narwhal clicks (Koblitz et al. 2016; Zahn et al. 2021a; Zahn et al. 2021b; Jones et al. 2022). This is partly because narwhal clicks have considerably more energy between 20–30 kHz than beluga clicks (Frouin-Mouy et al. 2017; Jones et al. 2022). Beluga clicks also do not contain a low frequency component that is sometimes observed in narwhal echolocation between 3 and 14 kHz (Stafford et al. 2012). For events where species designation was in doubt from concatenated click spectrograms or mean spectra, raw sound file spectrograms were manually audited in Raven Pro (version 1.6.5; K. Lisa Yang Center for Conservation Bioacoustics at the Cornell Lab of Ornithology 2023). Additionally, the presence of whistles aided manual species designation. Marcoux et al. (2012) describe beluga whistles as having more diversified contours than those produced by narwhals (Sjare & Smith 1986b; e.g., Belikov & Bel'Kovich 2007). The presence of

highly variable whistles below 20 kHz along with high frequency echolocation (click energy mainly >30 kHz) supported beluga species assignment. Finally, manually classified events were compared with an independently labeled dataset from a different human analyst of the same recordings at a 6-hour resolution to ensure no whale detections were missed or incorrectly classified.

4.3.4 *TOL Statistics*

Upon completion of the manual species classification for all acoustic events, the difference in the spectral distribution of energy between beluga and narwhal clicks was visually explicit in concatenated click spectrograms and mean spectra. In order to quantify this observed difference, we built upon methods developed by Frouin-Mouy et al. (2017) and calculated the TOL difference between two sets of one-third octave bands in R (version 4.3.1; R Core Team 2023). One-third octave band-edge frequencies were calculated using the American National Standards Institute (ANSI) standard base-ten center frequencies also known as decidecade bands (ANSI, 2004). Three one-third octave bands were selected that best represented differences in spectral energy within the recording frequency bandwidth for the two species: 16 kHz (14,125–17,783 Hz), 25 kHz (22,387–28,184 Hz), and 40 kHz (35,481–44,668 Hz). We refer to these one-third octave bands by their nominal center frequencies throughout in lieu of the actual frequency range for simplicity. In this study, we considered whether the TOL in narwhal clicks consistently increased between 16 to 25 kHz with little difference between 25 to 40 kHz. Conversely, beluga clicks were expected to have little difference between 16 to 25 kHz and a large TOL difference between 25 to 40 kHz.

For TOL calculations, 1 kHz high pass filtered waveforms extracted from PAMGuard were analyzed and mean power spectra were produced for each acoustic event (512 pt FFT). The

TOL was calculated by summing the squared pressures within the upper and lower one-third octave limits from mean spectra. Then the difference was computed between the 1) 16 and 25 kHz and 2) 25 and 40 kHz one-third octave bands. The result was two TOL ratios with potential use in beluga and narwhal click classification. Hereafter we refer to these two metrics as the 16 to 25 kHz TOL ratio and 25 to 40 kHz TOL ratio.

4.3.5 *Acoustic Classification Model Testing*

Manual species identification of SoundTrap recordings from the Fisher Islands and Kong Oscar sites yielded two labeled datasets of hourly acoustic events. Parameter values calculated for all clicks contained in these events (see Methods Section C) were used to test the performance of the model developed by Zahn et al. (2021b). Zahn et al. (2021b) used the BANTER (Bio-Acoustic eveNT classifiER) model which is a two-stage classifier consisting of many RF models with the capacity to incorporate several call types (Breiman 2001; Rankin et al. 2017). The BANTER model in Zahn et al. (2021b) was trained using data from hand-dipped Reson TC4013-5 receivers (500 kHz sampling rate; sensitivity -215 dB ± 2 dB re 1 V/µPa; flat ± 2 dB frequency response 1–150 kHz) deployed in beluga and narwhal wintering grounds in Baffin Bay during March 2013 (see Methods in Zahn et al. 2021b). Since the Nyquist frequency of the Reson recordings was more than three times the Nyquist frequency of the SoundTrap recordings, the BANTER model was modified to only include detectors 2 and 3 (20–50 and 50–70 kHz, respectively) to match the classifier set applied to the SoundTrap dataset (see Methods Section C). Therefore, only clicks with peak frequencies between 20–70 kHz from Reson recordings were used to train the BANTER model. The BANTER training data were not decimated since this study aimed to see whether a model trained with data recorded at a high sampling rate could predict observations recorded at a lower sampling rate.

RF models use bootstrap sampling to build thousands of decision trees to produce a final ensemble tree. Random subsets drawn and used as training data are referred to as “in-bag” samples and the remaining observations are called “out-of-bag” (OOB) samples. OOB samples are used as testing data to estimate model prediction errors and accuracy. The BANTER model was used to predict the species of the Fisher Islands and Kong Oscar SoundTrap acoustic events separately in case there were site-specific differences.

Since TOL ratio statistics (see Methods Section D) provided a promising new metric to differentiate beluga and narwhal clicks, we added the 16 to 25 kHz and 25 to 40 kHz TOL ratios as event level measures to the BANTER model for potential improvement. Adding the TOL ratio event level variables to the BANTER model did not change the OOB correct classification rate during model development compared to the base model without TOL ratio variables. As with the base BANTER model without TOL ratio variables, the BANTER model with the newly added event level measures was used to predict acoustic events from the Fisher Islands and Kong Oscar sites separately.

We also evaluated the predictive strength of the TOL ratio metrics by building single RF models using only those two variables (16 to 25 kHz and 25 to 40 kHz TOL ratios). Three RF models were built using different training datasets that included TOL ratio estimates from: 1) Fisher Islands and Kong Oscar (pooled), 2) Fisher Islands, and 3) Kong Oscar. RF models have three primary parameters that can be adjusted: *mtry* defines the number of randomly selected variables used to split observations at each node, *sampsize* indicates the number of observations (i.e., acoustic events) that are randomly subset to build each tree, and *ntree* specifies how many individual trees are built in the forest. Since we were using two variables for classification, the only possible value for *mtry* was one. To evaluate model sensitivity to *sampsize*, each model was

fit over all possible values of *sampsize* and model accuracies were determined. For the RF models developed, the accuracies varied by less than 0.01% and therefore were not sensitive to permutations in *sampsize*. As in Zahn et al. (2021b), we report model results when *sampsize* was equal to half the total sample size for the smallest (i.e., minority) species class. RF models were configured such that equal subsamples were drawn from each species group without replacement to account for unbalanced datasets and prevent overfitting to the majority class. Models were constructed with ten thousand trees (*ntree*) and model stability was confirmed. All acoustic classification model development and evaluation for BANTER and RF models were conducted using the *banter* (version 0.9.6; Rankin et al. 2017), *randomForest* (version 4.7-1.1; Liaw & Wiener 2002), and *rfPermute* (version 2.5.1; Archer 2021) packages in R.

The Fisher Islands and Kong Oscar datasets functioned as complimentary training and testing datasets. Thus, site-specific RF models were tested with a dataset different from the one used to train the model. The Fisher Islands RF model was used to predict Kong Oscar acoustic events and the Kong Oscar RF model was used to predict Fisher Islands acoustic events. In RF classification models, observations (i.e., acoustic events) are assigned to a class (i.e., species) based on the percentage of trees in the forest voting for each species. For all models, the uncertainty of model predictions was evaluated by examining the distribution of votes for each acoustic event within a species class. Acoustic events were predicted with high model certainty when a majority of the trees voted for the correct species class.

4.4 RESULTS

4.4.1 *Manual Species Identification*

SoundTrap instruments recorded for 138 days (~4.5 months; 5 August–20 December 2019) at the Fisher Islands site and 165 days (~5.5 months; 5 August 2019–16 January 2020) at the Kong Oscar site. With a duty cycle of 40 minutes per hour, recordings totaled approximately 4,848 hours (~6.7 months) across sites. The PAMGuard Click Detector identified echolocation clicks including buzzes as well as non-echolocation high repetition rate calls, referred to in the literature as burst pulses, or pulsed calls (Figure 4.2). The low frequency component of narwhal clicks was visible between 3–5 kHz in some concatenated click spectrograms, possibly when whales were close to the moorings and the signal-to-noise ratio was high. During manual inspection of echolocation events using Raven Pro, lower frequency (<20 kHz) beluga whistles were observed in some events (Figure 4.2). However, echolocation clicks remained the dominant call type produced by both species over the recording period.

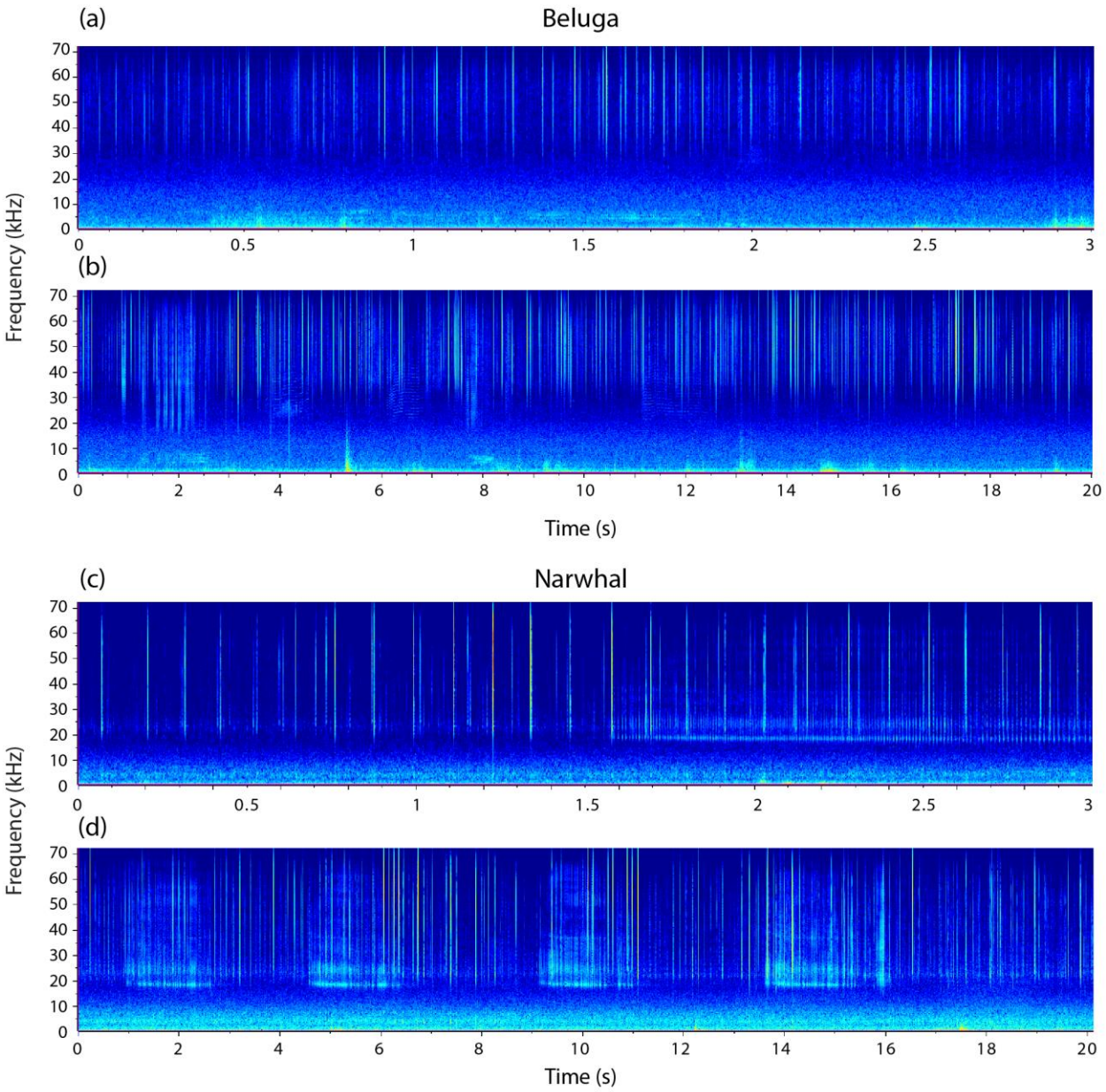

Figure 4.2. Selected spectrograms showing beluga (a, b) and narwhal (c, d) echolocation clicks with lighter and darker colors indicating higher and lower sound levels, respectively. All samples were recorded at the Fisher Islands site. Panels (a) and (b) also include beluga whistles in the 5–10 kHz range and (b) shows a few beluga pulsed calls. Panels (c) and (d) show narwhal burst pulses and echolocation click trains. Spectrograms were produced using a Hanning window, 50% overlap, and 512 point FFT for (a, c) and 1024 point FFT for (b, d) in Raven Pro 1.6.5. Note: the duration of the spectrogram (in seconds) differs between subplots with one short (3 sec) and one long (20 sec) duration example for each species.

Manual species identification of hourly acoustic event data revealed a clear visible difference between beluga and narwhal echolocation. Beluga clicks contained energy above 30 kHz with peak intensities typically occurring between 40–60 kHz (Figure 4.3). We note that true spectral peaks occurring in the 60–72 kHz range could not be identified due to the SoundTrap anti-aliasing filter having a -3 dB cut-off frequency at 64.8 kHz. Narwhal clicks consistently presented a relatively sharp low-frequency cut-off around 20 kHz (Figure 4.3) including signals produced during burst pulses and buzzes (Figure 4.2). Although the exact frequency of this lower limit varied between approximately 18 to 23 kHz, the presence of a steep increase in energy around 20 kHz provided an explicit method to distinguish narwhal clicks from those of beluga. A full catalogue of labeled beluga and narwhal acoustic event concatenated click spectrograms and mean spectra showed clear differences between species (Zahn et al. 2023).

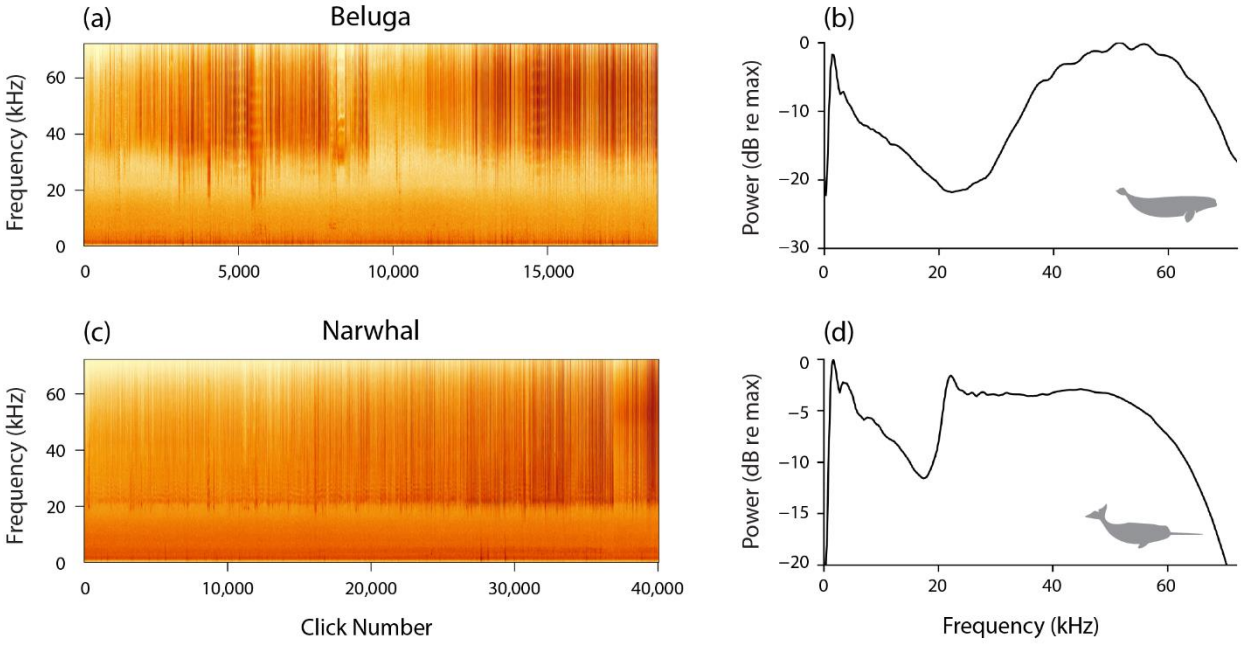

Figure 4.3. Concatenated click spectrograms (a, c) and mean power spectra (b, d) for example beluga (a, b) and narwhal (c, d) acoustic events. The number of clicks included in each concatenated click spectrogram is provided on the x-axis (a, c). Spectrograms and spectra were produced using a 512 point FFT and Hanning window from 1 kHz high pass waveforms.

Belugas and narwhals were detected at both the Fisher Islands and Kong Oscar sites, however the majority of detections were, by far, narwhal (92%). From the more than 6 months of acoustic data, which was divided into 1-hour time bins, a total of 201 hours contained narwhal and beluga clicks. From PAMGuard's click detectors 2 and 3 (i.e., clicks with peak frequencies between 20–50 and 50–70 kHz, respectively), there were more detections in total, and for each species, at the Fisher Islands site (117 events total; 776,679 detections) than the Kong Oscar site (84 events total; 241,920 detections). At the Fisher Islands, 12 events (141,098 detections) were beluga and 105 were narwhal (635,581 detections). At the Kong Oscar site, 4 events were beluga (1,653 detections) and 80 events were narwhal (240,267 detections). Narwhals were present in Melville Bay from the start of the recording period in early August until mid-November when

fall sea ice formation began (Figure 4.4). Belugas were detected only during the month of October (Figure 4.4).

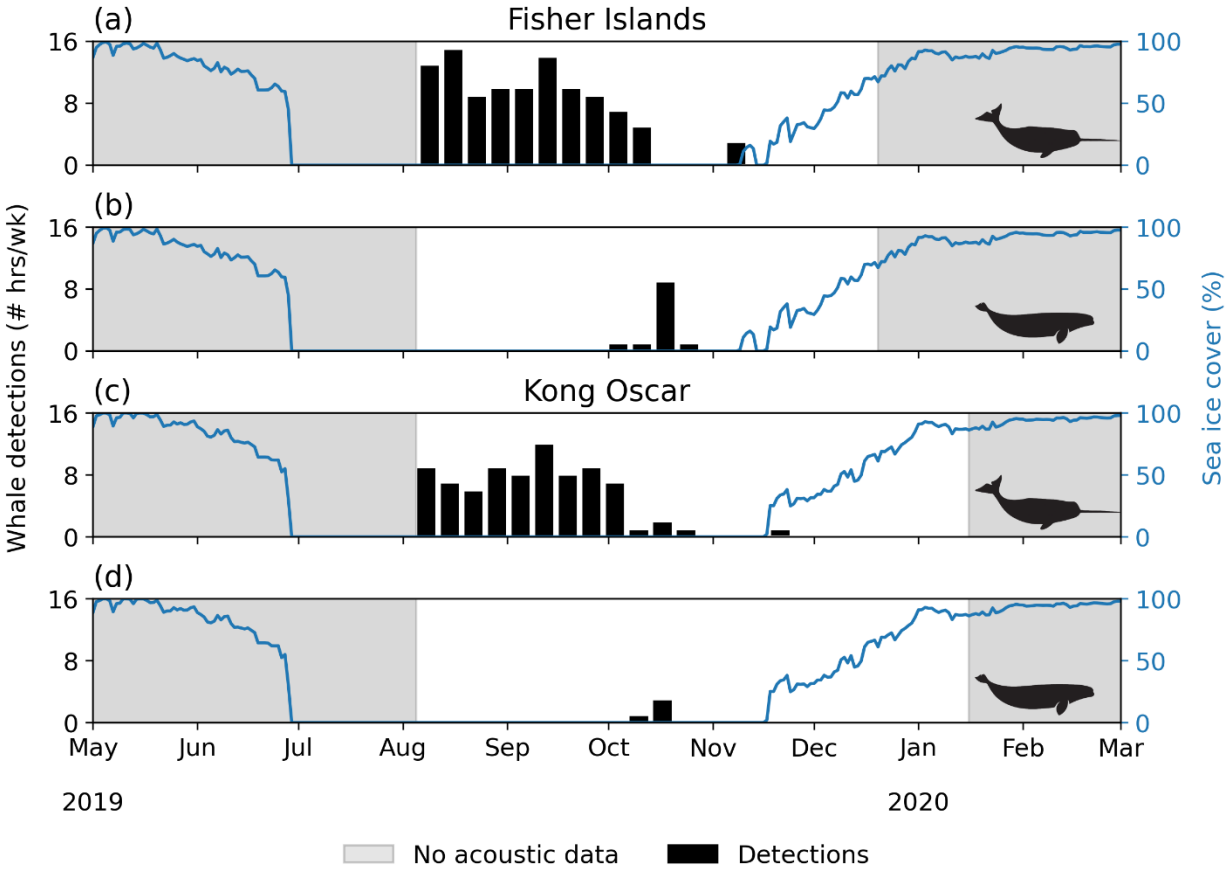

Figure 4.4. Time series of narwhal (a, c) and beluga (b, d) presence and percent sea ice cover (blue lines) at the Fisher Islands (a, b) and Kong Oscar (c, d) mooring sites from May 2019 to March 2020. Black bars provide the number of hours per week that narwhals and belugas were detected and thus indicate when whales were present. Gray shaded regions denote when no acoustic data were available. Hourly sea ice concentration data on the secondary (right side) y-axis were sourced from the ERA5 reanalysis product (Copernicus Climate Change Service, Climate Data Store 2022; Hersbach et al. 2022) and were averaged to a daily resolution.

4.4.2 *TOL Ratios*

Consistent trends between selected TOL were observed between beluga and narwhal acoustic events. Beluga echolocation power spectra had little change in TOL between the 16 to 25 kHz bands in contrast to narwhal power spectra that showed a large increase in magnitude between these bands (Figure 4.5). Conversely, a large difference was seen between the 25 and 40 kHz TOL in beluga spectra that was absent in narwhal spectra (Figure 4.5). The mean 16 to 25 kHz TOL ratio was 2.69 dB (median: 2.91 dB) in beluga spectra and -7.07 dB (median: -7.03 dB) in narwhal spectra. The mean 25 to 40 kHz TOL ratio was -8.74 dB (median: -10.3 dB) in beluga spectra and 1.35 dB (median: 0.62 dB) in narwhal spectra. All SoundTrap beluga events had a decrease in TOL between the 16 and 25 kHz bands, corresponding to the decreasing noise level with increasing frequency. The difference between TOL ratios (i.e., 16 to 25 kHz TOL ratio minus the 25 to 40 kHz TOL ratio) was positive for beluga spectra and negative for narwhal spectra (Figure 4.5).

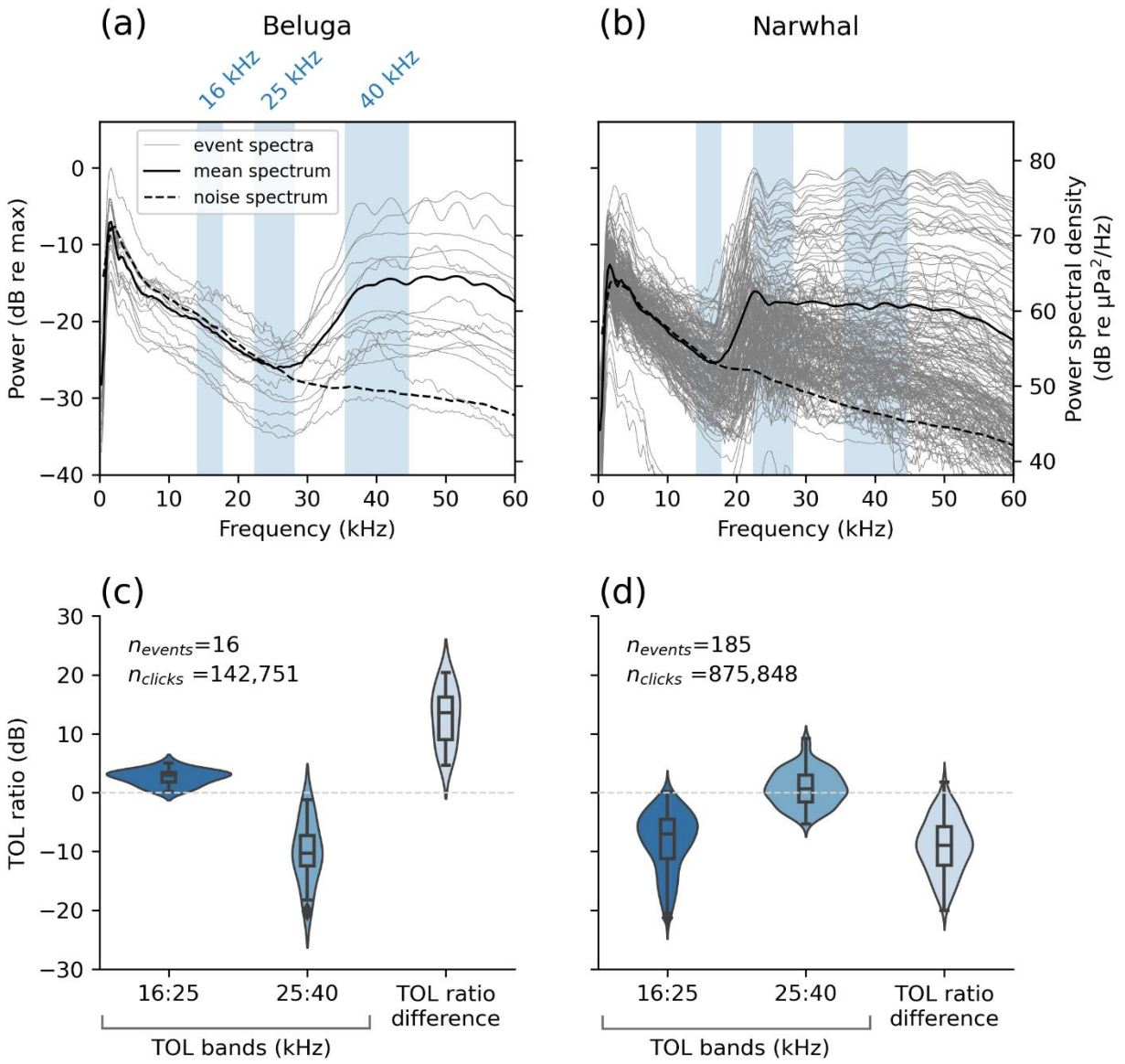

Figure 4.5. Mean power spectra for beluga (a) and narwhal (b) acoustic events. Mean spectra for individual acoustic events are shown in gray, and the overall mean spectra across events are shown in black with the noise floor provided as a dashed line. The average noise spectrum was computed using samples extracted from waveform clips that immediately preceded each click. Primary y-axes in (a) and (b) provide normalized power (dB) with respect to the maximum and the secondary y-axes show corresponding power spectral density magnitudes (dB re 1 µPa^2/Hz). Blue shaded areas in (a) and (b) demarcate the frequency bandwidths of the 16, 25, and 40 kHz one-third octave bands. Violin plots with inset box plots show the distribution of the TOL ratios (dB) between the 16 to 25 kHz and 25 to 40 kHz one-third octave bands and the difference

between these two ratios (i.e., 16:25 kHz TOL ratio subtracted from 25:40 kHz TOL ratio) for beluga (c) and narwhal (d) acoustic events.

4.4.3 *Acoustic Classification*

The BANTER acoustic classifier trained with Reson data performed well with correct classification rates of 94% and above when used to predict SoundTrap acoustic events (Table 4.2). BANTER models correctly classified 100% of the narwhal events, and misclassifications occurred only with beluga events. Model performance was unchanged (i.e., did not improve) when TOL variables were added as event-level measures. Due to the lower sampling rate of the SoundTrap recordings, beluga parameter estimates (e.g., peak frequency) were lower compared to those estimated from the Reson training dataset (Zahn et al. 2021b). The dissimilarity between the training and testing datasets may also be due to differences in the hydrophone's frequency response and pre-processing methods (e.g., high pass filters) for the two datasets. Nevertheless, the lower parameter values calculated for the SoundTrap beluga events more closely resembled narwhal parameter estimates from the Reson dataset, resulting in incorrect beluga species assignment. A summary of SoundTrap acoustic event parameter estimates for BANTER variables is provided in Supplementary Table S4.2. Examination of BANTER event classifier votes (i.e., percent of trees in the forest voting for each species) indicated high confidence for narwhal species assignment and low confidence for beluga predictions where many beluga events had nearly equal proportions of trees voting for beluga and narwhal species assignment (see Supplementary Figure S4.1).

Table 4.2. Confusion matrices for BANTER predictions of SoundTrap beluga and narwhal acoustic events at the Fisher Islands and Kong Oscar sites. Results are shown from the BANTER model trained with and without TOL ratio variables. The predictions were unchanged when TOL variables were added. Rows indicate the original acoustic event species assignment and columns show event predictions by the classifier. Model accuracy, or percentage correctly classified (95% confidence interval), is included for each class.

	Beluga	Narwhal	Accuracy (95% CI)
(a) BANTER with and without TOL variables			
Fisher Islands predictions			
Beluga	5	7	41.7% (15.2 – 72.3%)
Narwhal	0	105	100% (96.5 – 100%)
Overall			94.0% (88.1 – 97.6%)
Kong Oscar predictions			
Beluga	3	1	75.0% (19.4 – 99.4%)
Narwhal	0	80	100% (95.5 – 100%)
Overall			98.8% (93.5 – 100%)

During the model development stage, OOB correct classification rates were high for RF models built for each dataset (>99%; Table 4.3). All acoustic events were correctly assigned in both models except for one narwhal event misclassification from the Fisher Islands. For all RF models developed, variable importance scores indicated the 16 to 25 kHz TOL ratio was the more important variable for correct species classification. However, exploratory runs of RF models with only the 16 to 25 kHz TOL ratio variable resulted in decreased accuracy, and thus the 25 to 40 kHz TOL ratio variable was also important for correct predictions. Visualizing the distribution of RF model votes confirmed high confidence in OOB predictions for all RF models developed (Supplementary Figure S4.1).

Table 4.3. RF confusion matrices for model development using the TOL ratios between the 16 to 25 kHz and 25 to 40 kHz one-third octave bands. Three RF models were trained using acoustic events from separate datasets: 1) both sites, 2) Fisher Islands site, and 3) Kong Oscar site. Rows indicate the original acoustic event species assignment and columns show predictions by the classifier. OOB percent correct (95% confidence interval) classification rates provide model accuracy.

	Beluga	Narwhal	OOB accuracy (95% CI)
Both sites			
Beluga	16	0	100% (79.4 – 100%)
Narwhal	1	184	99.5% (97.0 – 100%)
Overall			99.5% (97.3 – 100%)
Fisher Islands			
Beluga	12	0	100% (73.5 – 100%)
Narwhal	1	104	99.0% (94.8 – 100%)
Overall			99.1% (95.3 – 100%)
Kong Oscar			
Beluga	4	0	100% (39.8 – 100%)
Narwhal	0	80	100% (95.5 – 100%)
Overall			100% (95.7 – 100%)

RF models built with only TOL ratio variables predicted the species identity of acoustic events with extremely high accuracy (100%; Table 4.4). The Fisher Islands RF model correctly predicted all of the acoustic events from the Kong Oscar dataset. Similarly, the Kong Oscar RF model predicted all of the acoustic events from the Fisher Islands dataset.

Table 4.4. RF confusion matrices for model predictions using the TOL ratios between the 16 to 25 kHz and 25 to 40 kHz bands. Individual RF models built for each site were tested with data from the other site to evaluate model performance. Rows show the original acoustic event species assignment and columns indicate classifier predictions. Model accuracy, or percentage of total acoustic events correctly classified (95% confidence interval), is provided.

	Beluga	Narwhal	Accuracy (95% CI)
Fisher Islands predicts Kong Oscar			
Beluga	4	0	100% (39.8 – 100%)
Narwhal	0	80	100% (95.5 – 100%)
Overall			100% (95.7 – 100%)
Kong Oscar predicts Fisher Islands			
Beluga	12	0	100% (73.5 – 100%)
Narwhal	0	105	100% (96.5 – 100%)
Overall			100% (96.9 – 100%)

4.5 DISCUSSION

Our results provide compelling evidence for identifying beluga and narwhal clicks with high certainty. We tested a previously developed acoustic classifier (Zahn et al. 2021b) and demonstrated the predictive strength of two new model parameters derived from one-third octave frequency bands. The differences in TOL between the 16 to 25 and 25 to 40 kHz one-third octave bands proved to be robust metrics for automated and manual species identification. This study builds on existing literature (e.g., Frouin-Mouy et al. 2017; Jones et al. 2022) and together indicate that among the diverse vocalizations produced by Arctic toothed whales, echolocation clicks are dependable signals for beluga and narwhal acoustic classification.

4.5.1 *Visual Species Identification*

We show beluga and narwhal clicks can reliably be identified through visual inspection of spectrograms. Across all acoustic events examined here, narwhal clicks contained a distinct spectral peak just above 20 kHz where spectral energy sharply decreased below 20 kHz and remained relatively flat between 20 and 60 kHz. The frequency peak near 20 kHz is consistent with existing literature documenting narwhal spectra (Møhl et al. 1990; Stafford et al. 2012; Koblitz et al. 2016; Frouin-Mouy et al. 2017; Zahn et al. 2021b; Jones et al. 2022). Pulsed calls and buzzes produced by narwhals and detected by the PAMGuard Click Detector also contained increased energy near 20 kHz. Only in lower ambient noise conditions were the low frequency components of narwhal clicks between 3–5 kHz observed. In contrast to narwhal clicks, beluga click spectra mostly had energy above 30 kHz. Unlike the sharp 20 kHz lower limit seen in narwhal spectra, spectral energy in beluga clicks increased more gradually from 30 kHz and peaked between 40–50 kHz, which is potentially a consequence of a 72 kHz Nyquist frequency and an anti-aliasing filter attenuating energy above ~60 kHz. Beluga pulsed calls that were detected in our analyses contained energy from 20 kHz and above, but they did not present a clear 20 kHz edge like those produced by narwhals.

These results corroborate findings by Jones et al. (2022) where beluga and narwhal clicks from moored High-frequency Acoustic Recording Packages (HARPs) with a 200 kHz sampling rate were analyzed. Jones et al. (2022) found beluga clicks had higher peak frequencies (55–60 kHz) than narwhal clicks (23 kHz) at lower received levels (<130 dB peak-peak). At high received levels (>150 dB peak-peak), both species had peak frequencies between 50 and 60 kHz. Broadly, Jones et al. (2022) summarize that narwhal clicks had more energy than beluga clicks below 40 kHz. Yet, spectral peaks vary depending on the orientation of the whale relative to the

receiver and the specifications of the recorder. For example, peak frequencies of on-axis clicks were higher for both species, estimated to be 71±15 kHz for narwhals (Koblitz et al. 2016) and 97±7 kHz for belugas (Zahn et al. 2021a). Nonetheless, existing literature supports the assertion that belugas produce clicks with greater energy at higher frequencies compared to narwhals.

4.5.2 *Acoustic Classifier Performance*

When testing with lower sampling rate recordings, the BANTER model from Zahn et al. (2021b) classified species with high overall correct classification rates of 94% for the Fisher Islands site and 98.8% for the Kong Oscar site. These results suggest that the BANTER model trained with data from a Reson hydrophone (500 kHz sampling rate) is generalizable such that it can predict species assignment of clicks recorded at lower sampling rates (e.g., SoundTrap with 144 kHz sampling rate). However, the small sample size of the beluga class resulted in wide prediction intervals and high classification uncertainty for identifying beluga clicks. Further, the lower Nyquist frequency of the SoundTrap recordings and different frequency response compared to the Reson recordings resulted in underestimated click parameter estimates in the testing dataset compared to the training dataset (Zahn et al. 2021b). Therefore, some SoundTrap beluga event parameter estimates resembled those from Reson narwhal events, leading to misclassifications. We speculate that the BANTER model's overall correct prediction rates would increase if there were a larger beluga event sample size since the model would have more data to differentiate between species. Adding TOL ratio event-level variables did not improve species classifications, indicating that TOL ratios estimated from the training dataset did not predict the testing dataset well. These results highlight disparities between the training and testing datasets and emphasize the need for caution when utilizing datasets from recorders with different specifications in acoustic classification.

RF models using TOL statistics had stronger predictions than BANTER predictions, likely due to the fact that the training dataset was acquired and processed exactly the same as the testing dataset. Our results confirm that narwhal clicks had a larger difference between the 16 and 25 kHz one-third octave bands compared to belugas, whereas beluga clicks had a larger difference between the 25 and 40 kHz bands compared to narwhals. OOB correct classification rates were high for all RF models developed (>99%; Table 4.3). Similarly, RF models trained with data from one site (i.e., Kong Oscar or Fisher Islands) correctly predicted 100% of the acoustic events from the other site (Table 4.4).

In summary, our model results found that the recording system's sampling rate influenced model predictions. Parameters used in the BANTER model (e.g., peak frequency) will vary depending on the sampling rate and frequency response of the recording system, but the TOL ratio variables employed here will be unaffected as long as the sampling rate is at least 96 kHz with a flat frequency response between 14–45 kHz. However, ambient noise levels will influence 16 and 25 kHz TOL estimates where higher noise levels will decrease the relative magnitude within these bands. Nevertheless, the TOL ratio between the 16 to 25 and 25 to 40 kHz bands is sufficiently large that beluga and narwhal clicks remain differentiable in contrasting environments (see Supplementary Figure S4.2).

4.5.3 *Future Recommendations*

The present study marks an important step in automating beluga and narwhal acoustic detection for future passive acoustic monitoring programs. Based on the results presented herein, we highlight that the lowermost part of echolocation click spectra (<50 kHz) for narwhals and belugas contain enough critical information for species classification. Therefore, we recommend a minimum sampling rate of 96 kHz for classification of these two species, although recorders

with higher sampling rates (~400 kHz or more) are needed for general signal characterization involving parameters such as peak frequency and centroid frequency. Given the sensory function of echolocation, acoustic properties of clicks appear to be less variable than social calls, making them consistent metrics for species classification across subpopulations. To fully implement an auto-detector and classifier for recordings near glaciated coastlines, future work must describe and classify transient ice sounds to isolate biotic and abiotic sounds. While this was outside of the scope of the present study, we show highly accurate automated species predictions once cetacean clicks are separated.

Arctic ecosystems are being altered by climate change and trans-Arctic shipping routes will be used with greater frequency in the next decade (Meier et al. 2014; Melia et al. 2016; Lannuzel et al. 2020). Efforts to monitor changes to ambient noise levels and endemic Arctic odontocete distributions are becoming increasingly important, especially for effective management of beluga and narwhal stocks for harvest by Arctic communities in Canada and Greenland (Hobbs et al. 2019). We verified that beluga and narwhal clicks are differentiable, and moreover, discrete parameters exist to automatically classify them at high success rates. With the increasing prevalence of autonomous recorders being used to monitor cetaceans globally, our results are directly applicable to future passive acoustics research. Going forward, we encourage sustained observations using long-term passive acoustics from fixed platforms (e.g., moored HARPs or SoundTrap) to track species occurrence of resident and non-resident species and monitor increased human activity in the Arctic.

4.6 Acknowledgements

This work was funded by the US Office of Naval Research (award no. N00014-17-1-2774) and supported by the NASA Oceans Melting Greenland EVS-2 mission. M.J.Z. was partially

supported by the Cooperative Institute for Climate, Ocean, & Ecosystem Studies (CICOES) under NOAA Cooperative Agreement NA20OAR4320271, Contribution No. 2023-1312. M.S. was supported by the Danish Cooperation for Environment in the Arctic (DANCEA, MST-2020-64692). We thank everyone who contributed to the data collection, in particular Jens Koblitz and Marianne Rasmussen, and development of the BANTER model that provided foundations for this study. We are also grateful to Jennifer L. K. McCullough for her assistance with PAMGuard and the BANTER model, Ben Cohen for Landsat 8 imagery support, and Alex Douglass for his statistical advice. We thank Shannon Rankin for her helpful input on previous versions of this manuscript.

4.7 Data Availability

Acoustic data from moorings is available upon request from authors. Sea ice concentration ERA5 hourly data are supplied by the Copernicus Climate Change Service Climate Data Store at https://doi.org/10.24381/cds.adbb2d47. R and Python code used to produce all analyses including classification models and figures for this manuscript are publicly available on Github: https://github.com/mjzahn/beluga_narwhal_click_classifier (last commit: 4 November, 2023).

4.8 Supplemental Materials

The supplementary information below includes additional tables and figures that support this manuscript. A catalogue of concatenated click spectrograms and mean power spectra for all acoustic event data from this study is available on Zenodo (Zahn et al. 2023).

Table S4.1. Descriptions of BANTER acoustic parameters calculated using the *PAMpal* package.

Variable Code	Variable Name	Unit	Description
peak	Peak frequency	kHz	Frequency value with the highest dB level
peak2	Second peak frequency	kHz	Frequency value with the second highest dB level
peak3	Third peak frequency	kHz	Frequency value with the third highest dB level
trough	Frequency trough	kHz	Frequency value between peak and peak2 with the lowest dB value; also called spectral notch
trough2	Second frequency trough	kHz	Frequency value between peak2 and peak3 with the lowest dB value
peakToPeak2	First peak to second peak	kHz	Difference between the frequency values of peak and peak2
peakToPeak3	First peak to third peak	kHz	Difference between the frequency values of peak and peak3
peak2ToPeak3	Second peak to third peak	kHz	Difference between the frequency values of peak2 and peak3
Q_10dB	-10 dB resonant quality factor	kHz	Metric of frequency pureness at -10 dB calculated by dividing the center frequency by the bandwidth
Q_3dB	-3 dB resonant quality factor	kHz	Metric of frequency pureness at -3 dB calculated by dividing the center frequency by the bandwidth
fmin_10dB	-10 dB frequency minimum	kHz	-10 dB frequency minimum
fmin_3dB	-3 dB frequency minimum	kHz	-3 dB frequency minimum
fmax_10dB	-10 dB frequency maximum	kHz	-10 dB frequency maximum
fmax_3dB	-3 dB frequency maximum	kHz	-3 dB frequency maximum
BW_10dB	-10 dB bandwidth	kHz	-10 dB bandwidth
BW_3dB	-3 dB bandwidth	kHz	-3 dB bandwidth
centerkHz_10dB	-10 dB center frequency	kHz	[min frequency + (max frequency - min frequency)]/2 at -10 dB
centerkHz_3dB	-3 dB center frequency	kHz	[min frequency + (max frequency - min frequency)]/2 at -3 dB
duration	Click duration	µs	Time defined by the number of samples above 100 times the 40th percentile of the Teager Kaiser energy level
ici	Inter-click interval	sec	Time interval between consecutive clicks; mode approximated for each event

Table S4.2. Summary of BANTER signal parameter measurements for all beluga and narwhal acoustic events from the SoundTrap data, inclusive of both the Kong Oscar and Fisher Islands sites. A 20 kHz Butterworth high pass filter was applied prior to calculating parameter values for each click. Mean, standard deviation, and median are provided.

		Beluga			Narwhal		
Variable	Unit	Mean	Std	Median	Mean	Std	Median
peak	kHz	39.1	7.4	38.6	31.6	7.2	29.6
peak2	kHz	42.4	13.1	40.2	35.5	12.5	36.8
peak3	kHz	31.6	18.5	27.0	30.3	23.7	43.2
trough	kHz	37.6	11.6	32.8	38.4	11.9	40.4
trough2	kHz	35.6	16.0	38.4	23.7	18.4	28.0
peakToPeak2	kHz	15.8	4.3	15.2	13.7	5.2	12.8
peakToPeak3	kHz	15.0	8.5	13.6	11.9	10.0	12.0
peak2ToPeak3	kHz	19.5	11.2	19.0	13.6	11.5	12.4
Q_10dB	kHz	3.9	2.3	2.8	4.8	5.0	3.3
Q_3dB	kHz	16.0	10.3	11.9	19.9	12.2	17.9
fmin_10dB	kHz	33.9	6.3	31.3	25.7	5.6	24.3
fmin_3dB	kHz	38.3	6.7	38.6	29.3	6.4	27.7
fmax_10dB	kHz	47.6	8.6	46.8	37.4	10.5	34.5
fmax_3dB	kHz	41.7	6.5	41.5	31.6	7.3	29.7
BW_10dB	kHz	13.7	7.6	13.3	11.8	9.3	8.5
BW_3dB	kHz	3.4	1.8	3.4	2.3	2.0	1.8
centerkHz_10dB	kHz	40.8	6.5	40.9	31.6	7.0	29.8
centerkHz_3dB	kHz	40.0	6.5	40.1	30.4	6.8	28.7
duration	µs	90.5	81.0	73.1	157.1	266.1	76.6
ici	ms	40.6	45.4	14.1	82.7	87.8	75.2

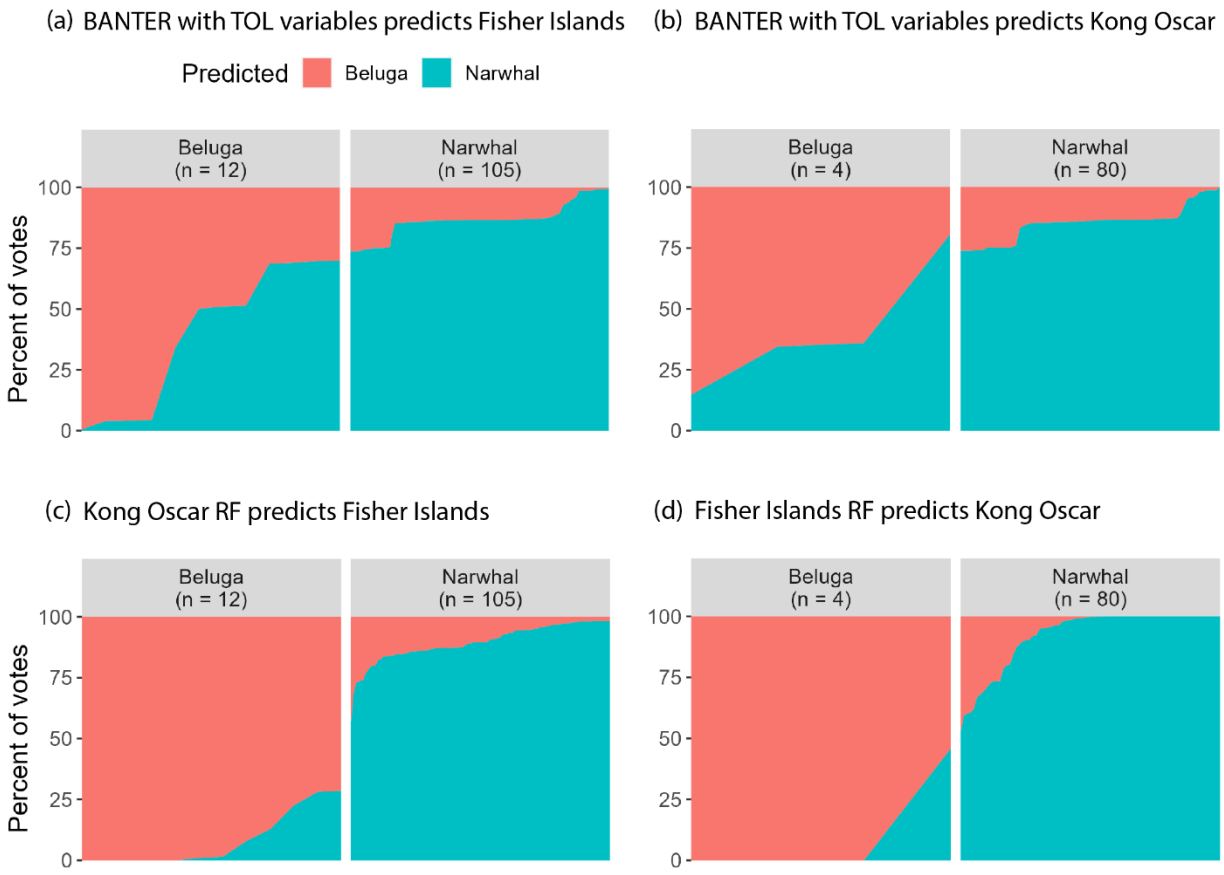

Figure S4.1. Distribution of model votes for each sample (i.e., acoustic event) in each class demonstrating overall model confidence in its predictions. The distributions show the percentage of trees in the forest voting for each species. Model predictions are colored in salmon (pink) for beluga and turquoise for narwhal. Model votes using the BANTER model with one-third octave (TOL) event level variables are shown for predictions from (a) the Fisher Islands and (b) Kong Oscar datasets. Model votes using Random Forest (RF) models trained with TOL variables are shown in (c) and (d).

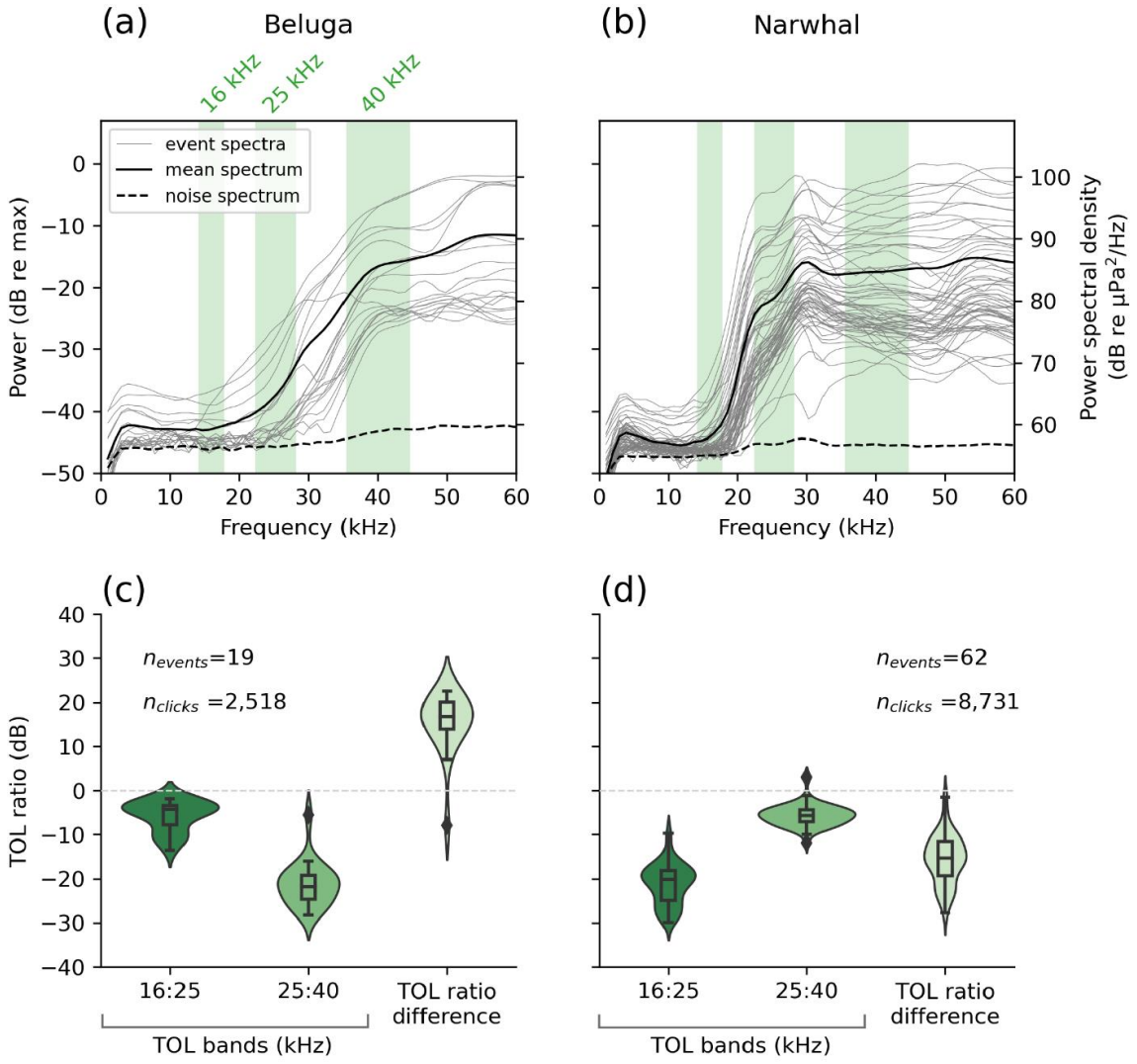

Figure S4.2. Mean power spectra for beluga (a) and narwhal (b) acoustic events published in Zahn et al. (2021b) from Reson recorders (500 kHz sampling rate). Power spectra in (a) and (b) are truncated to only show energy below 60 kHz to match the Nyquist frequency of the SoundTrap recording system (144 kHz sampling rate). Mean spectra for individual acoustic events are shown in gray. The overall mean spectra across events are shown in black with the noise floor provided as a dashed line. Green shaded areas in (a) and (b) demarcate the frequency bandwidths of the 16, 25, and 40 kHz one-third octave bands. Violin plots with inset box plots show the distribution of the TOL ratios (dB) between the 16 to 25 kHz and 25 to 40 kHz one-third octave bands and the difference between these two ratios (i.e., 16:25 kHz TOL ratio minus the 25:40 kHz TOL ratio) for beluga (c) and narwhal (d) acoustic events.

Chapter 5. SEASONAL HYDROGRAPHY AND UNIQUE PLUME SIGNATURES FROM MOORINGS AT NORTHWEST GREENLAND GLACIER FRONTS

5.1 ABSTRACT

Greenland's marine-terminating glaciers connect the ice sheet to the ocean and provide a critical boundary where heat, freshwater, and nutrient exchanges take place. Buoyant freshwater runoff from inland ice sheet melt is discharged at the base of marine-terminating glaciers, forming a vigorous upwelling plume. It is understood that subglacial plumes modify waters near glacier fronts and increase submarine glacier melt by entraining warm ambient waters at depth. However, ocean observations along Greenland's coastal margins remain biased toward summer months which limits accurate estimation of ocean forcing on glacier retreat and acceleration. Here, we fill a key observational gap in northwest Greenland by describing seasonal hydrographic variation at glacier fronts in Melville Bay using *in situ* observations from moorings deployed year-round, CTDs, and profiling floats. We evaluated local and remote forcing using remote sensing and reanalysis data products alongside a high-resolution ocean model. Analysis of the year-round hydrographic data revealed consistent above-sill seasonality in temperature and salinity with site-specific plume signatures determined by glacier depth and runoff rate. The warmest, saltiest waters occurred in spring (April–May) and primed glaciers for enhanced submarine melt in summer when meltwater plumes entrain deep waters. Waters were coldest and freshest in early winter (November–December) after summer sea ice and glacier melt provided cold freshwater along the shelf. Ocean variability was greatest in the fall, coincident with large storms and wind events

before sea ice formation. Results increase our mechanistic understanding of Greenland ice-ocean interactions and enable improvements in ocean model parameterization.

5.2 INTRODUCTION

Greenland's marine-terminating, or tidewater, glaciers connect the ice sheet to the ocean and provide important gateways for heat, meltwater, and nutrient fluxes. Mass loss of the Greenland ice sheet results from the discharge of ice into the ocean through glacier dynamics and deficits in surface mass balance (i.e., difference in snow accumulation and meltwater runoff) (Mouginot et al. 2019; Choi et al. 2021). Due to a warming climate, tidewater glaciers have been delivering solid ice and meltwater runoff from the ice sheet to the ocean at increasing rates with significant contributions to global sea level rise (Chen et al. 2017; IPCC 2019; IMBIE Team 2020). Marine-terminating glaciers have submerged fronts in ocean inlets and fjords that can be over 1 km deep, and consequently, these glaciers are sensitive to ocean temperatures where warmer (cooler) waters have been linked to glacier acceleration (deceleration) and retreat (advance) (Holland et al. 2008; Gladish et al. 2015a; Gladish et al. 2015b; Khazendar et al. 2019; Wood et al. 2021). However, the mechanisms driving glacier retreat are complex and consist of interactions between the atmosphere, ice, ocean, and land geography (e.g., ocean bathymetry and steep fjord topography) (Straneo & Heimbach 2013; Mouginot et al. 2015; Fried et al. 2018; Wood et al. 2021; Slater & Straneo 2022). For the ocean's contribution to glacier retreat, researchers have relied on remote sensing and modeled simulations to estimate melt rates at the ice-ocean interface due to the paucity of sustained *in-situ* ocean measurements near Greenland's glacier fronts (Sciascia et al. 2013; Fried et al. 2015; Carroll et al. 2016; Straneo et al. 2019; Catania et al. 2020; Jackson et al. 2020). Much of the empirical data that exist are from southeast and

central west Greenland (Straneo et al. 2010; Harden et al. 2014; Carroll et al. 2018), and prior to this study, there were no year-round observations from the northwest sector.

Warming in the subpolar North Atlantic Ocean, observed in the 1990s and consistently since 2016 (Bersch et al. 2007; Desbruyères et al. 2021; Jackson et al. 2022), increases heat transport to Greenland's marine-terminating glaciers via a network of coastal currents (Straneo & Heimbach 2013; Khazendar et al. 2019). Generally, waters circulating around Greenland on its continental shelf and within its fjords is composed of a colder, fresher surface polar water (PW) layer in the upper 100–200 m above a warmer, saltier Atlantic water (AW) layer below 200 m with an intermediary mixed water layer in between (Straneo et al. 2010; Wood et al. 2021). PW is sourced from the Arctic and Greenland glacial ice melt (Myers et al. 2009; Rykova et al. 2015). AW is of subtropical origin from North Atlantic Current and Gulf Stream (Cuny et al. 2002; Pickart et al. 2005). AW is shunted across coastal shelves into drainage basins and fjords where it comes into direct contact with glacier fronts (Straneo et al. 2010; Fenty et al. 2016; Straneo et al. 2016). The distribution of water masses along Greenland's shelf and their characteristics vary seasonally and regionally depending on thermohaline circulation patterns, seafloor geometry, atmospheric forcing, and the annual sea ice cycle (Straneo et al. 2010; Harden et al. 2014; Jackson et al. 2014; Carroll et al. 2018). The intrusion of warm, subpolar AW into Greenland's fjords has been shown to undercut glacier termini and increase glacier retreat and acceleration (Holland et al. 2008; Straneo et al. 2010; Straneo & Heimbach 2013; Harden et al. 2014; Carroll et al. 2018; Rignot et al. 2021; Wood et al. 2021). However, the seasonality and magnitude of warm waters reaching Greenland's glaciers and the factors influencing subsurface glacial melt are active areas of research.

Over the last decade, the formation of subglacial meltwater plumes formed at the base of Greenland's glaciers has been identified as a fundamental mechanism that enhances submarine melt at the glacier face by entraining warm AW (Straneo et al. 2011; Straneo & Heimbach 2013; Bendtsen et al. 2015; Carroll et al. 2016; Morlighem et al. 2019; Slater & Straneo 2022). Freshwater runoff originating from inland ice sheet surface melt and basal frictional melt is ejected at the base of marine-terminating glaciers as turbulent plumes (Chu 2014; Mankoff et al. 2016; Slater et al. 2022). The more buoyant plume rises towards the surface and mixes ambient waters until reaching neutral buoyancy. Increased runoff due to atmospheric forcing on the ice sheet can increase near-glacier ocean mixing and heat transport to the glacier front, increasing ambient melt and undercutting of the glacier terminus (Fried et al. 2015; Sutherland et al. 2019; Slater & Straneo 2022). Upwelled plume waters also bring nutrients to the surface photic zone, initiating regional primary production and biological activity (Cape et al. 2018; Williams et al. 2021; Kanna et al. 2022; Møller et al. 2023).

Recent work has demonstrated the physical and biological importance of subglacial plumes to Greenland's coastal ecosystems (Meire et al. 2017; Slater et al. 2022; Oliver et al. 2023). Yet, empirical observations of plumes are limited due to sampling constraints from hazardous conditions near calving glaciers and the high risk of instrument loss. Glacier termini have highly heterogenous morphologies across their faces, and how these fine-scale characteristics influence plume processes remains unexplained. A mechanistic understanding of fundamental local processes at the ice-ocean boundary is needed to accurately parameterize climate model simulations (Catania et al. 2020), but resolving complex regional ice-ocean dynamics (meter scale) with pan-Greenland trends in glacier retreat (1,000 km scale) remains a considerable challenge. NASA launched the Earth Venture-Suborbital Oceans Melting

Greenland (OMG) mission to address existing knowledge gaps surrounding Greenland's ice-ocean dynamics by collecting observations on the continental shelf (Fenty et al. 2016). The OMG campaign obtained oceanographic observations around Greenland at an unprecedented spatial scale and confirmed that the ocean plays an important role in Greenland glacier acceleration and retreat (Fenty et al. 2016; Wood et al. 2021). However, ocean observations along Greenland's margins are still biased toward summer months with relatively few year-round measurements.

Here, we describe year-round hydrographic variability at glacier fronts in Melville Bay based on moored instruments deployed from August 2018 to August 2020. We leverage *in situ* measurements from moorings, profiling floats, and CTDs together with reanalysis and an ocean numerical model to investigate the timing, magnitude, and exogenous forcing of the seasonal variability. We also discuss the heterogeneity and drivers of plume characteristics across sites. Knowledge of ocean variability at the glacier-ocean interface is needed to understand the mechanisms by which Greenland's glaciers are melting and predict how changes due to warming temperatures will impact local ecosystems and the global climate.

5.3 Methods and Data

5.3.1 *Program Design*

Seafloor-mounted oceanographic moorings were deployed near glacier fronts in Melville Bay (Greenlandic: *Qimusseriarsuaq*), Northwest Greenland between 74°N and 76.5°N. Melville Bay features a large trough that is open to Baffin Bay to the southwest. To the east, the inner continental shelf consists of a discontinuous network of valleys and sills between 400–1,000 m deep that influence how water travels inshore and interacts with glacier fronts (Figure 5.1). A

total of six ocean moorings were deployed from the R/V *Sanna* at three sites over two years (2018–2020) and five were successfully recovered. Moorings were positioned in front of Rink, Kong Oscar (Nuussuup Sermia), and Sverdrup (Tuttulissuaq) glaciers (Bjørk et al. 2015). In this study, we refer to ocean mooring locations by the name of the nearest glacier because there are no placenames for the inlets in which they were deployed. The 2019–2020 mooring located near Sverdrup glacier was destroyed by icebergs and was unrecoverable. The 2019–2020 Rink glacier mooring site was shifted to the Fisher Islands due to inaccessibility of the original site from heavy ice conditions (Figure 5.1b). The approximate linear distance between the 2020 glacier front (Joughin et al. 2021) and mooring locations are 12 km for Rink, 25.7 km for the Fisher Islands, 17.2 for Kong Oscar, and 11.7 km for Sverdrup. Hereafter we refer to the Rink and Fisher Islands mooring locations jointly as Rink/Fisher.

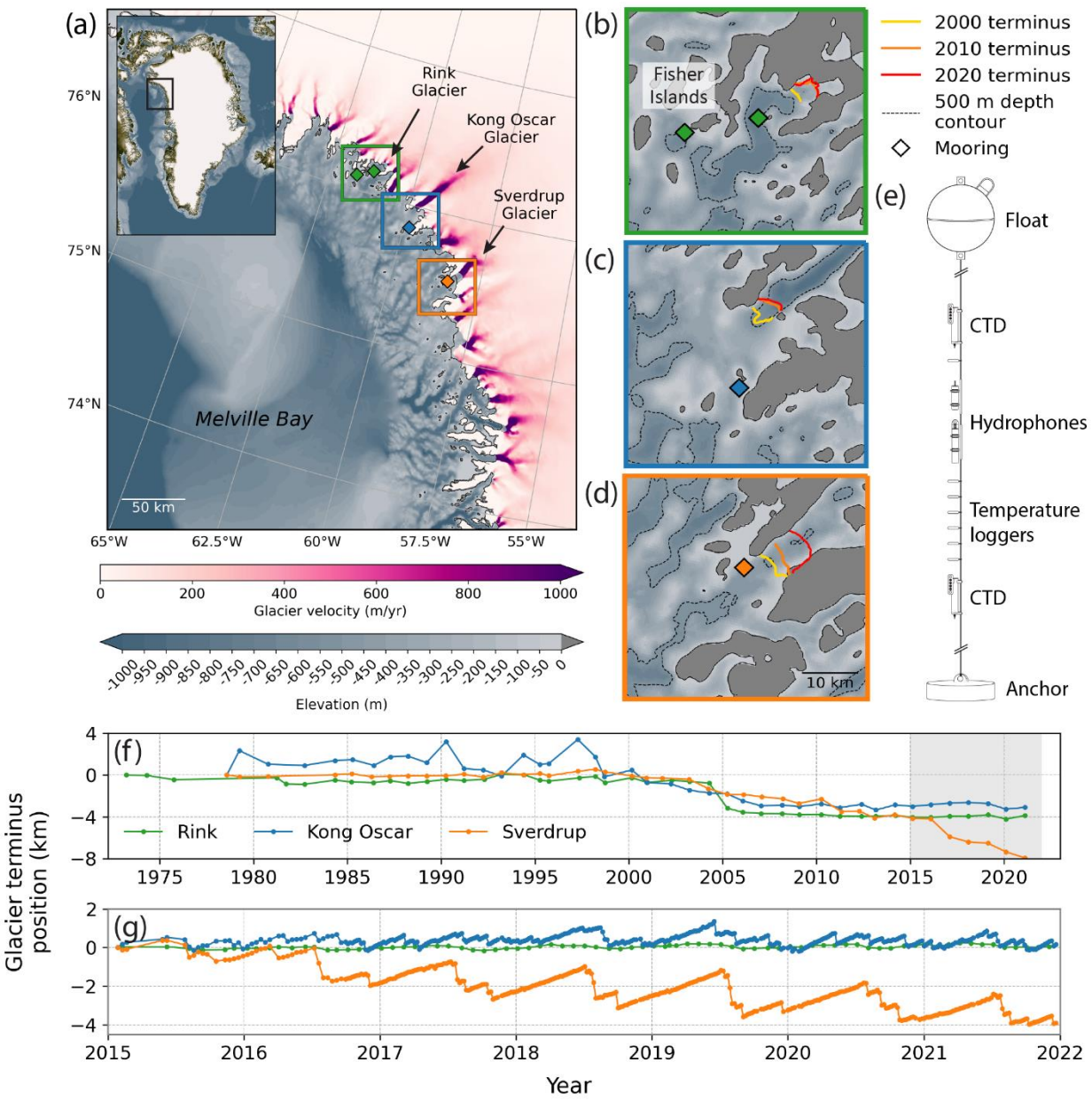

Figure 5.1. Map showing the study region in Melville Bay, Northwest Greenland (a) with inset maps for ocean mooring locations that were positioned in front of three glaciers: Rink glacier (b), Kong Oscar glacier (c), and Sverdrup glacier (d). A schematic of hydrographic and passive acoustic instrumentation included on each mooring is also provided in (e). The MEaSUREs Greenland glacier ice velocity 2019 annual mosaic (Joughin 2022) is overlaid on ocean bathymetry from the International Bathymetric Chart of the Arctic Ocean (Jakobsson et al. 2012) in (a). Below-ice bed topography from BedMachine V5 (Morlighem et al. 2017; Morlighem et

al. 2022) is displayed in (b-d) with dashed lines along the 500-meter depth contour and glacier terminus positions for three years (2000, 2010, 2020) from SAR mosaics (Joughin et al. 2021). Colored diamonds indicate locations for each mooring site (green: Rink/Fisher, blue: Kong Oscar, orange: Sverdrup). Annual (f) and seasonal (g) glacier terminus variability normalized to zero at start of time series where decreasing (increasing) values indicate glacier retreat (advance). The shaded region in (f) shows the timeframe in (g). Estimates in (g) are available at ~monthly frequency for Rink glacier (green) and ~weekly for Kong Oscar (blue) and Sverdrup (orange) (Black & Joughin 2022).

Moorings were equipped with oceanographic sensors and passive acoustic recorders. Each mooring had two instruments that measured conductivity (salinity), temperature, and depth (CTD) with one positioned shallower at ~100 m and one deeper at ~300 m. Temperature loggers were staggered in between CTDs to fill profile gaps (Figure 5.1e, Table 1). Two hydrophones were placed below the shallow CTD to measure the acoustic presence of narwhals near each glacier front. Moored temperature and salinity measurements provide high-resolution, year-round patterns of ocean properties that can be linked to ecosystem processes (Woodgate et al. 2015; Janout et al. 2016; e.g., Danielson et al. 2022).

5.3.2 *Selected Glacier Fronts*

Our study sites include three glaciers with different characteristics and the aim to represent the variety of ice dynamics observed at Melville Bay glacier fronts. Kong Oscar glacier is the largest, fastest-flowing glacier, followed by Sverdrup and Rink. At present, Rink glacier has two termini with shallow grounding depths (mean: 113 m, maximum: 243 m). Kong Oscar is the deepest glacier (mean: 578 m, maximum: 747 m) and produces the most solid ice discharge (i.e., icebergs; Mankoff 2020b; Mankoff et al. 2020b). Sverdrup has an intermediate grounding depth (mean: 254 m, maximum: 532 m) but has the widest glacier front. Estimates of mean freshwater

runoff are smallest for Rink. The runoff arising from Kong Oscar and Sverdrup are similar, but Sverdrup is slightly higher. Supporting Table S5.1 provides a summary of each glacier's properties.

From 1980–2000, the terminus positions of Rink and Sverdrup were stable (i.e., neither appreciably advancing nor retreating) while Kong Oscar advanced and retreated within a 4 km range (Figure 5.1f). Between ~2000 and 2006, all three glaciers retreated. From 2006 to present-day, Kong Oscar and Rink have been stable, but Sverdrup has continued to retreat. Sverdrup has the largest seasonal terminus variability, advancing/retreating ±2 km each year (Figure 5.1g). The terminus position of Kong Oscar glacier varies by half the magnitude of Sverdrup's (±1 km). Seasonal terminus location variability of Rink glacier is effectively invariant (±0.1 km). If Rink glacier retreats in the future, it may shoal and become land-terminating (Figure 5.1b).

5.3.3 *Data Processing and Evaluation*

5.3.3.1 Moored Observations

Moored CTDs sampled every 3 minutes and temperature loggers every 20 seconds. CTD pressure data were analyzed to identify anomalous spikes when the mooring was hit by icebergs with deep keels and depressed down the water column. Spikes, typically lasting 1–6 hours and spanning 10–50 m, were flagged and removed. Depth corrections were made for occasions when the mooring was dragged and settled at a new depth. Measurements were averaged into hourly, daily, and weekly datasets. Daily mean temperature and salinity provided a sufficient timescale to examine seasonal patterns and thus was the temporal resolution used in downstream analyses. Temperature and salinity profiles were made by linearly interpolating between observations in the vertical (depth) dimension.

The relationship between temperature and salinity was explored using T-S plots and known water mass densities from previous work (Curry et al. 2014). In T-S space, mixed Arctic waters exhibit a positive relationship between temperature and salinity where saltier waters are warmer and fresher waters are cooler. The timing of observations in relation to the T-S mixing line were considered in order to identify which months diverged from this line. Months where observations generally fell along the mixing line were identified and used to fit a linear model. A linear regression was run separately for each mooring as the slope of the mixing line varied slightly between each dataset. *In situ* temperature observations from the moorings were then used to predict salinity from the modeled fit. Predicted salinity values were subtracted from the *in situ* salinity observations to determine when and where (i.e., at what depths) salinity deviated from the mixing line. By plotting profiles of the difference between the observed and predicted salinities, key processes are identifiable, including evidence of subglacial plumes and upwelling or downwelling.

5.3.3.2 Local Atmospheric and Ice Forcing

The influence of ice and atmosphere dynamics on local ocean variability was examined by relating several key processes to the mooring observations. Year-round timeseries of sea ice cover, vertical velocity (derived from wind stress), air-sea heat fluxes, glacier ice velocity, glacier terminus advance/retreat, and subglacial freshwater runoff were plotted alongside the moored temperature and salinity measurements. Daily averages were calculated from hourly estimates of sea ice cover, wind stress, and air-sea heat fluxes (sum of shortwave radiation, longwave radiation, sensible, and latent heat fluxes) from the ERA5 reanalysis product (Copernicus Climate Change Service, Climate Data Store 2022; Hersbach et al. 2022). ERA5 estimates were provided on a nominal 0.25x0.25° grid which corresponds to a ~6.9x27.8 km grid

cell at 76°N. The closest ERA5 grid cell to each mooring location was used. The Rink mooring location was selected to represent the Rink/Fisher site.

Vertical velocity (m/day) was derived from daily wind stress to evaluate the potential role of Ekman pumping in ocean variability at the three sites. Only grid cells with <20% land cover were used. Wind stress curl was computed from individual vector components of the wind stress and was scaled by percent sea ice for each grid cell. Ekman pumping, or the vertical velocity at the base of the Ekman layer, $\boldsymbol{w_{ek}}$, was calculated by dividing the wind stress curl by a reference density ($\boldsymbol{\rho}$ = 1027 kg/m^3) and the Coriolis parameter at 75°N. Daily vertical velocity was computed for the entire mooring deployment to compare with other variable time series. However, when fast ice forms and covers Melville Bay during winter months, sea ice inhibits the transfer of momentum between wind and the ocean surface. Therefore, we accounted for the influence of sea ice in our vertical velocity calculations by setting wind stress to zero when the concentration of sea ice in a grid cell exceeded 50%. We note that the interactions between wind, sea ice, and the ocean's surface are complex, particularly at the sea ice edge. The movement of sea ice itself induces drag on the ocean surface, and further, the heterogeneity of sea ice creates highly variable surface drag conditions, making it difficult to estimate the degree to which wind stress acts on the ocean (Cole et al. 2017; Brenner et al. 2021). For our purposes, 50% sea ice concentration was used as an approximation for when sea ice cover substantially limits the force of wind imparted on the ocean. When Ekman pumping was suspected from observing large fluctuations in isotherms and isohalines in the mooring data, an additional analysis was conducted to compare wind-driven vertical motion to isopycnal variability. A one-dimensional ordinary differential equation (ODE) was constructed to model vertical motion over time. The

ODE included time-integrated vertical velocity and a relaxation term to represent the water column returning towards initial conditions (see additional methods in Supporting Text S5.1).

Measurements of glacier ice velocity, glacier terminus position, and subglacial runoff were compared to moored hydrographic observations at each site to investigate ice-ocean interactions between the glacier face and surrounding water. Ice velocity (m/yr) from Sentinel 2A, 2B, and Landsat 8 imagery were extracted from the NASA MEaSUREs ITS_LIVE project (Gardner et al. 2018; Gardner et al. 2022) using a point measured at the glacier centerline and approximately half the glacier width up from the 2019–2020 glacier front. Relative glacier length (km) was normalized and represents the advance (positive) and retreat (negative) of each glacier terminus (Black & Joughin 2022; Black & Joughin 2023). Relative length estimates were available at a weekly frequency for Kong Oscar and Sverdrup and monthly for Rink. The freshwater runoff dataset was derived from two regional climate models, Regional Atmospheric Climate Model (RACMO; Noël et al. 2019) and Modèle Atmosphérique Régional (MAR; Fettweis et al. 2017), and was available as a daily timeseries (Mankoff 2020a; Mankoff et al. 2020a). Land and ice basins with runoff outlets in front of Rink, Kong Oscar, and Sverdrup glaciers were considered in our analyses. However, subglacial runoff from each glacier ice basin provided the largest freshwater input.

5.3.3.3 Bathymetry and Cross-Shelf Hydrography

The presence or absence of sills and troughs within a tidewater glacier fjord can inhibit or facilitate warm, AW from reaching the glacier front (Schaffer et al. 2017; Schaffer et al. 2020). Oceanic sills are shallow sites that restrict water flow whereas troughs are deep pathways that enable water movement. We investigated the role of bathymetry and hydrographic patterns across the continental shelf by constructing transects beginning from each glacier front and

ending at the edge of the continental shelf. Transects were hand-drawn along the thalweg, known as the line of lowest elevation along a valley or channel, using QGIS software (QGIS Development Team 2022). Bathymetric data were sourced from IceBridge BedMachine Greenland, Version 5 (Morlighem et al. 2017; Morlighem et al. 2022). During mooring deployment/recovery cruises, ship based CTDs were taken from the R/V *Sanna.* In addition to these CTD profiles, airborne-expendable CTDs (AXCTDs) from NASA's OMG program were used to build temperature and salinity transects from the same year. Only CTD profiles that were on or near the thalwegs were included and observations between profiles were linearly interpolated for visualizing transect results.

While thalwegs provide the line of lowest elevation, we developed an algorithm to extract lines of highest elevation, or ridgelines, on either side of the thalweg channel (Supporting Text S5.2 and Figure S5.1). Thalwegs and ridgelines were plotted alongside CTD transects to examine inshore-offshore hydrographic patterns. Thalwegs provided the lower bound and the ridgelines the upper bound for bathymetric constraints across the shelf.

5.3.3.4 Remote Forcing

In addition to releasing over one thousand AXCTDs on Greenland's continental shelf during the summer, NASA's OMG campaign deployed autonomous profiling floats in major troughs along the shelf to obtain measurements at a higher temporal resolution. Three floats were deployed in Melville Bay and were programmed to profile the water column approximately every five days. The first float was released in 2017 but lasted less than a month due to environmental and technical complications. Here, we utilize float data from the latter two Autonomous Profiling Explorer (APEX) floats (Teledyne Webb Research): APEX Floats F9185 (22 October 2020–16 December 2021) and F9444 (20 September 2021–3 September 2023). In sum, the two floats provide nearly

3 years of data from the Melville Bay trough beginning in October 2020. The northbound West Greenland Current (WGC) follows Greenland's western boundary and is generally composed of a colder, fresher coastal current—referred to as the West Greenland Coastal Current (WGCC)—on the shelf and a warmer, saltier wedge on the slope (Myers et al. 2009; Lin et al. 2018; Pacini et al. 2020). Despite asynchronous observations between the float and mooring data, the timing and magnitude of offshore hydrographic seasonality provided a valuable comparison with the variability observed in the inshore mooring time series. By relating APEX float data to the moored observations, we examined whether upstream waters from the WGC that are advected inshore contributed to the hydrographic patterns observed at the glacier fronts. To accompany the offshore float data, we utilized a high resolution solution from the Estimating the Circulation and Climate of the Ocean (ECCO) Consortium to investigate seasonality in the WGC and remote forcing on glacier front hydrography in Melville Bay. Six years (2015–2020) of daily temperature and salinity from the ECCO model were analyzed (additional methods available in Supporting Text S5.3 and Figures S5.2–S5.4).

Table 5.1. Summary of ocean mooring instrumentation and deployments.

Mooring	Date deployed	Date recovered	Seafloor depth (m)	Latitude (°N)	Longitude (°W)	CTD instrument (depths, m)	Temperature logger (depths, m)
Rink	25 Aug 2018	5 Aug 2019	703	76.1605	61.2791	SBE 37-SM MicroCAT RS-232 (76, 328)	SBE 56 (125[a], 203, 266, 408, 488, 568, 648, 658)
Fisher	5 Aug 2019	11 Aug 2020	370	76.1038	61.7270	SBE 37-SM MicroCAT RS-232 (137, 377)	SBE 56 (187, 202, 227, 252, 277, 302, 327, 352)
Kong Oscar	24 Aug 2018	4 Aug 2019	251	75.8437	59.8429	SBE 37-SM MicroCAT RS-232 (104, 240)	SBE 56 (123, 143, 162, 182, 201, 220)
Kong Oscar	4 Aug 2019	10 Aug 2020	250	75.8418	59.8431	SBE 37-SM MicroCAT RS-232 (94, 226)	SBE 56 (113, 133, 153, 173, 193, 213)
Sverdrup	22 Aug 2018	3 Aug 2019	385	75.5413	58.4105	SBE 37-SM MicroCAT RS-232 (118, 355)	SBE 56 (153, 188, 223, 258, 293, 311, 337)

Note. The sampling interval was 180 seconds for the CTD instruments and 20 seconds for the temperature sensors. [a]This temperature logger stopped recording 25 days before the mooring recovery.

5.4 RESULTS

5.4.1 *Seasonal Hydrographic Variability and Subglacial Plume Signatures*

Seasonal variability in temperature and salinity was consistent across the three sites (Rink/Fisher, Kong Oscar, and Sverdrup). Time series of unmodified upper and lower CTD measurements at varying depths (Supporting Figure S5.6) were consistent with depth-averaged trends (Figure 5.2). Temperature and salinity reached a maximum in late spring (April–May) and a minimum in early winter (November–December). Temperature varied by approximately 1.25°C across depths and salinity varied by 0.8 psu between 120–140 m and 0.4 psu between 220–240 m. Hydrographic variability on a sub-monthly timescale and between sites was greater at shallower depths demonstrated by larger fluctuations in mean temperature and salinity within 120–140 m compared to 220–240 m (Figure 5.2). Shallow CTD observations also had a greater spread in T-S space than those from deep CTDs (Figure 5.3). Temperature and salinity profiles between 100 and 250 m showed that the Rink/Fisher site was slightly warmer than the Kong Oscar and Sverdrup sites within the AW layer (Supporting Figure S5.11).

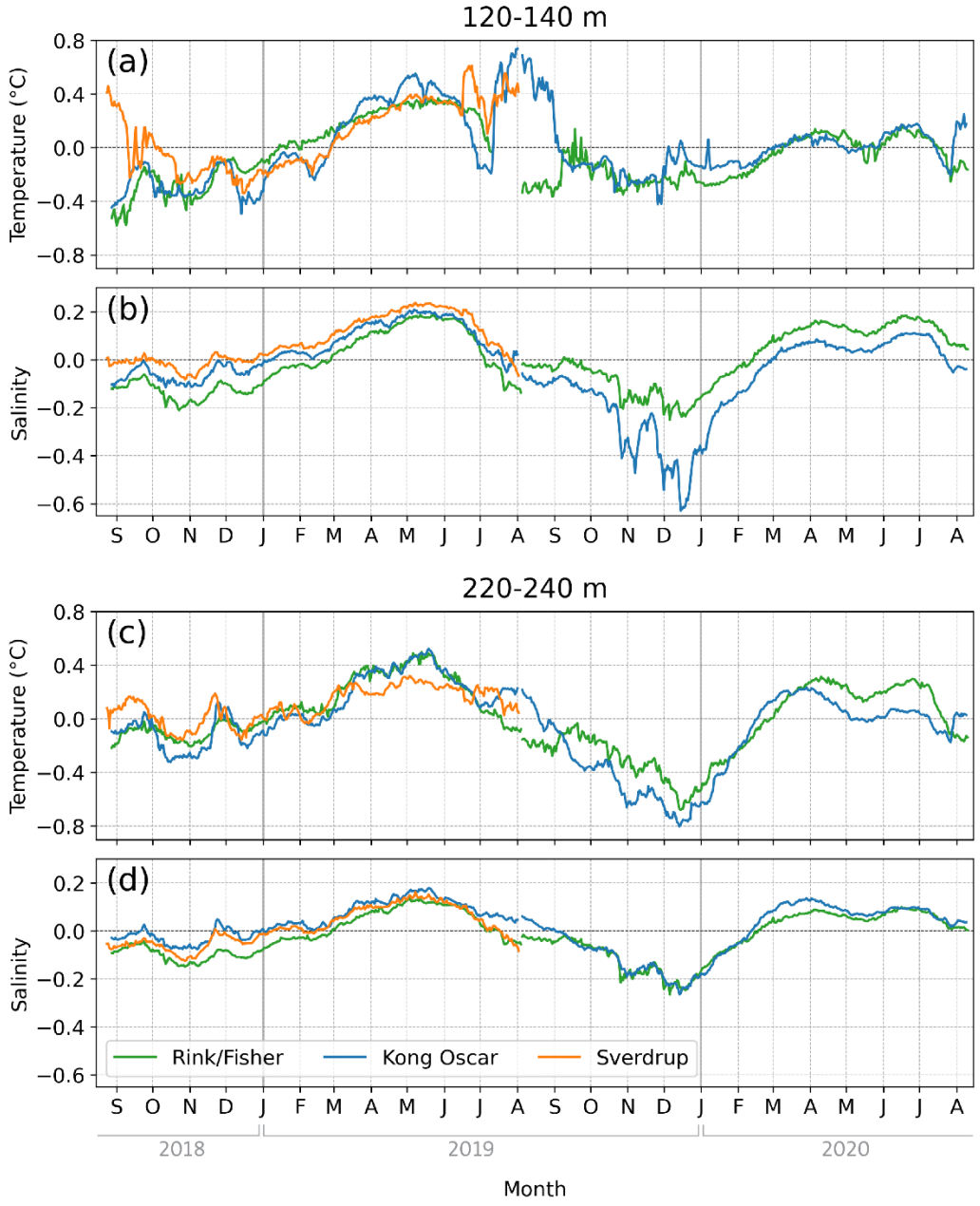

Figure 5.2. Daily mean temperature and salinity anomalies between 120–140 m (a, b) and 220–240 m (c, d) deep from moored observations at the three sites (green: Rink/Fisher, blue: Kong Oscar, orange: Sverdrup) with respect to each site's mean values. Mean temperatures in (a) and (c) are -0.07°C and 0.64°C, respectively. Mean salinities in (b) and (d) are 33.60 and 33.91 psu, respectively.

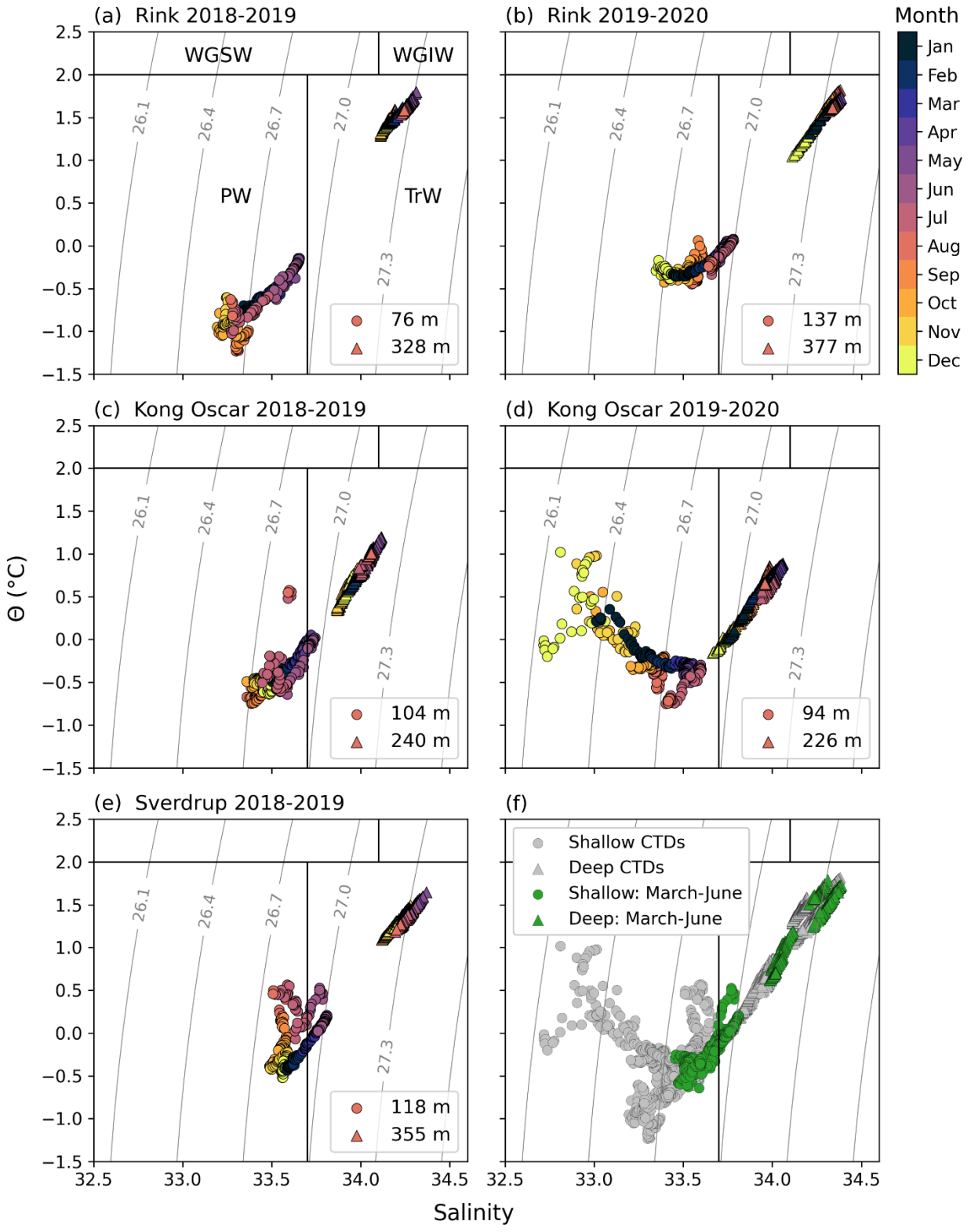

Figure 5.3. Potential temperature-salinity (T-S) plots for CTD observations (daily means) from each mooring (shallow CTD: circles, deep CTD: triangles) colored by month (a–e). Green points

in (f) show CTD observations from all five moorings that occurred between March and June and gray points show the remaining observations between July and February. Grey contours show lines of constant potential density in kg/m^3. Water masses are outlined as West Greenland Shelf Water (WGSW; $\theta < 7$ °C; $S < 34.1$), West Greenland Irminger Water (WGIW; $\theta > 2$°C; $S > 34.1$), Polar Water (PW; $\theta \leq 2$ °C; $S \leq 33.7$), and Transitional Water (TrW; $\theta > 2$ °C; $S > 33.7$) following Curry et al. (2014). Note: Curry et al. (2014) refer to PW as Arctic Water but we use PW to distinguish it from Atlantic Water (AW).

Investigation of T-S variability from moored CTD observations at intermediate depths (~100–350 m) revealed the presence of PW ($\theta \leq 2$ °C; $S \leq 33.7$) and Transitional Water (TrW; $\theta > 2$ °C; $S > 33.7$) (Curry et al. 2014) at the three sites (Figure 5.3). Generally, observations showed a positive, linear relationship where saltier, warmer waters were found below fresher, colder waters. The larger T-S variability seen in shallow CTDs (~100 m) differed in magnitude and timing between sites. The greatest departure from the mixing line was found at Kong Oscar between November 2019 and January 2020 (Figure 5.3d). Observations between March and June remained on the mixing line, indicating that the most stable period was during the spring (Figure 5.3f).

Freshwater anomalies computed from the difference in predicted (T-S linear fit) and observed (*in situ* moored CTDs) salinity clearly identified when and where CTD observations followed or deviated from the mixing line (Figure 5.4). Minimal to no differences in predicted and observed salinity were seen between March and June. The largest anomalies occurred from late summer to early winter at Kong Oscar and Sverdrup. Late summer anomalies between July and September at Kong Oscar and Sverdrup coincided with the timing of freshwater runoff and are characteristic of subglacial plumes (Figure 5.4). Subglacial plumes temporarily freshen waters near the glacier face and initiate vertical mixing where warm deep water masses are

advected upwards. There was a ~1–2 month lag between the onset of freshwater runoff in May/June and the arrival of upwelling plume waters (July) seen at Kong Oscar and Sverdrup. Rink/Fisher presented minimal variation compared to the other sites with no evident plume signature (Figure 5.4a). The estimated runoff rate for the Rink glacier ice outlet is less than one quarter the rate estimated for Kong Oscar and Sverdrup glaciers which have near-equal magnitudes. The prominent freshwater anomaly observed at Kong Oscar from November to January (2019–2020; Figure 5.4b) corresponded to the observations that departed from the T-S mixing line noted above (Figure 5.3d). During this time, freshwater progressively filled the upper 200 m until mid-December when it began to diminish. The freshwater anomaly observed in fall 2019 at Kong Oscar was associated with a strong wind-driven downwelling event and is discussed further in the following section (see Section 3.2).

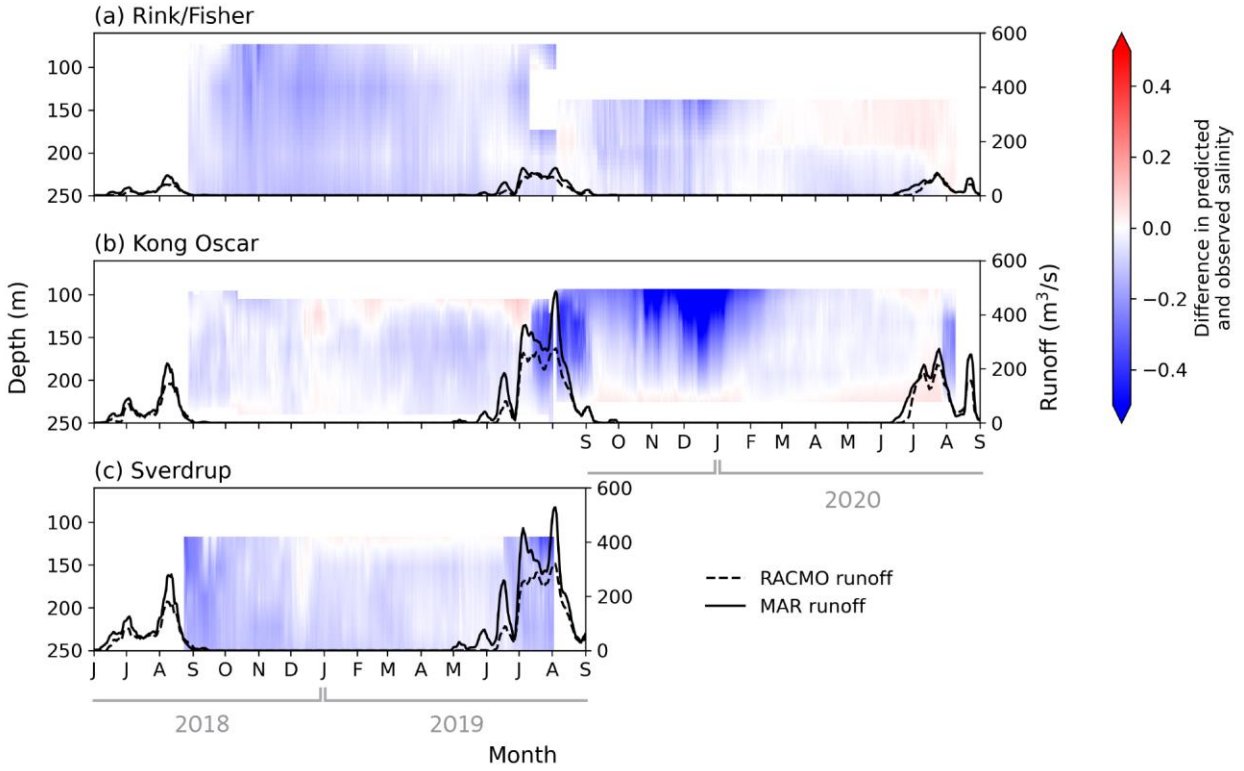

Figure 5.4. Profiles showing the difference in predicted salinity from the T-S linear fit and *in situ* salinity observations for Rink/Fisher (a), Kong Oscar (b), and Sverdrup (c). Blue colors represent fresher waters than predicted and red indicates waters saltier than predicted. Freshwater runoff from two regional climate models (RACMO and MAR) is shown for comparison with the freshwater anomalies (Mankoff 2020a; Mankoff et al. 2020a). Freshwater runoff is reported for each glacier ice outlet and does not include other nearby land and ice outlets.

5.4.2 *Local Forcing*

Relating key ice and atmosphere processes to the mooring temperature and salinity profiles revealed their seasonal influence on local hydrography. Beginning in June, increased insolation caused melting of the ice sheet, glaciers, sea ice, and icebergs. During these summer months, sea ice retreated, glaciers retreated, glacier ice velocity increased, and the ocean absorbed heat (Figures 5.5–5.7). What proceeded was a seasonal nearshore freshwater pulse and deepening of

isopycnals from June through December as meltwater flowed into coastal waters. Freshwater runoff increased in June following summer ice sheet melt, reached a maximum in July/August, and stopped in September (Figures 5.5–5.7f).

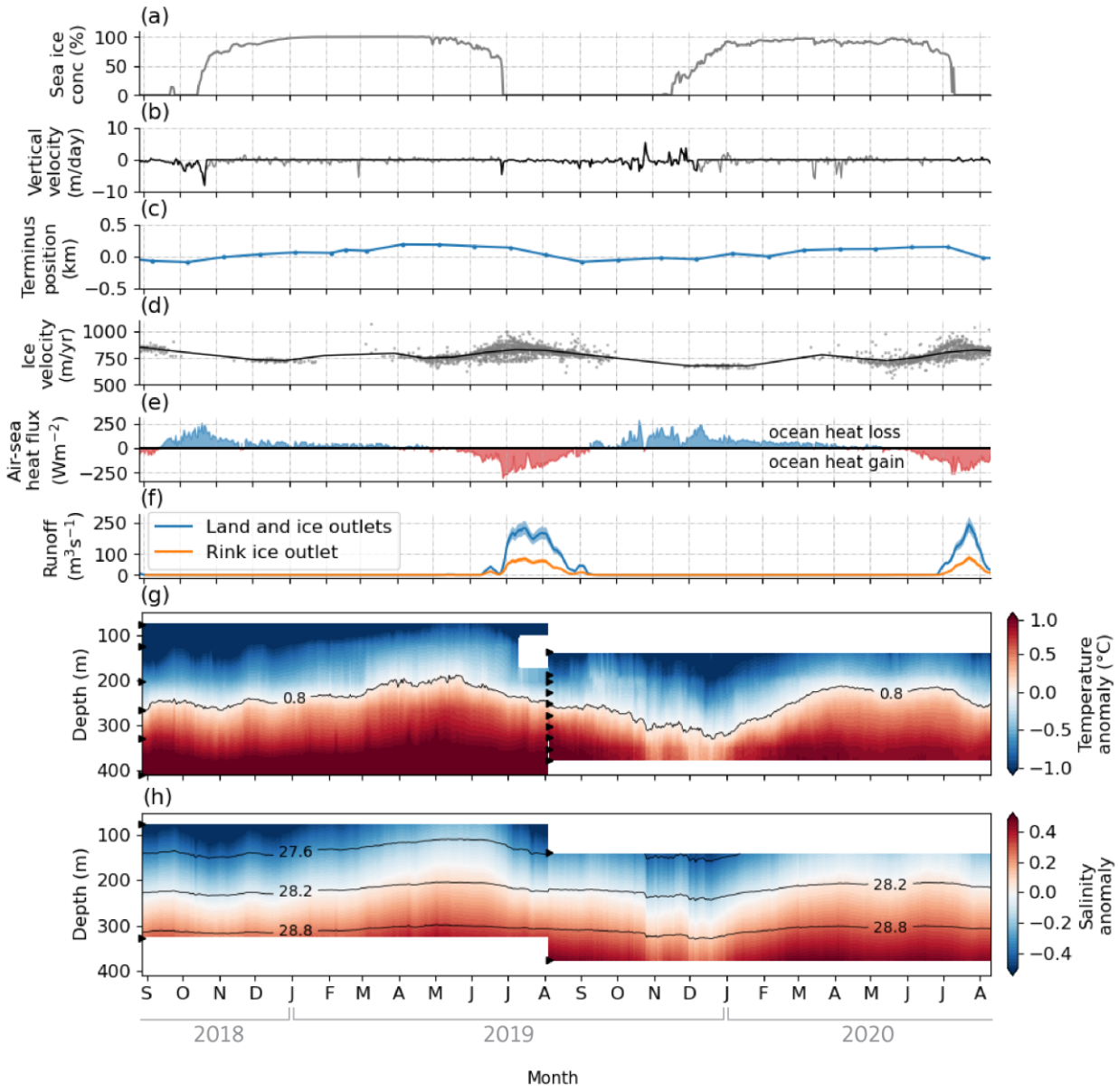

Figure 5.5. Timeseries of key variables to relate local ice and atmospheric processes to ocean variability at the Rink/Fisher mooring site. Sea ice concentration (a), vertical velocity (b), terminus position (c), glacier ice velocity (d), air-sea heat flux (e), freshwater runoff (f), and

profiles of temperature (g) and salinity (h) anomalies are shown between August 2018 and August 2020 with respect to overall mean values (across depths and sampling period). Although temperature loggers for the 2018–2019 Rink mooring recorded down to 658 m, the upper 400 m are shown here (g) to better match the sampling range in 2019–2020. The black line in (b) shows vertical velocity when sea ice is accounted for (i.e., wind stress is zero when sea ice concentration is above 50%) and the gray line is without considering the presence of sea ice. Increasing values for the relative terminus position (c) indicate glacier advance and decreasing values mean glacier retreat. The black line in (d) is the 30-day running mean of individual ice velocity estimates from satellite imagery (gray points). Air-sea heat flux values (e) are positive for atmosphere heat gain (ocean heat loss). Runoff (f) is shown for all land and ice outlets near the Rink glacier terminus (blue) and only the Rink glacier ice outlet (orange). Runoff is plotted with 15% uncertainty following Mankoff et al. (2020a). The mean temperature isotherm (0.8°C) is overlaid in (g) and potential density isopycnals are shown in (h). Horizontal triangles in (g) and (h) show the depths where hydrographic sensors were located within each profile. Specific details about the source and derivation of each dataset shown are provided in section 2.2.2.

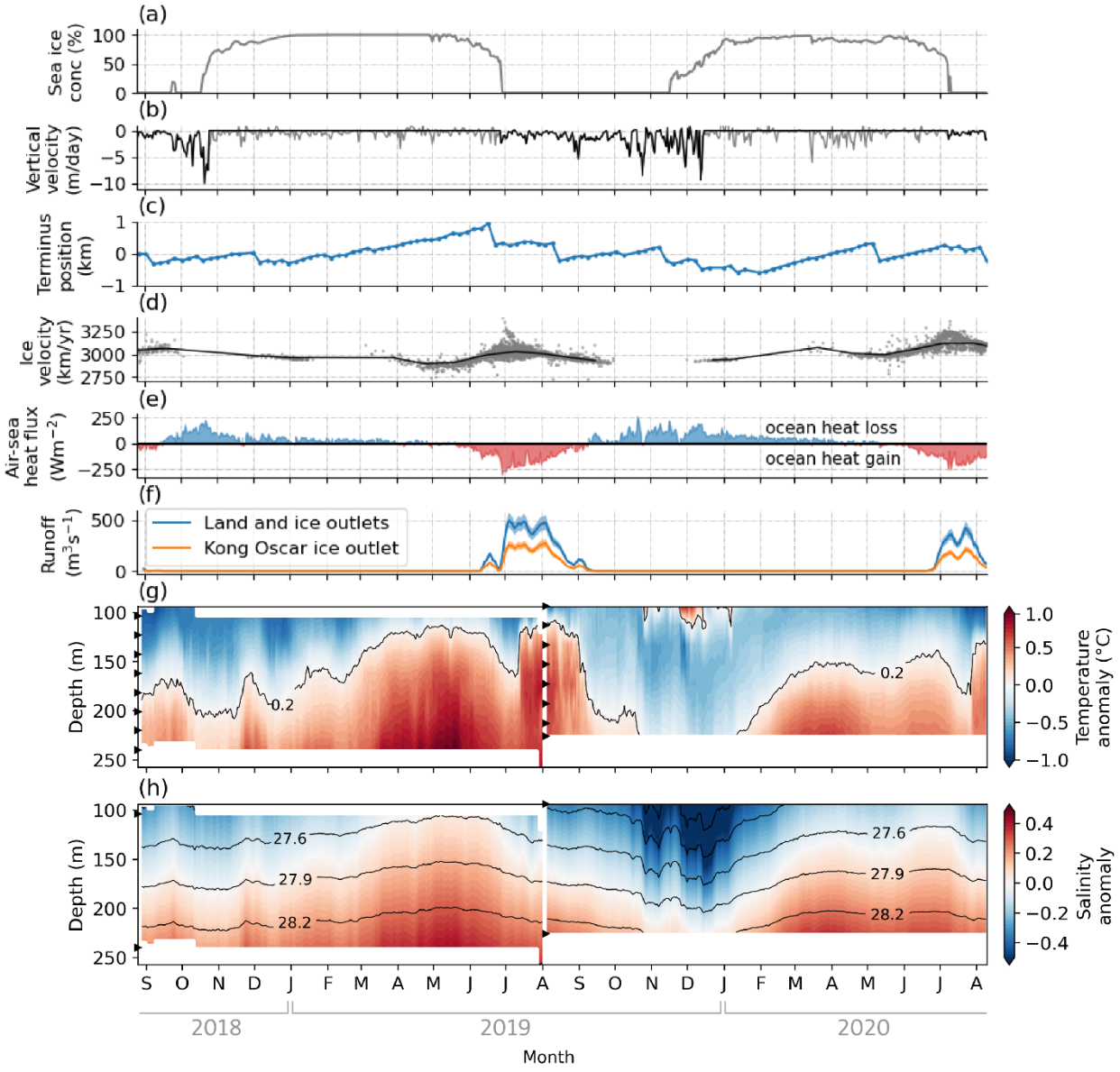

Figure 5.6. Same as Figure 5.5 but for the Kong Oscar mooring site between August 2018 and August 2020. The mean temperature isotherm of 0.2°C is overlaid in (g).

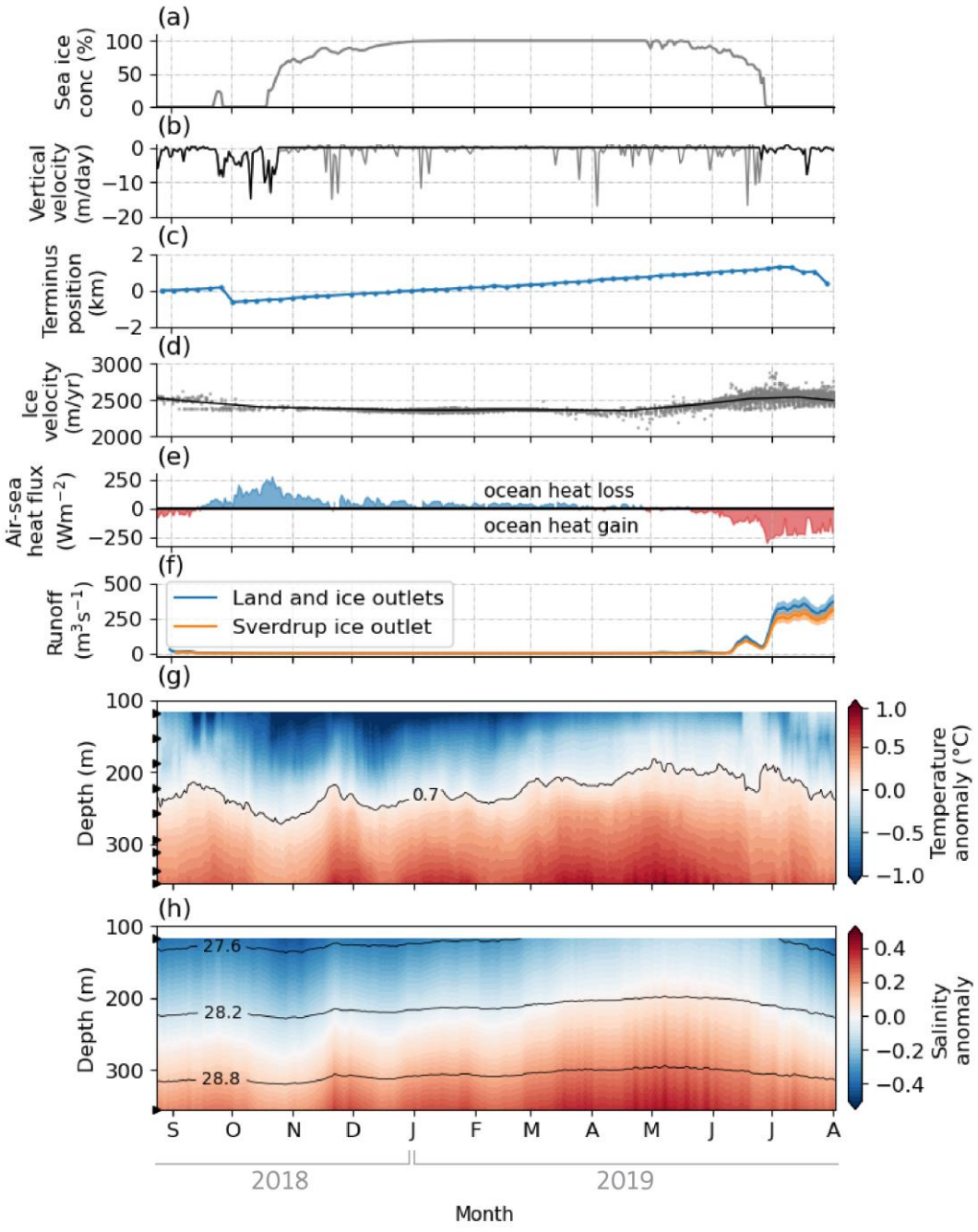

Figure 5.7. Same as Figure 5.5 but for the Sverdrup mooring site between August 2018 and August 2019. The mean temperature isotherm of 0.7°C is overlaid in (g).

The transition between summer and fall occurred by mid-September when the ocean began to lose heat, freshwater input from runoff stopped, and local winds increased. Northbound

low pressure systems traveling up the west Greenland coast brought cyclonic winds to Melville Bay and created downwelling-favorable conditions along the coast (Supporting Figures S5.7–S5.8). Wind speeds were strongest in the fall and winter but only influenced ocean vertical motion when sufficient open water existed (i.e., minimal sea ice). Fall sea ice formation began one month later and was more gradual in 2019 (~18 October) than in 2018 (~17 November; Figures 5.5a, 5.6a, 5.7a). The magnitude of vertical velocity varied between sites but was largely negative (downward) motion with the exception of Rink/Fisher where a few upwelling events occurred in October and November 2019 (Figures 5.5b, 5.6b, 5.7b). Further exploration of the freshwater anomaly in fall 2019 at Kong Oscar showed close alignment between modeled vertical motion and isopycnal variability (Supporting Figure S5.9), indicating wind-driven mixing. In addition to wind-driven vertical motion, ocean heat loss between September and January led to downward buoyancy-driven circulation as colder (i.e., denser) waters sank. In the winter and spring (December–May), Melville Bay was covered in landfast ice, glaciers advanced and decelerated, and warm, salty waters shoaled. During this period, sea ice cover inhibited wind-driven mixing and isotherms were smooth (g,h in Figures 5.5–5.7), reflecting stability in the water column. The fast ice broke-up late-June following the temperature and salinity maximum.

While the seasonal trends described above were consistent across the three sites, differences in plume dynamics were found. Total runoff, inclusive of land and ice outlets, was largest at Kong Oscar, followed by Sverdrup, and then Rink/Fisher (Figures 5.5f, 5.6f, 5.7f). However, Kong Oscar and Sverdrup had near equal runoff rates when considering only the contribution from the glacier ice basin and no other nearby land/ice sources. Subglacial plume signatures in local hydrography also differed between sites. Positive temperature anomalies in

shallow waters between June and September provided evidence of subglacial plumes as warm temperatures at depth rose toward the surface. Temperature signatures for plumes were observed for Kong Oscar and Sverdrup but not for Rink/Fisher (Figures 5.5g, 5.6g, 5.7g). Evidence of the plume was most visible at Kong Oscar.

5.4.3 *Impacts of Bathymetry and Remote Forcing*

Along-thalweg summer CTD transects extending from each glacier front to the edge of the inner shelf showed the modification of near-terminus water from glacier freshwater input (Figure 5.8). Isopycnals deepened near all glacier fronts, indicating the presence of a deeper PW wedge that borders the coastline (Figure 5.8c–h). The upper cold, fresh layer (PW) and deeper warm, salty layer (TrW and WGIW) were intensified and more stratified farther offshore. Compared to offshore profiles, inshore profiles were warmer and fresher in near-surface waters (<200 m) and cooler and fresher at depth, consistent with subglacial plume mixing near the glacier termini.

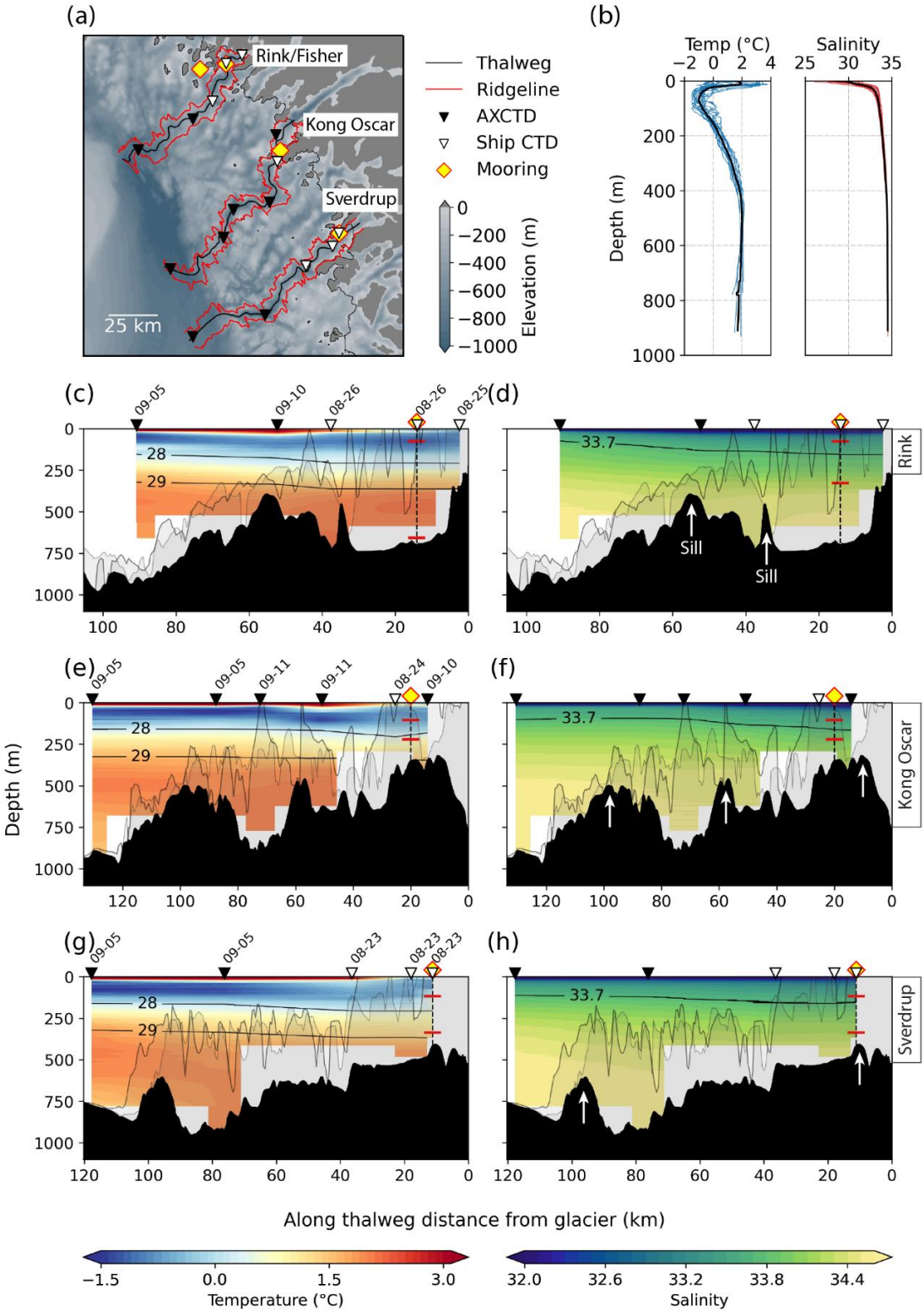

Figure 5.8. Example cross-shelf CTD transects for summer 2018 at each glacier site: Rink/Fisher (c, d), Kong Oscar (e, f), and Sverdrup (g, h). Panel (a) shows the location of hand-drawn

thalwegs (black), ridgelines produced from our program (red; see section 2.3.3), and 2018 ship-based CTDs (white inverted triangles) and AXCTDs (black triangles) used in the transects (c–h). Temperature (blue) and salinity (red) profiles for all 2018 CTDs used in the transects are presented in (b) with mean profiles shown in black. The thalweg distance (km) begins at the glacier front and increases going offshore. Along thalweg temperature transects are shown on the left (c, e, g) with potential density isopycnals, and salinity transects are shown on the right (d, f, h) with the 33.7 isohaline overlaid. In all transects (c–h), the shaded black region shows the bathymetry along each thalweg and the shaded gray region shows the ridgeline elevations to either side of the thalweg. CTD locations are plotted at the top of each transect with sampling dates (MM-DD) provided on temperature transects. White arrows in (d, f, h) indicate locations of sills along each thalweg. Mooring locations for each site are shown in (c–h) with upper and lower bounds (horizontal red lines) marking the depth range covered by temperature sensors. Mooring locations displayed on transects are for reference only; no mooring data were used in the creation of the temperature or salinity transects. Since the Rink/Fisher mooring site differed between years, the 2018–2019 Rink mooring location and sensor depths are pictured in (c) and (d) because the location of the 2019–2020 Fisher mooring was not on the tranect (a).

Visualization of thalweg and ridgeline bathymetry for the three sites showed that the seafloor geometry across the shelf is highly variable with many peaks and troughs (Figure 5.8c–h). The mean ridgeline depth, inclusive of all three sites, was 359 m and the mean thalweg depth was 665 m. For all sites, ridgelines reached the surface around 30–40 km from the glacier front, forming nearby islands and small inlets (Figure 5.8). The warm, freshwater lens at the surface, known as the seasonal surface mixed layer, was visible throughout most of the transect except for the closest 30–40 km in front of the glacier termini.

Thalweg bathymetry extending from each glacier front generally deepened going offshore but contained sills that inhibited horizontal water movement. The Rink/Fisher thalweg had two sills, one inshore at 447 m and the other offshore at 393 m (Figure 5.8d). However, we

note that both sills were deeper than the grounding line of the glacier (223 m). The Kong Oscar transect had three sills at 317, 458, and 497 m with the shallowest one 11 km from the glacier front (Figure 5.8f). Sverdrup had one outer sill at 606 m and one inner sill at 407 m (Figure 5.8h). All moorings, with the exception of the 2018–2019 Rink/Fisher mooring, did not measure temperature or salinity below sill depths (see moorings plotted in Figure 5.8c–h). The 2018–2019 Rink/Fisher mooring was instrumented with temperature loggers down to 658 m (Table 1) and positioned in a trough between the glacier front and inshore sill. Examination of the full-depth Rink/Fisher temperature profile revealed a distinct difference in seasonal hydrography above and below the sill at ~400 m. The consistent seasonal pattern observed at all sites was visible above the sill for Rink/Fisher and little change in temperature was observed below the sill (Supporting Figure S5.10).

Offshore profiling float data from the Melville Bay trough showed clear seasonality in temperature and salinity down to ~500 m (Figure 5.9). A summer seasonal mixed layer of warm, fresh water was visible from July to September in near-surface waters <50 m (Figure 5.9a,b). By fall (September–October), air-sea heat fluxes changed sign and waters began to cool. Accordingly, surface freshwater melt accumulated during summer along the coast became denser and propagated downward (i.e., PW layer thickened) throughout winter in the upper ~100 m. Similarly, seasonality was observed in ECCO temperature and salinity estimates along the WGC and showed the progression of warm, saline AW propagating northward (Supporting Figure S5.4–S5.5).

The core AW layer in the Melville Bay trough was identified between 320–380 m in the profiling float and ECCO data. At these depths, temperatures reached a maximum in November and December, coinciding with temperatures near glacier fronts changing sign and beginning to

warm (Figure 5.9e). Maximum temperature and salinity offshore occurred approximately 4–5 months before corresponding maxima observed in inshore moored observations (April–May). Temperature from the float data varied annually by ~0.5°C and salinity by ~0.2. Empirical data from APEX floats showed a longer cooling and freshening period (December–September: 9 months) in the trough than at glacier fronts (May–December: 7 months) between 320–380 m.

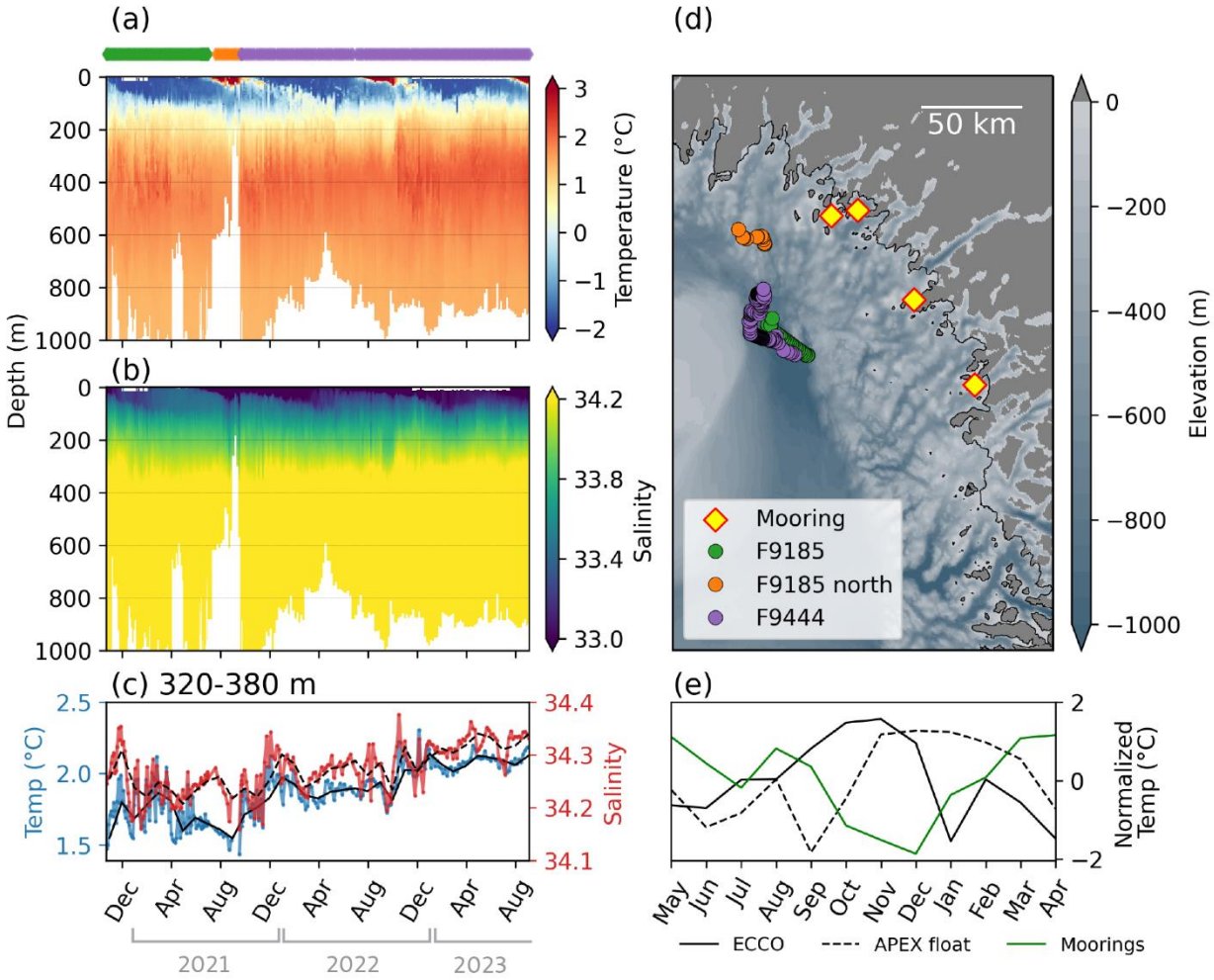

Figure 5.9. APEX float temperature (a) and salinity (b) profiles, intermediate depth (320–380 m) mean temperature and salinity time series (c), and float profile locations (d) for F9185 (22 October 2020–16 December 2021) and F9444 (20 September 2021–3 September 2023). The comparison between monthly mean temperature (detrended and normalized) for the ECCO

solution, APEX floats, and mooring time series between 320–380 m is shown in (e). For (c), individual profile mean temperature (blue) and salinity (red) observations are shown with overlaid monthly means in solid and dashed black lines, respectively. Profile GPS locations in (d) were linearly interpolated for occasions when the float could not obtain a fix. Colored diamonds above temperature and salinity profiles in (a) correspond to the colored profile locations in (d). Orange circles show positions for when F9185 drifted north, outside of the Melville Bay trough. Observations outside of the trough (F9185 north) were not included in calculations for the APEX float time series in (e).

5.5 DISCUSSION

5.5.1 *Melville Bay Seasonal Hydrography*

Examination of mooring data at three glacier fronts in Melville Bay revealed consistent above-sill seasonality across sites, indicating that similar exogenous forces shape hydrographic variability at Northwest Greenland glacier termini. The warmest, saltiest waters were observed in late spring (April–May maximum) before ice sheet surface melt began and cold meltwater flowed from glaciers to the shelf. The coldest, freshest waters occurred in early winter (November–December minimum) after the summer melt season.

Based on moored temperature and salinity profiles and from investigating observations in T-S space, we propose that hydrographic variability at Melville Bay glacier fronts consists of three primary phases: variable, intermediate (or recovery), and stable. The open-water season in summer and fall constitutes the variable phase due to local atmosphere and ice dynamics. Variation in temperature and salinity was greatest between July and November, coincident with local plume-driven mixing and large wind events before winter sea ice formation. The shift from plume-driven upwelling to wind-driven downwelling created a dynamic setting between summer and fall. Ekman pumping was most notably observed at the Kong Oscar site in fall 2019 which

may be associated with the longer open-water season of 2019. Fast-ice formation occurred one month later in 2019 than in 2018. The intermediate period occurs in winter (December–February) as waters recover from the variable phase. It is during the intermediate phase that the renewal of warm, salty waters takes place as AW shoals and transitions to the stable phase in spring between March and June. During this time, inshore waters were most stable following winter months when local forcing from glacier dynamics (e.g., runoff, calving) was minimized and sea ice acted as a barrier to wind-generated Ekman pumping. The shoaling of AW in spring primes glaciers for enhanced submarine melt in July due to warm water entrainment from summer subglacial plumes.

5.5.2 *Local and Remote Forcing*

Our results indicate that Melville Bay hydrography is shaped by both local and remote forcing. Local effects of freshwater runoff, wind stress, sea ice, air-sea heat fluxes, and glacier behavior (i.e., speed and advance/retreat) on glacier front hydrography modulated sub-monthly variability, particularly in summer and fall. Conversely, we speculate that remote forcing from upstream currents controls the renewal of warm, salty AW inshore near glacier fronts during spring (Figure 5.9). This conclusion is supported by float profile observations of warmer, saltier waters offshore and seasonality observed in the ECCO solution and float data. When offshore temperatures in the Melville Bay trough peak in November–December, temperatures near glacier fronts changed sign and began to warm, suggesting warm, salty waters are advected inshore and contribute to the renewal of AW from December to May. Generally, local conditions modify inshore waters on shorter timescales (weeks) compared to remote effects (months to years). Future work to quantify the seasonality of PW in the WGCC will help elucidate what fraction of

the freshwater pulse observed in our moorings (March–December; Figure 5.2) originates from local summer melt versus remote circulation pathways.

Altogether, observations from moorings, CTDs, and profiling floats verify heat transport from the North Atlantic to glacier fronts in Melville Bay in concordance with existing literature (Carr et al. 2013; Porter et al. 2014; Willis et al. 2018; Wood et al. 2018; Morlighem et al. 2019). Although waters are modified as they travel poleward from the southern tip of Greenland along the west coast, we confirm the presence of Atlantic-origin water in the form of TrW (-0.5–2°C) based on water mass properties in T-S space (Figure 5.3). Ocean waters surrounding Greenland experience progressive heat loss as northbound warm, saline AW meet cold, fresh PW from outlets of tidewater glaciers and the Arctic Ocean. Waters along southeast Greenland and the Irminger Sea experience the warmest mean AW temperatures (8–10°C), owing to their proximity to the North Atlantic Current (Straneo et al. 2012). Conversely, AW in Melville Bay is much colder due to mixing of AW and PW and released heat during transit via air-sea temperature exchanges (Rignot et al. 2012; Straneo et al. 2012; Rysgaard et al. 2020). However, unlike typical fjord systems where in- and outflowing water follow a single or few primary channels, marine-terminating glaciers in Melville Bay are exposed to shelf waters that have traveled across the shelf through numerous pathways. Despite the dilution of AW along Greenland's western boundary, deep glaciers in Melville Bay will be susceptible to increased submarine melt with increasing ocean temperatures, referred to as the "Atlantification" of the Arctic (Årthun et al. 2012; Asbjørnsen et al. 2020; Ingvaldsen et al. 2021).

5.5.3 *Evidence of Plume and Role of Bathymetry*

Our results provide empirical evidence of subglacial plume signatures from mooring profiles where anomalously warm, fresh waters were observed at shallow depths less than 200 m. Direct

observations of subglacial plumes have been collected using CTDs (Bendtsen et al. 2015; Fenty et al. 2016; Mankoff et al. 2016; Straneo et al. 2016; Willis et al. 2018) and imagery from cameras and satellites (Fried et al. 2015; Schild et al. 2016), but to our knowledge, there has not been a complete hydrographic timeseries of subglacial plume upwelling prior to the present study. Meltwater plumes driven by upwelling runoff were seen in hydrographic profiles for Kong Oscar and Sverdrup but not for Rink/Fisher (Figure 5.4). Known features of these glaciers (see section 2.2) explain the observed differences in plume signatures. Kong Oscar and Sverdrup are midsized glaciers with deep grounding lines (>300 m) so buoyant meltwater runoff released at the base of their termini creates a larger density gradient and more turbulent upwelling plume. Conversely, Rink is a shallow glacier (<300 m grounding depth) so the rising plume equilibrates with ambient waters more quickly. Additionally, Kong Oscar and Sverdrup discharge four-times the volume of freshwater runoff compared to Rink (Figure 5.4) and thus produce larger plumes with greater mixing potential. Therefore, we expect warm water entrainment is substantially higher for Kong Oscar and Sverdrup than for Rink. Our results support the conclusion that the glacier grounding depth and runoff rate determine the magnitude of the rising plume, and thus undercutting potential, at glacier fronts.

Seafloor geometry at or near the glacier front controls onshore-offshore horizontal water flow in addition to the vertical motion of the plume. Glacier basin walls and coastal islands—illustrated here as ridgelines extending above sea level—spatially coincided with the dissolution of the surface mixed layer. These findings suggest that the local topography near the glacier fronts may constrain locally modified waters formed from the mixing of runoff, subglacial melt, and iceberg melt during the summer (Figure 5.8). However, freshwater export is also influenced by water density gradients and near-terminus circulation. Plume signatures from the moored

observations began 30–45 days after the onset of freshwater runoff (Figure 5.3b,c) consistent with other studies showing delayed freshwater export (Sanchez et al. 2023). Furthermore, we show ocean sills restricted cross-shelf circulation, where seasonal hydrographic variability was observed above the sill depth but was largely invariant below the sill. Renewal of below-sill basin waters occurred in the spring when isopycnals shoaled and dense coastal inflows spilled over shallow ridges. Based on the sill depths of the three transects, the mean ridgeline depth (359 m), and offshore float profiles, we expect the majority of ocean variability within the Melville Bay shelf occurs in the upper 400 m.

We attribute the consistent seasonality observed in our three study sites to the lack of long, narrow fjord channels in Melville Bay which exposes glacier fronts to shelf waters and exogenous forcing in a similar way. Compared to much of Greenland's coastline, this region is unique in that tidewater glaciers terminate directly into Melville Bay as opposed to being situated in deep, extended fjords tens of kilometers in length. More uniform exchange between in- and offshore waters leads to the same seasonal progression of temperature and salinity (Figure 5.2). However, during the summer and fall variable phase, unique glacier characteristics drive site-specific plume signatures that temporarily modify nearshore waters and create a heterogeneous oceanographic environment along the coast.

5.5.4 *Factors Controlling Glacier Retreat*

There is a growing body of literature demonstrating the ocean's role in driving the retreat and acceleration of Greenland's marine-terminating glaciers (Fenty et al. 2016; Khazendar et al. 2019; Wood et al. 2021). It has been shown that while submarine glacier melt in south Greenland is largely due to ocean warming, in Northwest Greenland it is primarily governed by atmospheric warming via increased runoff and warm water entrainment (Slater & Straneo 2022). Yet,

understanding the relative contributions of ice, ocean, and atmosphere forcings on glacier behavior is difficult with limited empirical observations. Glacier model simulations for Northwest Greenland glaciers support the hypothesis that ocean forcing can initiate glacier retreat while the glacier bed geometry determines the rate and magnitude of the retreat (Morlighem et al. 2019; Wood et al. 2021). Generally, glaciers on a retrograde (i.e., downhill going inland) bed slope are expected to be more susceptible to retreat compared to prograde (i.e., uphill going inland) slopes (Catania et al. 2018). In the present study, we investigated three glaciers with different behavior within the same region, each ~50 km apart. Although our results showed consistent hydrographic seasonality across sites, the thermal forcing experienced by each glacier front varies due to differences in glacier grounding line depths and runoff rates. As a relatively shallow glacier (243 m deep), Rink encounters the lowest thermal forcing compared to Kong Oscar (747 m deep) and Sverdrup (532 m deep). Rink has also retreated along a prograde slope to form two termini tightly bound by land (Figure 5.1b). Therefore, it is not surprising that Rink presents little to no seasonal and interannual terminus position variability and has remained stable in recent years.

After all three glaciers were destabilized in the late-1990s and retreated (Wood et al. 2021), Rink and Kong Oscar found new stable positions, but Sverdrup continued to retreat (Figure 5.1f). The bathymetry directly in front of Kong Oscar glacier has yet to be mapped but is expected to be a steep retrograde slope (Supporting Figure S5.12). Based on the characteristics of Kong Oscar, continued retreat of the glacier is expected. However, we speculate that Kong Oscar is currently choked by narrow local bed topography which may be inhibiting further retreat (Figure 5.1c). Despite Kong Oscar being a faster glacier with more solid ice discharge, Sverdrup has a larger mean runoff rate and is almost twice the width of Kong Oscar. A definitive cause for

Sverdrup's ongoing retreat compared to Kong Oscar is unclear, but it may be the combination of a deep grounding line along a retrograde slope, sufficiently high runoff, and a wide channel that results in continued destabilization of the terminus. Still, evaluating additional variables and the interactive effects between ice mélange, sea ice, subglacial plumes, and glacier characteristics (e.g., width, ice velocity, and bed slope) remains a considerable challenge in predicting glacier behavior.

5.5.5 *Oceanographic Setting of Melville Bay Glacier Fronts and Future Work*

The clear seasonality observed in our mooring data closely aligns with the seasonal pattern seen in intermediate depth waters (~260 m deep) at the mouth of two fjords in central west Greenland (Carroll et al. 2018). Warm waters from the WGC are shunted through Uummannaq trough to fjords in central west Greenland, reaching a temperature maximum in spring (April–May; Carroll et al., 2018). Similarly, we show above-sill waters that have transited through the Melville Bay trough to glacier fronts also peak in April–May. In Davis Strait, WGIW reach maximum temperatures between November and December (Curry et al. 2014), ~5 months before Carrol et al. (2018) observed a peak in temperature of intermediate depth waters. However, since we find a similar ~5 month lag in temperature maxima at Melville Bay glacier fronts, it is possible that the thickening of the PW layer (i.e., freshening and cooling) observed along the inner west Greenland shelf is controlled more by seasonal freshwater runoff and to a lesser extent advection from upstream WGCC waters.

Moored observations from southeast Greenland fjords and the continental shelf provide a stark difference in hydrographic variability compared to those in west Greenland. Notably, the prevalent northeasterly winds in Baffin Bay are much weaker than the extreme along-shore winds observed in southeast Greenland. Moored observations in southeast Greenland near

Helheim and Kangerdlugssuaq glaciers show significant variability over very short (daily) timescales (Straneo et al. 2010; Jackson et al. 2014). These rapid changes in fjord hydrography are due to the absence of shallow sills and high-velocity barrier winds along the southeast Greenland coast that drive rapid cross-shelf exchange with fjord waters without bathymetric constrictions (Straneo et al. 2010; Harden et al. 2014). Outside of the fjord, Harden et al. (2014) suggest that the thickening of the PW layer in the East Greenland Coastal Current (EGCC), which feeds into the WGCC, during winter and spring originates from advection of Arctic PW export through Fram Strait as opposed to being sourced from Greenland runoff. Further research is needed to investigate the relative contributions of Greenland runoff and PW exported from the Arctic in Greenland's coastal currents (i.e., EGCC and WGCC).

For Melville Bay specifically, we encourage future work to assess how the hydrographic seasonality described herein is related to biological processes. For instance, subglacial plumes are expected to bring nutrient-rich waters to the photic zone and promote primary productivity (Meire et al. 2017; Kanna et al. 2022). However, as summer plumes fuel primary production, autumn storms that cause downwelling can quench it as nutrients in the surface layer are not replenished. Our results showing year-round variability in temperature and salinity provide the necessary physical basis to understand larger ecological dynamics, including seasonal habitat-use of Melville Bay glacier fronts by marine mammals and seabirds (Laidre et al. 2016; Straneo et al. 2022).

5.6 Conclusions

Coastal waters at glacier fronts in Melville Bay exhibited consistent above-sill seasonality in temperature and salinity with unique plume signatures driven by seafloor geometry and glacier dynamics. Analysis of *in situ* observations, reanalysis and glacier data products, and a high-

resolution ocean model indicated seasonal modulation of local and remote forcing on regional glacier front hydrography. Temperature and salinities reached a maximum in late spring (April–May) after the winter fast ice period and a minimum in early winter (November–December) following the summer melt season. We found that springtime ocean warming primes glacier fronts for submarine melt via summer subglacial plume mixing. Late summer and fall variability were largely driven by local processes, including vertical mixing from runoff and wind-driven downwelling. During winter when Melville Bay is covered in fast ice, the water column gradually stabilized as warm, salty water shoaled. Results support the assertion that runoff rates and outlet depths (i.e., glacier grounding depth) determine the magnitude of buoyant meltwater plumes in glacier front hydrography. To our knowledge, the mooring data presented here are the only year-round observations that have been made in Melville Bay, and further, they provide the first complete hydrographic time series of subglacial plume upwelling near glacier fronts. Understanding year-round ocean variability along Greenland enables calibration and validation of global ocean numerical models and informs our understanding of ocean-ice interactions including plume dynamics. It also provides a foundational understanding of how the physical environment evolves throughout the year which can be linked to biological and ecological processes, such as primary production and the seasonal occurrence of narwhals at glacier fronts in Melville Bay.

5.7 ACKNOWLEDGEMENTS

This research was funded by the US Office of Naval Research (award no. N00014-17-1-2774) and the NASA Oceans Melting Greenland EVS-2 mission. M.J.Z. was partially supported by the Cooperative Institute for Climate, Ocean, & Ecosystem Studies (CICOES) under NOAA Cooperative Agreement NA20OAR4320271, Contribution No. 2023-1296. We thank Taryn

Black for providing glacier length datasets in advance and Carine van der Boog for sharing code to process profiling float data. We also thank Ken Mankoff for his assistance in providing updated runoff estimates to cover our sampling period.

5.8 Data Availability

All mooring and CTD data from the OMG Narwhals project and bathymetry, AXCTD, profiling float, and elevation data from the OMG mission are available via NASA/Caltech's JPL Physical Oceanography Distributed Active Archive Center (PO.DAAC) at https://podaac.jpl.nasa.gov/omg. BedMachine version 5 data are provided by the NSIDC at https://doi.org/10.5067/GMEVBWFLWA7X. ERA5 hourly data are supplied by the Copernicus Climate Change Service Climate Data Store at https://doi.org/10.24381/cds.adbb2d47. Freshwater runoff data are available at https://doi.org/10.22008/promice/freshwater. Ice velocity data were extracted from the NASA MEaSUREs ITS_LIVE project at https://its-live.jpl.nasa.gov. Glacier terminus positions are accessible through NSIDC at https://doi.org/10.5067/DGBOSSIULSTD. All analyses were conducted using Python (version 3.9.7) and relied on the *xarray* (Hoyer & Hamman 2017), *cartopy* (Met Office 2010 - 2015), *pandas* (McKinney 2010; The pandas development team 2023), and *NumPy* (Harris et al. 2020) packages. The code used to produce all analyses and figures for this manuscript are publicly available on Github: https://github.com/mjzahn/OMG_Narwhals_hydrography-manuscript.

5.9 Supplemental Materials

Text S5.1. Ordinary Differential Equation (ODE) to model vertical motion over time

Given the downwelling favorable conditions along the Melville Bay coast during the fall, we suspected wind-driven vertical motion to account for some of the isopycnal variation observed at

Kong Oscar. To model vertical motion for each timestep (equal to 1 day), we used the following equations:

$$\frac{dh}{dt} = \text{vertical motion} + \text{relaxing term}$$
$$= w_{ek} - \left(\frac{h_t}{\tau}\right) \quad \text{(S5.1)}$$

$$h_{t+1} = h_t + dt\frac{dh}{dt} \quad \text{(S5.2)}$$

where h refers to the change in vertical height (or depth) in the water column each day (dt = 1 day) and is negative downwards. The initial height, h_0, is zero and represents the initial depth (m) that the water column is returning towards over the relaxation period, τ. The relaxation period parameter (τ), expressed in number of days, was adjusted until the best approximation of h to the observed Kong Oscar isopycnal was achieved.

Text S5.2. Algorithm to extract ridgelines along seafloor

To identify ridges, the program searches along lines extending from the thalweg for the elevation maximum (Supporting Figure S5.1a). Here, a radius extending 8 km on either side of the thalweg was used. The procedure was initially designed so that search lines extended perpendicular to the thalweg. However, in regions where tight curves were present in the thalweg, search lines overlapped which led to discontinuous ridges. Therefore, a reference line that runs roughly parallel to the thalweg is used to define the angle at which search lines extend from the thalweg. The reference may have bends to better match the thalweg trajectory. If multiple elevation maxima are identified, the program is configured to extract one local maximum based on a set of conditions in an effort to find one continuous ridge. Outlier points are identified based on spatial coordinates and are smoothed by using nearby points to interpolate a corrected position (Supporting Figure S5.1b). Ridgelines produced by the program were validated by comparing them with hand-drawn ridgelines created in QGIS and the results showed good agreement.

Text S5.3. Evaluating remote forcing using high resolution ECCO solution

The ECCO model domain covered central and northwest Greenland from approximately 68°N to 78°N across Baffin Bay from 39°W to 77°W (Figure S5.2). The area of each grid cell along the West Greenland coast and used in our analyses was approximately 3600 m^2. To identify seasonality of Atlantic water (AW) propagating north in the West Greenland Current, we analyzed seven transects of temperature and salinity along the horizontal (x) dimension at evenly distributed intervals (every 25 rows) across the y dimension: rows 0, 25, 50, 75, 100, 125, 150 (Figure S5.2). For each transect, boxes were isolated (dimensions x and z) where the core AW layer occurred. AW boxes were identified using seasonal mean temperature and salinity profiles and isopycnal boundaries. Potential densities of 27.3 and 27.4 kgm^{-3} were used to define the upper and lower depth limits (example for row 0 provided in Figure S5.3). AW boxes were extracted, detrended, and normalized by their standard deviation. Monthly time series were plotted for each AW box to evaluate seasonality along the central and northwest Greenland coast (Figure S5.4). The most northerly AW box from row 150 in Melville Bay was compared to the APEX float and Melville Bay seasonality (Figure 5.9e in main text).

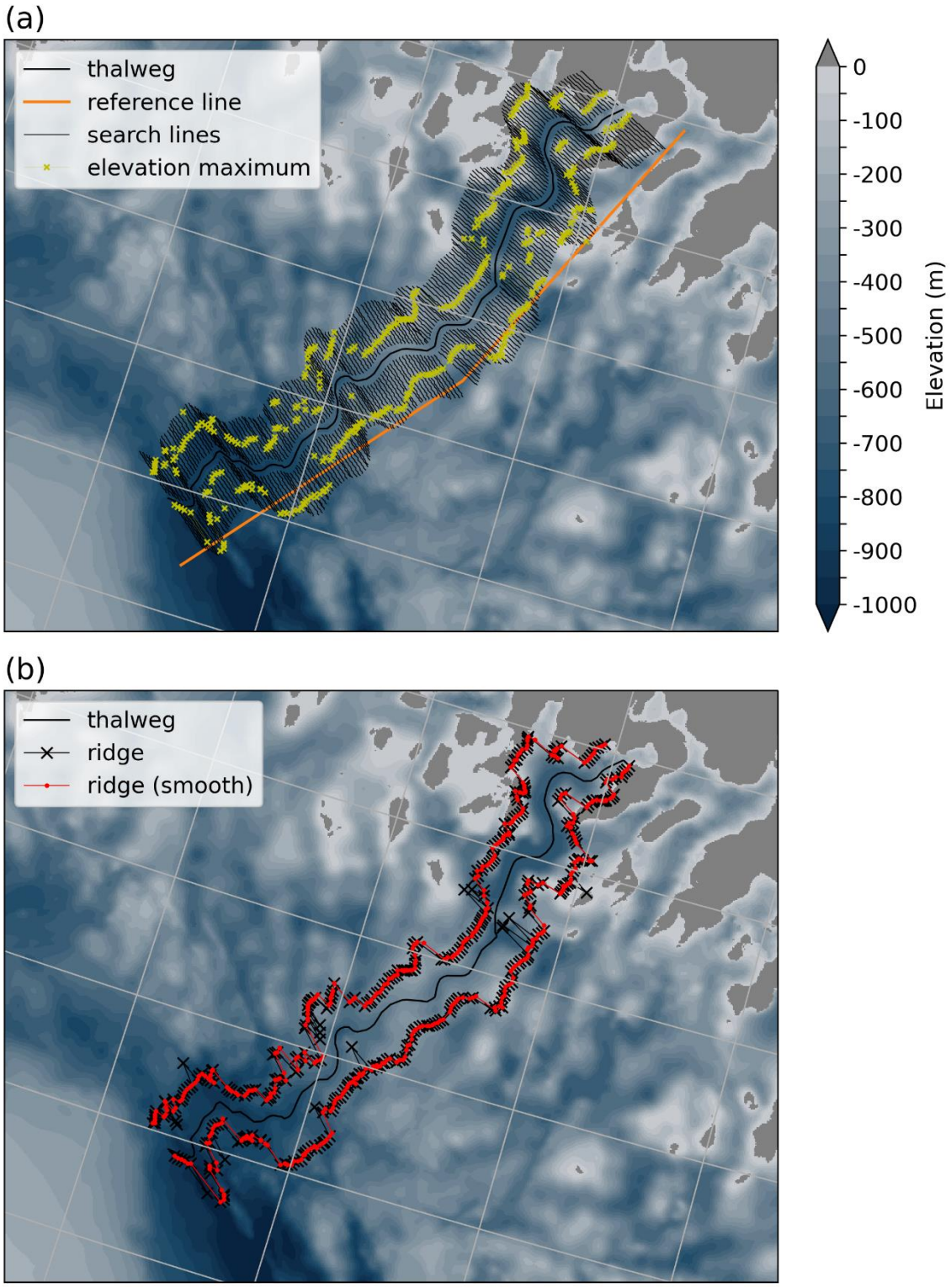

Figure S5.1. Ridgeline algorithm example from the Rink glacier transect showing the procedure for identifying elevation maximums (a) and smoothing (b).

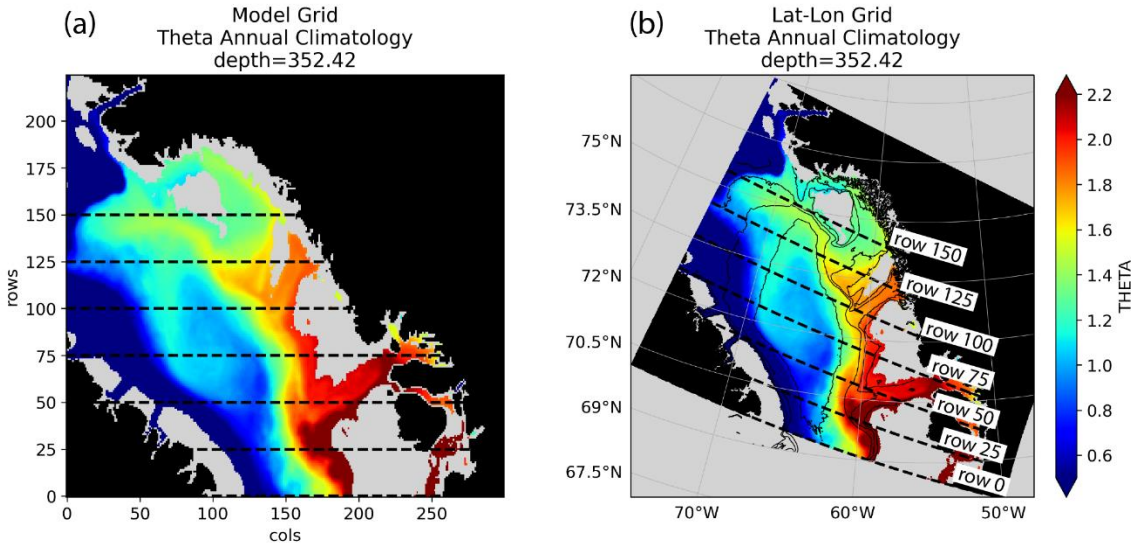

Figure S5.2. Annual potential temperature climatology (2015–2020) at 352 m from the ECCO solution in the model grid (a) and coordinate (b) projections.

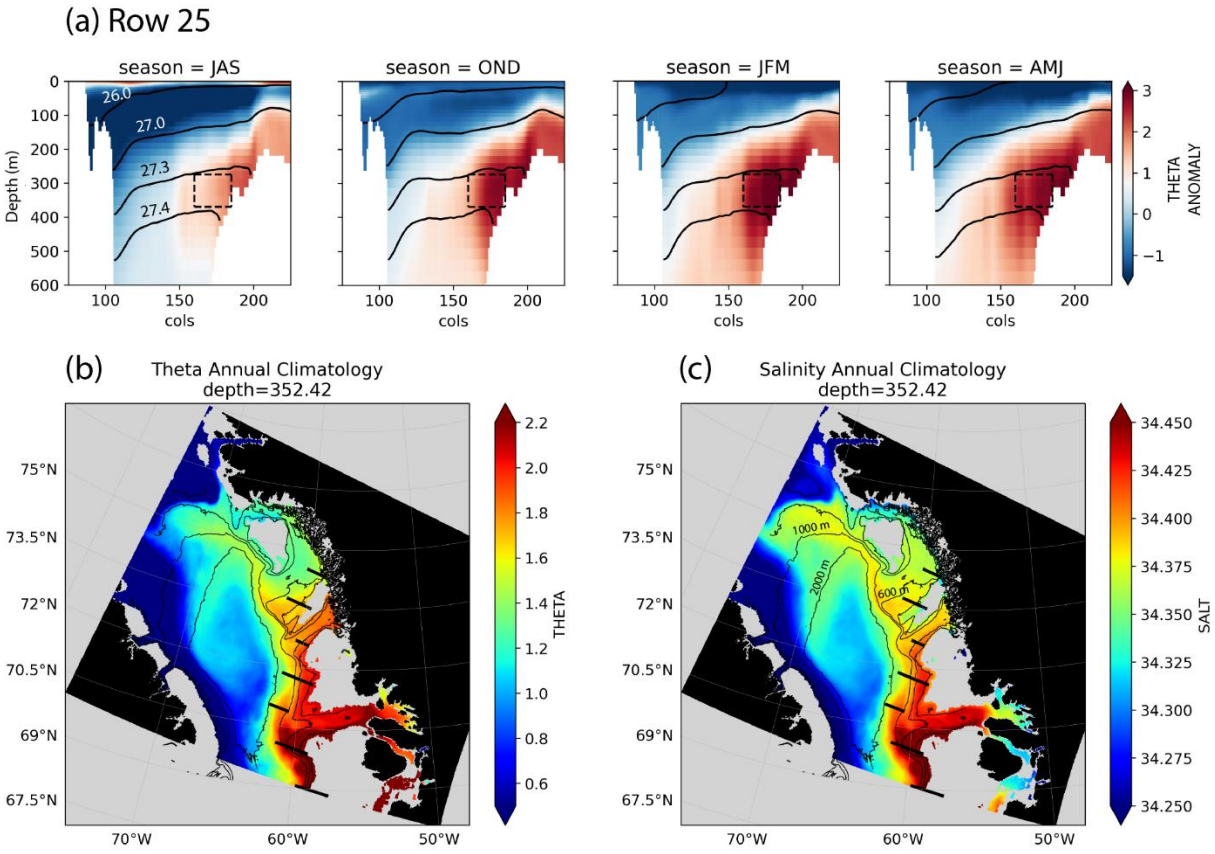

Figure S5.3. Example row 25 transect (a) showing the potential temperature anomaly profiles with overlaid isopycnals for the four seasons (Summer=July, August, September; Fall=October, November, December; Winter=January, February, March; Spring=April, May, June). The dashed line box in (a) shows the AW box extracted for calculating seasonal time series. ECCO potential temperature (b) and salinity (c) annual climatologies at 352 m are provided with black lines showing the AW boxes selected for each row transect.

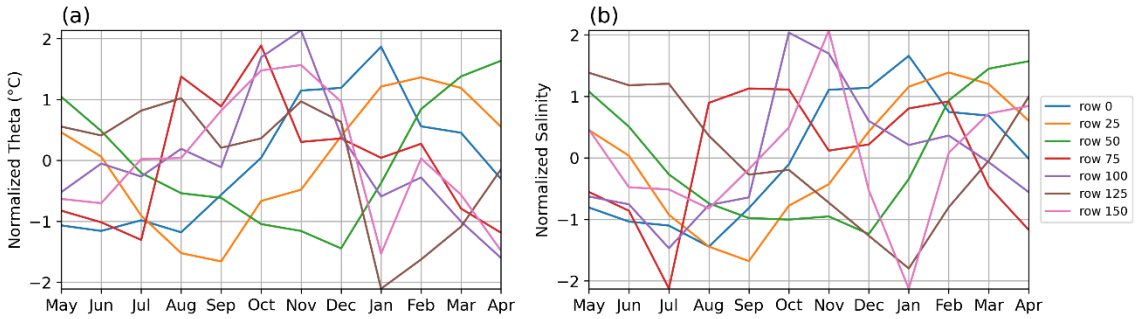

Figure S5.4. ECCO monthly potential temperature (a) and salinity (b) time series for each row transect. All ECCO estimates were detrended prior to taking monthly means and normalized by their standard deviation.

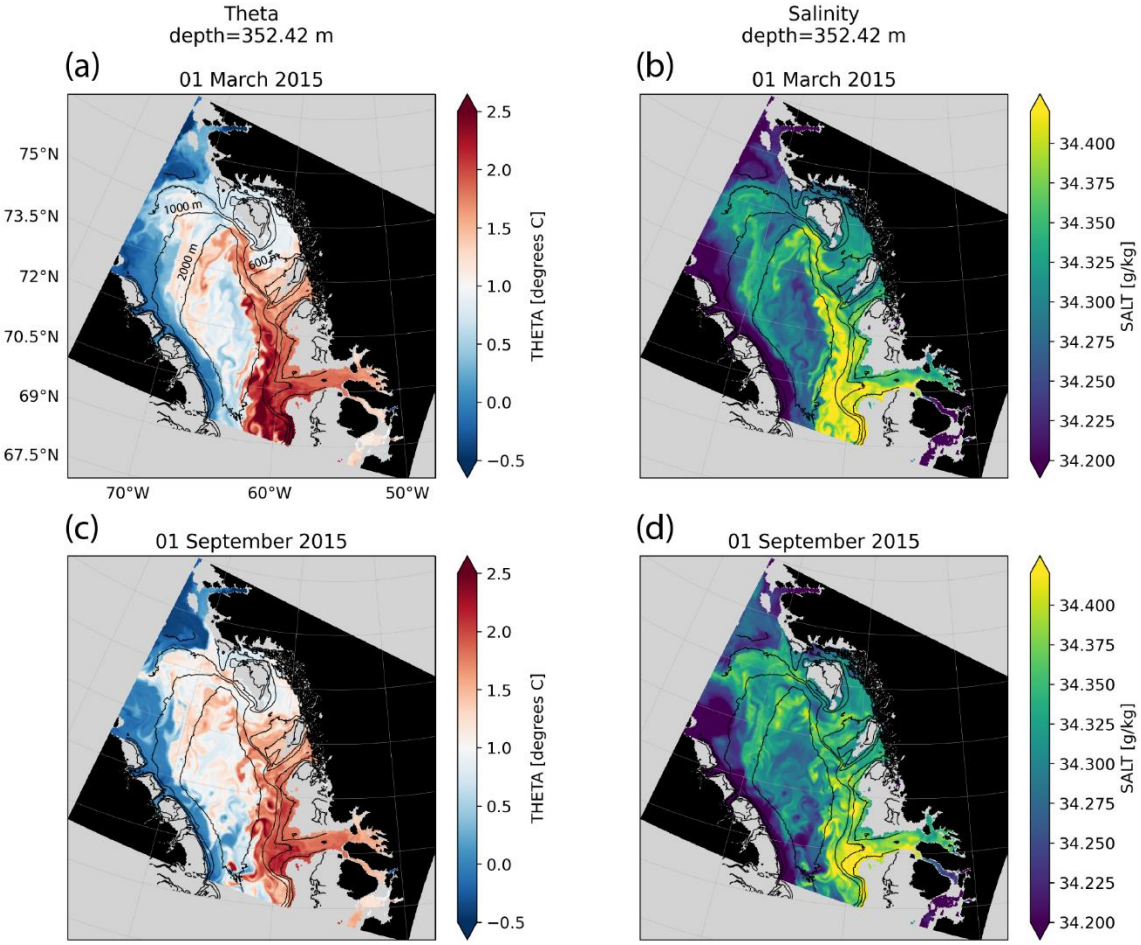

Figure S5.5. Example snapshots showing potential temperature (a, c) and salinity (b, d) in West Greenland at approximately 350 m deep from the ECCO solution on 01 March, 2015 (a, b) and 01 September, 2015 (c, d).

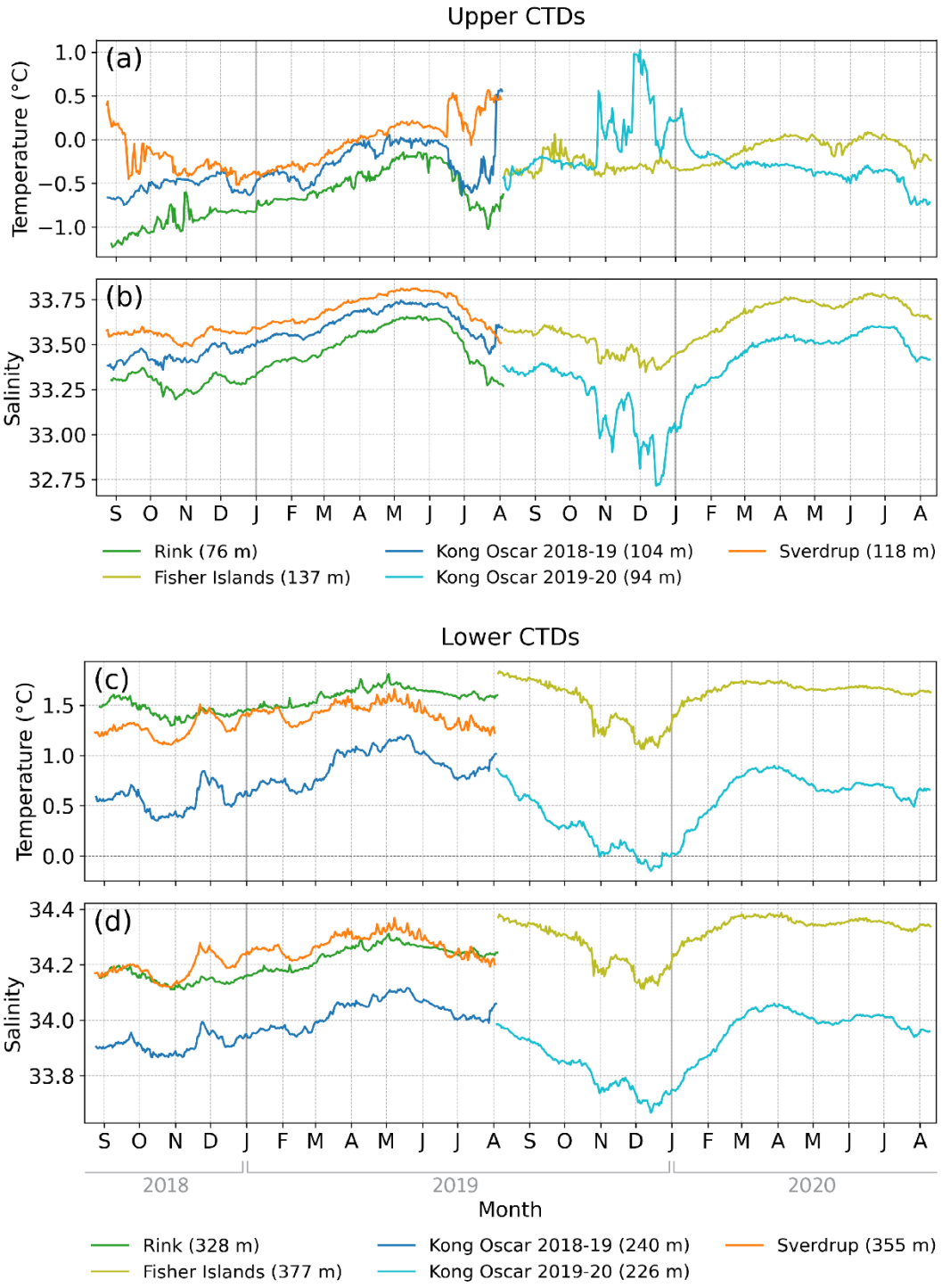

Figure S5.6. Daily absolute temperature (°C) and salinity (PSU) for the upper (a, b) and lower (c, d) CTDs fixed to each mooring: Rink/Fisher (green/olive), Kong Oscar (blue), Sverdrup (orange). Note that the depths at which each CTD was positioned varies across each mooring site and year.

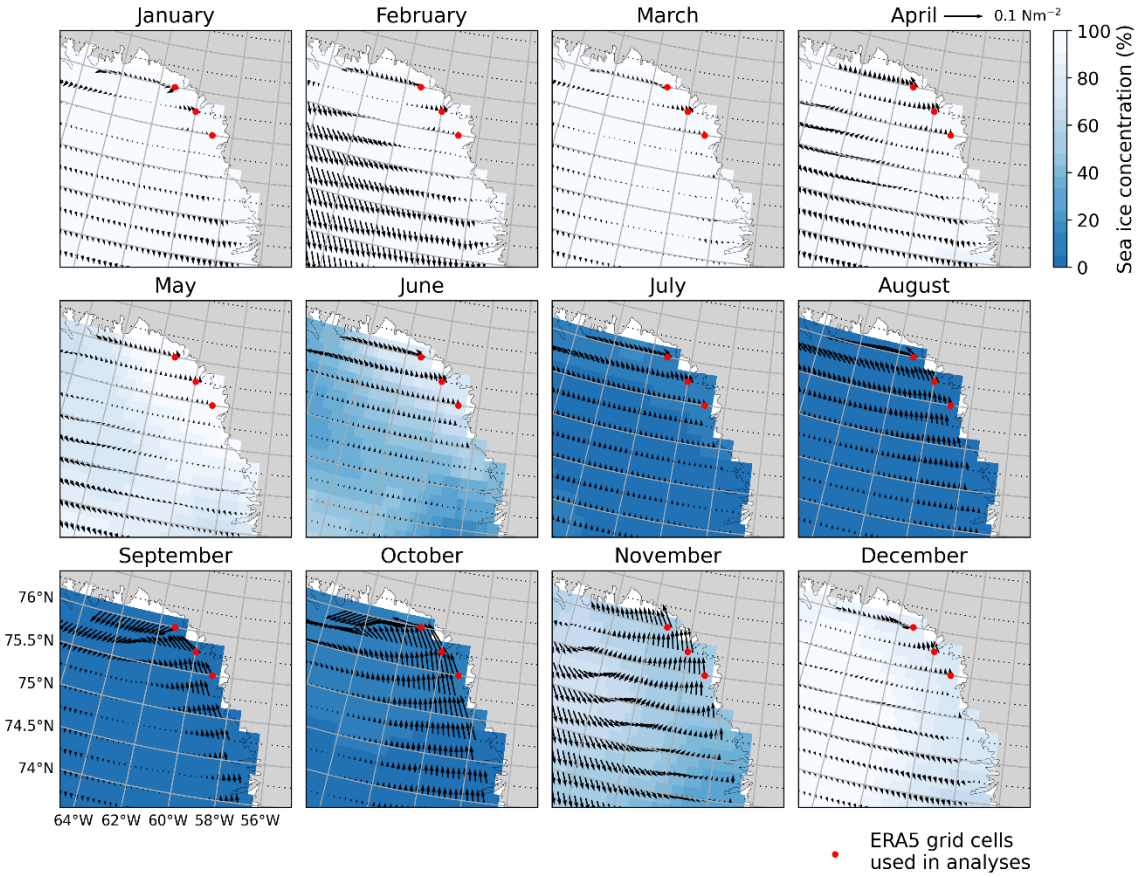

Figure S5.7. Melville Bay monthly mean sea ice concentration (%) and wind stress (Nm^{-2}) for 2018–2020 from the ERA5 reanalysis. Black vectors indicate the direction and magnitude of the wind stress. Red dots show the three ERA5 grid cells used in analyses to investigate local forcing at each mooring site.

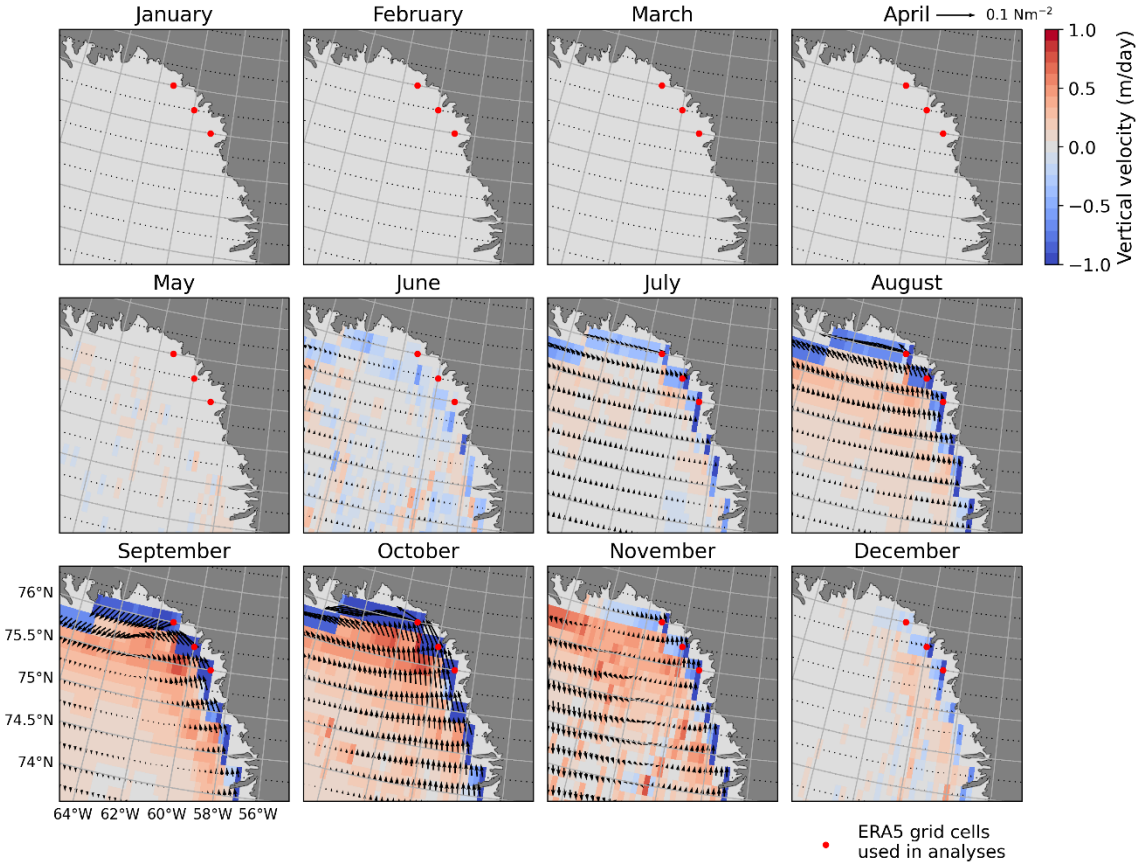

Figure S5.8. Melville Bay monthly mean vertical velocity, or Ekman pumping (w_{ek}), in m/day for 2018–2020. For Ekman pumping calculations, wind stress was set to zero when the concentration of sea ice was >50% to account for ice blocking the transfer of momentum between wind and the ocean surface. Black vectors indicate the direction and magnitude of the wind stress after the sea ice correction was applied. Red dots show the three ERA5 grid cells used in analyses to investigate local forcing at each mooring site.

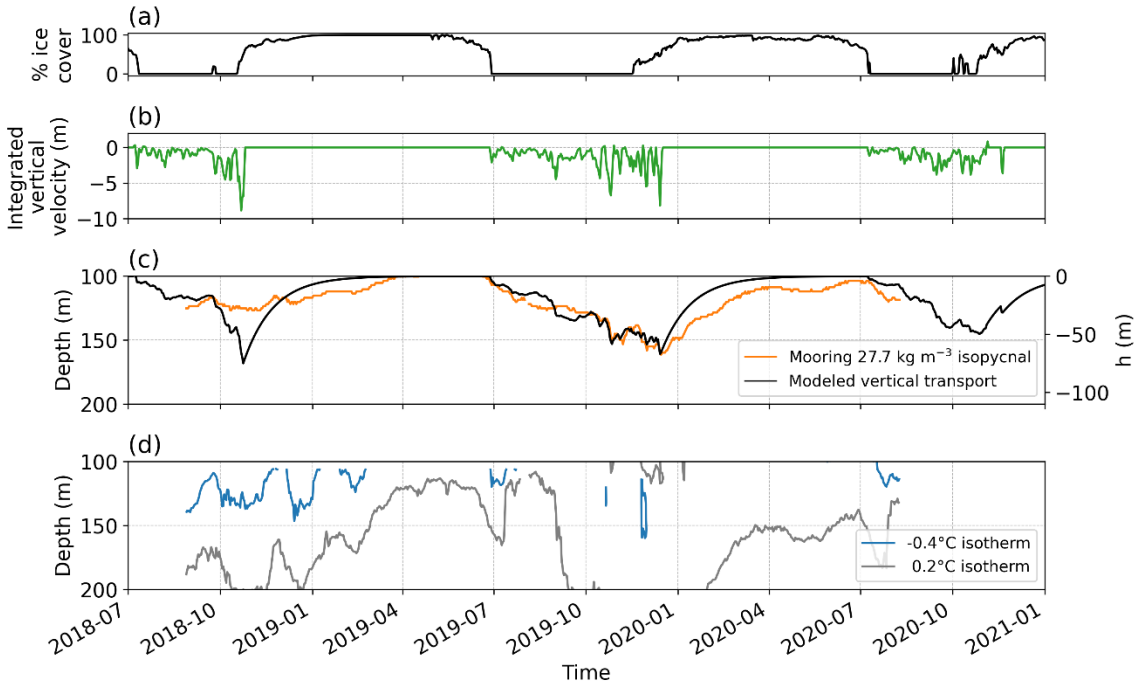

Figure S5.9. Comparison of modeled vertical motion (see Text S5.1) to isopycnal and isotherm variability at the Kong Oscar mooring site between August 2018 to August 2020. Percent sea ice cover (a) and integrated vertical velocity (b) are also shown to visualize the relationship between wind, ice, and ocean interactions. For vertical velocity calculations, wind stress was set to zero when percent sea ice was greater than 50%. The 1027.7 kgm^{-3} (σ_Θ = 27.7) isopycnal shown in orange in (c) was selected because it was observed in the mooring profile for the entire sampling period. The black line in (c) is the ODE output for the modeled change in height, $\boldsymbol{h}$, of a water mass over time. Two isotherms (-0.4 and 0.2°C) are plotted in (d).

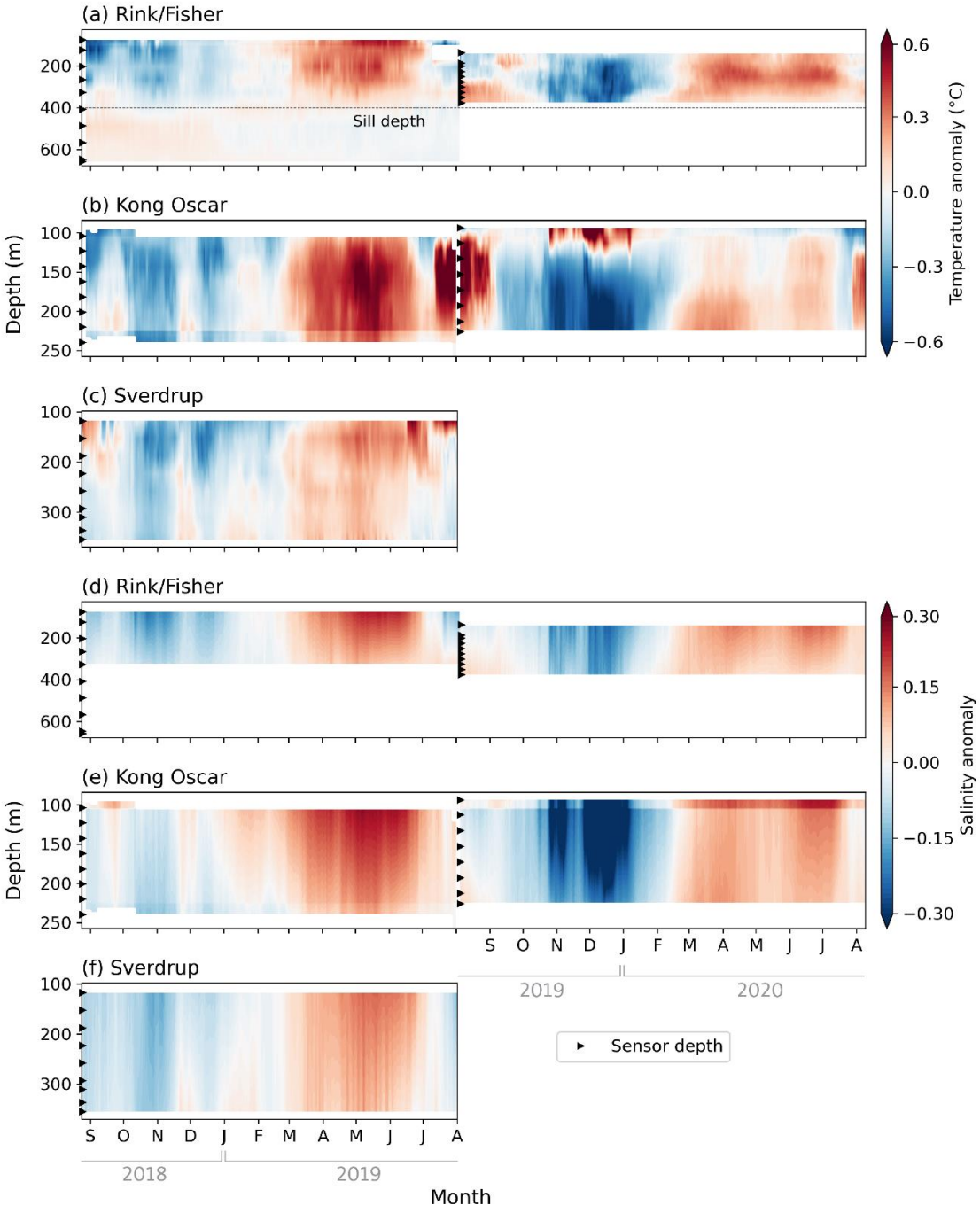

Figure S5.10. Temperature (a–c) and salinity (d–f) anomalies that were computed over the time coordinate to show how temperature and salinity vary for a given depth over time. All temperature (salinity) measurements were subtracted by their depth's mean temperature (salinity). Note: the y-axes do not show the same depth range; the entire sampling range of each mooring is plotted here. Black triangles show the depths of temperature logger and CTD sensors for each mooring. The horizontal dashed line in (a) shows the sill depth at 400 m.

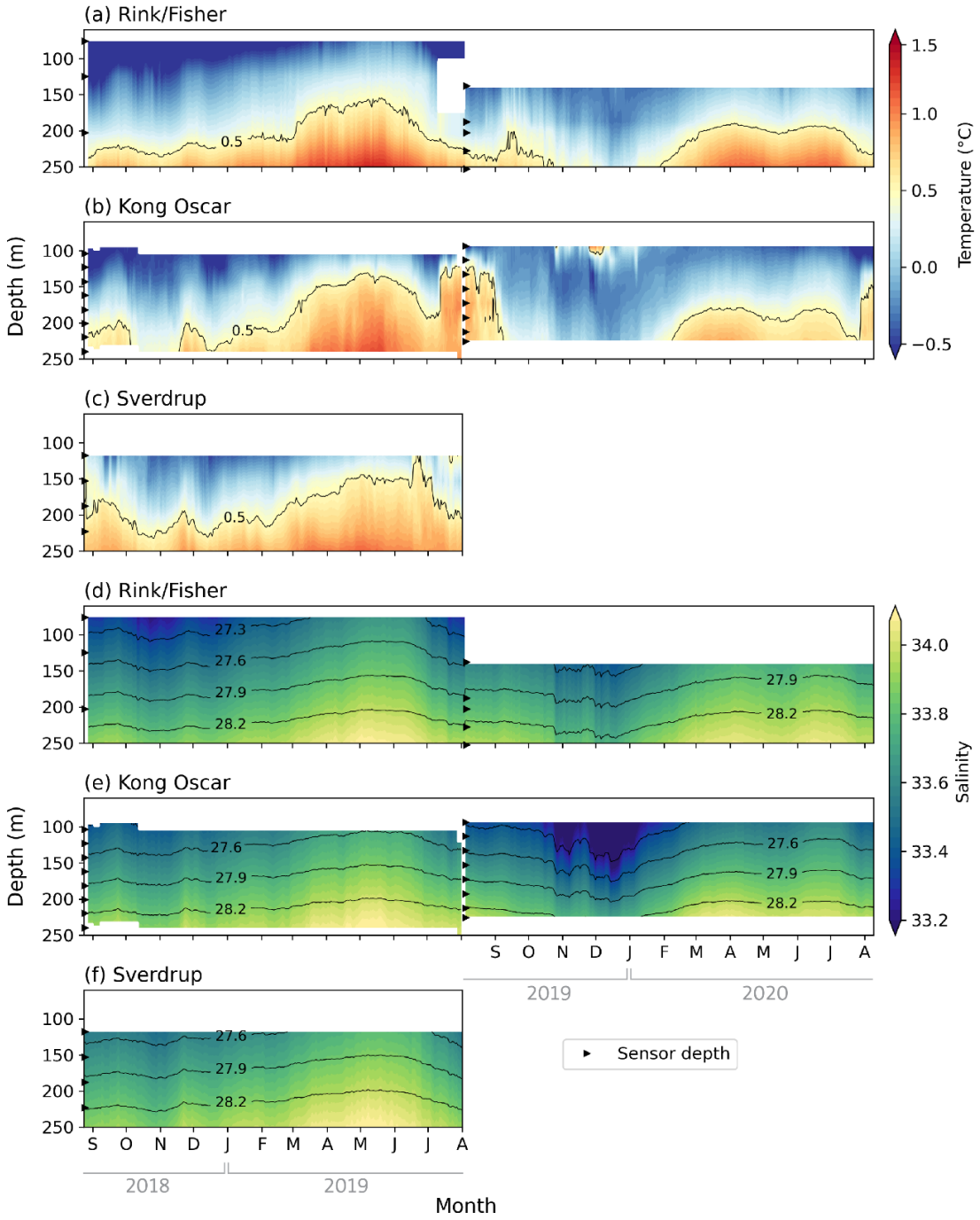

Figure S5.11. Temperature (a–c) and salinity (d–f) profiles for all moorings and within the same depth range of 60 and 250 meters. Black triangles show the depths of temperature logger and CTD sensors for each mooring.

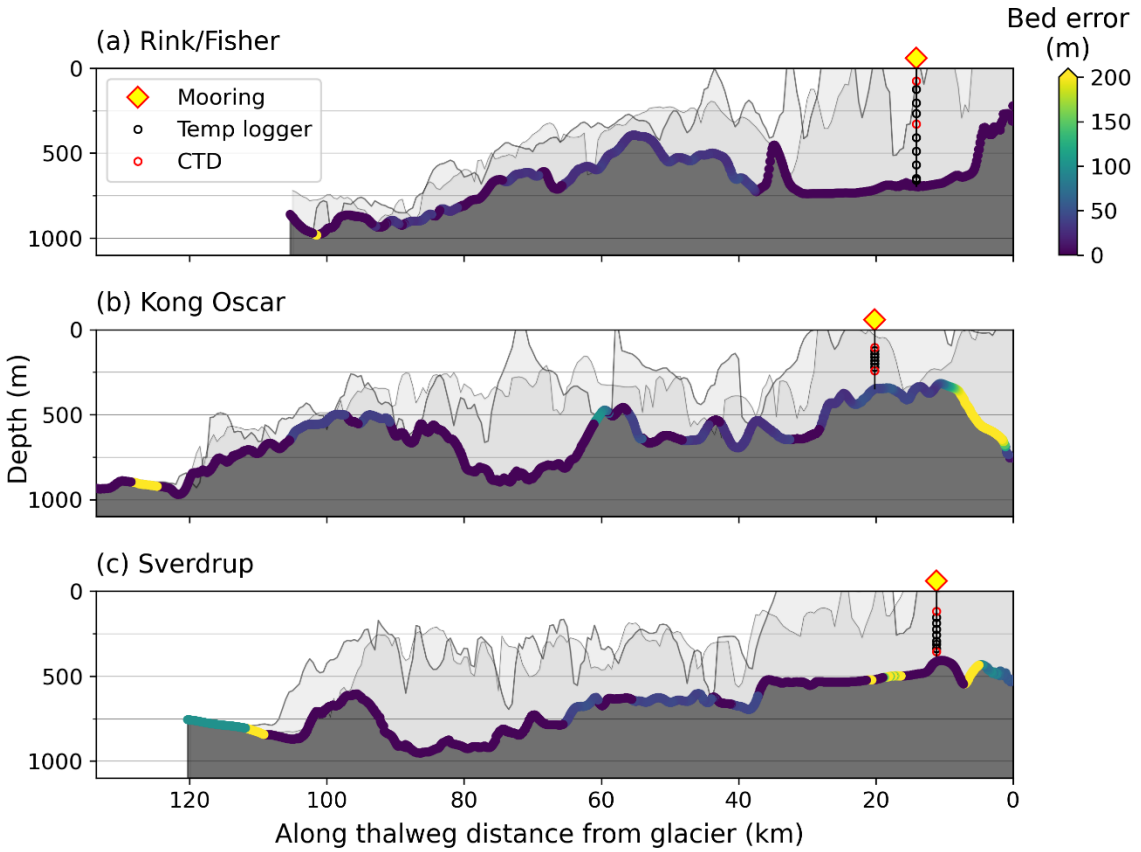

Figure S5.12. Along thalweg (dark gray) and ridgeline (light gray) bathymetry for Rink/Fisher (a), Kong Oscar (b), and Sverdrup (c) sites. Bathymetry error (in meters) is provided in color (0 = purple, ≥200 = yellow) along the thalweg transect. Yellow diamonds show mooring locations with the vertical position of CTD (red circles) and temperature logger (black circles) sensors in the water column. Note: the 2018–2019 mooring array is shown for (a) Rink/Fisher because the 2019–2020 mooring was positioned in the Fisher Islands and did not fall along the thalweg extending from the Rink glacier front (see Figure 5.8a).

Table S5.1. Summary of glacier properties for the three sites: Rink glacier, Kong Oscar glacier, and Sverdrup glacier. The definition for how each variable was determined is provided and the data source. Note: Rink glacier has two termini and both were used when estimating glacier width, ice front thickness, grounding line, and surface elevation.

Variable (units)	Rink	Kong Oscar	Sverdrup	Definition	Source
Glacier front thickness (m)	316 (215)	837 (673)	660 (404)	Maximum (mean) thickness along linear distance across 2019–2020 glacier ice front	BedMachine V5 (Morlighem et al. 2022)
Glacier front ocean depth, or grounding line (m)	-243 (-113)	-747 (-578)	-532 (-254)	Maximum (mean) depth across 2019–2020 glacier ice front (linear distance)	BedMachine V5 (Morlighem et al. 2022)
Glacier front surface elevation (m)	176 (103)	140 (95)	200 (150)	Maximum (mean) surface elevation across 2019–2020 glacier ice front (linear distance)	BedMachine V5 (Morlighem et al. 2022)
Glacier width (m)	6497	4427	7222	Measured in QGIS as linear distance across 2019–2020 glacier ice front	BedMachine V5 in QGIS with MODIS satellite imagery
Runoff ice outlet depth (m)	-250	-457	-187	Mankoff et al. (2020) obtained depth from BedMachine at outlet location for glacier ice basin	(Mankoff et al. 2020a)
Mean runoff from MAR (m^3s^{-1})	33.30	121.03	147.92	Average for summer months (June, July, August) 2018 through 2020 for the glacier ice basin outlet	(Mankoff et al. 2020a)
Mean runoff from RACMO (m^3s^{-1})	23.89	87.72	102.17	Average for summer months (June, July, August) 2018 through 2020 for the glacier ice basin outlet	(Mankoff et al. 2020a)
Mean ice velocity (m/yr)	798	3030	2413	Average for sampling period (2018-07-01 to 2020-09-30) from Sentinel 2A, 2B, and Landsat 8	ITS_LIVE Regional Glacier and Ice Sheet Surface Velocities (Gardner et al. 2018; Gardner et al. 2022)
Mean solid ice discharge (Gt/yr)	0.94	8.28	5.17	Average for sampling period (2018-07-01 to 2020-09-30)	(Mankoff 2020b; Mankoff et al. 2020b)

Chapter 6. CONCLUSIONS

6.1 SUMMARY

This dissertation identified previously undescribed characteristics of Arctic odontocete echolocation and hydrographic variability in northwest Greenland, a region that supports both belugas and narwhals seasonally. We used a unique acoustic dataset of beluga and narwhal echolocation from central west Greenland that was ideal for comparison as recordings were obtained from the same region and season, collected using the same hydrophone array, and each recording was paired with visual confirmation of the species present. We estimated standard click parameters for beluga echolocation and we found that they have a narrow sonar beam, similar to the narwhal (Koblitz et al. 2016). We also showed that belugas scan their environment while echolocating to increase their acoustic field of view. Beluga and narwhal click characteristics were compared and key variables were identified for species acoustic classification. An acoustic classifier that was trained using the dataset from central west Greenland was tested with a new long-term dataset from ocean moorings near glacier fronts in Melville Bay, Northwest Greenland. We found narwhal clicks had a steep increase between the 16 and 25 kHz one-third octave levels (TOL) that was absent in beluga spectra, and beluga clicks had a large increase between the 25 and 40 kHz TOL that was lacking in narwhal spectra. Random Forests classification models that used TOL ratio variables correctly predicted the species identity of click detections with extremely high accuracy. Together, results from chapters 2, 3, and 4 fill critical knowledge gaps in the acoustic ecology of belugas and narwhals and provide valuable quantities for species acoustic classification in future long-term passive acoustic studies.

In chapter 5, the focus shifted from passive acoustics to physical oceanography where hydrographic data from the same ocean moorings from chapter 4 were used to describe the seasonality in ocean properties in Melville Bay. While year-round hydrographic variability has been described for fjords in northeast, southeast, and central west Greenland, it has not been measured for northwest Greenland prior to this work. We showed the same seasonal cycle in temperature and salinity across the three locations studied but found differences in subglacial plume signatures. The most visible plume was observed for the deepest glacier that produced high rates of freshwater runoff, and no plume was seen for the shallowest glacier with comparatively little runoff. Peak temperatures near the glacier fronts occurred in spring just before summer when waters cooled and freshened along the shelf from sea ice and glacier ice melt. Chapter 5 provides a meaningful contribution to the broader understanding of ice-ocean interactions and a valuable physical basis for investigating biological processes along Greenland's continental shelf in the future.

6.2 Future Work

Many foundational questions remain surrounding beluga and narwhal ecology—particularly for understudied subpopulations—that hinder targeted conservation efforts and sustainable management (e.g., harvest quotas) given increasing threats from climate change and human disturbance (Ragen et al. 2008; Hobbs et al. 2019). With virtual certainty, climate change has been altering Arctic ecosystems with expected negative effects on marine mammals (Laidre et al. 2008; Moore & Huntington 2008; Post et al. 2013; Laidre et al. 2015). Advancements in passive acoustic methods will enable people to monitor changes to ambient sound levels due to increased vessel traffic and to beluga and narwhal distributions and behavior. Passive acoustic recorders are often complemented with *in situ* oceanographic sensors, and this dissertation encourages future long-

term studies using these methods to continue investigating when and why belugas and narwhals utilize certain habitats. In particular, innovations in profiling floats (e.g., APEX float) to house both acoustic recorders and CTD instruments will enable detection of Arctic odontocetes and ocean conditions in near-real time. To our knowledge, hydrophones have been integrated into profiling floats only once (QUEphone, Matsumoto et al. 2013), but all oceanographic sensors had to be removed because of space limitations. Aside from floats, we see direct applications of the acoustic variables and models developed in chapters 3 and 4 to parameterize detection algorithms within any autonomous underwater vehicle system (e.g., floats, gliders, sail drone).

There is still much to be learned about the seasonality of physical and biological oceanographic processes along Greenland's coasts. Patterns and associations between the hydrography, bathymetry, and exogenous forcing that were described in chapter 5 can be used to make inferences about regional productivity in each of the glacier front regions. More specifically, research is underway that leverages both the acoustic and physical oceanographic data from the Melville Bay moorings to investigate relationships between narwhal occurrence and environmental covariates, including temperature and salinity. We encourage future studies to take a similar approach to identify key characteristics of core beluga and narwhal habitats which are needed to assess future risks due to climate change. From the broader climate science perspective, results will also help constrain ice-ocean numerical models to estimate changes to global sea levels and climate patterns arising from Greenland ice sheet dynamics and continued Atlantic water warming. Glacier dynamics are a major driver of mass loss of the Greenland ice sheet (Mouginot et al. 2019) and glaciers in the northwest and central west sectors of Greenland are predicted to be leading contributors to ice sheet mass loss (Choi et al. 2021). Glacier fronts are highly heterogenous in form and behavior, and ongoing work will continue to describe fine-scale

processes (e.g., subglacial plumes and melt rates) at the glacier-ocean boundary for more accurate model predictions. Above all, it is clear interdisciplinary research is needed to make informed predictions about Greenland's changing coastal ecosystems (Straneo et al. 2022).

REFERENCES

Ahonen H., Stafford K.M., Lydersen C., Berchok C.L., Moore S.E. & Kovacs K.M. 2021. Inter-annual variability in acoustic detection of blue and fin whale calls in the Northeast Atlantic High Arctic between 2008 and 2018. *Endangered Species Research 45*, 209–224, doi: 10.3354/esr01132.

Ahonen H., Stafford K.M., Lydersen C., Steur L.D. & Kovacs K.M. 2019. A multi-year study of narwhal occurrence in the western Fram Strait—detected via passive acoustic monitoring. *Polar Research 38*, 3468, doi: 10.33265/polar.v38.3468.

American National Standards Institute. 2004. *Specification for Octave-Band and Fractional-Octave-Band Analog and Digital Filters*. New York: ANSI S1.11-2004.

Ames A.E., Beedholm K. & Madsen P.T. 2020. Lateralized sound production in the beluga whale (*Delphinapterus leucas*). *The Journal of Experimental Biology 223*, jeb226316, doi: 10.1242/jeb.226316.

Ames A.E., Blackwell S.B., Tervo O.M. & Heide-Jørgensen M.P. 2021. Evidence of stereotyped contact call use in narwhal (*Monodon monoceros*) mother-calf communication. *PloS one 16*, e0254393, doi: 10.1371/journal.pone.0254393.

Anderson M.J. 2001. A new method for non-parametric multivariate analysis of variance. *Austral Ecology 26*, 32–46, doi: 10.1046/j.1442-9993.2001.01070.x.

Anderson M.J. 2006. Distance-based tests for homogeneity of multivariate dispersions. *Biometrics 62*, 245–253, doi: 10.1111/j.1541-0420.2005.00440.x.

Anderson M.J. 2017. Permutational Multivariate Analysis of Variance (PERMANOVA). *Wiley StatsRef: Statistics Reference Online*, doi: 10.1002/9781118445112.stat07841.

Archer E. 2021. rfPermute: Estimate permutation p-values for Random Forest importance metrics. Accessed on the internet at https://github.com/EricArcher/rfPermute.

Archer F.I., Rankin S., Stafford K.M., Castellote M. & Delarue J. 2020. Quantifying spatial and temporal variation of North Pacific fin whale (*Balaenoptera physalus*) acoustic behavior. *Marine Mammal Science 36*, 224–245, doi: 10.1111/mms.12640.

Årthun M., Eldevik T., Smedsrud L.H., Skagseth Ø. & Ingvaldsen R.B. 2012. Quantifying the influence of Atlantic heat on Barents Sea ice variability and retreat. *Journal of Climate 25*, 4736–4743, doi: 10.1175/JCLI-D-11-00466.1.

Asbjørnsen H., Årthun M., Skagseth Ø. & Eldevik T. 2020. Mechanisms underlying recent arctic atlantification. *Geophysical Research Letters 47*, doi: 10.1029/2020gl088036.

Au W.W.L. 1993. *Sonar of Dolphins*. New York: Springer.

Au W.W.L. & Benoit-Bird K.J. 2003. Automatic gain control in the echolocation system of dolphins. *Nature 423*, 861–863, doi: 10.1038/nature01727.

Au W.W.L., Branstetter B., Moore P.W. & Finneran J.J. 2012. The biosonar field around an Atlantic bottlenose dolphin (*Tursiops truncatus*). *The Journal of the Acoustical Society of America 131*, 569–576, doi: 10.1121/1.3662077.

Au W.W.L., Ford J.K.B., Horne J.K. & Newman Allman K.A. 2004. Echolocation signals of free-ranging killer whales (*Orcinus orca*) and modeling of foraging for chinook salmon (*Oncorhynchus tshawytscha*). *The Journal of the Acoustical Society of America 115*, 901–909, doi: 10.1121/1.1642628.

Au W.W.L., Pawloski J.L., Nachtigall P.E., Blonz M. & Gisner R.C. 1995. Echolocation signals and transmission beam pattern of a false killer whale (*Pseudorca crassidens*). *The Journal of the Acoustical Society of America 98*, 51–59, doi: 10.1121/1.413643.

Au W.W.L., Penner R.H., Carder D.A. & Scronce B. 1985. Demonstration of adaptation in beluga whale echolocation signals. *The Journal of the Acoustical Society of America 77*, 726–730, doi: 10.1121/1.392341.

Au W.W.L., Penner R.H. & Turl C.W. 1987. Propagation of beluga echolocation signals. *The Journal of the Acoustical Society of America 82*, 807–813, doi: 10.1121/1.395278.

Baumann-Pickering S., Simonis A.E., Oleson E.M., Baird R.W., Roch M.A. & Wiggins S.M. 2015. False killer whale and short-finned pilot whale acoustic identification. *Endangered Species Research 28*, 97–108, doi: 10.3354/esr00685.

Baumann-Pickering S., Wiggins S.M., Hildebrand J.A., Roch M.A. & Schnitzler H.-U. 2010. Discriminating features of echolocation clicks of melon-headed whales (*Peponocephala electra*), bottlenose dolphins (*Tursiops truncatus*), and Gray's spinner dolphins (*Stenella longirostris longirostris*). *The Journal of the Acoustical Society of America 128*, 2212–2224, doi: 10.1121/1.3479549.

Beedholm K., Malinka C., Ladegaard M. & Madsen P.T. 2021. Do echolocating toothed whales direct their acoustic gaze on- or off-target in a static detection task? *The Journal of the Acoustical Society of America 149*, 581–590, doi: 10.1121/10.0003357.

Belikov R.A. & Bel'Kovich V.M. 2007. Whistles of beluga whales in the reproductive gathering off Solovetskii Island in the White Sea. *Acoustical Physics 53*, 528–534, doi: 10.1134/S1063771007040148.

Bendtsen J., Mortensen J., Lennert K. & Rysgaard S. 2015. Heat sources for glacial ice melt in a west Greenland tidewater outlet glacier fjord: The role of subglacial freshwater discharge. *Geophysical Research Letters 42*, 4089–4095, doi: 10.1002/2015gl063846.

Bersch M., Yashayaev I. & Koltermann K.P. 2007. Recent changes of the thermohaline circulation in the subpolar North Atlantic. *Ocean Dynamics 57*, 223–235, doi: 10.1007/s10236-007-0104-7.

Bjørk A.A., Kruse L.M. & Michaelsen P.B. 2015. Brief communication: Getting Greenland's glaciers right - A new data set of all official Greenlandic glacier names. *Cryosphere 9*, 2215–2218, doi: 10.5194/tc-9-2215-2015.

Black T. & Joughin I. 2022. MEaSUREs weekly to monthly Greenland outlet glacier terminus positions from Sentinel-1 mosaics, version 1, doi: 10.5067/DGBOSSIULSTD.

Black T. & Joughin I. 2023. Weekly to monthly terminus variability of Greenland's marine-terminating outlet glaciers. *The Cryosphere 17*, 1–13, doi: 10.5194/tc-17-1-2023.

Blackwell S.B., Greene C.R. & Richardson W.J. 2004. Drilling and operational sounds from an oil production island in the ice-covered Beaufort Sea. *The Journal of the Acoustical Society of America 116*, 3199–3211, doi: 10.1121/1.1806147.

Blackwell S.B., Tervo O.M., Conrad A.S., Sinding M.H.S., Hansen R.G., Ditlevsen S. & Heide-Jørgensen M.P. 2018. Spatial and temporal patterns of sound production in East Greenland narwhals. *PloS One 13*, e0198295, doi: 10.1371/journal.pone.0198295.

Blevins-Manhard R., Atkinson S. & Lammers M. 2017. Spatial and temporal patterns in the calling behavior of beluga whales, *Delphinapterus leucas*, in Cook Inlet, Alaska. *Marine Mammal Science 33*, 112–133, doi: 10.1111/mms.12353.

Breiman L. 2001. Random Forests. *Machine learning 45*, 5–32, doi: 10.1023/A:1010933404324.

Brenner S., Rainville L., Thomson J., Cole S. & Lee C. 2021. Comparing observations and parameterizations of ice-ocean drag through an annual cycle across the Beaufort sea. *Journal of Geophysical Research, C: Oceans 126*, doi: 10.1029/2020jc016977.

Cape M.R., Straneo F., Beaird N., Bundy R.M. & Charette M.A. 2018. Nutrient release to oceans from buoyancy-driven upwelling at Greenland tidewater glaciers. *Nature Geoscience 12*, 34–39, doi: 10.1038/s41561-018-0268-4.

Carr J.R., Vieli A. & Stokes C. 2013. Influence of sea ice decline, atmospheric warming, and glacier width on marine-terminating outlet glacier behavior in northwest Greenland at seasonal to interannual timescales. *Journal of Geophysical Research: Earth Surface 118*, 1210–1226, doi: 10.1002/jgrf.20088.

Carroll D., Sutherland D.A., Curry B., Nash J.D., Shroyer E.L., Catania G.A., Stearns L.A., Grist J.P., Lee C.M. & de Steur L. 2018. Subannual and seasonal variability of Atlantic-origin waters in two adjacent west Greenland fjords. *Journal of Geophysical Research: Oceans 123*, 6670–6687, doi: 10.1029/2018JC014278.

Carroll D., Sutherland D.A., Hudson B., Moon T., Catania G.A., Shroyer E.L., Nash J.D., Bartholomaus T.C., Felikson D., Stearns L.A., Noël B.P.Y. & van den Broeke M.R.

2016. The impact of glacier geometry on meltwater plume structure and submarine melt in Greenland fjords. *Geophysical Research Letters 43*, 9739–9748, doi: 10.1002/2016gl070170.

Castellote M., Leeney R.H., O'Corry-Crowe G., Lauhakangas R., Kovacs K.M., Lucey W., Krasnova V., Lydersen C., Stafford K.M. & Belikov R. 2013. Monitoring white whales (*Delphinapterus leucas*) with echolocation loggers. *Polar Biology 36*, 493–509, doi: 10.1007/s00300-012-1276-2.

Castellote M., Mooney A., Andrews R., Deruiter S., Lee W.J., Ferguson M. & Wade P. 2021. Beluga whale (*Delphinapterus leucas*) acoustic foraging behavior and applications for long term monitoring. *PloS One 16*, e0260485, doi: 10.1371/journal.pone.0260485.

Castellote M., Mooney T.A., Quakenbush L., Hobbs R., Goertz C. & Gaglione E. 2014. Baseline hearing abilities and variability in wild beluga whales (*Delphinapterus leucas*). *The Journal of Experimental Biology 217*, 1682–1691, doi: 10.1242/jeb.093252.

Castellote M., Small R.J., Lammers M.O., Jenniges J., Mondragon J., Garner C.D., Atkinson S., Delevaux J.M.S., Graham R. & Westerholt D. 2020. Seasonal distribution and foraging occurrence of Cook Inlet beluga whales based on passive acoustic monitoring. *Endangered Species Research 41*, 225–243, doi: 10.3354/esr01023.

Castellote M., Small R.J., Lammers M.O., Jenniges J.J., Mondragon J. & Atkinson S. 2016. Dual instrument passive acoustic monitoring of belugas in Cook Inlet, Alaska. *The Journal of the Acoustical Society of America 139*, 2697–2707, doi: 10.1121/1.4947427.

Castellote M., Stafford K.M., Neff A.D. & Lucey W. 2015. Acoustic monitoring and prey association for beluga whale, *Delphinapterus leucas*, and harbor porpoise, *Phocoena phocoena*, off two river mouths in Yakutat Bay, Alaska. *Marine Fisheries Review 77*, 1–10, doi: 10.7755/MFR.77.1.1.

Castellote M., Thayre B., Mahoney M., Mondragon J., Lammers M.O., Small R.J., Inlet C., Shelden K.E.W. & Vos D.J. 2018. Anthropogenic noise and the endangered Cook Inlet beluga whale, *Delphinapterus leucas*: Acoustic considerations for management. *Marine Fisheries Review 80*, 63–88, doi: 10.7755/MFR.80.3.3.

Catania G.A., Stearns L.A., Moon T.A., Enderlin E.M. & Jackson R.H. 2020. Future evolution of Greenland's marine-terminating outlet glaciers. *Journal of Geophysical Research: Earth Surface 125*, e2018JF004873, doi: 10.1029/2018JF004873.

Catania G.A., Stearns L.A., Sutherland D.A., Fried M.J., Bartholomaus T.C., Morlighem M., Shroyer E. & Nash J. 2018. Geometric controls on tidewater glacier retreat in central western Greenland. *Journal of Geophysical Research. Earth surface 123*, 2024–2038, doi: 10.1029/2017jf004499.

Chambault P., Blackwell S.B. & Heide-Jørgensen M.P. 2023. Extremely low seasonal prey capture efficiency in a deep-diving whale, the narwhal. *Biology Letters 19*, 20220423, doi: 10.1098/rsbl.2022.0423.

Chambault P., Tervo O.M., Garde E., Hansen R.G., Blackwell S.B., Williams T.M., Dietz R., Albertsen C.M., Laidre K.L., Nielsen N.H., Richard P., Sinding M.H.S., Schmidt H.C. & Heide-Jørgensen M.P. 2020. The impact of rising sea temperatures on an Arctic top predator, the narwhal. *Scientific Reports 10*, 1–10, doi: 10.1038/s41598-020-75658-6.

Chen X., Zhang X., Church J.A., Watson C.S., King M.A., Monselesan D., Legresy B. & Harig C. 2017. The increasing rate of global mean sea-level rise during 1993–2014. *Nature Climate Change 7*, 492–495, doi: 10.1038/nclimate3325.

Chmelnitsky E.G. & Ferguson S.H. 2012. Beluga whale, *Delphinapterus leucas*, vocalizations from the Churchill River, Manitoba, Canada. *The Journal of the Acoustical Society of America 131*, 4821–4835, doi: 10.1121/1.4707501.

Choi Y., Morlighem M., Rignot E. & Wood M. 2021. Ice dynamics will remain a primary driver of Greenland ice sheet mass loss over the next century. *Communications Earth & Environment 2*, doi: 10.1038/s43247-021-00092-z.

Chu V.W. 2014. Greenland ice sheet hydrology: A review. *Progress in Physical Geography: Earth and Environment 38*, 19–54, doi: 10.1177/0309133313507075.

Cole S.T., Toole J.M., Lele R., Timmermans M.-L., Gallaher S.G., Stanton T.P., Shaw W.J., Hwang B., Maksym T., Wilkinson J.P., Ortiz M., Graber H., Rainville L., Petty A.A., Farrell S.L., Richter-Menge J.A. & Haas C. 2017. Ice and ocean velocity in the Arctic marginal ice zone: Ice roughness and momentum transfer. *Elementa 5*, doi: 10.1525/elementa.241.

Comiso J.C. & Hall D.K. 2014. Climate trends in the Arctic as observed from space. *WIREs Climate Change 5*, 389–409, doi: 10.1002/wcc.277.

Copernicus Climate Change Service, Climate Data Store. 2022. ERA5 hourly data on single levels from 1979 to present. Copernicus Climate Change Service (C3S) Climate Data Store (CDS), doi: 10.24381/cds.adbb2d47.

Crawford R.E. & Jorgenson J.K. 1996. Quantitative studies of Arctic cod (*Boreogadus saida*) schools: Important energy stores in the Arctic food web. *Arctic Institute of North America 49*, 181–193, doi: 10.14430/arctic1196.

Cuny J., Rhines P.B., Niiler P.P. & Bacon S. 2002. Labrador Sea boundary currents and the fate of the Irminger Sea Water. *Journal of Physical Oceanography 32*, 627–647, doi: 10.1175/1520-0485(2002)032<0627:LSBCAT>2.0.CO;2.

Curry B., Lee C.M. & Petrie B. 2011. Volume, freshwater, and heat fluxes through Davis Strait, 2004-05. *Journal of physical oceanography 41*, 429–436, doi: 10.1175/2010JPO4536.1.

Curry B., Lee C.M., Petrie B., Moritz R.E. & Kwok R. 2014. Multiyear volume, liquid freshwater, and sea ice transports through Davis Strait, 2004-10. *Journal of Physical Oceanography 44*, 1244–1266, doi: 10.1175/JPO-D-13-0177.1.

Danielson S., University of Alaska Fairbanks, Grebmeier J., Iken K., Berchok C., Britt L., Dunton K., Eisner L., Farley E., Fujiwara A., Hauser D., Itoh M., Kikuchi T., Kotwicki S., Kuletz K., Mordy C., Nishino S., Peralta-Ferriz C., Pickart R., Stabeno P., Stafford K., Whiting A. & Woodgate R. 2022. Monitoring Alaskan Arctic shelf ecosystems through collaborative observation networks. *Oceanography* , doi: 10.5670/oceanog.2022.119.

de Freitas M., Jensen F.H., Tyne J., Bejder L. & Madsen P.T. 2015. Echolocation parameters of Australian humpback dolphins (*Sousa sahulensis*) and Indo-Pacific bottlenose dolphins (*Tursiops aduncus*) in the wild. *The Journal of the Acoustical Society of America 137*, 3033–3041, doi: 10.1121/1.4921277.

Desbruyères D., Chafik L. & Maze G. 2021. A shift in the ocean circulation has warmed the subpolar North Atlantic Ocean since 2016. *Communications Earth & Environment 2*, 1–9, doi: 10.1038/s43247-021-00120-y.

Dietz R. & Heide-Jørgensen M.P. 1995. Movements and swimming speed of narwhals, *Monodon monoceros*, equipped with satellite transmitters in Melville Bay, northwest Greenland. *Canadian Journal of Zoology 73*, 2106–2119, doi: 10.1139/z95-248.

Dietz R., Heide-Jørgensen M.P., Richard P., Orr J., Laidre K. & Schmidt H.C. 2008. Movements of narwhals (*Monodon monoceros*) from Admiralty Inlet monitored by satellite telemetry. *Polar Biology 31*, 1295–1306, doi: 10.1007/s00300-008-0466-4.

Dietz R., Heide-Jørgensen M.P., Richard P.R. & Acquarone M. 2001. Summer and fall movements of narwhals (*Monodon monoceros*) from northeastern Baffin Island towards northern Davis Strait. *Arctic 54*, 244–261, doi: 10.14430/arctic785.

Doidge D.W. & Finley K.J. 1993. Status of the Baffin Bay population of beluga, *Delphinapterus leucas*. *Canadian Field-Naturalist 107*, 533–546. https://www.biodiversitylibrary.org/page/34810675#page/553/mode/1up.

Erbe C. & Farmer D.M. 2000. Zones of impact around icebreakers affecting beluga whales in the Beaufort Sea. *The Journal of the Acoustical Society of America 108*, 1332–1340, doi: 10.1121/1.1288938.

Erbe C., Reichmuth C., Cunningham K., Lucke K. & Dooling R. 2016. Communication masking in marine mammals: A review and research strategy. *Marine Pollution Bulletin 103*, 15–38, doi: 10.1016/j.marpolbul.2015.12.007.

Falk B., Jakobsen L., Surlykke A. & Moss C.F. 2014. Bats coordinate sonar and flight behavior as they forage in open and cluttered environments. *The Journal of Experimental Biology 217*, 4356–4364, doi: 10.1242/jeb.114132.

Fenty I., Willis J.K., Khazendar A., Dinardo S., Forsberg R., Fukumori I., Holland D., Jakobsson M., Moller D., Morison J., Münchow A., Rignot E., Schodlok M., Thompson A.F., Tinto K., Rutherford M. & Trenholm N. 2016. Oceans Melting Greenland: Early results from NASA's ocean-ice mission in Greenland. *Oceanography 29*, 72–83, doi: 10.5670/oceanog.2016.100.

Fettweis X., Box J.E., Agosta C., Amory C., Kittel C., Lang C., van As D., Machguth H. & Gallée H. 2017. Reconstructions of the 1900–2015 Greenland ice sheet surface mass balance using the regional climate MAR model. *The Cryosphere 11*, 1015–1033, doi: 10.5194/tc-11-1015-2017.

Finneran J.J., Schlundt C.E., Dear R., Carder D.A. & Ridgway S.H. 2002. Temporary shift in masked hearing thresholds in odontocetes after exposure to single underwater impulses from a seismic watergun. *The Journal of the Acoustical Society of America 111*, 2929–2940, doi: 10.1121/1.1479150.

Fisher F.H. & Simmons V.P. 1977. Sound absorption in sea water. *The Journal of the Acoustical Society of America 62*, 558–564, doi: 10.1121/1.381574.

Fletcher N.H. 1992. *Acoustic Systems in Biology*. Oxford University Press.

Ford J.K.B. & Fisher H.D. 1978. Underwater acoustic signals of the narwhal (*Monodon monoceros*). *Canadian Journal of Zoology 56*, 552–560, doi: 10.1139/z78-079.

Fried M.J., Catania G.A., Bartholomaus T.C., Duncan D., Davis M., Stearns L.A., Nash J., Shroyer E. & Sutherland D. 2015. Distributed subglacial discharge drives significant submarine melt at a Greenland tidewater glacier. *Geophysical Research Letters 42*, 9328–9336, doi: 10.1002/2015gl065806.

Fried M.J., Catania G.A., Stearns L.A., Sutherland D.A., Bartholomaus T.C., Shroyer E. & Nash J. 2018. Reconciling drivers of seasonal terminus advance and retreat at 13 central west Greenland tidewater glaciers. *Journal of Geophysical Research: Earth surface 123*, 1590–1607, doi: 10.1029/2018jf004628.

Frost K.J. & Lowry L.F. 1990. Distribution, abundance, and movements of beluga whales, *Delphinapterus leucas*, in coastal waters of western Alaska. In T.G. Smith, D.J.S. Aubin & J.R. Geraci (eds.): *Advances in research on the beluga whale, Delphinapterus leucas*. Pp. 39–57. Canadian Bulletin of Fisheries and Aquatic Sciences.

Frouin-Mouy H., Kowarski K., Martin B. & Bröker K. 2017. Seasonal trends in acoustic detection of marine mammals in Baffin Bay and Melville Bay, Northwest Greenland. *Arctic 70*, 59–76, doi: 10.14430/arctic4632.

Garde E., Hansen S.H., Ditlevsen S., Tvermosegaard K.B., Hansen J., Harding K.C. & Heide-Jørgensen M.P. 2015. Life history parameters of narwhals (*Monodon monoceros*) from Greenland. *Journal of Mammalogy 96*, 866–879, doi: 10.1093/jmammal/gyv110.

Garde E., Heide-Jørgensen M.P., Hansen S.H., Nachman G. & Forchhammer M.C. 2007. Age-specific growth and remarkable longevity in narwhals (*Monodon monoceros*) from West Greenland as estimated by aspartic acid racemization. *Journal of Mammalogy 88*, 49–58, doi: 10.1644/06-MAMM-A-056R.1.

Garde E., Tervo O.M., Sinding M.-H.S., Nielsen N.H., Cornett C. & Heide-Jørgensen M.P. 2022. Biological parameters in a declining population of narwhals (*Monodon monoceros*) in Scoresby Sound, Southeast Greenland. *Arctic Science 20*, doi: 10.1139/as-2021-0009.

Gardner A.S., Fahnestock M. & Scambos T. 2022. ITS_LIVE regional glacier and ice sheet surface velocities, doi: 10.5067/6II6VW8LLWJ7.

Gardner A.S., Moholdt G., Scambos T., Fahnstock M., Ligtenberg S., van den Broeke M. & Nilsson J. 2018. Increased West Antarctic and unchanged East Antarctic ice discharge over the last 7 years. *The Cryosphere 12*, 521–547, doi: 10.5194/tc-12-521-2018.

Garland E.C., Castellote M. & Berchok C.L. 2015. Beluga whale (*Delphinapterus leucas*) vocalizations and call classification from the eastern Beaufort Sea population. *The Journal of the Acoustical Society of America 137*, 3054–3067, doi: 10.1121/1.4919338.

Ghose K. & Moss C.F. 2006. Steering by hearing: A bat's acoustic gaze is linked to its flight motor output by a delayed, adaptive linear law. *The Journal of Neuroscience*, 1704–1710, doi: 10.1523/JNEUROSCI.4315-05.2006.

Gillespie D., Mellinger D.K., Gordon J. & Al. E. 2008. PAMGUARD: semiautomated, open source software for real-time acoustic detection and localization of cetaceans. *Proceedings of the Institute of Acoustics Institute of Acoustics 30*, 54–62.

Gillooly J.F. & Ophir A.G. 2010. The energetic basis of acoustic communication. *Proceedings of the Royal Society B 277*, 1325–1331, doi: 10.1098/rspb.2009.2134.

Gladish C.V., Holland D.M. & Lee C.M. 2015a. Oceanic boundary conditions for Jakobshavn Glacier. Part II: Provenance and sources of variability of disko bay and Ilulissat Icefjord waters, 1990-2011. *Journal of Physical Oceanography 45*, 33–63, doi: 10.1175/JPO-D-14-0045.1.

Gladish C.V., Holland D.M., Rosing-Asvid A., Behrens J.W. & Boje J. 2015b. Oceanic boundary conditions for Jakobshavn Glacier. Part I: Variability and renewal of Ilulissat Icefjord waters, 2001-14. *Journal of Physical Oceanography 45*, 3–32, doi: 10.1175/JPO-D-14-0044.1.

Graham Z.A., Garde E., Heide-Jørgensen M.P. & Palaoro A.V. 2020. The longer the better: Evidence that narwhal tusks are sexually selected. *Biology Letters 16*, 2–6, doi: 10.1098/rsbl.2019.0950.

Gregersen U., Hopper J.R. & Knutz P.C. 2013. Basin seismic stratigraphy and aspects of prospectivity in the NE Baffin Bay, Northwest Greenland. *Marine and Petroleum Geology 46*, 1–18, doi: 10.1016/j.marpetgeo.2013.05.013.

Griffiths E.T., Archer F., Rankin S., Keating J.L., Keen E., Barlow J., Jeffrey E., Griffiths E.T., Archer F., Rankin S., Keating J.L., Keen E., Barlow J. & Moore J.E. 2020. Detection and classification of narrow-band high frequency echolocation clicks from drifting recorders. *The Journal of the Acoustical Society of America 147*, 3511–3522, doi: 10.1121/10.0001229.

Gurevich V.S. & Evans W.E. 1976. Echolocation discrimination of complex planar targets by the Beluga whale (*Delphinapterus leucas*). *The Journal of the Acoustical Society of America 60*, S5, doi: 10.1121/1.2003442.

Halliday W.D., Barclay D., Barkley A.N., Cook E., Hilliard R.C., Hussey N.E., Jones J.M., Juanes F., Niemi A., Nudds S., Pine M.K. & Richards C. 2021a. Underwater sound levels in the Canadian Arctic, 2014–2019. *Marine Pollution Bulletin 168*, 112437, doi: 10.1016/j.marpolbul.2021.112437.

Halliday W.D., Pine M.K., Citta J.J., Harwood L., Donna D., Hauser W., Hilliard R.C., Lea E.V., Loseto L.L., Quakenbush L. & Insley S.J. 2021b. Potential exposure of beluga and bowhead whales to underwater noise from ship traffic in the Beaufort and Chukchi Seas. *Ocean and Coastal Management 204*, 105473, doi: 10.1016/j.ocecoaman.2020.105473.

Halliday W.D., Pine M.K. & Insley S.J. 2020. Underwater noise and Arctic marine mammals: review and policy recommendations. *Environmental Reviews 28*, 438–448, doi: 10.1139/er-2019-0033.

Harden B.E., Straneo F. & Sutherland D.A. 2014. Moored observations of synoptic and seasonal variability in the East Greenland Coastal Current. *Journal of Geophysical Research: Oceans 119*, 8838–8857, doi: 10.1038/175238c0.

Harington C.R. 2008. The evolution of Arctic marine mammals. *Ecological Applications 18*, S23–S40, doi: 10.1890/06-0624.1.

Harris C.R., Millman K.J., van der Walt S.J., Gommers R., Virtanen P., Cournapeau D., Wieser E., Taylor J., Berg S., Smith N.J., Kern R., Picus M., Hoyer S., van Kerkwijk M.H., Brett M., Haldane A., Del Río J.F., Wiebe M., Peterson P., Gérard-Marchant P., Sheppard K., Reddy T., Weckesser W., Abbasi H., Gohlke C. & Oliphant T.E. 2020. Array programming with NumPy. *Nature 585*, 357–362, doi: 10.1038/s41586-020-2649-2.

Hauser D.D.W., Laidre K.L., Parker-Stetter S.L., Horne J.K., Suydam R.S. & Richard P.R. 2015. Regional diving behavior of Pacific Arctic beluga whales *Delphinapterus leucas* and possible associations with prey. *Marine Ecology Progress Series 541*, 245–264, doi: 10.3354/meps11530.

Hauser D.D.W., Laidre K.L., Stafford K.M., Stern H.L., Suydam R.S. & Richard P.R. 2017a. Decadal shifts in autumn migration timing by Pacific Arctic beluga whales are related to delayed annual sea ice formation. *Global Change Biology 23*, 2206–2217, doi: 10.1111/gcb.13564.

Hauser D.D.W., Laidre K.L. & Stern H.L. 2018. Vulnerability of Arctic marine mammals to vessel traffic in the increasingly ice-free Northwest Passage and Northern Sea Route. *Proceedings of the National Academy of Sciences 115*, 7617–7622, doi: 10.1073/pnas.1803543115.

Hauser D.D.W., Laidre K.L., Stern H.L., Moore S.E., Suydam R.S. & Richard P.R. 2017b. Habitat selection by two beluga whale populations in the Chukchi and Beaufort seas. *PloS One 12*, e0172755, doi: 10.1371/journal.pone.0172755.

Hauser D.D.W., Laidre K.L., Suydam R.S. & Richard P.R. 2014. Population-specific home ranges and migration timing of Pacific Arctic beluga whales (*Delphinapterus leucas*). *Polar Biology 37*, 1171–1183, doi: 10.1007/s00300-014-1510-1.

Heide-Jørgensen M.P., Blackwell S.B., Tervo O.M., Samson A.L., Garde E., Hansen R.G., Ngô M.C., Conrad A.S., Trinhammer P., Schmidt H.C., Sinding M.-H.S., Williams T.M. & Ditlevsen S. 2021. Behavioral response study on seismic airgun and vessel exposures in narwhals. *Frontiers in Marine Science 8*, 658173, doi: 10.3389/fmars.2021.658173.

Heide-Jørgensen M.P., Blackwell S.B., Williams T.M., Sinding M.H.S., Skovrind M., Tervo O.M., Garde E., Hansen R.G., Nielsen N.H., Ngô M.C. & Ditlevsen S. 2020. Some like it cold: Temperature-dependent habitat selection by narwhals. *Ecology and Evolution 10*, 8073–8090, doi: 10.1002/ece3.6464.

Heide-Jørgensen M.P., Dietz R., Laidre K.L. & Richard P. 2002. Autumn movements, home ranges, and winter density of narwhals (*Monodon monoceros*) tagged in Tremblay Sound, Baffin Island. *Polar Biology 25*, 331–341, doi: 10.1007/s00300-001-0347-6.

Heide-Jørgensen M.P., Dietz R., Laidre K.L., Richard P., Orr J. & Schmidt H.C. 2003a. The migratory behaviour of narwhals (*Monodon monoceros*). *Canadian Journal of Zoology 81*, 1298–1305, doi: 10.1139/Z03-117.

Heide-Jørgensen Mads Peter, Hansen R.G., Westdal K., Reeves R.R. & Mosbech A. 2013. Narwhals and seismic exploration: Is seismic noise increasing the risk of ice entrapments? *Biological Conservation 158*, 50–54, doi: 10.1016/j.biocon.2012.08.005.

Heide-Jørgensen M.P., Laidre K.L., Borchers D., Marques T.A., Stern H. & Simon M. 2010. The effect of sea-ice loss on beluga whales (*Delphinapterus leucas*) in West Greenland. *Polar Research 29*, 198–208, doi: 10.3402/polar.v29i2.6061.

Heide-Jørgensen M.P., Nielsen N.H., Hansen R.G., Schmidt H.C., Blackwell S.B. & Jørgensen O.A. 2015. The predictable narwhal: Satellite tracking shows behavioural similarities between isolated subpopulations. *Journal of Zoology 297*, 54–65, doi: 10.1111/jzo.12257.

Heide-Jørgensen M.P., Richard P., Dietz R., Laidre K.L., Orr J. & Schmidt H.C. 2003b. An estimate of the fraction of belugas (*Delphinapterus leucas*) in the Canadian high Arctic that winter in West Greenland. *Polar Biology 26*, 318–326, doi: 10.1007/s00300-003-0488-x.

Heide-Jørgensen M. P., Richard P.R., Dietz R. & Laidre K.L. 2013. A metapopulation model for Canadian and West Greenland narwhals. *Animal Conservation 16*, 331–343, doi: 10.1111/acv.12000.

Hersbach H., Bell B., Berrisford P., Biavati G., Horányi A., Muñoz Sabater J., Nicolas J., Peubey C., Radu R., Rozum I., Schepers D., Simmons A., Soci C., Dee D. & Thépaut J.-N. 2022. ERA5 hourly data on single levels from 1979 to present. Copernicus Climate Change Service (C3S) Climate Data Store (CDS). *Copernicus Climate Change Service (C3S) Climate Data Store (CDS)*, doi: 10.24381/cds.adbb2d47.

Hobbs R., Reeves R., Prewitt J.S., Desportes G., Breton-Honeyman K., Christensen T., Citta J.J., Ferguson S.H., Frost K.J., Garde E., Gavrilo M., Ghazal M., Glazov D.M., Gosselin J.F., Hammill M.O., Hansen R.G., Harwood L., Heide-Jørgensen M.P., Inglangasuk G., Kovacs K.M., Krasnova V.V., Kuznetsova D.M., Lee D.S., Lesage V., Litovka D.I., Lorenzen E.D., Lowry L.F., Lydersen C., Matthews C.J.D., Meschersky I.G., Mosnier A., O'Corry-Crowe G., Postma L.D., Quakenbush L.T., Shpak O.V., Skovrind M., Suydam R.S. & Watt C.A. 2019. Global review of the conservation status of Monodontid stocks. *Marine Fisheries Review 81*, 1–53, doi: 10.7755/MFR.81.3–4.1.

Holland D.M., Thomas R.H., De Young B., Ribergaard M.H. & Lyberth B. 2008. Acceleration of Jakobshavn Isbrae triggered by warm subsurface ocean waters. *Nature Geoscience 1*, 659–664, doi: 10.1038/ngeo316.

Hoyer S. & Hamman J. 2017. xarray: N-D labeled arrays and datasets in Python. *Journal of Open Research Software 5*, doi: 10.5334/jors.148.

Huntington H.P. 2009. A preliminary assessment of threats to Arctic marine mammals and their conservation in the coming decades. *Marine Policy 33*, 77–82, doi: 10.1016/j.marpol.2008.04.003.

IMBIE Team. 2020. Mass balance of the Greenland Ice Sheet from 1992 to 2018. *Nature 579*, 233–239, doi: 10.1038/s41586-019-1855-2.

Ingvaldsen R.B., Assmann K.M., Primicerio R., Fossheim M., Polyakov I.V. & Dolgov A.V. 2021. Physical manifestations and ecological implications of Arctic Atlantification. *Nature Reviews Earth & Environment 2*, 874–889, doi: 10.1038/s43017-021-00228-x.

Innes S., Heide-Jørgensen M.P., Laake J.L., Laidre K.L., Cleator H.J., Richard P. & Stewart R.E.A. 2002. Surveys of belugas and narwhals in the Canadian High Arctic in 1996. *NAMMCO Scientific Publications 4*, 169–190, doi: 10.7557/3.2843.

Intergovernmental Panel on Climate Change (IPCC). 2022. Polar Regions. *The Ocean and Cryosphere in a Changing Climate: Special Report of the Intergovernmental Panel on Climate Change*. Pp. 203–320. Cambridge University Press, doi: 10.1017/9781009157964.005.

Intergovernmental Panel on Climate Change (IPCC). 2021. Summary for Policymakers. In V. Masson-Delmotte, P. Zhai, A. Pirani, S.L. Connors, C. Péan, S. Berger, N. Caud, Y. Chen, L. Goldfarb, M.I. Gomis, M. Huang, K. Leitzell, E. Lonnoy, J.B.R. Matthews, T.K. Maycock, T. Waterfield, O. Yelekçi, R. Yu & B. Zhou (eds.): *Climate Change 2021: The Physical Science Basis. Contribution of Working Group I to the Sixth Assessment Report of the Intergovernmental Panel on Climate Change*. Cambridge University Press, doi: 10.1260/095830507781076194.

Intergovernmental Panel on Climate Change (IPCC). 2019. Summery for Policymakers. In H.O. Pörtner, D.C. Roberts, V. Masson-Delmotte, P. Zhai, M. Tignor, E. Poloczanska, K. Mintenbeck, M. Nicolai, A. Okem, J. Petzold, B. Rama & N. Weyer (eds.): *IPCC Special Report on the Ocean and Cryosphere in a Changing Climate*. P. 34. Cambridge University Press. Accessed on the internet at https://www.ipcc.ch/srocc/home/.

Jackson D.A. 1993. Stopping rules in principal components analysis: a comparison of heuristical and statistical approaches. *Ecology 74*, 2204–2214.

Jackson L.C., Biastoch A., Buckley M.W., Desbruyères D.G., Frajka-Williams E., Moat B. & Robson J. 2022. The evolution of the North Atlantic Meridional Overturning Circulation since 1980. *Nature Reviews Earth & Environment 3*, 241–254, doi: 10.1038/s43017-022-00263-2.

Jackson R.H., Nash J.D., Kienholz C., Sutherland D.A., Amundson J.M., Motyka R.J., Winters D., Skyllingstad E. & Pettit E.C. 2020. Meltwater intrusions reveal mechanisms for rapid submarine melt at a tidewater glacier. *Geophysical Research Letters 47*, doi: 10.1029/2019gl085335.

Jackson R.H., Straneo F. & Sutherland D.A. 2014. Externally forced fluctuations in ocean temperature at Greenland glaciers in non-summer months. *Nature Geoscience 7,* 503–508, doi: 10.1038/ngeo2186.

Jakobsson M., Mayer L., Coakley B., Dowdeswell J.A., Forbes S., Fridman B., Hodnesdal H., Noormets R., Pedersen R., Rebesco M., Schenke H.W., Zarayskaya Y., Accettella D., Armstrong A., Anderson R.M., Bienhoff P., Camerlenghi A., Church I., Edwards M., Gardner J.V., Hall J.K., Hell B., Hestvik O., Kristoffersen Y., Marcussen C., Mohammad R., Mosher D., Nghiem S.V., Pedrosa M.T., Travaglini P.G. & Weatherall P. 2012. The international bathymetric chart of the Arctic Ocean (IBCAO) Version 3.0. *Geophysical Research Letters 39*, L12609, doi: 10.1029/2012GL052219.

Janout M.A., Hölemann J., Waite A.M., Krumpen T., von Appen W.J. & Martynov F. 2016. Sea-ice retreat controls timing of summer plankton blooms in the Eastern Arctic Ocean. *Geophysical Research Letters 43*, 12,493-12,501, doi: 10.1002/2016GL071232.

Jensen F.H., Johnson M., Ladegaard M., Wisniewska D.M. & Madsen P.T. 2018. Narrow acoustic field of view drives frequency scaling in toothed whale biosonar. *Current Biology: CB 28*, 3878–3885, doi: 10.1016/j.cub.2018.10.037.

Jensen F.H., Rocco A., Mansur R.M., Smith B.D., Janik V.M. & Madsen P.T. 2013. Clicking in shallow rivers: short-range echolocation of Irrawaddy and Ganges river dolphins in a shallow, acoustically complex habitat. *PloS One 8*, e59284, doi: 10.1371/journal.pone.0059284.

Jensen F.H., Wahlberg M., Beedholm K., Johnson M., De Soto N.A. & Madsen P.T. 2015. Single-click beam patterns suggest dynamic changes to the field of view of echolocating Atlantic spotted dolphins (*Stenella frontalis*) in the wild. *The Journal of Experimental Biology 218*, 1314–1324, doi: 10.1242/jeb.116285.

Jones J.M., Frasier K.E., Westdal K.H., Ootoowak A.J., Wiggins S.M. & Hildebrand J.A. 2022. Beluga (*Delphinapterus leucas*) and narwhal (*Monodon monoceros*) echolocation click detection and differentiation from long-term Arctic acoustic recordings. *Polar Biology*, doi: 10.1007/s00300-022-03008-5.

Joughin I. 2022. MEaSUREs Greenland Annual Ice Sheet Velocity Mosaics from SAR and Landsat, Version 4. 2019-12-01 subset, doi: 10.5067/RS8GFZ848ZU9.

Joughin I., Moon T., Joughin J. & Black T. 2021. MEaSUREs annual Greenland outlet glacier terminus positions from SAR mosaics, version 2, doi: 10.5067/ESFWE11AVFKW.

K. Lisa Yang Center for Conservation Bioacoustics at the Cornell Lab of Ornithology. 2023. Raven Pro: Interactive Sound Analysis Software (Version 1.6.5) [Computer software]. Accessed on the internet at https://ravensoundsoftware.com.

Kacimi S. & Kwok R. 2022. Arctic Snow Depth, Ice Thickness, and Volume From ICESat-2 and CryoSat-2: 2018–2021. *Geophysical Research Letters 49*, e2021GL097448, doi: 10.1029/2021gl097448.

Kanna N., Sugiyama S., Ando T., Wang Y., Sakuragi Y., Hazumi T., Matsuno K., Yamaguchi A., Nishioka J. & Yamashita Y. 2022. Meltwater discharge from marine-terminating glaciers drives biogeochemical conditions in a Greenlandic fjord. *Global Biogeochemical Cycles 36*, doi: 10.1029/2022gb007411.

Keil P., Mauritsen T., Jungclaus J., Hedemann C., Olonscheck D. & Ghosh R. 2020. Multiple drivers of the North Atlantic warming hole. *Nature Climate Change 10*, 667–671, doi: 10.1038/s41558-020-0819-8.

Kellogg W.N. 1959. Size discrimination by reflected sound in a bottle-nose porpoise. *Journal of Comparative and Physiological Psychology 52*, 509–514, doi: 10.1037/h0046277.

Khazendar A., Fenty I.G., Carroll D., Gardner A., Lee C.M., Fukumori I., Wang O., Zhang H., Seroussi H., Moller D., Noël B.P.Y., van den Broeke M.R., Dinardo S. & Willis J. 2019.

Interruption of two decades of Jakobshavn Isbrae acceleration and thinning as regional ocean cools. *Nature Geoscience 12*, 277–283, doi: 10.1038/s41561-019-0329-3.

Kloepper L.N., Buck J.R., Liu Y. & Nachtigall P.E. 2018. Off-axis targets maximize bearing Fisher Information in broadband active sonar. *The Journal of the Acoustical Society of America 143*, EL43–EL48, doi: 10.1121/1.5021709.

Koblitz J.C., Stilz P., Rasmussen M.H. & Laidre K.L. 2016. Highly directional sonar beam of narwhals (*Monodon monoceros*) measured with a vertical 16 hydrophone array. *PloS One 11*, e0162069, doi: 10.1371/journal.pone.0162069.

Koblitz J.C., Wahlberg M., Stilz P., Madsen P.T., Beedholm K. & Schnitzler H.-U. 2012. Asymmetry and dynamics of a narrow sonar beam in an echolocating harbor porpoise. *The Journal of the Acoustical Society of America 131*, 2315–2324, doi: 10.1121/1.3683254.

Kochanowicz Z., Dawson J., Halliday W.D., Sawada M., Copland L., Ann N., Nicoll A., Ferguson S.H., Heide-Jørgensen M.P., Marcoux M., Watt C. & Yurkowski D.J. 2021. Using western science and Inuit knowledge to model ship-source noise exposure for cetaceans (marine mammals) in Tallurutiup Imanga (Lancaster Sound), Nunavut , Canada. *Marine Policy 130*.

Kovacs K.M., Lydersen C., Overland J.E. & Moore S.E. 2011. Impacts of changing sea-ice conditions on Arctic marine mammals. *Marine biodiversity: a journal of the Senckenberg Research Institute / Senckenberg Forschungsinstitut und Naturmudeum 41*, 181–194, doi: 10.1007/s12526-010-0061-0.

Kwok R. 2018. Arctic sea ice thickness, volume, and multiyear ice coverage: losses and coupled variability (1958-2018). *Environmental Research Letters: ERL [Web site] 13*, 105005, doi: 10.1088/1748-9326/aae3ec.

Kyhn L.A., Jensen F.H., Beedholm K., Tougaard J., Hansen M. & Madsen P.T. 2010. Echolocation in sympatric peale's dolphins (*Lagenorhynchus australis*) and commerson's dolphins (*Cephalorhynchus commersonii*) producing narrow-band high-frequency clicks. *The Journal of Experimental Biology 213*, 1940–1949, doi: 10.1242/jeb.042440.

Kyhn L.A., Tougaard J., Jensen F., Wahlberg M., Stone G., Yoshinaga A., Beedholm K. & Madsen P.T. 2009. Feeding at a high pitch: Source parameters of narrow band, high-frequency clicks from echolocating off-shore hourglass dolphins and coastal Hector's dolphins. *The Journal of the Acoustical Society of America 125*, 1783–1791, doi: 10.1121/1.3075600.

Ladegaard M., Jensen F.H., De Freitas M., Da Silva V.M.F. & Madsen P.T. 2015. Amazon river dolphins (*Inia geoffrensis*) use a high-frequency short-range biosonar. *The Journal of Experimental Biology 218*, 3091–3101, doi: 10.1242/jeb.120501.

Ladegaard M. & Madsen P.T. 2019. Context-dependent biosonar adjustments during active target approaches in echolocating harbour porpoises. *The Journal of Experimental Biology 222*, doi: 10.1242/jeb.206169.

Laidre K.L. & Heide-Jørgensen M.P. 2011. Life in the lead: Extreme densities of narwhals *Monodon monoceros* in the offshore pack ice. *Marine Ecology Progress Series 423*, 269–278, doi: 10.3354/meps08941.

Laidre K.L. & Heide-Jørgensen M.P. 2005. Winter feeding intensity of narwhals (*Monodon monoceros*). *Marine Mammal Science 21*, 45–57, doi: 10.1111/j.1748-7692.2005.tb01207.x.

Laidre K.L., Heide-Jørgensen M.P. & Dietz R. 2002. Diving behaviour of narwhals (Monodon monoceros) at two coastal localities in the Canadian High Arctic. *Canadian Journal of Zoology 80*, 624–635, doi: 10.1139/z02-041.

Laidre K.L., Heide-Jørgensen M.P., Dietz R., Hobbs R.C. & Jørgensen O.A. 2003. Deep-diving by narwhals *Monodon monoceros*: Differences in foraging behavior between wintering areas? *Marine Ecology Progress Series 261*, 269–281, doi: 10.3354/meps261269.

Laidre K.L., Heide-Jørgensen M.P., Jørgensen O.A. & Treble M.A. 2004. Deep-ocean predation by a high Arctic cetacean. *ICES Journal of Marine Science 61*, 430–440, doi: 10.1016/j.icesjms.2004.02.002.

Laidre K.L., Moon T., Hauser D.D.W., McGovern R., Heide-Jørgensen M.P., Dietz R. & Hudson B. 2016. Use of glacial fronts by narwhals (*Monodon monoceros*) in West Greenland. *Biology Letters 12*, doi: 10.1098/rsbl.2016.0457.

Laidre K.L., Stern H., Kovacs K.M., Lowry L., Moore S.E., Regehr E.V., Ferguson S.H., Wiig Ø., Boveng P., Angliss R.P., Born E.W., Litovka D., Quakenbush L., Lydersen C., Vongraven D. & Ugarte F. 2015. Arctic marine mammal population status, sea ice habitat loss, and conservation recommendations for the 21st century. *Conservation Biology 29*, 724–737, doi: 10.1111/cobi.12474.

Laidre K.L., Stirling I., Lowry L.F., Wiig Ø., Heide-Jørgensen M.P. & Ferguson S.H. 2008. Quantifying the sensitivity of Arctic marine mammals to climate-induced habitat change. *Ecological Applications 18*, S97–S125, doi: 10.1890/06-0546.1.

Lammers M.O. & Castellote M. 2009. The beluga whale produces two pulses to form its sonar signal. *Biology Letters 5*, 297–301, doi: 10.1098/rsbl.2008.0782.

Lammers M.O., Castellote M., Small R.J., Atkinson S., Jenniges J., Rosinski A., Oswald J.N. & Garner C. 2013. Passive acoustic monitoring of Cook Inlet beluga whales (*Delphinapterus leucas*). *The Journal of the Acoustical Society of America 134*, 2497–2504, doi: 10.1121/1.4816575.

Lannuzel D., Tedesco L., van Leeuwe M., Campbell K., Flores H., Delille B., Miller L., Stefels J., Assmy P., Bowman J., Brown K., Castellani G., Chierici M., Crabeck O., Damm E., Else B., Fransson A., Fripiat F., Geilfus N.X., Jacques C., Jones E., Kaartokallio H., Kotovitch M., Meiners K., Moreau S., Nomura D., Peeken I., Rintala J.M., Steiner N., Tison J.L., Vancoppenolle M., Van der Linden F., Vichi M. & Wongpan P. 2020. The future of Arctic sea-ice biogeochemistry and ice-associated ecosystems. *Nature Climate Change 10*, 983–992, doi: 10.1038/s41558-020-00940-4.

Lefort K.J., Garroway C.J. & Ferguson S.H. 2020. Killer whale abundance and predicted narwhal consumption in the Canadian Arctic. *Global Change Biology 26*, 4276–4283, doi: 10.1111/gcb.15152.

Lesage V. 2021. The challenges of a small population exposed to multiple anthropogenic stressors and a changing climate: the St. Lawrence Estuary beluga. *Polar Research 40*, doi: 10.33265/polar.v40.5523.

Lesage V., Barrette C., Kingsley M.C.S. & Sjare B. 1999. The effect of vessel noise on the vocal behavior of belugas in the St. Lawrence River estuary, Canada. *Marine Mammal Science 15*, 65–84, doi: 10.1111/j.1748-7692.1999.tb00782.x.

Lever J., Krzywinski M. & Altman N. 2017. Principal component analysis. *Nature Methods 14*, 641–642, doi: 10.1038/nmeth.4346.

Lewis A.E., Hammill M.O., Power M., Doidge D.W. & Lesage V. 2009. Movement and aggregation of eastern Hudson Bay beluga whales (*Delphinapterus leucas*): A comparison of patterns found through satellite telemetry and Nunavik Traditional Ecological Knowledge. *Arctic 62*, 13–24, doi: 10.14430/arctic109.

Liaw A. & Wiener M. 2002. Classification and regression by randomForest. *R News 2*, 18–22.

Lin P., Pickart R.S., Torres D.J. & Pacini A. 2018. Evolution of the freshwater coastal current at the southern tip of Greenland. *Journal of Physical Oceanography 48*, 2127–2140, doi: 10.1175/JPO-D-18-0035.1.

Louis M., Skovrind M., Castruita J.A.S., Garilao C., Kaschner K., Gopalakrishnan S., Haile J.S., Lydersen C., Kovacs K.M., Garde E., Heide-Jørgensen M.P., Postma L., Ferguson S.H., Willerslev E. & Lorenzen E.D. 2020. Influence of past climate change on phylogeography and demographic history of narwhals, *Monodon monoceros*. *Proceedings of the Royal Society B: Biological Sciences 287*, 20192964, doi: 10.1098/rspb.2019.2964.

Lydersen C. & Kovacs K.M. 2021. A review of the ecology and status of white whales (*Delphinapterus leucas*) in Svalbard, Norway. *Polar Research 40*, 5509, doi: 10.33265/polar.v40.5509.

Lydersen C., Martin A.R., Kovacs K.M. & Gjertz I. 2001. Summer and autumn movements of white whales *Delphinapterus leucas* in Svalbard, Norway. *Marine Ecology Progress Series 219*, 265–274.

Macaulay J.D.J., Malinka C.E., Gillespie D. & Madsen P.T. 2020. High resolution three-dimensional beam radiation pattern of harbour porpoise clicks with implications for passive acoustic monitoring. *The Journal of the Acoustical Society of America 147*, 4175–4188, doi: 10.1121/10.0001376.

Madsen P.T. 2005. Marine mammals and noise: Problems with root mean square sound pressure levels for transients. *The Journal of the Acoustical Society of America 117*, 3952–3957, doi: 10.1121/1.1921508.

Madsen P.T. & Wahlberg M. 2007. Recording and quantification of ultrasonic echolocation clicks from free-ranging toothed whales. *Deep-Sea Research Part I 54*, 1421–1444, doi: 10.1016/j.dsr.2007.04.020.

Madsen P.T., Wilson M., Johnson M., Hanlon R.T., Bocconcelli A., Aguilar de Soto N. & Tyack P.L. 2007. Clicking for calamari: Toothed whales can echolocate squid Loligo pealeii. *Aquatic Biology 1*, 141–150, doi: 10.3354/ab00014.

Mankoff K.D. 2020a. Freshwater runoff, doi: 10.22008/promice/freshwater.

Mankoff K.D. 2020b. Greenland Ice Sheet solid ice discharge from 1986 through last month: Discharge, doi: 10.22008/PROMICE/DATA/ICE_DISCHARGE/D/V02.

Mankoff K.D., Noël B., Fettweis X., Ahlstrøm A.P., Colgan W., Kondo K., Langley K., Sugiyama S., van As D. & Fausto R.S. 2020a. Greenland liquid water discharge from 1958 through 2019. *Earth System Science Data 12*, 2811–2841, doi: 10.5194/essd-12-2811-2020.

Mankoff K.D., Solgaard A., Colgan W., Ahlstrøm A.P., Khan S.A. & Fausto R.S. 2020b. Greenland Ice Sheet solid ice discharge from 1986 through March 2020. *Earth System Science Data 12*, 1367–1383, doi: 10.5194/essd-12-1367-2020.

Mankoff K.D., Straneo F., Cenedese C., Das S.B., Richards C.G. & Singh H. 2016. Structure and dynamics of a subglacial discharge plume in a Greenlandic fjord. *Journal of Geophysical Research: Oceans 121*, 3010–3028, doi: 10.1002/2016JC011764.Received.

Marcoux M., Auger-Methe M., Chmelnitsky E., Ferguson S.H. & Humphries M.M. 2011. Local passive acoustic monitoring of narwhal presence in the Canadian Arctic: a pilot project. *Arctic 64*, 307–316, doi: 10.14430/arctic4121.

Marcoux M., Auger-Méthé M. & Humphries M.M. 2012. Variability and context specificity of narwhal (*Monodon monoceros*) whistles and pulsed calls. *Marine Mammal Science 28*, 649–665, doi: 10.1111/j.1748-7692.2011.00514.x.

Marcoux M. & Hammill M.O. 2016. Model estimates of Cumberland Sound beluga (*Delphinapterus leucas*) population size and total allowable removals. *DFO Canadian Science Advisory Secretariat*.

Marques T.A., Thomas L., Martin S.W., Mellinger D.K., Ward J.A., Moretti D.J., Harris D. & Tyack P.L. 2013. Estimating animal population density using passive acoustics. *Biological reviews of the Cambridge Philosophical Society 88*, 287–309, doi: 10.1111/brv.12001.

Marshall J., Dobson F., Moore K., Rhines P., Visbeck M., D'Asaro E., Bumke K., Chang S., Davis R., Fischer K., Garwood R., Guest P., Harcourt R., Herbaut C., Holt T., Lazier J., Legg S., McWilliams J., Pickart R., Prater M., Renfrew I., Schott F., Send U. & Smethie W. 1998. The Labrador Sea Deep Convection Experiment. *Bulletin of the American Meteorological Society 79*, 2033–2058, doi: 10.1175/1520-0477(1998)079<2033:TLSDCE>2.0.CO;2.

Matsumoto H., Jones C., Klinck H., Mellinger D.K., Dziak R.P. & Meinig C. 2013. Tracking beaked whales with a passive acoustic profiler float. *The Journal of the Acoustical Society of America 133*, 731–740, doi: 10.1121/1.4773260.

Mattmüller R.M., Thomisch K., Van Opzeeland I., Laidre K.L. & Simon M. 2022. Passive acoustic monitoring reveals year-round marine mammal community composition off Tasiilaq, Southeast Greenland. *The Journal of the Acoustical Society of America 151*, 1380–1392, doi: 10.1121/10.0009429.

McCauley R.D., Day R.D., Swadling K.M., Fitzgibbon Q.P., Watson R.A. & Semmens J.M. 2017. Widely used marine seismic survey air gun operations negatively impact zooplankton. *Nature Ecology and Evolution 1*, 0195, doi: 10.1038/s41559-017-0195.

McCullough J.L.K., Simonis A.E., Sakai T. & Oleson E.M. 2021. Acoustic classification of false killer whales in the Hawaiian islands based on comprehensive vocal repertoire. *JASA Express Letters 1*, 071201, doi: 10.1121/10.0005512.

McGowen M.R., Spaulding M. & Gatesy J. 2009. Divergence date estimation and a comprehensive molecular tree of extant cetaceans. *Molecular Phylogenetics and Evolution 53*, 891–906, doi: 10.1016/j.ympev.2009.08.018.

McKinney W. 2010. Data structures for statistical computing in Python. In S. van der Walt & J. Millman (eds.): *Proceedings of the 9th Python in Science Conference* – Python in Science Conference. SciPy, doi: 10.25080/majora-92bf1922-00a.

Meier W.N., Hovelsrud G.K., van Oort B.E.H., Key J.R., Kovacs K.M., Michel C., Haas C., Granskog M.A., Gerland S., Perovich D.K., Makshtas A. & Reist J.D. 2014. Arctic sea ice in transformation: A review of recent observed changes and impacts on biology and human activity. *Reviews of Geophysics 52*, 185–217, doi: 10.1002/2013RG000431.

Meire L., Mortensen J., Meire P., Juul-Pedersen T., Sejr M.K., Rysgaard S., Nygaard R., Huybrechts P. & Meysman F.J.R. 2017. Marine-terminating glaciers sustain high productivity in Greenland fjords. *Global Change Biology 23*, 5344–5357, doi: 10.1111/gcb.13801.

Melia N., Haines K. & Hawkins E. 2016. Sea ice decline and 21st century trans-Arctic shipping routes. *Geophysical Research Letters 43*, 9720–9728, doi: 10.1002/2016gl069315.

Mellinger D.K., Stafford K.M., Moore S.E., Dziak R.P. & Matsumoto H. 2007. An overview of fixed passive acoustic observation methods for cetaceans. *Oceanography 20*, 36–45, doi: 10.5670/oceanog.2007.03.

Met Office. 2010 - 2015. *Cartopy: a cartographic python library with a matplotlib interface*. Exeter, Devon. Accessed on the internet at http://scitools.org.uk/cartopy.

Miller L.A., Pristed J., Mohl B. & Surlykke A. 1995. The click-sounds of narwhals (*Monodon monoceros*) in Inglefield Bay, Northwest Greenland. *Marine Mammal Science 11*, 491–502.

Møhl B., Surlykke A. & Miller L.A. 1990. High Intensity Narwhal Clicks. In J.A. Thomas & R.A. Kastelein (eds.): *Sensory Abilities of Cetaceans: Laboratory and Field Evidence*. Pp. 295–303. Boston, MA: Springer US, doi: 10.1007/978-1-4899-0858-2_18.

Møhl B., Wahlberg M., Madsen P.T., Heerfordt A. & Lund A. 2003. The monopulsed nature of sperm whale clicks. *The Journal of the Acoustical Society of America 114*, 1143–1154, doi: 10.1121/1.1586258.

Møhl B., Wahlberg M., Madsen P.T., Miller L.A. & Surlykke A. 2000. Sperm whale clicks: Directionality and source level revisited. *The Journal of the Acoustical Society of America 107*, 638–648, doi: 10.1121/1.428329.

Møller E.F., Christensen A., Larsen J., Mankoff K.D., Ribergaard M.H., Sejr M., Wallhead P. & Maar M. 2023. The sensitivity of primary productivity in Disko Bay, a coastal Arctic ecosystem, to changes in freshwater discharge and sea ice cover. *Ocean Science 19*, 403–420, doi: 10.5194/os-19-403-2023.

Moore S.E., Clarke J.T., Okkonen S.R., Grebmeier J.M., Berchok C.L. & Stafford K.M. 2022. Changes in gray whale phenology and distribution related to prey variability and ocean biophysics in the northern Bering and eastern Chukchi seas. *PloS One 17*, e0265934, doi: 10.1371/journal.pone.0265934.

Moore S.E. & Huntington H.P. 2008. Arctic marine mammals and climate change: Impacts and resilience. *Ecological Applications 18*, 157–165, doi: 10.1890/06-0571.1.

Moore S.E. & Reeves R.R. 2018. Tracking arctic marine mammal resilience in an era of rapid ecosystem alteration. *PLoS Biology 16*, 1–7, doi: 10.1371/journal.pbio.2006708.

Morisaka T., Yoshida Y., Akune Y., Mishima H. & Nishimoto S. 2013. Exchange of signature calls in captive belugas (*Delphinapterus leucas*). *Journal of Ethology 31*, 141–149, doi: 10.1007/s10164-013-0358-0.

Morlighem M., Williams C., Rignot E., An L., Arndt J.E., Bamber J., Catania G., Chauché N., Dowdeswell J.A., Dorschel B., Fenty I., Hogan K., Howat I., Hubbard A., Jakobsson M., Jordan T.M., Kjeldsen K.K., Millan R., Mayer L., Mouginot J., Noël B., O'Cofaigh C., Palmer S.J., Rysgaard S., Seroussi H., Siegert M.J., Slabon P., Straneo F., van den Broeke M.R., Weinrebe W., Wood M. & Zinglersen K. 2022. IceBridge BedMachine Greenland, Version 5. [bed], doi: 10.5067/GMEVBWFLWA7X.

Morlighem M., Williams C.N., Rignot E., An L., Arndt J.E., Bamber J.L., Catania G., Chauché N., Dowdeswell J.A., Dorschel B., Fenty I., Hogan K., Howat I., Hubbard A., Jakobsson M., Jordan T.M., Kjeldsen K.K., Millan R., Mayer L., Mouginot J., Noël B.P.Y., O'Cofaigh C., Palmer S., Rysgaard S., Seroussi H., Siegert M.J., Slabon P., Straneo F., van den Broeke M.R., Weinrebe W., Wood M. & Zinglersen K.B. 2017. BedMachine v3: Complete bed topography and ocean bathymetry mapping of Greenland from multibeam echo sounding combined with mass conservation. *Geophysical Research Letters 44*, 11051–11061, doi: 10.1002/2017GL074954.

Morlighem M., Wood M., Seroussi H., Choi Y. & Rignot E. 2019. Modeling the response of northwest Greenland to enhanced ocean thermal forcing and subglacial discharge. *Cryosphere 13*, 723–734, doi: 10.5194/tc-13-723-2019.

Mouginot J., Rignot E., Bjørk A.A., van den Broeke M., Millan R., Morlighem M., Noël B., Scheuchl B. & Wood M. 2019. Forty-six years of Greenland Ice Sheet mass balance from 1972 to 2018. *Proceedings of the National Academy of Sciences 116*, 9239–9244, doi: 10.1073/pnas.1904242116.

Mouginot J., Rignot E., Scheuchl B., Fenty I., Khazendar A., Morlighem M., Buzzi A. & Paden J. 2015. Fast retreat of Zachariæ Isstrøm, northeast Greenland. *Science 350*, 1357–1361, doi: 10.1126/science.aac7111.

Mudryk L.R., Dawson J., Howell S.E.L., Derksen C., Zagon T.A. & Brady M. 2021. Impact of 1, 2 and 4 °C of global warming on ship navigation in the Canadian Arctic. *Nature climate Change*, doi: 10.1038/s41558-021-01087-6.

Myers P.G., Donnelly C. & Ribergaard M.H. 2009. Structure and variability of the West Greenland Current in summer derived from 6 repeat standard sections. *Progress in Oceanography 80*, 93–112, doi: 10.1016/j.pocean.2008.12.003.

Myers P.G., Kulan N. & Ribergaard M.H. 2007. Irminger water variability in the West Greenland Current. *Geophysical Research Letters 34*, 2–7, doi: 10.1029/2007GL030419.

Nammco. 2022. Report of the 28th meeting of the NAMMCO Scientific Committee. Accessed on the internet at https://nammco.no/topics/scientific-committee-reports.

NAMMCO. 2017. *Report of the NAMMCO-JCNB Joint Scientific Working Group on Narwhal and Beluga*. Copenhagen, Denmark: North Atlantic Marine Mammal Commission. Accessed on the internet at http://nammco.wpengine.com/wp-content/uploads/2017/06/nammco-jcnb-jwg-report-march-2017-final-with-ex-summ.pdf.

Nielsen M.R. 2009. Is climate change causing the increasing narwhal (*Monodon monoceros*) catches in Smith Sound, Greenland? *Polar Research 28*, 238–245, doi: 10.1111/j.1751-8369.2009.00106.x.

Noël B., van de Berg W.J., Lhermitte S. & van den Broeke M.R. 2019. Rapid ablation zone expansion amplifies north Greenland mass loss. *Science Advances 5*, eaaw0123, doi: 10.1126/sciadv.aaw0123.

Norris K.S., Prescott J.H., Asa-Dorian P.V. & Perkins P. 1961. An experimental demonstration of echo-location behavior in the porpoise, *Tursiops truncatus* (Montagu). *The Biological Bulletin 120*, 163–176, doi: 10.2307/1539374.

O'Corry-Crowe G.M. 2018. Beluga Whale: *Delphinapterus leucas*. *Encyclopedia of Marine Mammals*. Pp. 93–96.

Oksanen J., Blanchet F.G., Friendly M., Kindt R., Legendre P., McGlinn D., Minchin P.R., O'Hara R.B., Simpson G.L., Solymos P., Stevens M.H.H., Szoecs E. & Wagner H. 2020. Vegan: community ecology package. R package version 2.5-7. Accessed on the internet at https://cran.r-project.org/package=vegan.

Oliver H., Slater D., Carroll D., Wood M., Morlighem M. & Hopwood M.J. 2023. Greenland subglacial discharge as a driver of hotspots of increasing coastal chlorophyll since the early 2000s. *Geophysical Research Letters 50*, doi: 10.1029/2022gl102689.

Onarheim I.H., Eldevik T., Smedsrud L.H. & Stroeve J.C. 2018. Seasonal and regional manifestation of Arctic sea ice loss. *Journal of Climate 31*, 4917–4932, doi: 10.1175/JCLI-D-17-0427.1.

Otosaka I.N., Shepherd A., Ivins E.R., Schlegel N.-J., Amory C., van den Broeke M.R., Horwath M., Joughin I., King M.D., Krinner G., Nowicki S., Payne A.J., Rignot E., Scambos T., Simon K.M., Smith B.E., Sørensen L.S., Velicogna I., Whitehouse P.L., A, Geruo, Agosta C., Ahlstrøm A.P., Blazquez A., Colgan W., Engdahl M.E., Fettweis X., Forsberg R., Gallée H., Gardner A., Gilbert L., Gourmelen N., Groh A., Gunter B.C., Harig C., Helm V., Khan S.A., Kittel C., Konrad H., Langen P.L., Lecavalier B.S., Liang C.-C., Loomis B.D., McMillan M., Melini D., Mernild S.H., Mottram R., Mouginot J., Nilsson J., Noël B., Pattle M.E., Peltier W.R., Pie N., Roca M., Sasgen I., Save H.V., Seo K.-W., Scheuchl B., Schrama E.J.O., Schröder L., Simonsen S.B., Slater T., Spada G., Sutterley T.C., Vishwakarma B.D., van Wessem J.M., Wiese D., van der Wal W. & Wouters B. 2023. Mass balance of the Greenland and Antarctic ice sheets from 1992 to 2020. *Earth System Science Data 15*, 1597–1616, doi: 10.5194/essd-15-1597-2023.

Overland J., Dunlea E., Box J.E., Corell R., Forsius M., Kattsov V., Olsen M.S., Pawlak J., Reiersen L.O. & Wang M. 2019. The urgency of Arctic change. *Polar Science 21*, 6–13, doi: 10.1016/j.polar.2018.11.008.

Overland J. & Wang M. 2013. When will the summer Arctic be nearly sea ice free? *Geophysical Research Letters 40*, 2097–2101, doi: 10.1002/grl.50316.

Pacini A., Pickart R.S., Bahr F., Torres D.J., Ramsey A.L., Holte J., Karstensen J., Oltmanns M., Straneo F., Le Bras I.A., Moore G.W.K. & Femke de Jong M. 2020. Mean conditions and seasonality of the west Greenland boundary current system near cape farewell. *Journal of Physical Oceanography 50*, 2849–2871, doi: 10.1175/JPO-D-20-0086.1.

Panova E.M., Belikov R.A., Agafonov A.V., Kirillova O.I., Chernetsky A.D. & Bel'kovich V.M. 2016. Intraspecific variability in the vowel-like sounds of beluga whales (*Delphinapterus leucas*): Intra- and interpopulation comparisons. *Marine Mammal Science 32*, 452–465, doi: 10.1111/mms.12266.

Pearson K. 1901. On lines and planes of closest fit to systems of points in space. *Philosophical Magazine 2*, 559–572.

Penner R.H., Turl C.W. & Au W.W. 1986. Target detection by the beluga using a surface-reflected path. *The Journal of the Acoustical Society of America 80*, 1842–1843, doi: 10.1121/1.394301.

Pickart R.S., Torres D.J. & Fratantoni P.S. 2005. The East Greenland spill jet. *Journal of Physical Oceanography 35*, 1037–1053, doi: 10.1175/JPO2734.1.

Podolskiy E.A. & Sugiyama S. 2020. Soundscape of a narwhal summering ground in a glacier fjord (Inglefield Bredning, Greenland). *Journal of Geophysical Research: Oceans 125*, e2020JC016116, doi: 10.1029/2020JC016116.

Porter D.F., Tinto K.J., Boghosian A., Cochran J.R., Bell R.E., Manizade S.S. & Sonntag J.G. 2014. Bathymetric control of tidewater glacier mass loss in northwest Greenland. *Earth and Planetary Science Letters 401*, 40–46, doi: 10.1016/j.epsl.2014.05.058.

Post E., Bhatt U.S., Bitz C.M., Brodie J.F., Fulton T.L., Hebblewhite M., Kerby J., Kutz S.J., Stirling I. & Walker D.A. 2013. Ecological Consequences of Sea-Ice Decline. *Science 341*, 519–525.

QGIS Development Team. 2022. QGIS Geographic Information System. QGIS Association. Accessed on the internet at https://www.qgis.org.

R Core Team. 2021. R: A language and environment for statistical computing. Accessed on the internet at http://www.r-project.org/.

R Core Team. 2023. R: A language and environment for statistical computing. *R Foundation for Statistical Computing*. Accessed on the internet at http://www.r-project.org/.

Radtke C.L., Terhune J.M., Frouin-Mouy H. & Rouget P.A. 2023. Vocal count responses of narwhals to bulk carrier noise in Milne Inlet, Nunavut, Canada. *Marine Mammal Science 39*, 1057–1075, doi: 10.1111/mms.13028.

Ragen T.J., Huntington H.P. & Hovelsrud G.K. 2008. Conservation of Arctic marine mammals faced with climate change. *Ecological Applications 18*, S166–S174, doi: 10.1890/06-0734.1.

Rankin S., Archer F., Keating J.L., Oswald J.N., Oswald M., Curtis A. & Barlow J. 2017. Acoustic classification of dolphins in the California Current using whistles, echolocation clicks, and burst pulses. *Marine Mammal Science 33*, 520–540, doi: 10.1111/mms.12381.

Rantanen M., Karpechko A.Y., Lipponen A., Nordling K., Hyvärinen O., Ruosteenoja K., Vihma T. & Laaksonen A. 2022. The Arctic has warmed nearly four times faster than the globe since 1979. *Communications Earth & Environment 3*, 1–10, doi: 10.1038/s43247-022-00498-3.

Rasmussen M.H., Koblitz J.C. & Laidre K.L. 2015. Buzzes and high-frequency clicks recorded from narwhals (*Monodon monoceros*) at their wintering ground. *Aquatic Mammals 41*, 256–264, doi: 10.1578/AM.41.3.2015.256.

Redfern J.V., Mckenna M.F., Moore T.J., Calambokidis J., Deangelis M.L., Becker E.A., Barlow J., Forney K.A., Fiedler P.C. & Chivers S.J. 2013. Assessing the risk of ships striking large whales in marine spatial planning. *Conservation Biology 27*, 292–302, doi: 10.1111/cobi.12029.

Reeves R.R., Ewins P.J., Agbayani S., Heide-Jørgensen M.P., Kovacs K.M., Lydersen C., Suydam R., Elliott W., Polet G., Van Dijk Y. & Blijleven R. 2014. Distribution of endemic cetaceans in relation to hydrocarbon development and commercial shipping in a warming Arctic. *Marine Policy 44*, 375–389, doi: 10.1016/j.marpol.2013.10.005.

Richard P.R., Heide-Jørgensen M.P. & St. Aubin D. 1998a. Fall movements of belugas (*Delphinapterus leucas*) with satellite-linked transmitters in Lancaster Sound, Jones Sound, and Northern Baffin Bay. *Arctic 51*, 5–16. Accessed on the internet at http://www.jstor.org/stable/40511798.

Richard P.R., Laake J.L., Hobbs R.C., Heide-Jørgensen M.P., Asselin N.C. & Cleator H. 2010. Baffin Bay narwhal population distribution and numbers: aerial surveys in the Canadian High Arctic, 2002-04. *Arctic 63*, 85–99, doi: 10.14430/arctic649.

Richard P.R., Orr J.R., Dietz R. & Dueck L. 1998b. Sightings of Belugas and Other Marine Mammals in the North Water, Late March 1993. *Arctic 51*, 1–4. Accessed on the internet at http://www.jstor.org/stable/40511797.

Rignot E., An L., Chauche N., Morlighem M., Jeong S., Wood M., Mouginot J., Willis J.K., Klaucke I., Weinrebe W. & Muenchow A. 2021. Retreat of Humboldt Gletscher, north

Greenland, driven by undercutting from a warmer ocean. *Geophysical Research Letters 48*, e2020GL091342, doi: 10.1029/2020GL091342.

Rignot E., Fenty I., Menemenlis D. & Xu Y. 2012. Spreading of warm ocean waters around Greenland as a possible cause for glacier acceleration. *Annals of Glaciology 53*, 257–266, doi: 10.3189/2012AoG60A136.

Roch M.A., Stinner-sloan J., Baumann-pickering S. & Wiggins S.M. 2015. Compensating for the effects of site and equipment variation on delphinid species identification from their echolocation clicks. *The Journal of the Acoustical Society of America 137*, doi: 10.1121/1.4904507.

Ross J.C. & Allen P.E. 2014. Random Forest for improved analysis efficiency in passive acoustic monitoring. *Ecological Informatics 21*, 34–39, doi: 10.1016/j.ecoinf.2013.12.002.

Roy N., Simard Y., Gervaise C. & Dtn E. 2010. 3D tracking of foraging belugas from their clicks: Experiment from a coastal hydrophone array. *Applied Acoustics 71*, 1050–1056, doi: 10.1016/j.apacoust.2010.05.008.

Runge M.C., Stroeve J.C., Barrett A.P. & McDonald-Madden E. 2016. Detecting failure of climate predictions. *Nature Climate Change 6*, 861–864, doi: 10.1038/NCLIMATE3041.

Rutenko A.N. & Vishnyakov A.A. 2006. Time sequences of sonar signals generated by a beluga whale when locating underwater objects. *Acoustical Physics 52*, 314–323, doi: 10.1134/S1063771006030122.

Rykova T., Straneo F. & Bower A.S. 2015. Seasonal and interannual variability of the West Greenland Current system in the Labrador Sea in 1993-2008. *Journal of Geophysical Research: Oceans 120*, 1318–1332, doi: 10.1002/2014jc010386.

Rykova T., Straneo F., Lilly J.M. & Yashayaev I. 2009. Irminger current anticyclones in the Labrador Sea observed in the hydrographic record, 1990-2004. *Journal of Marine Research 67*, 361–384, doi: 10.1357/002224009789954739.

Rysgaard S., Boone W., Carlson D., Sejr M.K., Bendtsen J., Juul-Pedersen T., Lund H., Meire L. & Mortensen J. 2020. An updated view on water masses on the pan-West Greenland continental shelf and their link to proglacial fjords. *Journal of Geophysical Research: Oceans 125*, 1–10, doi: 10.1029/2019JC015564.

Sakai T. 2021. PAMpal: Load and process passive acoustic data. Accessed on the internet at http://cran.r-project.org/package=PAMpal.

Sakai T. 2023. PAMpal standardClickCalcs. Accessed on the internet at https://taikisan21.github.io/PAMpal/StandardCalcs.html.

Sanchez R., Slater D. & Straneo F. 2023. Delayed freshwater export from a Greenland tidewater glacial fjord. *Journal of Physical Oceanography 53*, 1291–1309, doi: 10.1175/JPO-D-22-0137.1.

Schaffer J., Kanzow T., von Appen W.J., von Albedyll L., Arndt J.E. & Roberts D.H. 2020. Bathymetry constrains ocean heat supply to Greenland's largest glacier tongue. *Nature Geoscience 13*, 227–231, doi: 10.1038/s41561-019-0529-x.

Schaffer J., von Appen W.-J., Dodd P.A., Hofstede C., Mayer C., de Steur L. & Kanzow T. 2017. Warm water pathways toward Nioghalvfjerdsfjorden Glacier, Northeast Greenland. *Journal of Geophysical Research: Oceans 122*, 4004–4020, doi: 10.1002/2016JC012462.

Schevill W.E. & Lawrence B. 1956. Food-finding by a captive porpoise (*Tursiops truncatus*). *Breviora 53*, 1–15.

Schevill W.E. & Lawrence B. 1949. Underwater listening to the white porpoise (*Delphinapterus leucas*). *Science 109*, 143–144, doi: 10.1126/science.109.2824.143.

Schild K.M., Hawley R.L. & Morriss B.F. 2016. Subglacial hydrology at Rink Isbræ, West Greenland inferred from sediment plume appearance. *Annals of Glaciology 57*, 118–127, doi: 10.1017/aog.2016.1.

Sciascia R., Straneo F., Cenedese C. & Heimbach P. 2013. Seasonal variability of submarine melt rate and circulation in an East Greenland fjord. *Journal of Geophysical Research: Oceans 118*, 2492–2506, doi: 10.1002/jgrc.20142.

Seibert A.-M., Koblitz J.C., Denzinger A. & Schnitzler H.-U. 2013. Scanning behavior in echolocating common pipistrelle bats (*Pipistrellus pipistrellus*). *PloS One 8*, e60752, doi: 10.1371/journal.pone.0060752.

Shapiro A.D. 2006. Preliminary evidence for signature vocalizations among free-ranging narwhals (*Monodon monceros*). *The Journal of the Acoustical Society of America 120*, 1695–1705, doi: 10.1121/1.2226586.

Shuert C.R., Marcoux M., Hussey N.E., Heide-Jørgensen M.P., Dietz R. & Auger-Méthé M. 2022. Decadal migration phenology of a long-lived Arctic icon keeps pace with climate change. *Proceedings of the National Academy of Sciences 119*, e2121092119, doi: 10.1073/pnas.2121092119.

Silber G.K., Vanderlaan A.S.M., Tejedor A., Johnson L., Taggart T., Brown M.W., Bettridge S. & Sagarminaga R. 2012. The role of the International Maritime Organization in reducing vessel threat to whales: Process, options, action and effectiveness. *Marine Policy 36*, 1221–1233, doi: 10.1016/j.marpol.2012.03.008.

Simões Amorim T.O., de Castro F.R., Moron J.R., Duque B.R., Di Tullio J.C., Secchi E.R. & Andriolo A. 2019. Integrative bioacoustics discrimination of eight delphinid species in

the western South Atlantic Ocean. *PloS One 14*, e0217977, doi: 10.1371/journal.pone.0217977.

Simon M., Wahlberg M. & Miller L.A. 2007. Echolocation clicks from killer whales (*Orcinus orca*) feeding on herring (*Clupea harengus*). *The Journal of the Acoustical Society of America 121*, 749–752, doi: 10.1121/1.2404922.

Sjare B.L. & Smith T.G. 1986a. The relationship between behavioral activity and underwater vocalizations of the white whale, *Delphinapterus leucas*. *Canadian Journal of Zoology 64*, 2824–2831, doi: 10.1134/S000143701201016X.

Sjare B.L. & Smith T.G. 1986b. The vocal repertoire of white whales, *Delphinapterus leucas*, summering in Cunningham Inlet, Northwest Territories. *Canadian Journal of Zoology 64*, 407–415, doi: 10.1139/z86-063.

Slater D.A., Carroll D., Oliver H., Hopwood M.J., Straneo F., Wood M., Willis J.K. & Morlighem M. 2022. Characteristic depths, fluxes, and timescales for Greenland's tidewater glacier fjords from subglacial discharge-driven upwelling during summer. *Geophysical Research Letters 49*, 1–9, doi: 10.1029/2021gl097081.

Slater D.A. & Straneo F. 2022. Submarine melting of glaciers in Greenland amplified by atmospheric warming. *Nature Geoscience 15*, 794–799, doi: 10.1038/s41561-022-01035-9.

Smith A.B., Kloepper L.N., Yang W.-C., Huang W.-H., Jen I.-F., Rideout B.P. & Nachtigall P.E. 2016. Transmission beam characteristics of a Risso's dolphin (*Grampus griseus*). *The Journal of the Acoustical Society of America 139*, 53–62, doi: 10.1121/1.4937752.

Smith L.C. & Stephenson S.R. 2013. New Trans-Arctic shipping routes navigable by midcentury. *Proceedings of the National Academy of Sciences 110*, E1191–E1195, doi: 10.1073/pnas.1214212110.

Smith T.G. & Martin A.R. 1994. Distribution and movements of belugas, *Delphinapterus leucas*, in the Canadian High Arctic. *Canadian Journal of Fisheries and Aquatic Sciences 51*, 1653–1663, doi: 10.1139/f94-166.

Soldevilla M.S., Henderson E.E., Campbell G.S., Wiggins S.M., Hildebrand J.A. & Roch M.A. 2008. Classification of Risso's and Pacific white-sided dolphins using spectral properties of echolocation clicks. *The Journal of the Acoustical Society of America 124*, 609–624, doi: 10.1121/1.2932059.

Sousa-Lima R.S., Norris T.F., Oswald J.N. & Fernandes D.P. 2013. A review and inventory of fixed autonomous recorders for passive acoustic monitoring of marine mammals. *Aquatic Mammals 39*, 23–53, doi: 10.1578/AM.39.1.2013.23.

Southall B.L., Nowacek D.P., Bowles A.E., Senigaglia V., Bejder L. & Tyack P.L. 2021. Marine mammal noise exposure criteria: Assessing the severity of marine mammal behavioral

responses to human noise. *Aquatic Mammals 47*, 421–464, doi: 10.1578/am.47.5.2021.421.

Stafford K.M., Citta J.J., Okkonen S.R. & Zhang J. 2021. Bowhead and beluga whale acoustic detections in the western Beaufort Sea 2008–2018. *PloS One 16*, e0253929, doi: 10.1371/journal.pone.0253929.

Stafford K.M., Farley E.V., Ferguson M., Kuletz K.J. & Levine R. 2022. Northward range expansion of aubarctic upper trophic level animals into the Pacific Arctic region. *Oceanography 35*, 158–166, doi: 10.5670/oceanog.2022.101.

Stafford K.M., Laidre K.L. & Heide-Jørgensen M.P. 2012. First acoustic recordings of narwhals (*Monodon monoceros*) in winter. *Marine Mammal Science 28*, 197–207, doi: 10.1111/j.1748-7692.2011.00500.x.

Stewart R.E.A., Campana S.E., Jones C.M. & Stewart B.E. 2006. Bomb radiocarbon dating calibrates beluga (*Delphinapterus leucas*) age estimates. *Canadian Journal of Zoology 84*, 1840–1852, doi: 10.1139/Z06-182.

Stewart R.E.A., Lesage V., Lawson J.W., Cleator H. & Martin K.A. 2011. Science technical review of the draft Environmental Impact Statement (EIS) for Baffinland's Mary River Project.

Straneo F., Curry R.G., Sutherland D.A., Hamilton G.S., Cenedese C., Våge K. & Stearns L.A. 2011. Impact of fjord dynamics and glacial runoff on the circulation near Helheim Glacier. *Nature Geoscience 4*, 322–327, doi: 10.1038/ngeo1109.

Straneo F., Hamilton G.S., Stearns L.A. & Sutherland D.A. 2016. Connecting the Greenland Ice Sheet and the ocean: A case study of Helheim Glacier and Sermilik Fjord. *Oceanography 29*, 34–45, doi: 10.5670/oceanog.2016.97.

Straneo F., Hamilton G.S., Sutherland D.A., Stearns L.A., Davidson F., Hammill M.O., Stenson G.B. & Rosing-Asvid A. 2010. Rapid circulation of warm subtropical waters in a major glacial fjord in East Greenland. *Nature Geoscience 3*, 182–186, doi: 10.1038/ngeo764.

Straneo F. & Heimbach P. 2013. North Atlantic warming and the retreat of Greenland's outlet glaciers. *Nature 504*, 36–43, doi: 10.1038/nature12854.

Straneo F., Scripps Institution of Oceanography, Slater D., Bouchard C., Cape M., Carey M., Ciannelli L., Holte J., Matrai P., Laidre K., Little C., Meire L., Seroussi H. & Vernet M. 2022. An interdisciplinary perspective on Greenland's changing coastal margins. *Oceanography* , doi: 10.5670/oceanog.2022.128.

Straneo F., Sutherland D.A., Holland D., Gladish C., Hamilton G.S., Johnson H.L., Rignot E., Xu Y. & Koppes M. 2012. Characteristics of ocean waters reaching greenland's glaciers. *Annals of Glaciology 53*, 202–210, doi: 10.3189/2012AoG60A059.

Straneo F., Sutherland D.A., Stearns L., Catania G., Heimbach P., Moon T., Cape M.R., Laidre K.L., Barber D., Rysgaard S., Mottram R., Olsen S., Hopwood M.J. & Meire L. 2019. The case for a sustained Greenland Ice Sheet-Ocean Observing System (GrIOOS). *Frontiers in Marine Science 6*, doi: 10.3389/fmars.2019.00138.

Surlykke A., Ghose K. & Moss C.F. 2009. Acoustic scanning of natural scenes by echolocation in the big brown bat, *Eptesicus fuscus*. *The Journal of Experimental Biology 212*, 1011–1020, doi: 10.1242/jeb.024620.

Sutherland D.A., Jackson R.H., Kienholz C., Amundson J.M., Dryer W.P., Duncan D., Eidam E.F., Motyka R.J. & Nash J.D. 2019. Direct observations of submarine melt and subsurface geometry at a tidewater glacier. *Science 365*, 369–374, doi: 10.1126/science.aax3528.

Sutherland D.A. & Pickart R.S. 2008. The East Greenland Coastal Current: Structure, variability, and forcing. *Progress in Oceanography 78*, 58–77, doi: 10.1016/j.pocean.2007.09.006.

Talley L.D., Pickard G.L., Emery W.J. & Swift J.H. 2011. *Descriptive Physical Oceanography: An Introduction*. 6th ed. London, UK: Elsevier.

Tang C.C.L., Ross C.K., Yao T., Petrie B., DeTracey B.M. & Dunlap E. 2004. The circulation, water masses and sea-ice of Baffin Bay. *Progress in Oceanography 63*, 183–228, doi: 10.1016/j.pocean.2004.09.005.

Tervo O.M., Blackwell S.B., Ditlevsen S., Garde E., Hansen R.G., Samson A.L., Conrad A.S. & Heide-Jørgensen M.P. 2023. Stuck in a corner: Anthropogenic noise threatens narwhals in their once pristine Arctic habitat. *Science Advances 9*, eade0440, doi: 10.1126/sciadv.ade0440.

The pandas development team. 2023. *pandas-dev/pandas: Pandas*. Zenodo, doi: 10.5281/ZENODO.3509134.

Turl C.W. & Penner R.H. 1989. Differences in echolocation click patterns of the beluga (*Delphinapterus leucas*) and the bottlenose dolphin (*Tursiops truncatus*). *The Journal of the Acoustical Society of America 86*, 497–502, doi: 10.1121/1.398229.

Turl C.W., Penner R.H. & Au W.W.L. 1987. Comparison of target detection capabilities of the beluga and bottlenose dolphin. *The Journal of the Acoustical Society of America 82*, 1487–1491, doi: 10.1121/1.395192.

Turl C.W., Skaar D.J. & Au W.W. 1991. The echolocation ability of the beluga (*Delphinapterus leucas*) to detect targets in clutter. *The Journal of the Acoustical Society of America 89*, 896–901, doi: 10.1121/1.1894651.

United Nations Conference on Trade and Development (UNCTAD). 2021. *Review of Maritime Transport 2021*. New York: United Nations Publications.

Urick R.J. 1983. *Principles of Underwater Sound*. 3rd Edition. New York: McGraw-Hill.

Vacquié-Garcia J., Lydersen C., Ims R.A. & Kovacs K.M. 2018. Habitats and movement patterns of white whales *Delphinapterus leucas* in Svalbard, Norway in a changing climate. *Movement Ecology 6*, doi: 10.1186/s40462-018-0139-z.

Våge K., Pickart R.S., Sarafanov A., Knutsen Ø., Mercier H., Lherminier P., van Aken H.M., Meincke J., Quadfasel D. & Bacon S. 2011. The Irminger Gyre: Circulation, convection, and interannual variability. *Deep-Sea Research: Part I, Oceanographic Research Papers 58*, 590–614, doi: 10.1016/j.dsr.2011.03.001.

Våge K., Pickart R.S., Thierry V., Reverdin G., Lee C.M., Petrie B., Agnew T.A., Wong A. & Ribergaard M.H. 2009. Surprising return of deep convection to the subpolar North Atlantic Ocean in winter 2007-2008. *Nature Geoscience 2*, 67–72, doi: 10.1038/ngeo382.

Vergara V., Michaud R. & Barrett-Lennard L.G. 2010. What can captive whales tell us about their wild counterparts? Identification, usage, and ontogeny of contact calls in belugas (*Delphinapterus leucas*). *International Journal of Comparative Psychology 23*, 278–309. Accessed on the internet at http://www2.gsu.edu/~wwwscp/ijcp-2010-3/05.Vergara_etal_FINAL.pdf.

Vergara V. & Mikus M.A. 2019. Contact call diversity in natural beluga entrapments in an Arctic estuary: Preliminary evidence of vocal signatures in wild belugas. *Marine Mammal Science 35*, 434–465, doi: 10.1111/mms.12538.

Villadsgaard A., Wahlberg M. & Tougaard J. 2007. Echolocation signals of wild harbour porpoises, *Phocoena phocoena*. *The Journal of Experimental Biology 210*, 56–64, doi: 10.1242/jeb.02618.

Wahlberg M., Jensen F.H., Soto N.A., Beedholm K., Bejder L., Oliveira C., Rasmussen M., Simon M., Villadsgaard A. & Madsen P.T. 2011. Source parameters of echolocation clicks from wild bottlenose dolphins (*Tursiops aduncus* and *Tursiops truncatus*). *The Journal of the Acoustical Society of America 130*, 2263–2274, doi: 10.1121/1.3624822.

Wahlberg M., Møhl B. & Teglberg Madsen P. 2001. Estimating source position accuracy of a large-aperture hydrophone array for bioacoustics. *The Journal of the Acoustical Society of America 109*, 397–406, doi: 10.1121/1.1329619.

Walmsley S.F., Rendell L., Hussey N.E. & Marcoux M. 2020. Vocal sequences in narwhals (*Monodon monoceros*). *The Journal of the Acoustical Society of America 147*, 1078–1091, doi: 10.1121/10.0000671.

Wang M. & Overland J.E. 2009. A sea ice free summer Arctic within 30 years? *Geophysical Research Letters 36*, L07502, doi: 10.1029/2009GL037820.

Williams P.L., Burgess D.O., Waterman S., Roberts M., Bertrand E.M. & Bhatia M.P. 2021. Nutrient and carbon export from a tidewater glacier to the coastal ocean in the Canadian arctic archipelago. *Journal of Geophysical Research: Biogeosciences 126*, doi: 10.1029/2021jg006289.

Williams T.M., Blackwell S.B., Tervo O., Garde E., Sinding H.S., Richter B. & Peter M. 2022. Physiological responses of narwhals to anthropogenic noise : A case study with seismic airguns and vessel traffic in the Arctic. *Functional Ecology 36*, 2251–2266, doi: 10.1111/1365-2435.14119.

Willis J., Jet Propulsion Laboratory, Caltech, Carroll D., Fenty I., Kohli G., Khazendar A., Rutherford M., Trenholm N. & Morlighem M. 2018. Ocean-ice interactions in Inglefield gulf: Early results from NASA's oceans melting Greenland mission. *Oceanography 31*, doi: 10.5670/oceanog.2018.211.

Wisniewska D.M., Johnson M., Beedholm K., Wahlberg M. & Madsen P.T. 2012. Acoustic gaze adjustments during active target selection in echolocating porpoises. *The Journal of Experimental Biology 215*, 4358–4373, doi: 10.1242/jeb.074013.

Wood M., Rignot E., Fenty I., An L., Bjørk A., van den Broeke M., Cai C., Kane E., Menemenlis D., Millan R., Morlighem M., Mouginot J., Noël B., Scheuchl B., Velicogna I., Willis J.K. & Zhang H. 2021. Ocean forcing drives glacier retreat in Greenland. *Science Advances 7*, 1–11, doi: 10.1126/sciadv.aba7282.

Wood M., Rignot E., Fenty I., Menemenlis D., Millan R., Morlighem M., Mouginot J. & Seroussi H. 2018. Ocean-induced melt triggers glacier retreat in Northwest Greenland. *Geophysical Research Letters 45*, 8334–8342, doi: 10.1029/2018GL078024.

Woodgate R.A., Stafford K.M. & Prahl F.G. 2015. A synthesis of year-round interdisciplinary mooring measurements in the Bering Strait (1990–2014) and the RUSALCA years (2004–2011). *Oceanography 28*, 46–67, doi: 10.5670/oceanog.2015.57.

Yang L., Sharpe M., Temple A.J., Jiddawi N., Xu X. & Berggren P. 2020. Description and classification of echolocation clicks of Indian Ocean humpback (*Sousa plumbea*) and Indo-Pacific bottlenose (*Tursiops aduncus*) dolphins from Menai Bay, Zanzibar, East Africa. *PloS One 15*, e0230319, doi: 10.1371/journal.pone.0230319.

Yang W.-C., Chen C.-F., Chuah Y.-C., Zhuang C.-R., Chen I.-H. & Kellar N.M. 2021. Anthropogenic sound exposure-induced stress in captive dolphins and implications for cetacean health. *Frontiers in Marine Science 8*, 606736, doi: 10.3389/fmars.2021.606736.

Zahn M.J., Ladegaard M., Simon M., Stafford K.M., Sakai T. & Laidre K.L. 2023. Catalogue of Arctic Toothed Whale Click Spectra and Spectrograms from SoundTrap Recordings (1.0.0) [Data set]. *Zenodo*, doi: 10.5281/zenodo.10076260.

Zahn M.J., Laidre K.L., Stilz P., Rasmussen M.H. & Koblitz J.C. 2021a. Vertical sonar beam width and scanning behavior of wild belugas (*Delphinapterus leucas*) in West Greenland. *PloS One 16*, e0257054, doi: 10.1371/journal.pone.0257054.

Zahn M.J., Rankin S., Mccullough J.L.K., Koblitz J.C., Archer F., Rasmussen M.H. & Laidre K.L. 2021b. Acoustic differentiation and classification of wild belugas and narwhals

using echolocation clicks. *Scientific Reports 11*, 22141, doi: 10.1038/s41598-021-01441-w.

Zhong M., Castellote M., Dodhia R., Ferres J.L., Keogh M., Brewer A., Zhong M., Castellote M., Dodhia R., Ferres J.L., Keogh M. & Brewer A. 2020. Beluga whale acoustic signal classification using deep learning neural network models. *The Journal of the Acoustical Society of America 147*, 1834–1841, doi: 10.1121/10.0000921.

Zimmer W.M.X., Johnson M.P., Madsen P.T. & Tyack P.L. 2005. Echolocation clicks of free-ranging Cuvier's beaked whales (*Ziphius cavirostris*). *The Journal of the Acoustical Society of America 117*, 3919–3927, doi: 10.1121/1.1910225.